Title

Investigating the transgenerational inheritance of environmental cues in C. elegans

Author

Truong, Lisa

Publication Date

2022

Peer reviewed|Thesis/dissertation

UNIVERSITY OF CALIFORNIA

Los Angeles

Investigating the transgenerational inheritance of environmental cues in *C. elegans*

A dissertation submitted in partial satisfaction of the requirements for the degree

Doctor of Philosophy in Human Genetics

by

Lisa Truong

2022

ABSTRACT OF THE DISSERTATION

Investigating the transgenerational inheritance of environmental cues in *C. elegans*

by

Lisa Truong

Doctor of Philosophy in Human Genetics

University of California, Los Angeles, 2022

Professor Patrick Allard, Co-Chair

Professor Matteo Pellegrini, Co-Chair

In sexually reproducing organisms, germ cell development is vital for the faithful transmission of the genome and epigenome across generations. Recent studies have shown that germ cell development is affected by different environmental toxicants, resulting in a decrease in germ cell health and number. Here, we examine the transgenerational impact and mechanisms of two prevalent toxicants, the plastic manufacturing chemical Bisphenol A and ethanol, in *Caenorhabditis elegans*. Both have well-described impacts on the developing fetus; however, their effects on developing germ cells and subsequent generations are less explored. We hypothesize that exposure disrupts the epigenetic machinery in germ cells, causing changes in histone modifications, fertility defects, and germline dysfunction in a transgenerational manner. First, we show that BPA exposure causes a transgenerational two-fold increase in germline chromatin desilencing coupled with a reduction and redistribution of histone H3K9me3 and H3K27me3. We show that the alteration of repressive histone levels is required for the observed transgenerational 43% increase in germline apoptosis and 85%

increase in embryonic lethality. By performing a genetic rescue using RNAi, we identified the chromatin modifying enzymes H3K9 and H3K27 demethylases (*jmjd-2, jmjd-3,* and *utx-1*) to be responsible for the transgenerational effects of BPA, since RNAi alone was able to restore the chromatin into a silenced state and rescue fertility defects. This confirms our idea that epigenetic memory is mediated by histone marks. Next, an increase in apoptosis suggests possible perturbations in the germline checkpoint machinery. To understand which checkpoint BPA perturbs, we used mutants of each checkpoint to rescue the effect. This revealed that BPA perturbs the synapsis checkpoint since a *pch-2* mutant decreased BPA induced apoptosis by two-fold whereas mutants of the DNA damage checkpoint, *spo-11* and *cep-1*, did not. Furthermore, visualization of the synaptonemal complex (SC) using a SYP-3::GFP strain revealed perturbations in proper SC assembly and aggregation of SC proteins resulting from ancestral BPA exposure. The formation of these aggregates was further associated with increases in embryonic lethality transgenerationally at the F3. In parallel, we also explored another common toxicant, ethanol, but instead we built the complete transgenerational transcriptional map of ethanol using single cell RNA-seq approaches. Together, my work identified the molecular drivers of environmental transgenerational effects on the germline machinery and reproductive health. We hope to further understand how it induces germline dysfunction, carrying important implications for human reproductive health in the context of environmental exposures.

The dissertation of Lisa Truong is approved.

Amander Therese Clark

Alison Renee Frand

Patrick Allard, Committee Co-Chair

Matteo Pellegrini, Committee Co-Chair

University of California, Los Angeles

2022

Dedicated to the most important people in my world,

Mom, Dad, Monica, and Steven

Table of Contents

List of Tables and Figures

Chapter 4

Single-nucleus resolution mapping of the adult *C. elegans* and its application to elucidate inter- and trans-generational response to alcohol exposure

Acknowledgements

Thank you to my wonderful PI, Dr. Patrick Allard, for all his support and guidance during my journey. It has been such an amazing experience. He has really encouraged and challenged me to think outside the box, while always being someone who I can depend on to care for me when I needed it most, both inside and outside of the lab. His patience and guidance has really shaped me into the scientist that I am today and I will always be grateful for the time I have spent under his wing. They say that you can tell a lot about a PI by looking at his lab and Patrick's lab has always been filled with generous, helpful, enthusiastic, and caring souls, a true reflection of Patrick himself. I count myself lucky to have been your pupil.

I would also like to thank the wonderful members of the Allard lab, both past and present. You have all made our lab such an accepting place to learn and grow. I will miss all our adventures together from out of state conferences to boba trips down the block. It has been such a rewarding experience getting the opportunity to brainstorm with you all and I have learned so much from each and every one of you. I would like to give special thanks to Dr. Jessica Camacho and Dr. Yichang Chen, my mentors and comrades who I can always count on to keep me company as I work late into the nights and on weekends. Thank you for your guidance, for your words of wisdom, and for always having my back. A special thanks to Dr. Roxane Verdikt for her immense knowledge and deep understanding about every experiment known to man. I can always count on you to answer my questions regarding experimental setup and I always appreciate your enthusiasm for teaching. I would also like to thank all the lab mates that I have been lucky enough to get to collaborate with including Yen-Wei Chen, Rio Barrere-Cain, Abby Bline, Carly Moore, and Courtney McClure. A special thank you to Hui Jiang and Yannie Kang for being such supportive lab mates both inside and outside of lab and always offering their help when I needed it. Lastly, I wanted to thank my wonderful undergraduate students, without whom a lot of this work would not have been possible.

I would also like to thank my committee members, Dr. Matteo Pellegrini, Dr. Amander Clark, and Dr. Alison Frand. Your guidance and mentorship is truly invaluable. Thank you for challenging me to think outside the box and for teaching me to think like a scientist. I always enjoy our meetings because I learn so much from every one of you and getting the opportunity to discuss my projects with you really paved the way for the trajectory of these projects.

Thank you to all my friends and family for being the greatest support system. Thank you so much for believing in me, especially during the times when it was hard for me to believe in myself. A special thank you to my parents for giving me the opportunity to pursue a career in science and for always supporting my passions no matter where they lead me. I could not have gotten this far without you.

Thank you to all my funding sources from UCLA, NIH, and especially the Genomic Analysis Training Program (GATP) for allowing me to advance my scientific training and to share my work with a broader audience through multiple conferences and meetings. A special thanks to Dr. Jeanette Papp and Dr. Eric Sobel for their mentorship through the GATP.

Chapter 1 is a version of a previous publication: Camacho J, Truong L, Kurt Z, Chen Y-W, Morselli M, Gutierrez G, Pellegrini M, Yang X, and Allard P. The Memory of Environmental Chemical Exposure in *C. elegans* Is Dependent on the Jumonji Demethylases *jmjd-2* and *jmjd-3/utx-1*. Cell Reports. 2018 May;23(8):2392-404. I would like to also acknowledge the contributions of the co-authors in this paper. Thank you Jessica Camacho for her contribution in designing, conducting experiments, and writing the paper, Kurt Zeyneb, Yen-Wei Chen, and Dr. Yang for their help with RNA-seq and ChIP-seq data analysis, Gerardo Gutierrez for conducting experiments, Marco Morselli and Dr. Pellegrini for conducting the RNA-seq experiments, Dr. Patrick Allard for designing experiments, interpreting data, and writing the manuscript.

Dr. Patrick Allard is the principal investigator who directed and supervised all parts of the research in this dissertation. Thank you to Dr. Allard as well as the whole committee for providing insight regarding the writing and editing of each dissertation chapter.

LISA TRUONG

EDUCATION

University of California Los Angeles, Los Angeles, CA
Ph.D Candidate in Human Genetics
Investigating the transgenerational inheritance of environmental cues in *C. elegans*
Cumulative GPA: 3.621

University of California Davis, Davis, CA
B.S. in Genetics and Genomics **June 12, 2015**
Areas of Concentration: Non-disjunction during meiosis and genetic diseases
Cumulative GPA: 3.56

HONORS AND AWARDS

Dissertation Year Fellowship **2021 – 2022**
Genomic Analysis and Interpretation Training Grant **2017 – 2019**

RESEARCH EXPERIENCE

University of California Los Angeles, Los Angeles, CA
Graduate Student **March 2016 – Current**

- Currently working with Dr. Patrick Allard in the department of Environmental Health Sciences to study the effects of environmental exposures such as Bisphenol A (BPA) and Ethanol exposure on gene expression and chromatin dynamics across multiple generations in *C. elegans.*

University of California Davis, Davis, CA
Undergraduate Genetic Researcher **Sept 2013 – June 2015**

- Worked with Dr. Engebrecht in the department of Molecular and Cellular Biology to study the effects of mutations in a*lt-1* on chromosomes and progeny using the model organism *C. elegans.*

University of California, Davis Medical Center, Sacramento, CA
Department of Neurology
Clinical Research Intern **April 2013 – June 2015**

- Assisted clinical research coordinators with several ongoing and new clinical trials as part of the Neuroimmunology Study Group, specifically on Multiple Sclerosis trials. Main Responsibilities include administering the Multiple Sclerosis Functional Composite (MSFC) test, Symbol Digit Modalities test

(SDMT), Sloan Low Contrast Visual Acuity test, and the Brief Visuospatial Memory Test – Revised (BVMT-R).

PUBLICATIONS

University of California Los Angeles, Los Angeles, CA
Cell Reports – Volume 23, Issue 8 (2018)

- The Memory of Environmental Chemical Exposure in *C. elegans* Is Dependent on the Jumonji Demethylases *jmjd-2* and *jmjd-3/utx-1*
- Camacho J, Truong L, Kurt Z, *et al*. The Memory of Environmental Chemical Exposure in *C. elegans* is Dependent on the Jumonji Demethylases jmjd-2 and jmjd-3/utx-1. *Cell Reports* 23(8), 2392-2404 (2018).

University of California Los Angeles, Los Angeles, CA
Environmental and Molecular Mutagenesis – Volume 59, Issue 7 (2018)

- *Caenorhabditis elegans* as an emerging model system in environmental epigenetics
- Weinhouse C, Truong L, Meyer JN, Allard P. *Caenorhabditis elegans* as an emerging model system in environmental epigenetics. *Environ Mol Mutagen* 59(7), 560-575 (2018).

PRESENTATIONS

San Diego Convention Center, San Diego, CA
61st Annual Meeting of the Society of Toxicology and ToxExpo
Student Poster Presenter **March 27 – 31, 2022**

- "Examining the Transgenerational Effects of Environmental Cues in *C. elegans*"

University of California, Los Angeles, Los Angeles, CA
UCLA Department of Human Genetics Academic Retreat
Best Poster Presentation Award
Student Poster Presenter **October 7, 2021**

- "Examining the Transgenerational Effects of Environmental Cues in *C. elegans*"

Green Acre Campus Pointe, San Diego, CA
Southern California Chapter of the Society of Toxicology (SCCSOT) Fall Regional Meeting
First Prize Poster Presentation
Student Poster Presenter **November 7, 2019**

- "Examining the Transgenerational Effects of Environmental Cues in *C. elegans*"

University of California Los Angeles, Los Angeles, CA
Genomic Analysis Training Program (GATP) Annual Joint Research Symposium
First Prize Poster Presentation
Student Poster Presenter **May 10, 2018**

- "The Jumonji demethylases *Jmjd-2* and *Jmjd-3*/*Utx-1* are required for the transgenerational effects of BPA in *C. elegans*"

CHAPTER 1

Introduction & Background

"Impacts of Toxicant Exposures and Single-cell Sequencing"

Part of Chapter 1 was published as a review in Environmental and Molecular Mutagenesis titled

"*Caenorhabditis elegans* as an Emerging Model System in Environmental Epigenetics"

1.1 Introduction

We are exposed to both natural and man-made toxicants in our environment each and every day. From our homes to our work-places, we constantly come into contact with chemicals that may have serious effects on our health and reproduction. For decades we have only focused on the effects of direct exposures. However, it is just as important to consider how these chemicals may affect future generations. This is especially true since emerging data has validated the direct negative effects of numerous toxicants and companies have begun to phase these chemicals out of production (Adeola, 2021). However, the removal of the exposure source does not erase the effects of these chemicals. Emerging studies continue to highlight the impact of in-utero exposure on multiple generations post exposure (Heard *et al.*, 2014). In this chapter, we will focus on the multigenerational impact of environmental exposures as well as introduce a new sequencing technique that we will be using to explore the tissue-specific multi- and trans-generational effects of environmental toxicants.

1.2 Germline and multigenerational effects of environmental cues

1.2.1 The importance of germ cell development and their sensitivity to environmental factors.

In most sexually reproducing organisms, the development of germ cells is tightly controlled to ensure that each half of the parental genomes is faithfully transmitted from one generation to the next. Failure of germ cells to properly differentiate is associated with birth defects as well as infertility, miscarriages, and stillbirths (Hunt *et al.,* 2008). In addition to inheriting the genome from its parents, the progeny also inherits its associate epigenetic marks which include DNA methylation and histone modifications. Increasing evidence has shown that these epigenetic modifications play important biological roles due to its role in regulating gene expression and ensuring genome stability (Harmston *et al.*, 2013). Germ cells also carry these epigenetic marks and perturbations are detrimental to the survival of the embryo (Kim *et al.*,

2014). The epigenome of germ cells is highly regulated during early development through the removal of DNA methylation and the addition of repressive histone modifications H3K9me3 and H3K27me3. Thus, the proper regulation of histone marks in early germ cells has been shown to be essential for heterochromatin silencing and germ cell differentiation and survival (Liu *et al*., 2014).

Chemical exposures can alter the epigenome of germ cells and these epigenetic modifications will then be passed on to subsequent generations. Studies have shown that germ cell development can be affected by many environmental factors. One study showed that Paracetamol (Acetaminophen) interferes with female reproductive development and perturbs proliferation of primordial germ cells resulting in a reduced number of germ cells, diminished follicle reserve, and reduced fertility in female fetuses (Holm *et al.,* 2016). In another study, mice treated with Phthalates, a chemical used to manufacture plastics, induces the production of multinucleated germ cells (MGCs) following *in utero* exposure in male fetuses (Mylchreest *et al.,* 2002). Lastly, mice and rats treated with Vinclozolin, a fungicide used in farming, resulted in an increase in apoptotic germ cell numbers following *in utero* exposure in male mice fetuses (Uzumcu *et al.,* 2004) and decreased sperm cell number and viability following *in utero* exposure in male rat fetuses (F1) as well as two generations after (F3), suggesting a possible transgenerational effect (Anway *et al.,* 2005). However, the exact mechanisms for this transgenerational inheritance is still unknown. The authors proposed that this transgenerational effect is mediated through DNA methylation (Anway *et al.,* 2005). However, this poses an issue since early germ cells undergo two waves of epigenetic reprogramming that decreases DNA methylation to its lowest levels (Gkountela *et al.*, 2015; Messerschmidt et al., 2014; Hackett *et al*., 2013) establishing a blank slate. Instead, I propose to that histone marks may play an important role in mediating epigenetic memory in the absence of DNA methylation.

1.2.2 *Caenorhabditis elegans* as an emerging model system for environmental epigenetics

C. elegans is a valuable model to study the effects of environmental exposures on the epigenome, as well as developmental plasticity (reviewed in Laubach et al., 2018), due to its ability to respond to a variety of environmental stressors, including osmolarity (Kishimoto et al., 2017), starvation (Rechavi et al., 2014), and temperature (Klosin et al., 2017), as well as chemical pollutants, such as heavy metals (Kishimoto et al., 2017; Rudgalvyte et al., 2017), nanoparticles (Schultz et al., 2016), and others. The extent to which *C. elegans* encounters anthropogenically produced or mobilized chemicals in its natural environment is not well studied, but ongoing study of wild nematode strains will enable characterization of chemical response and resistance outside of a controlled laboratory environment, potentially permitting the adoption of this organism in ecotoxicological studies.

As mentioned above, the combination of the ease of manipulation of the organism, the high degree of conservation of epigenetic regulatory pathways, and the availability of a wide range of molecular tools strongly recommends *C. elegans* for studies of the environmental influences on the epigenome, the types of epigenetic marks altered by exogenous cues, and the epigenetic mechanisms implicated in the nematode's response. The fast generation time and the high degree of conservation of epigenetic regulatory pathways (except cytosine methylation) enable the examination of multi- and trans-generational effects of environmental exposures, an exciting and compelling research topic within environmental epigenetics.

In addition, as most *C. elegans* are born hermaphrodites under typical conditions, but males and/or individuals that produce only sperm or eggs can be produced by temperature shifts, and through genetic manipulations, *C. elegans* can be used to isolate the effects of epigenetic changes in sperm or oocytes. Foundational work in the Strome and Kelly labs distinguished the germline epigenome from the epigenome in somatic cells (Strome 2005; Furuhashi et al., 2010), and described initial evidence for trans-generational inheritance of

responses to environmental stressors in *C. elegans* (Furuhashi et al., 2010; Arico et al., 2011; Kelly 2014).

1.2.3 Studying the Developmental Origins of Health and Disease (DOHaD) Paradigm using *Caenorhabditis elegans*

Environmental epigenetics research in *C. elegans* to date has focused on the Developmental Origins of Health and Disease (DOHaD) paradigm, or the increased risk of adult disease due to environmental exposures in early life, as well as extensions of this paradigm. The three most common exposure designs are: (1) somatic developmental exposure, often during larval development (DOHaD); (2) multigenerational effects of developmental exposure (DOHaD); and (3) experiments that extend DOHaD to test transgenerational effects of developmental exposure. We describe these designs and summarize existing research (Table I) using these designs below. However, we emphasize that environmental epigenetics research is not limited to these designs. Study designs in this subfield are likely to expand as new tools become available; for example, new single cell epigenomics techniques and genetically diverse nematode strains have already enabled new and exciting questions in environmental epigenetics; the advent of single cell epigenomics techniques and the availability of a wide range of nematode strains with varying genetic backgrounds will augment an expansion of research questions in this growing subfield.

A classic DOHaD experiment tests the effects of a developmental exposure on somatic tissues. For example, Rudgalvyte et al. (2017) used a chronic exposure paradigm throughout larval development to determine the impact of methylmercury on the epigenetic land-scape. The authors observed an enrichment of the active mark H3K4me3 in Phase II metabolism genes, the lipocalin-related protein gene *lpr-5*, and the cuticular collagen gene *dpy-7*, which is involved in formation of the outer cuticle, a natural barrier to chemicals (Rudgalvyte et al., 2017). Knockdown of *lpr-5* and *dpy-7* triggered increased lethality after methylmercury exposure,

supporting epigenetic control of chemical defense mechanisms in the nematode (Rudgalvyte et al., 2017).

A *multi-generational experiment* will expose several generations either directly by repeated exposure or indirectly, by exposing a gravid adult (P0) and therefore also exposing the embryo (F1) and the germline (F2) within the embryo. In contrast, a *trans-generational experiment* will expose one generation (P0) and examine a downstream generation that was never directly or indirectly exposed to the chemical (F3 and beyond). Thus, in *C. elegans*, the study of trans-generational effects at the F3 is greatly facilitated by its short generation time, reaching the F3 within 2 weeks by contrast to other common trans-generational models such as zebrafish and mice where such studies could span 6 months to a year.

1.2.4 Studies in *C. elegans* have suggested epigenetics pathways to be the mechanism of inheritance of environmental cues

The study of the implication of epigenetic pathways in environmental inheritance provides by far the richest body of work on environmental epigenetics in *C. elegans*. Taki et al. (2014b) examined the impact of nicotine exposure during larval development on microRNA (miRNA) expression. The authors observed that nicotine exposure was associated with differential expression of 40 miRNAs: 37 following high exposure, and 3 following low exposure, to nicotine (Taki et al., 2014b). These miRNAs clustered into distinct functional hubs, including metabolic and neuronal pathways (Taki et al., 2014b), suggesting that miRNA regulation might mediate some of nicotine's behavioral effects (Taki et al., 2013). In a follow-up trans-generational study, the authors identified a total of 14 miRNAs with differential expression by nicotine exposure across more than one generation (Taki et al., 2014a).

Schultz et al. (2016) conducted a 10-generation continuous exposure study using silver ions and silver nanoparticles. Continuous exposure to silver nitrate, silver nanoparticles, and sulfidized ("aged") silver nanoparticles sensitized the worms to later exposures: F2 worms

showed the greatest decrease in lifespan and greatest reproductive toxicity, effects that were attenuated but sustained until the F10. While these results clearly showed a sensitization of the nematodes' response to several toxicants over many generations, the study did not explore the role of epigenetic pathways in that sensitization. There are additional reports of stressors causing heritable phenotypes, including dietary restriction (Hibshman et al., 2016).

In one of the most striking studies of trans-generational effects, Klosin *et al.* (2017) observed loss of silencing of a heterochromatic gene array that persisted for 14 generations following five generations of exposure to high temperature. Even a single generation of exposure triggered loss of silencing that lasted for seven generations (Klosin *et al.*, 2017). The inheritance occurred through both sperm and oocytes, and was associated with decreased H3K9me3 levels (Klosin *et al.*, 2017). Gene array silencing in unexposed animals required the H3K9 methyltransferase *set-25* (Klosin *et al.*, 2017). These results suggest that environmental exposures may perturb the balance between demethylase and methyltransferase activity required for maintenance of epigenetic patterning.

In contrast to the heat-induced effects on a repressive histone modification, arsenite exposure induces trans-generational effects on the activating mark H3K4me2. Yu and Liao (2016) observed increased H3K4me2 levels and reduced expression of the H3K4me2 demethylase, *spr-5*, for three generations following an initial developmental arsenite exposure.

Active histone marks were also targeted in the response to high hormone levels. Gamez-Del-Estal *et al.* (2014) showed that testosterone exposure induced abnormal behavioral patterns in *C. elegans*, which persisted for four generations after exposure cessation. Abnormal behaviors were abolished on treatment with RNAi to androgen receptor gene orthologs or with sodium butyrate, a histone deacetylase inhibitor, suggesting that activating acetylated histone proteins were required for abnormal responses.

Kishimoto *et al.* (2017) addressed overlap in trans-generational mechanisms using exposure to multiple stressors in parallel (arsenite, hyperosmosis, or starvation). Interestingly,

exposure to any of the three stressors during developmental stages resulted in increased adulthood resistance to lethal concentrations of the oxidative stressor, hydrogen peroxide (Kishimoto *et al.*, 2017). This resistance was inherited for three generations (Kishimoto *et al.*, 2017). Knockdown of individual H3K4 methyltransferase components, *wdr-5.1* and *set-2*, were sufficient to reverse inheritance of the resistance phenotype (Kishimoto *et al.*, 2017). Thus all 3 stressors appeared to use a similar mechanism that involved regulation of H3K4me3 levels.

TABLE I. Select Studies Relevant to Environmental Epigenetics in *C. elegans*

Stressor	Study design	Epigenetic mark	Main findings	Reference
Methylmercury	Developmental	H3K4me3	Phase II metabolism genes, *lpr-5*, *dpy-7*	Rudgalvyte et al., 2017
Nicotine	Developmental	miRNA	37 miRNA on high exposure, 3 on low exposure	Taki et al., 2013
Arsenite, hyperosmosis, starvation	Developmental	H3K4me3	Increased adulthood resistance to hydrogen peroxide required H3K4 methyltransferase subunits *wdr-5.1* and *set-2*, overlap in mechanism of all three stressors	Kishimoto et al., 2017
Dietary restriction	Developmental	None	Altered offspring size and starvation resistance mediated by insulin-like signaling	Hibshman et al., 2016
Nicotine	Transgenerational	miRNA	14 miRNA	Taki et al., 2014
Silver ions, silver nanoparticles	Transgenerational	None	Lifespan decrease, reproductive toxicity	Schultz et al., 2016
Temperature	Transgenerational	H3K9me3	Loss of silencing of heterochromatic array required H3K9 methyltransferase *set-25*	Klosin et al., 2017
Arsenite	Transgenerational	H3K4me2	Increased H3K4me2 and reduced H3K4me2 demethylase *spr-5* expression	Yu and Liao 2016
Testosterone	Transgenerational	Post-translational histone acetylation	Abnormal behaviors abolished on RNAi to androgen receptor gene orthologs or with HDAC sodium butyrate	Gamez-Del-Estal et al., 2014
Starvation-induced developmental arrest	Transgenerational	Small RNA	Small RNA targeted nutrient reservoir activity and vitellogenins, inheritance required argonaute factors *rde-4* and *hrde-1*	Rechavi et al., 2014
Arsenite, hyperosmosis, starvation	Transgenerational	H3K4me3	Increased adulthood resistance to hydrogen peroxide required H3K4 methyltransferase subunits *wdr-5.1* and *set-2*, overlap in mechanism of all three stressors	Kishimoto et al., 2017
Genetic	Transgenerational	H3K9me, small RNA	H3K9 mutants progressive decline in fertility, required argonaute factor *hdre-1* and H3K9 methyltransferase *met-2*	Lev et al., 2017
Bisphenol A (BPA)	Transgenerational	H3K9me3, H3K27me3	Germline transgene desilencing in exposed animals was coupled with decreased H3K9me3 and H3K27me3, as well as reproductive defects and embryonic lethality, for five generations. Repression was rescued by activation of Jumonji demethylases JMJD-2 and JMJD-3/UTX-1.	Camacho et al., 2018 (in press)

1.3 The emergence of a new sequencing technique: Single-cell sequencing

1.3.1 The development of single-cell sequencing technologies over the years

Single-cell sequencing refers to the sequencing and identification of a single-cell's genome or transcriptome. This technology allows for the identification of cell population differences and has paved the way for better understanding of how a multitude of factors, including gene expression, can change within specific cell types due to external or environmental factors, something that is overshadowed by previous bulk sequencing methods. Traditionally, sequencing methods such as RNA sequencing (RNA-seq) analyzes total RNA from a tissue sample or whole organisms (Wang *et al.*, 2009). While this method has the ability to identify global changes in the levels of transcripts in a tissue or sample, it treats the sample as a whole, revealing only the average of many cells without capturing sample heterogeneity. In contrast, single-cell sequencing technologies can detect heterogeneity between individual cells, elucidate novel cell types, and identify otherwise rare cell types whose signal would have been lost in bulk RNA-seq (Kolodziejczyk *et al.,* 2015; Macaulay *et al.,* 2016; Svensson *et al.,* 2018).

Single-cell sequencing technologies have improved exponentially in the past decade – moving from approximately 100 cells with multiplexing to 1,000 cells with integrated fluidic circuits and 10,000 cells with nanodroplet capture techniques (Svensson *et al.,* 2018). In addition to increasing in efficiency, sequencing capabilities move beyond just looking at the genome and transcriptome. Nagano *et al.* developed single-cell HiC to determine physical chromatin interactions at single cell resolution while Buenrostro *et al.* (2015) developed an Assay for Transposase Accessible Chromatin using sequencing (ATAC-seq) to map chromatin accessibility. Guo *et al.* developed single-cell reduced representation bisulfite sequencing (scRRBS) that enables single-cell and single-base resolution of DNA methylation. As methods continued to improve, Guo *et al.* developed a single-cell multi-omics sequencing technology (single-cellCOOL-seq) that simultaneously analyzes the chromatin state, DNA methylation, copy number variation, and ploidy in a single cell, combining the different layers epigenomic

information into one sequencing technique. As new single-cell technologies continue to develop, the cost continues to decrease, making this technology more accessible to researchers everywhere (Tang *et al.,* 2019).

1.3.2 The strengths of single-cell sequencing as compared to bulk sequencing methods

Single-cell sequencing has proven to be a powerful tool for delineating complex populations and studying rare cell types. It has contributed to a deeper understanding of complex human diseases such as breast cancer (Nguyen *et al.,* 2018) as well as mammalian organs including lung epithelium (Treutlein *et al.,* 2014), kidney (Brunskill *et al.,* 2014), and brain (Luo *et al.,* 2017; Pollen *et al,* 2014). Because of the high degree of heterogeneity the aforementioned tissues have, traditional sequencing methods are inadequate for capturing their biology. By utilizing single-cell methods, tissues can be more accurately analyzed, leading to the reclassification of different cell types within tissues and the identification of novel cell lineage markers during organ or disease development (Nguyen *et al.,* 2018; Treutlein *et al.,* 2014; Brunskill *et al.,* 2014; Luo *et al.,* 2017; Pollen *et al,* 2014; Wen and Tang, 2018). In addition, single-cell sequencing has been useful in studying rare cell types. Extensive transcriptional regulation and epigenetic reprogramming occurs during early stages of mammalian embryogenesis. However, the genetic and epigenetic regulation of these processes has been difficult to study due to the limited amount of input material and rarity of cell types. Using single-cell RNA-sequencing, Tang *et al.* (2010) overcame this barrier and were able to explore the transcriptional changes that occur in cells during their transition from the inner cell mass (ICM) cells of blastocysts to embryonic stem cells (ESCs) *in vitro*. In another study, Yan *et al.* (2013) identified 22,687 maternally expressed genes, including 8,701 long noncoding RNAs (lncRNAs) in human preimplantation embryos using single-cell RNA-sequencing (scRNA-seq) while Li *et al.* (2018) generated a genome-wide map of DNA methylation and chromatin accessibility in human preimplantation embryos using single-cell chromatin overall omic-scale landscape

sequencing (scCOOL-seq). In both cases, newly developed single cell technologies paved the way for the understanding of how the transcriptome and epigenome mediate embryonic development in preimplantation embryos.

Recently, single-cell sequencing studies in diverse species have comprehensively mapped the developmental trajectories of individual cells. In two zebrafish studies, researchers followed the transcriptional changes that occur as cells differentiated from pluripotent stem cells into more specialized cell types which revealed specific transcriptional trajectories. Wagner *et al.* created a single-cell transcriptional atlas of the zebrafish embryos using inDrops scRNA-seq at multiple time points up to 24 hours postfertilization. Here, they sequenced over 92,000 cells throughout zebrafish development to identify how the transcriptome changes during axis patterning, germ layer formation, and early organogenesis. In a second study, Farrell *et al.* used Drop-seq to generate single-cell transcriptomes for 38,731 cells during early zebrafish embryogenesis from the onset of zygotic transcription through early somitogenesis. Using a computational approach, Farrell *et al.* identified transcriptional trajectories of 25 distinct zebrafish cell types and used differential gene expression analysis to elucidate gene expression cascades that lead to each of these cell types. In a similar study involving *C. elegans*, Packer *et al.* sequenced and profiled the transcriptomes of 86,024 single cells from embryos ranging from gastrulation to terminal cell differentiation. Using the 10X Genomics platform, computational methods, and existing gene expression data, they mapped each single-cell transcriptome to its corresponding position in the well-established *C. elegans* lineage tree and identified the gene expression changes that direct the development of 502 preterminal and terminal cell types.

In addition to helping map cell lineages during embryogenesis, single-cell sequencing has also been useful in identifying and mapping different cell types in developed organisms. Sebe-Pedros, *et al.* performed whole-organism single-cell transcriptomics using massively parallel single-cell RNA-sequencing (MARS-Seq) to map both adult and larval cell types in the cnidarian Nematostella, identifying eight broad cell groups including cnidocytes, gastrodermis,

and neurons. Similarly, two studies in *C. elegans* have comprehensively mapped cell types present in both larvae (Cao *et al*., 2017) and adults (Preston *et al.*, 2019). In Cao *et al.*, single-cell combinatorial indexing RNA sequencing (sci-RNA-seq) was used to profile nearly 50,000 cells from L2 staged larvae. In Preston *et al.*, single-cells dissociated from whole day-one adults were sequenced using the 10X Chromium V1™ platform. Upon comparison of the two populations, wild-type and *daf-2* mutants, researchers identified cell-specific changes in gene expression.

1.3.3 Weaknesses of current single cell / single nucleus RNA-seq methods in *C. elegans*

Currently, single-cell methods have proven to be inefficient at isolating single cells from adult *C. elegans* neuronal and germline tissues and in some cases, end up damaging these sensitive cell types. In one study done by Taylor *et a*l., (2019) they profiled the expression of *C. elegans* neurons but were unable to isolate enough single cells from mature adult worms, which resulted in L4 stage larvae being used instead (Taylor *et al*., 2019). In another study, Preston *et al*. (2019) extracted single nuclei from adult *C. elegans* but failed to isolate amounts of neurons and germline nuclei that were proportional to what is found *in vivo* in the adult *C. elegans*, namely 10% neurons and 66% germline (Preston *et al*., 2019; Hobert O., 2013; Hirsh and Klass, 1976). This inability to recover a similar composition in extracted single cells as compared to populations *in vivo* especially for sensitive cell types indicates that existing single-cell dissociation methods are particularly harmful to neuronal and germline tissues.

Because single-cell methods are ineffective at extracting neurons and germline, many researchers have to forgo comprehensive single-cell data sets in exchange for ones that are specifically enriched for neurons or germline. For example, Han *et al.*, preferentially obtained *C. elegans* adult germline nuclei using a gentle homogenization and filtering method (Han *et al*., 2018; Han *et al*., 2019). In addition, many labs have also enriched their single-cell samples for neurons using fluorescent activated cell sorting (FACS) (Kaletsky *et al.,* 2016; Taylor *et al*.,

2019; Spencer *et al*., 2014). However, the method of FACS sorting itself can damage cells, reduce cell viability, and potentially cause biochemical perturbations (Binek *et al.*, 2019). For example, Preston *et al*. observed that the percent of viable cells decreased significantly after sorting and their final yield of neurons was 3% of all live cells (Preston *et al.,* 2019). Since approximately 10% of *C. elegans* cells are neuronal, this indicates that the combination of single-cell dissociation and FACS sorting significantly damaged neurons and decreased neuronal recovery for sequencing (Hobert, 2013).

Alternatively, researchers can enrich for the number of neuronal cells in their sample by using *C. elegans* mutants that lack a germline, such as the *glp* mutants (Arantes-Oliveira *et al*., 2002; Austin *et al*., 1987). Since approximately two thirds of the adult *C. elegans* nuclei are composed of germline nuclei, germline-less mutants would then have a significantly higher proportion of somatic cells which would in turn enrich for neurons during the extraction (Hirsh and Klass, 1976). However, this would forgo a comprehensive analysis of the adult *C. elegans* as a whole and will counteract the biggest advantage that single-cell methods provide: the advantage of portraying intercellular interactions (Macaulay *et al.,* 2016; Kolodziejczyk *et al*., 2015; Svensson *et al*., 2018). Using mutants that lack a germline also introduces confounding genetic factors that can modulate both the transcriptome and the epigenome since the germline is notorious for regulating pathways in other tissues, the most famous of which is lifespan and fat metabolism in *C. elegans* (Wang *et al.*, 2008; Lin *et al.,* 2001; Greer *et al.*, 2010). In addition, neuronal tissues and germline tissues are capable of an extraordinary amount of crosstalk (Hsin and Kenyon, 1999; Apfeld and Kenyon 1999; Davanapally *et al.,* 2015; Boulias and Horvitz, 2012; Arantes-Oliveira *et al.,* 2013). Therefore, this caveat of using germline-less mutants will result in us missing intercellular interactions as well as possibly introducing confounding genetic factors, further emphasizing the need to develop a single-nucleus extraction protocol that is robust enough to extract single nuclei from adult *C. elegans* but gentle enough to preserve sensitive cell types.

References

Adeola, F. O. (2021). Global Impact of Chemicals and Toxic Substances on Human Health and the Environment. *Handbook of Global Health*, 2227–2256. https://doi.org/10.1007/978-3-030-45009-0_96

Anway, M. D., Cupp, A. S., Uzumcu, N., & Skinner, M. K. (2005). Epigenetic transgenerational actions of endocrine disruptors and male fertility. *Science (New York, N.Y.)*, *308*(5727), 1466–1469. https://doi.org/10.1126/SCIENCE.1108190

Apfeld, J., & Kenyon, C. (1999). Regulation of lifespan by sensory perception in Caenorhabditis elegans. *Nature*, *402*(6763), 804–809. https://doi.org/10.1038/45544

Arantes-Oliveira, N., Apfeld, J., Dillin, A., & Kenyon, C. (2002). Regulation of life-span by germ-line stem cells in Caenorhabditis elegans. *Science (New York, N.Y.)*, *295*(5554), 502–505. https://doi.org/10.1126/SCIENCE.1065768

Arico, J. K., Katz, D. J., van der Vlag, J., & Kelly, W. G. (2011). Epigenetic Patterns Maintained in Early Caenorhabditis elegans Embryos Can Be Established by Gene Activity in the Parental Germ Cells. *PLOS Genetics*, *7*(6), e1001391. https://doi.org/10.1371/JOURNAL.PGEN.1001391

Austin, J., & Kimble, J. (1987). glp-1 is required in the germ line for regulation of the decision between mitosis and meiosis in C. elegans. *Cell*, *51*(4), 589–599. https://doi.org/10.1016/0092-8674(87)90128-0

Binek, A., Rojo, D., Godzien, J., Rupérez, F. J., Nunez, V., Jorge, I., Ricote, M., Vázquez, J., & Barbas, C. (2019). Flow Cytometry Has a Significant Impact on the Cellular Metabolome. *Journal of Proteome Research*, *18*(1), 169–181. https://doi.org/10.1021/ACS.JPROTEOME.8B00472/SUPPL_FILE/PR8B00472_SI_002.XLSX

Boulias, K., & Horvitz, H. R. (2012). The C. elegans microRNA mir-71 acts in neurons to promote germline-mediated longevity through regulation of DAF-16/FOXO. *Cell Metabolism*, *15*(4), 439–450. https://doi.org/10.1016/J.CMET.2012.02.014

Brunskill, E. W., Park, J. S., Chung, E., Chen, F., Magella, B., & Potter, S. S. (2014). Single cell dissection of early kidney development: multilineage priming. *Development (Cambridge, England)*, *141*(15), 3093–3101. https://doi.org/10.1242/DEV.110601

Buenrostro, J. D., Wu, B., Chang, H. Y., & Greenleaf, W. J. (2015). ATAC-seq: A Method for Assaying Chromatin Accessibility Genome-Wide. *Current Protocols in Molecular Biology / Edited by Frederick M. Ausubel ... [et Al.]*, *109*, 21.29.1. https://doi.org/10.1002/0471142727.MB2129S109

Camacho, J., Truong, L., Kurt, Z., Chen, Y. W., Morselli, M., Gutierrez, G., Pellegrini, M., Yang, X., & Allard, P. (2018). The Memory of Environmental Chemical Exposure in C. elegans Is Dependent on the Jumonji Demethylases jmjd-2 and jmjd-3/utx-1. *Cell Reports*, *23*(8), 2392–2404. https://doi.org/10.1016/j.celrep.2018.04.078

Cao, J., Packer, J. S., Ramani, V., Cusanovich, D. A., Huynh, C., Daza, R., Qiu, X., Lee, C., Furlan, S. N., Steemers, F. J., Adey, A., Waterston, R. H., Trapnell, C., & Shendure, J. (2017). Comprehensive single-cell transcriptional profiling of a multicellular organism. *Science*, *357*(6352), 661–667. https://doi.org/10.1126/SCIENCE.AAM8940/SUPPL_FILE/AAM8940_CAO_SM_TABLES_S1_TO_S14.XLSX

Devanapally, S., Ravikumar, S., & Jose, A. M. (2015). Double-stranded RNA made in C. Elegans neurons can enter the germline and cause transgenerational gene silencing. *Proceedings of the National Academy of Sciences of the United States of America*, *112*(7), 2133–2138. https://doi.org/10.1073/PNAS.1423333112

Farrell, J. A., Wang, Y., Riesenfeld, S. J., Shekhar, K., Regev, A., & Schier, A. F. (2018). Single-cell reconstruction of developmental trajectories during zebrafish embryogenesis. *Science*, *360*(6392). https://doi.org/10.1126/SCIENCE.AAR3131/SUPPL_FILE/AAR3131S1.MOV

Furuhashi, H., Takasaki, T., Rechtsteiner, A., Li, T., Kimura, H., Checchi, P. M., Strome, S., & Kelly, W. G. (2010). Trans-generational epigenetic regulation of C. elegans primordial germ cells. *Epigenetics and Chromatin*, *3*(1), 1–21. https://doi.org/10.1186/1756-8935-3-15/FIGURES/10

Gamez-Del-Estal, M. M., Contreras, I., Prieto-Pérez, R., & Ruiz-Rubio, M. (2014). Epigenetic effect of testosterone in the behavior of C. elegans. A clue to explain androgen-dependent autistic traits? *Frontiers in Cellular Neuroscience*, *8*(MAR). https://doi.org/10.3389/FNCEL.2014.00069

Gkountela, S., Zhang, K. X., Shafiq, T. A., Liao, W. W., Hargan-Calvopiña, J., Chen, P. Y., & Clark, A. T. (2015). DNA Demethylation Dynamics in the Human Prenatal Germline. *Cell*, *161*(6), 1425–1436. https://doi.org/10.1016/J.CELL.2015.05.012

Greer, E. L., Maures, T. J., Hauswirth, A. G., Green, E. M., Leeman, D. S., Maro, G. S., Han, S., Banko, M. R., Gozani, O., & Brunet, A. (2010). Members of the H3K4 trimethylation complex regulate lifespan in a germline-dependent manner in C. elegans. *Nature*, *466*(7304), 383–387. https://doi.org/10.1038/NATURE09195

Guo, F., Li, L., Li, J., Wu, X., Hu, B., Zhu, P., Wen, L., & Tang, F. (2017). Single-cell multi-omics sequencing of mouse early embryos and embryonic stem cells. *Cell Research 2017 27:8*, *27*(8), 967–988. https://doi.org/10.1038/cr.2017.82

Guo, H., Zhu, P., Wu, X., Li, X., Wen, L., & Tang, F. (2013). Single-cell methylome landscapes of mouse embryonic stem cells and early embryos analyzed using reduced representation bisulfite sequencing. *Genome Research*, *23*(12), 2126. https://doi.org/10.1101/GR.161679.113

Hackett, J. A., Sengupta, R., Zylicz, J. J., Murakami, K., Lee, C., Down, T. A., & Surani, M. A. (2013). Germline DNA demethylation dynamics and imprint erasure through 5-hydroxymethylcytosine. *Science (New York, N.Y.)*, *339*(6118), 448–452. https://doi.org/10.1126/SCIENCE.1229277

Han, M., Wei, G., McManus, C. E., Hillier, L. W., & Reinke, V. (2019). Isolated C. Elegans germ nuclei exhibit distinct genomic profiles of histone modification and gene expression. *BMC Genomics*, *20*(1), 1–15. https://doi.org/10.1186/S12864-019-5893-9/FIGURES/5

Han, M., Wei, G., McManus, C. E., & Reinke, V. (2018). A simple and effective method to isolate germ nuclei from C. elegans for genomic assays. *BioRxiv*, 371351. https://doi.org/10.1101/371351

Harmston, N., & Lenhard, B. (2013). Chromatin and epigenetic features of long-range gene regulation. *Nucleic Acids Research*, *41*(15), 7185–7199. https://doi.org/10.1093/NAR/GKT499

Heard, E., & Martienssen, R. A. (2014). Transgenerational Epigenetic Inheritance: myths and mechanisms. *Cell*, *157*(1), 95. https://doi.org/10.1016/J.CELL.2014.02.045

Hibshman, J. D., Hung, A., & Baugh, L. R. (2016). Maternal Diet and Insulin-Like Signaling Control Intergenerational Plasticity of Progeny Size and Starvation Resistance. *PLOS Genetics*, *12*(10), e1006396. https://doi.org/10.1371/JOURNAL.PGEN.1006396

Hirsh, D., Oppenheim, D., & Klass, M. (1976). Development of the reproductive system of Caenorhabditis elegans. *Developmental Biology*, *49*(1), 200–219. https://doi.org/10.1016/0012-1606(76)90267-0

Hobert, O. (2013). The neuronal genome of Caenorhabditis elegans. *WormBook : The Online Review of C. Elegans Biology*, 1–106. https://doi.org/10.1895/WORMBOOK.1.161.1

Hobert, O. (2010). Neurogenesis in the nematode Caenorhabditis elegans. *WormBook : The Online Review of C. Elegans Biology*, 1–24. https://doi.org/10.1895/WORMBOOK.1.12.2

Holm, J. B., Mazaud-Guittot, S., Danneskiold-Samsøe, N. B., Chalmey, C., Jensen, B., Nørregård, M. M., Hansen, C. H., Styrishave, B., Svingen, T., Vinggaard, A. M., Koch, H. M., Bowles, J., Koopman, P., Jégou, B., Kristiansen, K., & Kristensen, D. M. (2016). Intrauterine Exposure to Paracetamol and Aniline Impairs Female Reproductive Development by Reducing Follicle Reserves and Fertility. *Toxicological Sciences : An Official Journal of the Society of Toxicology*, *150*(1), 178–189. https://doi.org/10.1093/TOXSCI/KFV332

Hsin, H., & Kenyon, C. (1999). Signals from the reproductive system regulate the lifespan of C. elegans. *Nature*, *399*(6734), 362–366. https://doi.org/10.1038/20694

Hunt, P. A., & Hassold, T. J. (2008). Human female meiosis: what makes a good egg go bad? *Trends in Genetics : TIG*, *24*(2), 86–93. https://doi.org/10.1016/J.TIG.2007.11.010

Kaletsky, R., Lakhina, V., Arey, R., Williams, A., Landis, J., Ashraf, J., & Murphy, C. T. (2016). The C. elegans adult neuronal IIS/FOXO transcriptome reveals adult phenotype regulators. *Nature*, *529*(7584), 92–96. https://doi.org/10.1038/NATURE16483

Kelly, W. G. (2014). Transgenerational epigenetics in the germline cycle of Caenorhabditis elegans. *Epigenetics and Chromatin*, *7*(1), 1–17. https://doi.org/10.1186/1756-8935-7-6/FIGURES/6

Kim, S., Günesdogan, U., Zylicz, J. J., Hackett, J. A., Cougot, D., Bao, S., Lee, C., Dietmann, S., Allen, G. E., Sengupta, R., & Surani, M. A. (2014). PRMT5 Protects Genomic Integrity during Global DNA Demethylation in Primordial Germ Cells and Preimplantation Embryos. *Molecular Cell*, *56*(4), 564. https://doi.org/10.1016/J.MOLCEL.2014.10.003

Kishimoto, S., Uno, M., Okabe, E., Nono, M., & Nishida, E. (2017). Environmental stresses induce transgenerationally inheritable survival advantages via germline-to-soma communication in Caenorhabditis elegans. *Nature Communications*, *8*. https://doi.org/10.1038/NCOMMS14031

Klosin, A., Casas, E., Hidalgo-Carcedo, C., Vavouri, T., & Lehner, B. (2017). Transgenerational transmission of environmental information in C. elegans. *Science (New York, N.Y.)*, *356*(6335), 320–323. https://doi.org/10.1126/SCIENCE.AAH6412

Kolodziejczyk, A. A., Kim, J. K., Svensson, V., Marioni, J. C., & Teichmann, S. A. (2015). The Technology and Biology of Single-Cell RNA Sequencing. *Molecular Cell*, *58*(4), 610–620. https://doi.org/10.1016/J.MOLCEL.2015.04.005

Laubach, Z. M., Perng, W., Dolinoy, D. C., Faulk, C. D., Holekamp, K. E., & Getty, T. (2018). Epigenetics and the maintenance of developmental plasticity: extending the signalling theory framework. *Biological Reviews of the Cambridge Philosophical Society*, *93*(3), 1323–1338. https://doi.org/10.1111/BRV.12396

Li, L., Guo, F., Gao, Y., Ren, Y., Yuan, P., Yan, L., Li, R., Lian, Y., Li, J., Hu, B., Gao, J., Wen, L., Tang, F., & Qiao, J. (2018). Single-cell multi-omics sequencing of human early embryos. *Nature Cell Biology 2018 20:7*, *20*(7), 847–858. https://doi.org/10.1038/s41556-018-0123-2

Lin, K., Hsin, H., Libina, N., & Kenyon, C. (2001). Regulation of the Caenorhabditis elegans longevity protein DAF-16 by insulin/IGF-1 and germline signaling. *Nature Genetics*, *28*(2), 139–145. https://doi.org/10.1038/88850

Liu, S., Brind'Amour, J., Karimi, M. M., Shirane, K., Bogutz, A., Lefebvre, L., Sasaki, H., Shinkai, Y., & Lorincz, M. C. (2014). Setdb1 is required for germline development and silencing of H3K9me3-marked endogenous retroviruses in primordial germ cells. *Genes & Development*, *28*(18), 2041–2055. https://doi.org/10.1101/GAD.244848.114

Luo, C., Keown, C. L., Kurihara, L., Zhou, J., He, Y., Li, J., Castanon, R., Lucero, J., Nery, J. R., Sandoval, J. P., Bui, B., Sejnowski, T. J., Harkins, T. T., Mukamel, E. A., Behrens, M. M., & Ecker, J. R. (2017). Single-cell methylomes identify neuronal subtypes and regulatory elements in mammalian cortex. *Science*, *357*(6351), 600–604. https://doi.org/10.1126/SCIENCE.AAN3351/SUPPL_FILE/AAN3351_LUO_SM.PDF

Macaulay, I. C., Svensson, V., Labalette, C., Ferreira, L., Hamey, F., Voet, T., Teichmann, S. A., & Cvejic, A. (2016). Single-Cell RNA-Sequencing Reveals a Continuous Spectrum of

Differentiation in Hematopoietic Cells. *Cell Reports*, *14*(4), 966–977. https://doi.org/10.1016/J.CELREP.2015.12.082

Messerschmidt, D. M., Knowles, B. B., & Solter, D. (2014). DNA methylation dynamics during epigenetic reprogramming in the germline and preimplantation embryos. *Genes & Development*, *28*(8), 812. https://doi.org/10.1101/GAD.234294.113

Mylchreest, E., Sar, M., Wallace, D. G., & Foster, P. M. D. (2002). Fetal testosterone insufficiency and abnormal proliferation of Leydig cells and gonocytes in rats exposed to di(n-butyl) phthalate. *Reproductive Toxicology (Elmsford, N.Y.)*, *16*(1), 19–28. https://doi.org/10.1016/S0890-6238(01)00201-5

Nagano, T., Lubling, Y., Stevens, T. J., Schoenfelder, S., Yaffe, E., Dean, W., Laue, E. D., Tanay, A., & Fraser, P. (2013). Single cell Hi-C reveals cell-to-cell variability in chromosome structure. *Nature*, *502*(7469), 59–64. https://doi.org/10.1038/NATURE12593

Nguyen, Q. H., Pervolarakis, N., Blake, K., Ma, D., Davis, R. T., James, N., Phung, A. T., Willey, E., Kumar, R., Jabart, E., Driver, I., Rock, J., Goga, A., Khan, S. A., Lawson, D. A., Werb, Z., & Kessenbrock, K. (2018). Profiling human breast epithelial cells using single cell RNA sequencing identifies cell diversity. *Nature Communications 2018 9:1*, *9*(1), 1–12. https://doi.org/10.1038/s41467-018-04334-1

Packer, J. S., Zhu, Q., Huynh, C., Sivaramakrishnan, P., Preston, E., Dueck, H., Stefanik, D., Tan, K., Trapnell, C., Kim, J., Waterston, R. H., & Murray, J. I. (2019). A lineage-resolved molecular atlas of C. Elegans embryogenesis at single-cell resolution. *Science*, *365*(6459). https://doi.org/10.1126/SCIENCE.AAX1971/SUPPL_FILE/AAX1971_TABLES_S7_S8_S10_S11_S14.ZIP

Pollen, A. A., Nowakowski, T. J., Shuga, J., Wang, X., Leyrat, A. A., Lui, J. H., Li, N., Szpankowski, L., Fowler, B., Chen, P., Ramalingam, N., Sun, G., Thu, M., Norris, M., Lebofsky, R., Toppani, D., Kemp, D. W., Wong, M., Clerkson, B., … West, J. A. A. (2014). Low-coverage single-cell mRNA sequencing reveals cellular heterogeneity and activated signaling pathways in developing cerebral cortex. *Nature Biotechnology*, *32*(10), 1053–1058. https://doi.org/10.1038/NBT.2967

Preston, J. L., Stiffler, N., & Weitzman, M. (n.d.). *Organism-wide single-cell transcriptomics of long-lived C. elegans daf-2-/- mutants reveals tissue-specific reprogramming of gene expression networks*. https://doi.org/10.1101/509992

Rechavi, O., Houri-Ze'Evi, L., Anava, S., Goh, W. S. S., Kerk, S. Y., Hannon, G. J., & Hobert, O. (2014). Starvation-induced transgenerational inheritance of small RNAs in C. elegans. *Cell*, *158*(2), 277–287. https://doi.org/10.1016/J.CELL.2014.06.020

Rudgalvyte, M., Peltonen, J., Lakso, M., & Wong, G. (2017). Chronic MeHg exposure modifies the histone H3K4me3 epigenetic landscape in Caenorhabditis elegans. *Comparative Biochemistry and Physiology. Toxicology & Pharmacology : CBP*, *191*, 109–116. https://doi.org/10.1016/J.CBPC.2016.10.001

Schultz, C. L., Wamucho, A., Tsyusko, O. V., Unrine, J. M., Crossley, A., Svendsen, C., & Spurgeon, D. J. (2016). Multigenerational exposure to silver ions and silver nanoparticles

reveals heightened sensitivity and epigenetic memory in Caenorhabditis elegans. *Proceedings. Biological Sciences*, *283*(1832). https://doi.org/10.1098/RSPB.2015.2911

Sebé-Pedrós, A., Saudemont, B., Chomsky, E., Plessier, F., Mailhé, M. P., Renno, J., Loe-Mie, Y., Lifshitz, A., Mukamel, Z., Schmutz, S., Novault, S., Steinmetz, P. R. H., Spitz, F., Tanay, A., & Marlow, H. (2018). Cnidarian Cell Type Diversity and Regulation Revealed by Whole-Organism Single-Cell RNA-Seq. *Cell*, *173*(6), 1520-1534.e20. https://doi.org/10.1016/J.CELL.2018.05.019

Spencer, W. C., McWhirter, R., Miller, T., Strasbourger, P., Thompson, O., Hillier, L. D. W., Waterston, R. H., & Miller, D. M. (2014). Isolation of specific neurons from C. elegans larvae for gene expression profiling. *PloS One*, *9*(11). https://doi.org/10.1371/JOURNAL.PONE.0112102

Strome, S. (2005). Specification of the germ line. *WormBook : The Online Review of C. Elegans Biology*, 1–10. https://doi.org/10.1895/WORMBOOK.1.9.1

Svensson, V., Vento-Tormo, R., & Teichmann, S. A. (2018). Exponential scaling of single-cell RNA-seq in the past decade. *Nature Protocols*, *13*(4), 599–604. https://doi.org/10.1038/NPROT.2017.149

Taki, F. A., Pan, X., Lee, M. H., & Zhang, B. (2014). Nicotine exposure and transgenerational impact: A prospective study on small regulatory microRNAs. *Scientific Reports*, *4*. https://doi.org/10.1038/srep07513

Taki, F. A., Pan, X., Lee, M. H., & Zhang, B. (2014). Nicotine exposure and transgenerational impact: a prospective study on small regulatory microRNAs. *Scientific Reports*, *4*. https://doi.org/10.1038/SREP07513

Taki, F. A., Pan, X., & Zhang, B. (2014). Chronic Nicotine Exposure Systemically Alters MicroRNA Expression Profiles During Post-Embryonic Stages in Caenorhabditis elegans. *Journal of Cellular Physiology*, *229*(1), 79–89. https://doi.org/10.1002/jcp.24419

Tang, F., Barbacioru, C., Bao, S., Lee, C., Nordman, E., Wang, X., Lao, K., & Surani, M. A. (2010). Tracing the derivation of embryonic stem cells from the inner cell mass by single-cell RNA-Seq analysis. *Cell Stem Cell*, *6*(5), 468–478. https://doi.org/10.1016/J.STEM.2010.03.015

Tang, X., Huang, Y., Lei, J., Luo, H., & Zhu, X. (2019). The single-cell sequencing: New developments and medical applications. *Cell and Bioscience*, *9*(1), 1–9. https://doi.org/10.1186/S13578-019-0314-Y/FIGURES/2

Taylor, S. R., Santpere, G., Reilly, M., Glenwinkel, L., Poff, A., McWhirter, R., Xu, C., Weinreb, A., Basavaraju, M., Cook, S. J., Barrett, A., Abrams, A., Vidal, B., Cros, C., Rafi, I., Sestan, N., Hammarlund, M., Hobert, O., & Miller III, D. M. (2019). Expression profiling of the mature C. elegans nervous system by single-cell RNA-Sequencing. *BioRxiv*, 737577. https://doi.org/10.1101/737577

Treutlein, B., Brownfield, D. G., Wu, A. R., Neff, N. F., Mantalas, G. L., Espinoza, F. H., Desai, T. J., Krasnow, M. A., & Quake, S. R. (2014). Reconstructing lineage hierarchies of the

distal lung epithelium using single cell RNA-seq. *Nature*, *509*(7500), 371. https://doi.org/10.1038/NATURE13173

Uzumcu, M., Suzuki, H., & Skinner, M. K. (2004). Effect of the anti-androgenic endocrine disruptor vinclozolin on embryonic testis cord formation and postnatal testis development and function. *Reproductive Toxicology (Elmsford, N.Y.)*, *18*(6), 765–774. https://doi.org/10.1016/J.REPROTOX.2004.05.008

Wagner, D. E., Weinreb, C., Collins, Z. M., Briggs, J. A., Megason, S. G., & Klein, A. M. (2018). Single-cell mapping of gene expression landscapes and lineage in the zebrafish embryo. *Science*, *360*(6392), 981–987. https://doi.org/10.1126/SCIENCE.AAR4362/SUPPL_FILE/AAR4362_WAGNER_SM.PDF

Wang, M. C., O'Rourke, E. J., & Ruvkun, G. (2008). Fat metabolism links germline stem cells and longevity in C. elegans. *Science (New York, N.Y.)*, *322*(5903), 957–960. https://doi.org/10.1126/SCIENCE.1162011

Wang, Z., Gerstein, M., & Snyder, M. (2009). RNA-Seq: a revolutionary tool for transcriptomics. *Nature Reviews. Genetics*, *10*(1), 57. https://doi.org/10.1038/NRG2484

Wen, L., & Tang, F. (2018). Boosting the power of single-cell analysis. *Nature Biotechnology 2018 36:5*, *36*(5), 408–409. https://doi.org/10.1038/nbt.4131

Yan, L., Yang, M., Guo, H., Yang, L., Wu, J., Li, R., Liu, P., Lian, Y., Zheng, X., Yan, J., Huang, J., Li, M., Wu, X., Wen, L., Lao, K., Li, R., Qiao, J., & Tang, F. (2013). Single-cell RNA-Seq profiling of human preimplantation embryos and embryonic stem cells. *Nature Structural & Molecular Biology 2013 20:9*, *20*(9), 1131–1139. https://doi.org/10.1038/nsmb.2660

Yu, C. W., & Liao, V. H. C. (2016). Transgenerational Reproductive Effects of Arsenite Are Associated with H3K4 Dimethylation and SPR-5 Downregulation in Caenorhabditis elegans. *Environmental Science & Technology*, *50*(19), 10673–10681. https://doi.org/10.1021/ACS.EST.6B02173

CHAPTER 2

The memory of environmental chemical exposure in *C. elegans* is dependent on the Jumonji demethylases *jmjd-2* and *jmjd-3/utx-1*

Article

Cell Reports

The Memory of Environmental Chemical Exposure in *C. elegans* Is Dependent on the Jumonji Demethylases *jmjd-2* and *jmjd-3/utx-1*

Graphical Abstract

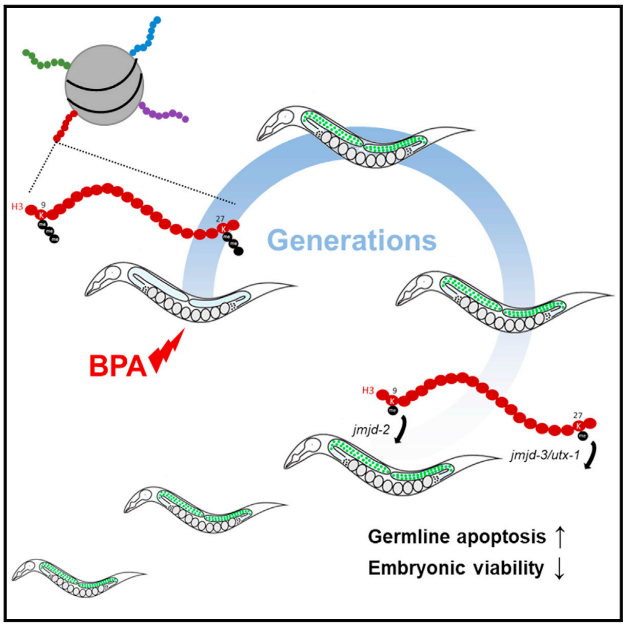

Authors

Jessica Camacho, Lisa Truong, Zeyneb Kurt, ..., Matteo Pellegrini, Xia Yang, Patrick Allard

Correspondence

pallard@ucla.edu

In Brief

Little is known about the mechanisms of inheritance of artificial environmental exposures. Camacho et al. describe the transgenerational reproductive dysfunctions caused by ancestral exposure to the model environmental compound Bisphenol A, and they provide a role for the regulation of repressive histone marks by histone demethylases in this process.

Highlights

- Bisphenol A elicits a 5-generation germline array desilencing effect in *C. elegans*
- The desilencing response tracks with germline apoptosis and embryonic lethality
- Ancestrally exposed F3 germlines show a dramatic reduction in H3K9me3 and H3K27me3
- JMJD-2 and JMD-3/UTX-1 demethylases are required for BPA's transgenerational effects

Data and Software Availability

GSE113187
GSE113266

Camacho et al., 2018, Cell Reports *23*, 2392–2404
May 22, 2018
https://doi.org/10.1016/j.celrep.2018.04.078

CellPress

OPEN ACCESS
CellPress

Cell Reports
Article

The Memory of Environmental Chemical Exposure in *C. elegans* Is Dependent on the Jumonji Demethylases *jmjd-2* and *jmjd-3/utx-1*

Jessica Camacho,[1] Lisa Truong,[2] Zeyneb Kurt,[3] Yen-Wei Chen,[1] Marco Morselli,[4] Gerardo Gutierrez,[1,5] Matteo Pellegrini,[4] Xia Yang,[1,3,6,7,8] and Patrick Allard[1,8,9,10,*]

[1]Molecular Toxicology Interdepartmental Program, University of California, Los Angeles, Los Angeles, CA 90095, USA
[2]Human Genetics and Genomic Analysis Training Program, University of California, Los Angeles, Los Angeles, CA 90095, USA
[3]Department of Integrative Biology and Physiology, University of California, Los Angeles, Los Angeles, CA 90095, USA
[4]Molecular, Cell and Developmental Biology Department, University of California, Los Angeles, Los Angeles, CA 90095, USA
[5]Department of Environmental and Occupational Health, California State University, Northridge, CA 91330, USA
[6]Bioinformatics Interdepartmental Program, University of California, Los Angeles, Los Angeles, CA 90095, USA
[7]Institute for Quantitative and Computational Biosciences, University of California, Los Angeles, Los Angeles, CA 90095, USA
[8]Molecular Biology Institute, University of California, Los Angeles, Los Angeles, CA 90095, USA
[9]Institute for Society and Genetics, University of California, Los Angeles, Los Angeles, CA 90095, USA
[10]Lead Contact
*Correspondence: pallard@ucla.edu
https://doi.org/10.1016/j.celrep.2018.04.078

SUMMARY

How artificial environmental cues are biologically integrated and transgenerationally inherited is still poorly understood. Here, we investigate the mechanisms of inheritance of reproductive outcomes elicited by the model environmental chemical Bisphenol A in *C. elegans*. We show that Bisphenol A (BPA) exposure causes the derepression of an epigenomically silenced transgene in the germline for 5 generations, regardless of ancestral response. Chromatin immunoprecipitation sequencing (ChIP-seq), histone modification quantitation, and immunofluorescence assays revealed that this effect is associated with a reduction of the repressive marks H3K9me3 and H3K27me3 in whole worms and in germline nuclei in the F3, as well as with reproductive dysfunctions, including germline apoptosis and embryonic lethality. Furthermore, targeting of the Jumonji demethylases JMJD-2 and JMJD-3/UTX-1 restores H3K9me3 and H3K27me3 levels, respectively, and it fully alleviates the BPA-induced transgenerational effects. Together, our results demonstrate the central role of repressive histone modifications in the inheritance of reproductive defects elicited by a common environmental chemical exposure.

INTRODUCTION

The elicitation and inheritance of phenotypes from environmental cues have been the subject of intense research and debate. Best understood is the transfer of biological information triggered by natural exposures, such as temperature, hyperosmotic stress, diet, or starvation, thanks to research advances in a variety of model systems from plants to rodents (reviewed in Heard and Martienssen, 2014). Recent reports have shown that the heritability of effects elicited by such natural cues across generations is conditioned by changes in the epigenome, or the molecular tags that alter gene expression and that are mitotically and/or meiotically heritable but do not entail a change in DNA sequence (Wu and Morris, 2001). These mechanisms include small RNA-based pathways (Gapp et al., 2014; Rechavi et al., 2014; Zhong et al., 2013) as well as through the regulation of the complex collection of covalent modifications of histone proteins (Gaydos et al., 2014; Greer et al., 2014; Kishimoto et al., 2017; Klosin et al., 2017; Siklenka et al., 2015). By contrast, the transgenerational inheritance of man-made environmental chemicals has remained controversial, particularly in mammalian settings. Several rodent studies have indicated that a one-generation parental (P)0 exposure to compounds, such as the fungicide Vinclozolin (Anway et al., 2005), or to mixtures of plastic compounds, such as Bisphenol A (BPA) and phthalates (Manikkam et al., 2013), is sufficient to cause a transgenerational decrease in the number and quality of germ cells in F3 and F4 adults, and it correlates with an alteration of DNA methylation patterns (Anway et al., 2005, 2006). However, some of these studies have been challenged (Heard and Martienssen, 2014; Hughes, 2014), have not provided a clear mechanism of inheritance, and have not explored the involvement of other epigenetic marks besides DNA methylation, such as histone modifications.

The nematode *Caenorhabditis elegans* has proven to be a valuable model system to study the effects of environmental exposures on the epigenome due to its ability to respond to a variety of stressors (Kishimoto et al., 2017; Klosin et al., 2017; Rechavi et al., 2014; Rudgalvyte et al., 2017). Here, we exploited the tractability of *C. elegans* to study the transgenerational impact of chemical exposure on reproductive function and dissect its underlying mechanisms of inheritance. These experiments were

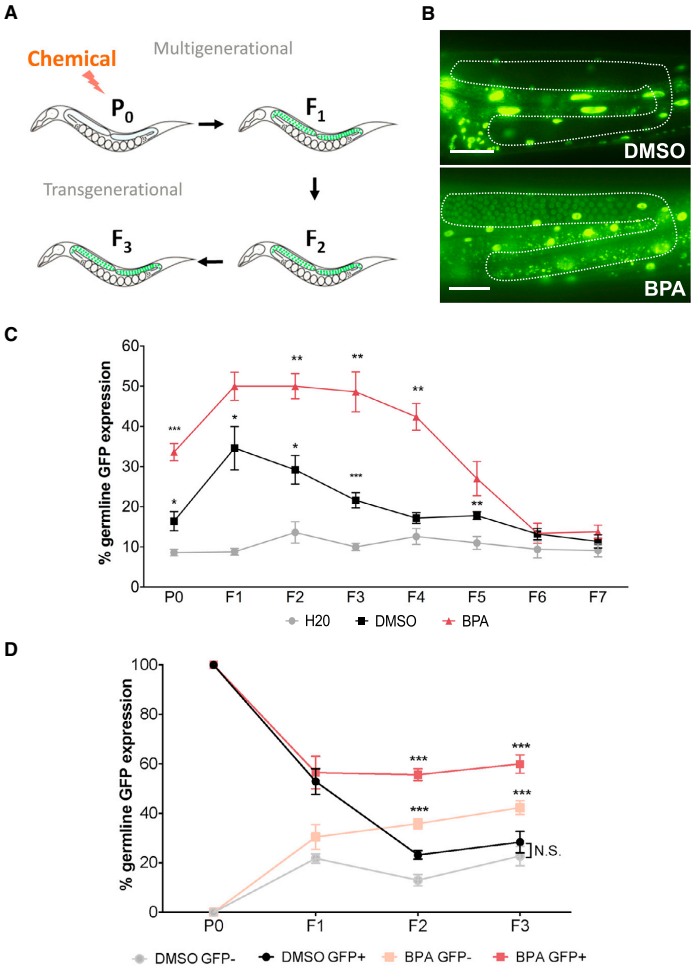

Figure 1. BPA Exposure Elicits a Transgenerational Desilencing of a Repetitive Array

(A) Exposure scheme. Nematodes are exposed to the chemicals of interest for 48 hr at the parental (P0) generation. Worms carrying the integrated array *pkIs1582* [*let-858*::GFP; *rol-6*(*su1006*)] express GFP in all somatic nuclei but silence the array in the germline. This strain is used to monitor the array desilencing over multiple generations.

(B) Representative example of silenced (top) and desilenced (bottom) *pkIs1582* array expression in F3 germlines (dashed lines). Scale bar, 50 μm.

(C) Percentage of worms displaying germline desilencing (y axis) at each generation (x axis). n = 5–10, 30 worms each; *p ≤ 0.05, **p ≤ 0.01, and ***p ≤ 0.001. Significance is indicated for BPA versus DMSO above the BPA line and DMSO versus water above the DMSO line.

(D) Lineage analysis of the germline desilencing response. Worms were sorted following exposure at the P0 generation based on their germline GFP expression. Their progeny was then followed and examined for 3 additional generations. n = 5–10, 30 worms each; ***p ≤ 0.001. BPA is compared to DMSO within each GFP status category (e.g., BPA/GFP+ versus DMSO/GFP+). All data are represented as mean ± SEM.

greatly facilitated by the nematode's short generation time, approximately 4 days at 20°C; its well-characterized distribution and regulation of chromatin marks (Bessler et al., 2010; Ho et al., 2014; Liu et al., 2011); and its ability to silence repetitive transgenes in the germline via repressive histone modifications in a fashion similar to the silencing of repetitive elements in mammalian germ cells (Kelly and Fire, 1998; Liu et al., 2014). Using these features, we investigated the mechanism of transgenerational inheritance following exposure to the model environmental chemical BPA. BPA is a widely used, high-production volume plastic manufacturing chemical highly prevalent in human samples (Vandenberg et al., 2010). We show that ancestral BPA exposure causes a histone 3, lysine 9 (H3K9) and a histone 3, lysine 27 (H3K27) trimethylation-dependent transgenerational chromatin-desilencing response in the germline that spans five generations and is associated with germline dysfunction and elevated progeny lethality.

RESULTS

Germline Transgene Desilencing following Chemical Exposure

To capture single, multi-, and transgenerational environmental effects stemming from chemical exposure, we used a germline desilencing reporter (Kelly et al., 1997). The assay that we developed (Figure 1A) is based on the strain NL2507 carrying an integrated low-complexity, highly repetitive array composed of a transgene coding for a fusion product between nuclear-localized LET-858 and GFP (*pkIs1582[let-858::GFP; rol-6(su1006)]*). This transgene is expressed in somatic cells, but it is transcriptionally silenced in the germline (Figure 1B) via accumulation of the repressive marks H3K9me3 and H3K27me3 (Kelly and Fire, 1998; Schaner and Kelly, 2006).

We first tested the reporter NL2507 strain in a chemical assay by using a variety of well-characterized inhibitors of chromatin-modifying enzymes (Figure S1). All drug exposures were performed at the P0 generation for 48 hr, encompassing the window of L4 stage to day 1 of adulthood. Drug responses were compared to the vehicle DMSO in the context of which a low rate of desilencing is observed (14.3% ± 1.6%). Following treatment with all tested inhibitors of H3K9 or H3K27 demethylases,

of non-selective methyltransferases or demethylases, as well as of histone acetyltransferases, the transgene expression remained silenced at levels comparable to the DMSO control. Conversely, HDAC inhibitors or methyltransferase inhibitors against either H3K9 or H3K27 all led to an increase in *pkIs1582* germline expression, with exposure to the class I HDAC inhibitor sodium butyrate and the SAM and EZH2 inhibitor 3-Deazaneplanocin A (DZnep) showing the highest levels of desilencing at P0, 32.5% ± 3.1% and 38.2% ± 1.9%, respectively ($p \leq 0.0001$ for both). Together, these results indicate that the desilencing of the *pkIs1582* array may serve as a sensitive and relevant indicator of chromatin mark-regulated transcriptional modulation.

BPA Exposure Causes a Heritable, Transgenerational Chromosomal Array-Desilencing Response

BPA was chosen as a test compound in the array-desilencing assay based on several lines of evidence that include changes in H3K27 histone methyltransferase Enhancer of Zeste homolog 2 (EZH2) expression (Bhan et al., 2014) and decreases in H3K9me3 levels in post-natal mouse oocytes (Trapphoff et al., 2013) and in H3K9 and H3K27 methylation levels in a variety of somatic cell types (Doherty et al., 2010; Singh and Li, 2012; Yeo et al., 2013).

First, we tested a range of BPA concentrations (10, 50, 100, and 500 μM), chosen based on previous dose-response analyses (Chen et al., 2016), to identify the lowest dose that led to a maximal desilencing effect. We initially performed the exposures at a single generation (P0) at L4 stage for 48 hr. We observed a dose-response relationship of the germline array desilencing across generations, reaching saturation at 100 μM (45.0% ± 3.3% desilencing at the F3, $p \leq 0.001$) (Figure S2A). We also tested additional 48-hr exposure windows, including from L1 to L4 (Figure S2B) and from day 0 of adulthood (24 hr post-L4) to day 2 (Figure S2C). In all cases, we observed a significant desilencing of the germline array in the F3, although the generational kinetics varied between exposure windows and none reached the maximum F3 desilencing levels achieved by the L4-to-day 1 exposure window (Figure S2A). Thus, for all subsequent experiments, we exposed the worms to a single 100-μM BPA dose from L4 to day 1. This external dose is below previously characterized *C. elegans* doses measured by gas chromatography-mass spectrometry (GC-MS) to lead to an internal BPA concentration within human physiological range (Chen et al., 2016).

We then examined the rate of array desilencing over six generations following the single P0 generation BPA exposure at 100 μM (Figure 1C). The solvent control DMSO led to a pronounced elevation in desilencing in F1 animals (34.6% ± 5.4% of worms display GFP expression in their germline) compared to water alone (8.6% ± 0.8%). However, GFP levels in the DMSO group sharply declined after the F1 generation and were statistically indistinguishable from the water control at the F4 generation. This effect of DMSO is likely due to its described positive activity in DNA relaxation, transcription enhancement, and promotion of an active chromatin state (Iwatani et al., 2006; Juang and Liu, 1987; Kim and Dean, 2004). By contrast, BPA exposure led to a dramatic increase in desilencing in the F1 generation (50.0% ± 3.5%). This BPA-induced desilencing rate was consistently higher than DMSO's and remained that way until the F5 generation. These results therefore indicate a potent transgenerational desilencing response stemming from BPA exposure and spanning 5 generations (P0–F4).

To determine whether most of the desilencing effect observed in the first transgenerational (F3) generation is primarily caused by descendants of strong P0 responders, we performed a series of lineage studies where individual P0 worms were segregated based on their germline GFP expression following BPA or DMSO exposure. Worms that showed germline desilencing at P0 following BPA exposure gave rise to F1, F2, and F3 progenies with a high rate of desilencing, nearing 60% (Figure 1D). By contrast, DMSO-exposed animals, whether silenced or desilenced at P0, showed a reduced rate of desilencing in the F2 and F3 generations, nearing 20%. Surprisingly, BPA-treated but GFP-negative P0 worms gave rise to progeny showing a higher rate of desilencing at each subsequent generation, such that there was a statistically significant difference when compared to DMSO in the F2 and F3 generations. In the latter, the proportion of descendants of BPA-exposed but GFP-negative P0s showing germline desilencing reached 42.3% ± 2.8% ($p \leq 0.01$ versus DMSO/GFP−). Interestingly, the mating of ancestrally exposed F1 hermaphrodites with unexposed males did not rescue the germline desilencing response, indicating that the primary mode of inheritance of BPA's effect is through the female germline (Figure S2D).

Collectively, these findings identify a matrilineal transgenerational inheritance of a repetitive array-desilencing response that is only partially conditioned by the ancestral (P0) response to BPA exposure.

BPA Exposure Causes a Transgenerational Alteration of the Germline Transcriptome

To investigate the impact of ancestral BPA exposure on the germline and distinguish it from that of DMSO, which also led to a mild transgenerational germline desilencing in the F3 compared to water, we performed RNA sequencing (RNA-seq) analysis on isolated F3 germlines. We identified a total of 264 transcripts that were differentially up- or downregulated at $p \leq 0.05$ in F3 germlines ancestrally exposed to BPA compared to DMSO, with 152 transcripts having a fold induction ≤ 0.5 or ≥ 1.5 (Table S1; Figure S3A). There was little overlap between the transcripts that were differentially expressed in all 3 groups, BPA versus DMSO, BPA versus water, and DMSO versus water (Figure S3B), suggesting that DMSO's transgenerational impact on the germline transcriptome is mostly distinct from that of BPA. A gene ontology analysis of the functional categories represented by the differentially expressed transcripts also highlighted the lack of overlap between the different treatment group comparisons. Interestingly, however, the second most represented functional category in the BPA versus DMSO group was reproduction, which was not represented in the DMSO versus water group (Figure S3C). This category includes 61 genes, many of them normally expressed in the germline tissue and essential for germline function (Table S2). These results therefore suggest that ancestral BPA exposure may deregulate reproductive processes by altering the germline transcriptome.

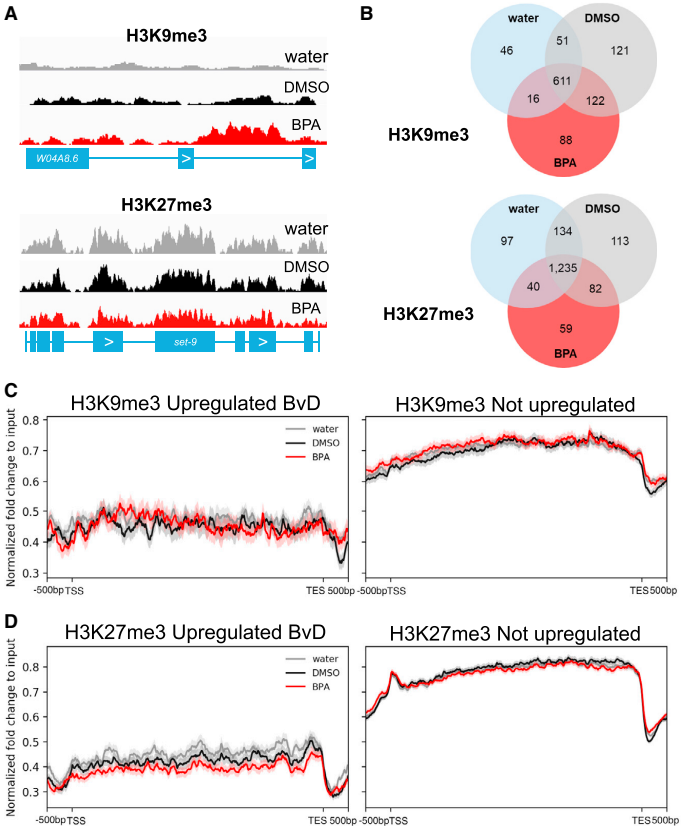

Figure 2. BPA-Induced Transgenerational Reduction in H3K9me3 and H3K27me3 Identified by ChIP-Seq

(A) Examples of ChIP-seq gene plots for H3K9me3 and H3K27me3 from F3 nematodes.

(B) Venn diagram from genes with peak calling in each of the treatment groups.

(C) Average H3K9me3 histone modification fold enrichment signals from gene bodies of either silenced upregulated genes (left panel) or silenced non-upregulated genes (right panel) after BPA treatment. Lightly shaded regions indicate the SE.

(D) Average H3K27me3 histone modification fold enrichment signals from gene bodies of either silenced upregulated genes (left panel) or silenced non-upregulated genes (right panel) after BPA treatment. Lightly shaded regions indicate the SE.

Ancestral BPA Exposure Leads to a Deregulation of Repressive Histone Marks in F3 Nematodes

Several recent reports in *C. elegans* have implicated various histone modifications as important mediators of a variety of environmental effects across generations (Kishimoto et al., 2017; Klosin et al., 2017). We therefore assessed whether BPA exposure in P0 worms could lead to observable changes in the chromatin of F3 worms. To this aim, we performed chromatin immunoprecipitation sequencing (ChIP-seq) in whole adult worms at the F3 generation ancestrally exposed to BPA, DMSO, and water. Just as for the RNA-seq analysis, these experiments were performed on a large population of worms that were not selected based on their GFP expression. We focused our analysis on two repressive marks, H3K9me3 and H3K27me3, which have both been previously implicated in chromatin silencing in the germline of a wide range of species as well as in the repression of low-complexity transgenes in the *C. elegans* germline (Bessler et al., 2010; Greer et al., 2014; Leung et al., 2014; Liu et al., 2014; Schaner and Kelly, 2006; Towbin et al., 2012).

We first mined the ChIP-seq data to identify genes with significantly altered H3K9me3 and H3K27me3 levels (see the Experimental Procedures; Figures 2A and 2B). Among the three conditions, water, DMSO, and BPA, we identified between 3,740 and 4,951 broad peaks for H3K9me3 and between 19,019 and 21,741 for H3K27me3 (Table S3). A total of 1,055 and 1,780 genes were associated with broad peak calls, i.e., showed enrichment in their gene bodies, for H3K9me3 and H3K27me3, respectively. The majority of these peak calls were shared among all three treatment groups, although the BPA treatment group generated 88 and 59 unique peaks for H3K9me3 and H3K27me3, respectively (Figure 2B). The gene ontology (GO) analysis of biological processes at false discovery rate (FDR) < 0.05 and $p < 0.001$ for the genes associated with a loss of H3K27me3 broad peaks in BPA samples compared to DMSO confirmed the relevance of the epigenomic effect detected, as the second most prominent GO category was related to the response to steroid hormone stimulus, in line with BPA's well-described estrogenic activity (Table S4).

Next we compared the ChIP-seq and RNA-seq datasets by examining the levels of H3K9me3 and H3K27me3 under all 3 treatment conditions in genes that either had a low expression level in DMSO (first quartile, i.e., silenced genes) and were not upregulated or were upregulated >2-fold based on the RNA-seq data. As expected, we found that upregulated genes had on average 40%–50% lower H3K9me3 and H3K27me3 compared to their not-upregulated counterparts (Figures 2C and 2D). The levels and distributions of the marks were consistent with their described patterns in the *C. elegans* larval chromatin, where both H3K9me3 and H3K27me3 predominantly occupy the gene body of silenced genes (Ho et al., 2014). Comparing the three treatment groups, we did not observe a difference in H3K9me3 based on expression levels, perhaps due to

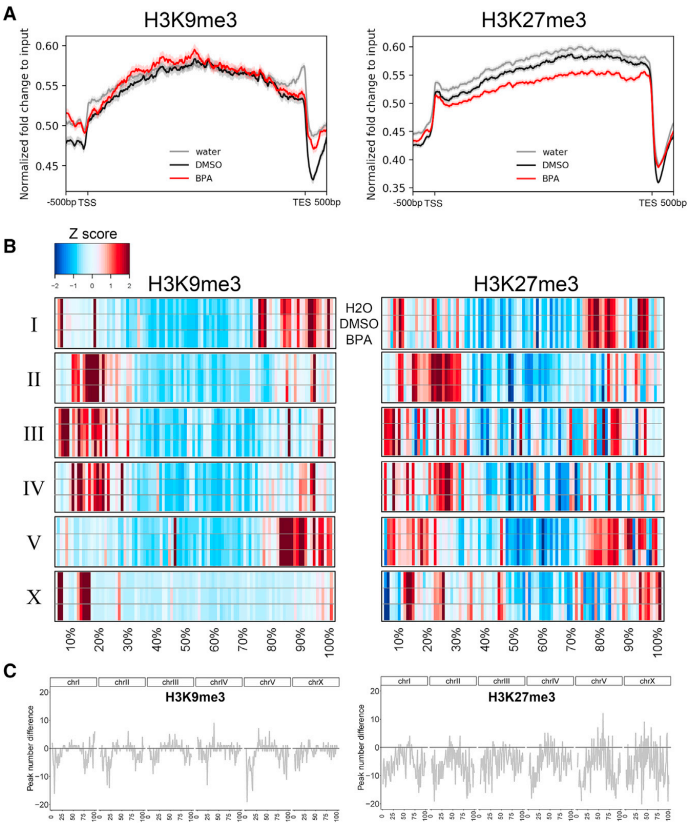

Figure 3. BPA Treatment Causes Transgenerational Intra-chromosomal Redistribution of Histone Modifications

(A) Average H3K9me3 (left) and H3K27me3 (right) histone modification fold enrichment signals from gene bodies of all genes. Shaded regions indicate SE.

(B) Heatmap of averaged H3K9me3 (left) and H3K27me3 (right) histone modification fold enrichment signals in 100 sub-regions across all chromosomes. *Z* scores were calculated on averaged values in each chromosome and sample.

(C) Difference in unique peak-calling numbers between BPA and DMSO from H3K9me3 (left) and H3K27me3 (right) along all chromosome sub-regions. The y axis indicates unique peak numbers calculated by BPA minus DMSO by region.

the tissue sources used for the two datasets (whole worms for ChIP-seq and isolated germlines for RNA-seq). However, we observed a decrease in H3K27me3 in the BPA treatment group compared to DMSO and water for genes that were upregulated (Figure 2D, lightly shaded area indicates SE). These results were similar for all genes, irrespective of expression level, where H3K27me3 was significantly reduced in the gene body compared to DMSO and water groups (Figure 3A).

Finally, we asked whether ancestral BPA exposure might not only affect H3K9me3 and H3K27me3 gene body levels but also their distribution along the chromosome axes. To this aim, we calculated the average fold enrichment of each mark over input by 1% increments along all 6 chromosomes. The data were normalized using a *Z* score for each individual chromosome and treatment group to allow the visualization of the marks' redistribution (Figure 3B). For each 1% increment, we also identified the number of peaks that were present in BPA but absent in DMSO (Figure 3C). These two complementary chromosome-wide analyses revealed a reduction of both marks from the distal chromosomal regions, largely heterochromatic (Garrigues et al., 2015), and a slight enrichment in the chromosome centers when comparing BPA to DMSO (Figures 3B and 3C). It also suggested a decrease of the marks' levels on the X chromosome. We validated the decrease in the levels of the marks by performing a multiplex histone post-translation modification (PTM) quantitation assay on pooled F3 whole-worm extracts (Table S5). The assay revealed a 25%–33% decrease in H3K9 mono-, di-, and trimethylation and a more pronounced 29%–56% decrease in H3K27 di- and trimethylation at the F3 generation in BPA-exposed P0 nematodes compared to DMSO. Conversely, another histone modification, H3K36me3, remained largely unchanged. Together, these results indicate a potent transgenerational impact of BPA on the chromatin, altering both the levels of the two repressive marks H3K9me3 and H3K27me3 as well as their distribution along chromosomal axes.

Ancestral BPA Exposure Leads to a Deregulation of Repressive Histone in the Germline

A transgenerational effect implies that the epigenomic alterations described above must also occur in the germline in order to be inherited. We therefore performed immunofluorescence against H3K9me3 and H3K27me3 in dissected germlines of the NL2507 strain containing the integrated *pkIs1582* transgene at the F3, when desilencing is pronounced, and at the F7, when germline desilencing has returned to control levels. At the pachytene stage of the F3 germline, we observed significant 26% and 24% reductions in global H3K9me3 and H3K27me3 levels, respectively, between BPA and DMSO (Figures 4A and 4B). By contrast, no significant differences were observed between water and DMSO. A similar decrease of total nuclear levels of these marks was seen in the strain PD7271, where the transgene is episomally maintained (*ccEx7271*): 23.3% and 34.6% reductions for H3K9me3 and H3K27me3, respectively (Figure S4). At the F7 generation, the germline levels of H3K9me3 and

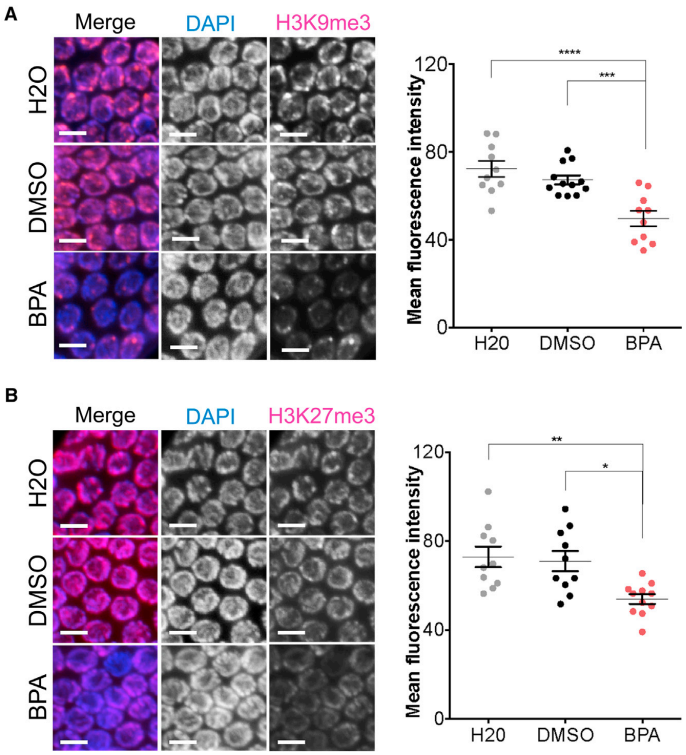

Figure 4. Ancestral BPA Exposure Decreases H3K9me3 and H3K27me3 Levels in F3 Germlines

(A and B) Immunofluorescence images of mid-to-late pachytene germline nuclei from F3 worms ancestrally exposed to DMSO or BPA and stained for H3K9me3 (A) or H3K27me3 (B). DAPI is represented in blue and the histone mark of interest in magenta in the merge. All images shown were selected representative images of the mean values obtained after quantification of all germline nuclei from that exposure group. The corresponding fluorescence intensity quantification is shown on the right panels. n = 11–12 worms, 10 nuclei per worm; *p ≤ 0.05, **p ≤ 0.01, ***p ≤ 0.001, and ****p ≤ 0.0001, one-way ANOVA with Sidak correction. Scale bar, 5 μm. All data are represented as mean ± SEM.

H3K27me3 in the BPA group were statistically indistinguishable from DMSO controls (Figure S5).

The use of the PD7271 *ccEx7271* array-bearing strain also allowed us to separately examine the levels of repressive modifications on the autosomes; the X chromosomes, which tend to lay apart from the rest of the chromosomes during the pachytene stage in hermaphrodites (Schaner and Kelly, 2006); and the extrachromosomal array (Figures 5A and 5B). We observed marked decreases in both H3K9me3 and H3K27me3 on autosomes (24.8% and 34.3%, respectively), X chromosomes (25.3% and 41.5%), and the extrachromosomal array (39.6% and 51.3%). We examined whether the trend toward a larger decrease of these marks on the X chromosomes compared to autosomes was significant by measuring the X:A ratio for each germline nucleus (Figure 5C). F3 germline nuclei showed a significant X:A ratio decrease in H3K27me3 levels when ancestrally exposed to BPA compared to DMSO (0.98 versus 1.09, respectively, a 10% decrease; p = 0.03), while H3K9me3 showed a trend toward a decreased X:A ratio between DMSO and BPA. Consistent with these results and with the described role of H3K27me3 in X silencing in the germline (Bender et al., 2006; Gaydos et al., 2012), we observed a modest but significant (p = 0.01) 2.36% increase in overall X-related genes with fragments per kilobase of transcript per million (FPKM) > 1 in our F3 germline RNA-seq data (Figure 5D).

Taken together, these experiments indicate a broad transgenerational impact on the germline chromatin of F3 nematodes not only confined to the repetitive arrays but also affecting the autosomes and the X chromosomes.

BPA Exposure Elicits a Transgenerational Increase in Embryonic Lethality and Germline Dysfunction

Next, we examined whether the transgenerational alteration of the germline chromatin was associated with reproductive defects. For these and all subsequent experiments, we chose to only compare BPA to DMSO, as BPA is dissolved in DMSO and the RNA-seq and ChIP-seq data indicated chromatin and expression BPA signatures distinct from those of DMSO. While the number of embryos produced was not dependent on ancestral exposure (Figure 6A), we observed a significant 85% (D = 3.83 and B = 7.07) increase in embryonic lethality in F3 worms ancestrally exposed to BPA when compared to DMSO (Figure 6B). We also examined the rate of embryonic lethality at the F7, a generation at which desilencing is not observed. Surprisingly, a trend between DMSO and BPA was still apparent even if it did not reach significance (86%, D = 3.58 and B = 6.67) (Figure 6B). The F3 embryonic lethality defect was not caused by the spurious expression of the *pkIs1582* transgene in the germline, as it was also observed in wild-type (N2) worms (Figure S6). Additionally, we assessed whether the increased embryonic lethality correlated with the transgene desilencing by separately assessing the embryonic survival of GFP-negative and GFP-positive F3 worms' progeny (Figure 6C). We observed a significantly higher level of embryonic lethality in the offspring of GFP-positive F3 worms ancestrally exposed to BPA when compared to both GFP-negative/BPA F3 offspring and GFP-positive/DMSO F3 offspring.

Finally, we monitored germline health by measuring the induction of germline apoptosis using acridine orange staining

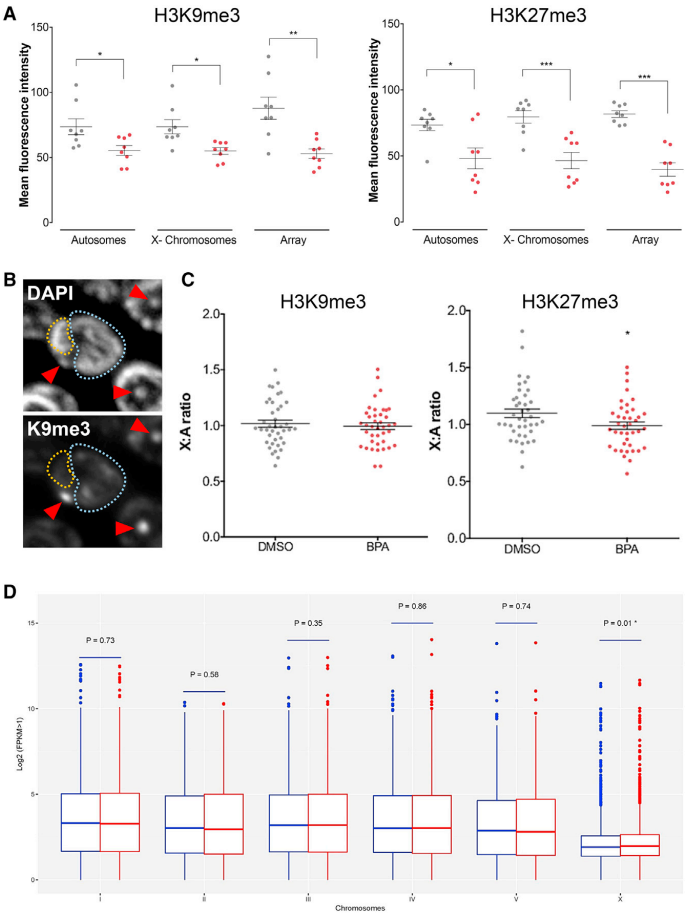

Figure 5. Ancestral BPA Exposure Leads to a Sharp Decrease in H3K9me3 and H3K27me3 on Autosomes, X Chromosomes, and an Extrachromosomal Array and an Up-regulation of X-Linked Genes

(A) Quantification of H3K9me3 and H3K27me3 levels on autosomes, X chromosomes, and an extrachromosomal array in the F3 generation following P0 exposure to either DMSO or BPA. Gray, DMSO; red, BPA. n = 8 worms, 5 nuclei per worm; *p $\leq$ 0.05, **p $\leq$ 0.01, and ***p $\leq$ 0.001.

(B) DAPI- (top) and H3K9me3- (bottom) stained nuclei. The colored dashed lines identify the autosomes (blue) and the X chromosomes (orange). The red arrowheads identify the extrachromosomal array that is enriched in H3K9me3.

(C) Fluorescence intensity quantification of H3K9me3 and H3K27me3 levels is shown on the right. Gray is the X:A ratio for DMSO and red for BPA. n = 8 worms, 5 nuclei per worm; *p $\leq$ 0.05.

(D) Gene expression data from dissected F3 germlines showing all transcripts with FKPM > 1 following ancestral DMSO (blue) or BPA (red) exposure. X-linked genes show a modest but significant overall 2.36% increase in expression (p = 0.01). All data are represented as mean ± SEM.

(Gartner et al., 2008) at the late prophase stage, when synapsis and recombination-dependent checkpoint activation results in programmed germline nuclear culling (Bhalla and Dernburg, 2005; Gartner et al., 2008). We observed a significant increase in germline apoptosis in F3 worms ancestrally exposed to BPA when compared to DMSO (Figures 6D and 6E), which was lost at the F7. Thus, together, these results show that ancestral BPA exposure elicits a clear transgenerational reproductive dysfunction effect. They also indicate that BPA-induced transgenerational effects mostly resolve by the F7.

Jumonji Histone Demethylase Activity Is Required for the Inheritance of BPA-Induced Transgenerational Effects

Since BPA exposure at the P0 generation was correlated with a decrease in repressive histone modifications in the germline of the F3 worms, we hypothesized that BPA's effects may be dependent on levels of these marks and on the activity of the enzymes that regulate them. This hypothesis was partially supported by the RNA-seq data from which 7 differentially expressed chromatin factors were identified: *sir-2.4*, ZK1127.3, *sop-2*, TO7E3.3, *met-2*, *jmjd-1.2*, and *set-26* (Table S1). MET-2, a SET domain histone H3 lysine 9 histone methyltransferase (HMTase) (Bessler et al., 2010), was significantly downregulated, while *set-26*, another H3K9 methyltransferase (Greer et al., 2014), was represented by two functionally equivalent transcript isoforms, one upregulated and one downregulated. Therefore, to functionally implicate the dysregulation of H3K9me3 and H3K27me3 in BPA's transgenerational outcomes, we attempted to rescue its effects by genetically or chemically modulating several histone demethylases after the initial P0 exposure but prior to the F3 (Figures 7A and S8A).

We first assessed whether the deregulation of repressive H3-lysine methylation marks by BPA is required for the transgenerational inheritance of BPA-induced effects. To this end, we used a feeding RNAi strategy to downregulate the expression of *jmjd-2* (H3K9me3/H3K36me3 histone lysine demethylase [KDM]) (Greer et al., 2014; Whetstine et al., 2006) or *jmjd-3/utx-1* (H3K27me3 KDM) (Agger et al., 2007), and we monitored two hallmarks of BPA's transgenerational effects, namely, the germline array desilencing as well as the increase in embryonic lethality. When compared to control RNAi, the downregulation of *jmjd-2* or *jmjd-3/utx-1* at the F1-to-F2 transition was sufficient to increase the levels of H3K9me3 and H3K27me3, respectively,

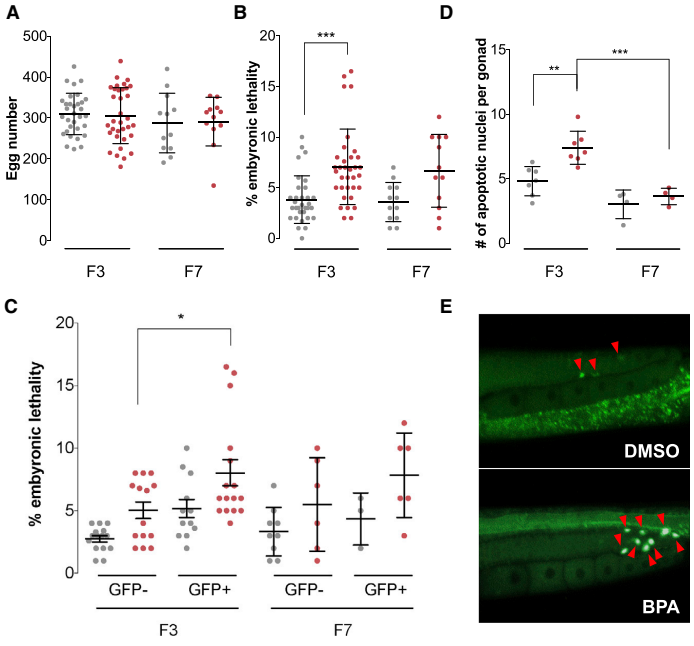

Figure 6. Transgenerational Impact of BPA on Fertility

(A) Number of eggs produced by F3 or F7 worms following P0 exposure to DMSO control (gray) or BPA (red).

(B) Percentage of lethality of embryos generated by F3 or F7 worms ancestrally exposed to either DMSO control or BPA. n = 23–33; ***p ≤ 0.001, two-way ANOVA.

(C) Embryonic lethality of F3 or F7 worms' progeny based on the GFP expression in the germline of F3 or F7 worms. n = 10; *p ≤ 0.05, two-way ANOVA.

(D) Number of apoptotic nuclei per gonadal arms of F3 or F7 worms. n = 7 repeats, 20 worms each; **p ≤ 0.01 and ***p ≤ 0.001, two-way ANOVA.

(E) Representative examples of acridine orange-stained F3 nematodes following P0 DMSO or BPA exposure. All data are represented as mean ± SEM.

in the F3 germlines (Figure 7B; quantification shown in Figure S7A). Also, while the control RNAi conditions slightly elevated the rates of desilencing and embryonic lethality compared to no-RNAi conditions, the downregulation of either *jmjd-2* or *jmjd-3/utx-1* led to a complete rescue of BPA-induced responses in the F3, except for the embryonic lethality effect under *jmjd-2* RNAi conditions, which was strongly reduced but did not reach significance (Figure 7C). Interestingly, single RNAi against *jmjd-3* or *utx-1* dramatically increased the proportion of desilenced germlines under both ancestral DMSO and BPA exposures, suggesting a partial compensation between *jmjd-3* and *utx-1* in the *C. elegans* germline (Figure S7B). This increase is similar to that of RNAi against the H3K27 HMT Polycomb Group complex member *mes-6* or against the SET domain H3K36 HMT *mes-4*, which functions to limit H3K27me3 spreading away from silenced chromatin (Figure S7B) (Gaydos et al., 2012).

We further implicated the deregulation of H3K9me3 and H3K27me3 as central to BPA's transgenerational effects by performing drug rescue experiments using the KDM4/JMJD-2 inhibitor IOX-1 (King et al., 2010), which has been shown to elevate H3K9me3 levels *in vitro* and in cell culture settings, (Hu et al., 2016; King et al., 2010; Schiller et al., 2014), and the potent selective Jumonji JMJD-3/UTX-1 H3K27 demethylase inhibitor GSK-J4 (Kruidenier et al., 2012). We first examined whether a combination of the two histone demethylase inhibitors would be sufficient to decrease the germline array desilencing and embryonic lethality effects. The co-treatment of the F1 generation with 100 μM IOX-1 and 100 μM GSK-J4 led to a significant reduction in BPA-induced array desilencing and embryonic lethality by 15.8% and 27.0%, respectively (Figure S8B). Finally, we tested the effect of the two inhibitors independently. Remarkably, F1 exposure to either IOX-1 or GSK-J4 was sufficient to suppress the elevation in array desilencing and embryonic lethality in P0 BPA-exposed worms compared to DMSO (Figure S8C). Thus, two distinct means of rescuing BPA's transgenerational effects, by RNAi or chemical inhibitors, indicate that the activity of either JMJD-2 or JMD-3/UTX-1 is required for the inheritance of BPA-induced reproductive effects.

DISCUSSION

In the present study, we aimed to characterize the molecular mechanisms of memory of environmental exposures using BPA as a model chemical. We showed that ancestral BPA exposure leads to a transgenerational decrease in the germline levels of H3K9me3 and H3K27me3 dependent on the activity of the JMJD-2 and JMJD-3/UTX-1 demethylases. Interestingly, our results indicate that, while the overt germline desilencing effect lasts only up to 5 generations, some modest impacts on reproduction extend at least until the F7 generation. These results therefore suggest that the transgenerational impact of BPA may differ depending on the type of genetic loci examined, with repetitive loci, such as the transgene, being less affected than other loci controlling *C. elegans* reproductive function.

We found that modulation of either JMJD-2 or JMJD-3/UTX-1 activity, chemically or genetically, is sufficient to dramatically reduce the inheritance of transgenerational effects. While JMJD-2 acts as both an H3K9me3 and H3K36me3 demethylase, the ability of *jmjd-2* RNAi to rescue desilencing's effects is likely caused by its action on H3K9me3, as H3K36me3 is considered an active mark in the *C. elegans* germline (Gaydos

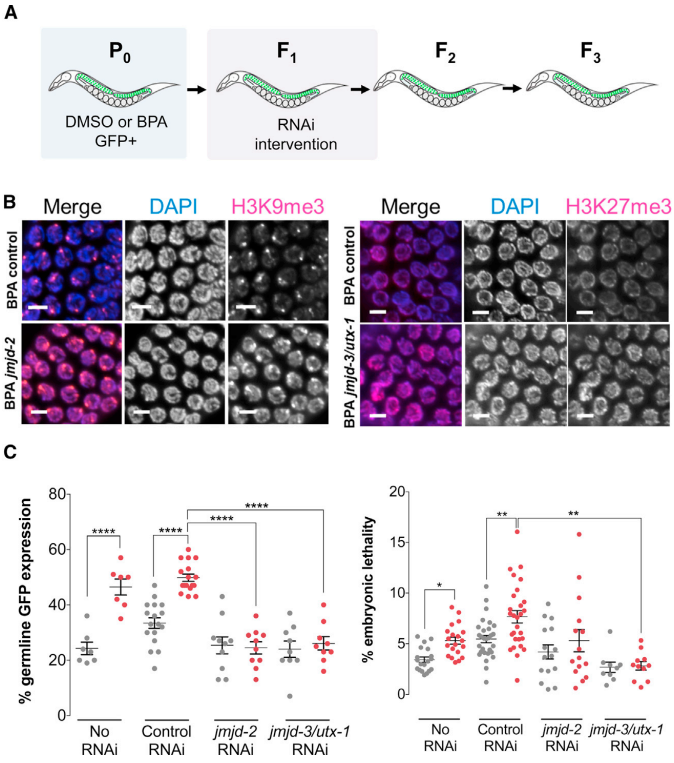

Figure 7. *jmjd-2* and *jmjd-3/utx-1* Demethylases Are Required for BPA-Induced Transgenerational Response

(A) Exposure and rescue experimental scheme. Following exposure to DMSO or BPA at the P0 generation, the progeny of GFP-positive P0 worms was collected and subjected to feeding RNAi until the F2. F3 worms were then collected and analyzed.

(B) Immunofluorescence images of mid-to-late pachytene germline nuclei from F3 worms ancestrally exposed to BPA and GFP-positive at the P0, stained for H3K9me3 or H3K27me3. DAPI is represented in blue and the histone mark of interest in magenta in the merge. All images shown were selected representative images of the mean values obtained after quantification of all germline nuclei from that exposure group (Figure S7A). Scale bar, 5 μm.

(C) RNAi rescue of ancestral DMSO- (gray) or BPA- (red) induced effects following either no F1 treatment, empty vector control, *jmjd-2*, or *jmjd-3/utx-1* feeding RNAi. n = 7–17 repeats, 30 worms each for desilencing assay and n = 4–8 repeats, 3–4 worms each for the embryonic lethality assay; $^{*}p \leq 0.05$, $^{**}p \leq 0.01$, and $^{****}p \leq 0.0001$, two-way ANOVA. All data are represented as mean ± SEM.

et al., 2012) and RNAi against *jmjd-2* increases its levels (Whetstine et al., 2006), which is inconsistent with the observed decrease in BPA-induced desilencing in *jmjd-2* RNAi F3 animals. Our results thus suggest a cooperation between H3K9me3 and H3K27me3 for proper chromatin silencing in the *C. elegans* germline. Such cooperation is understood in mammalian embryonic stem cells (ESCs) to emerge from the interaction between Jarid2/Jumonji and Polycomb Repressive Complex 2 (PRC2) (Pasini et al., 2010; Peng et al., 2009) and to be important for heterochromatin formation and/or maintenance through PRC2's effect on increasing the binding efficiency of HP1 to H3K9me3 (Boros et al., 2014). In *C. elegans*' embryonic or larval chromatin, there is a strong overlap between H3K27me3 and H3K9me3 at genome-wide levels (Garrigues et al., 2015; Ho et al., 2014). This overlap is particularly significant at chromosomal arms of heterochromatic nature as well as lamina-associated domains (Ho et al., 2014), something also observed in our data (Figure 3B). In the *C. elegans* meiotic germline, the overlap between H3K27me3 and H3K9me3 chromosomal distribution is likely to be high, as H3K27me3 distribution is greater than that of H3K9me3 (Bender et al., 2004; Bessler et al., 2010; Schaner and Kelly, 2006).

Our results are consistent with previous observations in mouse germ cells, where exposure of growing oocytes to low BPA concentrations decreased H3K9me3 levels (Trapphoff et al., 2013). However, the effect of BPA may also be context dependent, as an increase in EZH2 expression and, consequently, an elevation of H3K27me3 was detected in mammary tissues following BPA exposure (Doherty et al., 2010). Our work suggests that, at least in *C. elegans*, the tight regulation of H3K9 and H3K27 methylation is central to the epigenetic memory of ancestral exposures. It will be crucial to examine how histone-based epimutations may be inherited across generations in mammalian models, since the mammalian epigenome undergoes two distinct waves of reprogramming, once in the primordial germ cells (PGCs) and a second time after fertilization in the pre-implantation embryo (reviewed in Tang et al., 2016). During the first reprogramming in PGCs, there is a wide fluctuation in H3K9me2 level, which becomes depleted (Seki et al., 2005), and in H3K27me3 level, which is gradually enriched globally (Hajkova et al., 2008). However, H3K9me3 is maintained in a dotted pattern in the pericentric heterochromatic regions as well as on endogenous retroviruses (Liu et al., 2014; Seki et al., 2005). Thus, H3K9me3 could serve in mammals as a molecular mediator of exposure memory in the germline.

The centrality of H3K9me3 in the inheritance of natural environmental effects has recently been further highlighted in *C. elegans*, where temperature-mediated alteration of transgene expression was detected for up to 14 generations (Klosin et al., 2017). However, other environmental cues, such as starvation or hyperosmosis, have been shown, depending on the studies,

to require small RNA-based mechanisms and/or H3K4 trimethylase activity (Kishimoto et al., 2017; Rechavi et al., 2014). While these pathways may be mechanistically related, it will be necessary to examine whether a unifying mechanism of environmental inheritance can be identified, especially as we also identified a requirement for the regulation of H3K27 methylation for the transgenerational inheritance of BPA's exposure. Finally, our findings on the transgenerational memory of exposure to the model toxicant BPA and its impact on the germline's epigenome and reproduction also raise important questions for human risk from exposure, as our work identified transgenerational reproductive effects even in the absence of such a response in the earlier generations and at BPA concentrations lower than those previously characterized and that yielded internal concentrations close to those found in human reproductive tissues (Chen et al., 2016; Schönfelder et al., 2002; Vandenberg et al., 2010).

In conclusion, we have uncovered a transgenerational effect on reproduction stemming from exposure to the environmental chemical BPA and mediated in part by a deregulation of repressive histone modifications. These findings, therefore, highlight the need to comprehensively examine the effect of our chemical environment on the unique context of the germline epigenome, and they also offer interventional means to prevent the transmission of such effects across generations.

EXPERIMENTAL PROCEDURES

Culture Conditions and Strains

Standard methods of culturing and handling of *C. elegans* were followed (Stiernagle, 2006). Worms were maintained on nematode growth medium (NGM) plates streaked with OP50 *E. coli*, and all experiments were performed at 20°C (at 25°C, a pronounced desilencing of pkIs1582 is observed in the germline). Strains used in this study were obtained from the *C. elegans* Genetics Center (CGC) and include the following: NL2507 (*pkIs1582[let-858*::GFP; *rol-6*(*su1006*)]), PD7271 (*pha-1(e2123)* III; *ccEx7271*), and N2 (wild-type).

Chemical Exposure and GFP Scoring

The exposure and GFP germline desilencing assessments were performed as previously described (Lundby et al., 2016). Briefly, all chemicals tested were obtained from Sigma-Aldrich and were dissolved in DMSO to a stock concentration of 100 mM. Worms were synchronized by bleaching an adult population of the strain of interest, plating the eggs, and allowing the synchronized population to reach L4 larval stage (approximately 50 hr). These were then collected and incubated for 48 hr in 50 μL OP50 bacteria, 500 μL M9, and 0.5 μL of the chemical of interest for a final chemical concentration of 100 μM. After 48 hr, the worms were collected and allowed to recover on NGM plates for 1–2 hr (mixed population) or immediately plated as individual worms to separately labeled 35-mm seeded NGM plates (GFP+/− population sorting) and recovered there. Worms were scored for germline GFP expression using a Nikon H600L microscope at 40× magnification.

Apoptosis Assay and Embryonic Lethality Assessment

Apoptosis assay was performed by acridine orange staining on synchronized adult hermaphrodites collected at 20–24 hr post-L4, as previously described (Allard and Colaiácovo, 2011; Chen et al., 2016). Embryonic lethality was performed by monitoring the numbers of embryos produced by each worm of each day of its reproductive life and subsequent larvae hatched from these embryos. The ratio of the latter measure by the former and multiplied by 100 generates the rate of embryonic lethality.

Chemical Rescue

F1 L4 larvae were obtained from DMSO- or BPA-exposed GFP-positive P0 worm populations, and they were exposed for 48 hr to the chemical rescue drugs IOX-1 and GSK-J4 dissolved in DMSO to a stock concentration of 100 mM. In combination treatments, one drug was prepared at a higher concentration so that the final DMSO concentration never exceeded 0.11%. The exposed F1 adult worms were then allowed to recover on NGM plates, and their offspring were followed until the F3 generation for GFP scoring and embryonic lethality assessment.

RNAi Experiments

Worms were exposed to RNAi by feeding (Kamath and Ahringer, 2003) with *E. coli* strains containing either an empty control vector (L4440) or expressing double-stranded RNA. RNAi constructs against *jmjd-2*, *jmjd-3*, *utx-1*, *mes-4*, and *mes-6* were obtained from the Ahringer RNAi library and sequence verified. P0 worms were exposed to BPA or DMSO for 48 hr following the procedure described above. For *jmjd-2* and *jmjd-3*/*utx-1* RNAi, F1 adult worms from GFP-positive P0 worms were placed on plates of *E. coli* containing an empty control vector (L4440) or expressing double-stranded RNA to lay overnight. F2 worms were grown on RNAi bacteria from hatching until the first day of adulthood, at which point they were transferred to non-RNAi OP50 plates. The subsequent generation (F3) was collected at adulthood (24 hr post-L4) for further analysis. For *mes-4* and *mes-6* RNAi, the same procedure was followed but from the F2 to F3 generation to circumvent their associated maternal sterility phenotype.

Immunofluorescence

Immunofluorescence images were collected at 0.5-μm z intervals with an Eclipse Ni-E microscope (Nikon) and a cooled charge-coupled device (CCD) camera (model CoolSNAP HQ, Photometrics) controlled by the NIS Elements AR system (Nikon). The images presented and quantified are projections approximately halfway through 3D data stacks of *C. elegans* gonads, which encompass entire nuclei. Images were subjected to 3D landweber deconvolution analysis (5 iterations) with the NIS Elements AR analysis program (Nikon). H3K27me3 and H3K9me3 quantification in mid-late pachytene germ cell nuclei was performed with the ImageJ software. F3 worms were staged at L4, and gonad dissection and immunofluorescence were performed 20–24 hr post-L4, as previously described (Chen et al., 2016). Primary antibodies were used at the following dilutions: rabbit α-H3K9me3, 1:500 (Abcam); and mouse α-H3K27me2me3, 1:200 (Active Motif). Secondary antibodies were used at the following dilutions: Cy3 α-rabbit, 1:700; and TxRed α-mouse, 1:200, (Jackson ImmunoResearch).

Germline RNA Amplification and RNA-Seq Analysis

Total RNA was extracted from needle-dissected gonads of F3 adult worms obtained from a mixed population of H_2O-, DMSO-, and BPA-exposed P0 nematodes. The experiments were performed on 4 biological replicates of 30 gonads each that were processed through the NucleoSpin RNA XS, Macherey Nagel kit. cDNA was synthesized using the SMART-Seq v4 Ultra Low Input RNA Kit for sequencing, amplified 10×, and purified using agentcourt AMPure beads.

Nextera XT Library Prep Kit was used to prepare the sequencing libraries from 1 ng cDNA. Single-end sequencing at 50-bp length was performed on an Illumina Hiseq 4000 system (Illumina, CA, USA), and a total of ~350 million reads was obtained for 12 samples (3 treatment groups × 4 replicates/group). Data quality checks were performed using the FastQC tool (http://www.bioinformatics.babraham.ac.uk/projects/fastqc). RNA-seq reads passing quality control (QC) were analyzed using a pipeline comprised of HISAT (Kim et al., 2015), StringTie (Pertea et al., 2015), and Ballgown (Frazee et al., 2015) tools. HISAT was used to align reads against the *C. elegans* genome to discover the locations from which the reads originated and to determine the transcript splice sites. Then, StringTie was used to assemble the RNA-seq alignments into potential transcripts. Ballgown was used to identify the transcripts and genes that were differentially expressed between the BPA and DMSO groups, between the BPA and control (water) groups, and between the DMSO and control groups. FPKMs for each transcript were obtained by Ballgown and used as the expression measure. We filtered out the low-abundance transcripts and kept those having a mean FPKM > 1 across all samples. To test the transcriptional impact of BPA on individual chromosomes, we applied a Student's t test to determine whether the differences in the mean

log2(FPKM + 1) values between the BPA and DMSO groups were significant for all transcripts with FPKM > 1 on each chromosome. $p \leq 0.05$ was considered significant.

ChIP-Seq and Multiplex PTM Assay

Histone modification H3K9me3 and H3K27me3 ChIP-seq data were generated as a service by Active Motif using their in-house antibodies from 3 biological repeats of frozen F3 nematode populations, with 200 μL worms per sample repeat. The sequencing data were obtained through Illumina Nextseq and mapped to ce10 genome by Burrows-Wheeler Aligner (BWA) algorithm (Li and Durbin, 2009). Following pooling of the sequencing data per exposure category (Yang et al., 2014), the data were normalized to input and million reads to produce a signal track file by MACS2 (Zhang et al., 2008). For chromosome-wide mark distribution analysis, each chromosome was divided into 100 sub-regions and average fold enrichment score per base in sub-regions. We normalized signals with *Z* score for each chromosome and each sample.

For gene body histone modification analysis, deepTools (Ramírez et al., 2014) was utilized to obtain aggregated signal from −500 bp of the upstream transcription start site (TSS) to +500 bp of the downstream transcription end site (TES). We first summarized genes with multiple transcripts into a single gene by the one with the most significant difference from BPA and DMSO from RNA-seq results. Silenced genes were defined as genes expressed in the lowest 25% (Q1, 1,801 genes) of all genes in the DMSO group, and upregulated genes were defined as silenced genes upregulated more than 2-fold after BPA treatment (244 genes) based on RNA-seq results. We called peaks by MACS2 broad peak function with q value = 0.1 (cutoff). Broad peak is used as a peak-calling category when analyzing data for protein-DNA association with broader DNA coverage, such as for H3K9me3 and H3K27me3. It joins nearby narrower peak calling into one broader peak. To compare differential peak, unique peak method was used to compare BPA and DMSO samples (Steinhauser et al., 2016). Non-overlapping broad peaks called by MACS2 were defined as unique peaks. Unique peaks from BPA and DMSO in 100 sub-regions along each chromosome were compared. We further define peaked genes as genes with any peak calling in gene body region. Unless specified, analyses were conducted by R 3.4.0 (R Core Team, 2017) and Bioconductor (Huber et al., 2015).

The multiplex PTM quantitation assay was also generated as service by Active Motif on a Luminex platform, and it was performed on pooled samples (totaling 100 μL) generated from 3–4 individual repeats per exposure condition.

Statistical Analyses

Unless indicated otherwise, an unpaired t test assuming unequal variance with Welch's correction was applied. For multi-group comparisons, a one-way ANOVA with Sidak correction or two-way ANOVA was used.

DATA AND SOFTWARE AVAILABILITY

The accession numbers for the ChIP-seq and RNA-seq data reported in this paper are GEO: GSE113187 and GSE113266.

SUPPLEMENTAL INFORMATION

Supplemental Information includes eight figures and five tables and can be found with this article online at https://doi.org/10.1016/j.celrep.2018.04.078.

ACKNOWLEDGMENTS

P.A. is supported by NIH/NIEHS R01 ES02748701 and the Burroughs Wellcome Foundation. J.C. received support from NIH/NIEHS T32 ES015457 Training in Molecular Toxicology, the North American Graduate Fellowship, the NSF AGEP Competitive Edge, the NSF Graduate Research Fellowship, and the Eugene-Cota Robles Fellowship. L.T. is supported by the NIH Training Grant in Genomic Analysis and Interpretation T32 HG002536. G.G. is supported by NIH/NIEHS R25 ES02550703. Z.K. was supported by an American Heart Association post-doctoral fellowship (17POST33670739) and the Iris Cantor-UCLA Executive Advisory Board/CTSI Pilot Award. M.M. was supported by a Dissertation Year Fellowship (University of California, Los Angeles). X.Y. is supported by NIH/NIDDK R01 DK104363 and NIH/NINDS R21 NS103088.

AUTHOR CONTRIBUTIONS

J.C., L.T., M.M., and G.G. performed the experiments. J.C., L.T., Z.K., Y.-W.C., M.P., X.Y., and P.A. analyzed and interpreted the results. J.C., L.T., Z.K., Y.-W.C., X.Y., and P.A. wrote the manuscript.

DECLARATION OF INTERESTS

The authors declare no competing interests.

Received: September 7, 2017
Revised: March 15, 2018
Accepted: April 17, 2018
Published: May 22, 2018

REFERENCES

Agger, K., Cloos, P.A., Christensen, J., Pasini, D., Rose, S., Rappsilber, J., Issaeva, I., Canaani, E., Salcini, A.E., and Helin, K. (2007). UTX and JMJD3 are histone H3K27 demethylases involved in HOX gene regulation and development. Nature *449*, 731–734.

Allard, P., and Colaiácovo, M.P. (2011). Mechanistic insights into the action of Bisphenol A on the germline using C. elegans. Cell Cycle *10*, 183–184.

Anway, M.D., Cupp, A.S., Uzumcu, M., and Skinner, M.K. (2005). Epigenetic transgenerational actions of endocrine disruptors and male fertility. Science *308*, 1466–1469.

Anway, M.D., Leathers, C., and Skinner, M.K. (2006). Endocrine disruptor vinclozolin induced epigenetic transgenerational adult-onset disease. Endocrinology *147*, 5515–5523.

Bender, L.B., Cao, R., Zhang, Y., and Strome, S. (2004). The MES-2/MES-3/MES-6 complex and regulation of histone H3 methylation in C. elegans. Curr. Biol. *14*, 1639–1643.

Bender, L.B., Suh, J., Carroll, C.R., Fong, Y., Fingerman, I.M., Briggs, S.D., Cao, R., Zhang, Y., Reinke, V., and Strome, S. (2006). MES-4: an autosome-associated histone methyltransferase that participates in silencing the X chromosomes in the C. elegans germ line. Development *133*, 3907–3917.

Bessler, J.B., Andersen, E.C., and Villeneuve, A.M. (2010). Differential localization and independent acquisition of the H3K9me2 and H3K9me3 chromatin modifications in the Caenorhabditis elegans adult germ line. PLoS Genet. *6*, e1000830.

Bhalla, N., and Dernburg, A.F. (2005). A conserved checkpoint monitors meiotic chromosome synapsis in Caenorhabditis elegans. Science *310*, 1683–1686.

Bhan, A., Hussain, I., Ansari, K.I., Bobzean, S.A., Perrotti, L.I., and Mandal, S.S. (2014). Histone methyltransferase EZH2 is transcriptionally induced by estradiol as well as estrogenic endocrine disruptors bisphenol-A and diethylstilbestrol. J. Mol. Biol. *426*, 3426–3441.

Boros, J., Arnoult, N., Stroobant, V., Collet, J.F., and Decottignies, A. (2014). Polycomb repressive complex 2 and H3K27me3 cooperate with H3K9 methylation to maintain heterochromatin protein 1α at chromatin. Mol. Cell. Biol. *34*, 3662–3674.

Chen, Y., Shu, L., Qiu, Z., Lee, D.Y., Settle, S.J., Que Hee, S., Telesca, D., Yang, X., and Allard, P. (2016). Exposure to the BPA-Substitute Bisphenol S Causes Unique Alterations of Germline Function. PLoS Genet. *12*, e1006223.

Doherty, L.F., Bromer, J.G., Zhou, Y., Aldad, T.S., and Taylor, H.S. (2010). In utero exposure to diethylstilbestrol (DES) or bisphenol-A (BPA) increases EZH2 expression in the mammary gland: an epigenetic mechanism linking endocrine disruptors to breast cancer. Horm. Cancer *1*, 146–155.

Frazee, A.C., Pertea, G., Jaffe, A.E., Langmead, B., Salzberg, S.L., and Leek, J.T. (2015). Ballgown bridges the gap between transcriptome assembly and expression analysis. Nat. Biotechnol. *33*, 243–246.

Gapp, K., Jawaid, A., Sarkies, P., Bohacek, J., Pelczar, P., Prados, J., Farinelli, L., Miska, E., and Mansuy, I.M. (2014). Implication of sperm RNAs in transgenerational inheritance of the effects of early trauma in mice. Nat. Neurosci. *17*, 667–669.

Garrigues, J.M., Sidoli, S., Garcia, B.A., and Strome, S. (2015). Defining heterochromatin in C. elegans through genome-wide analysis of the heterochromatin protein 1 homolog HPL-2. Genome Res. *25*, 76–88.

Gartner, A., Boag, P.R., and Blackwell, T.K. (2008). Germline survival and apoptosis. WormBook1-20.

Gaydos, L.J., Rechtsteiner, A., Egelhofer, T.A., Carroll, C.R., and Strome, S. (2012). Antagonism between MES-4 and Polycomb repressive complex 2 promotes appropriate gene expression in C. elegans germ cells. Cell Rep. *2*, 1169–1177.

Gaydos, L.J., Wang, W., and Strome, S. (2014). Gene repression. H3K27me and PRC2 transmit a memory of repression across generations and during development. Science *345*, 1515–1518.

Greer, E.L., Beese-Sims, S.E., Brookes, E., Spadafora, R., Zhu, Y., Rothbart, S.B., Aristizábal-Corrales, D., Chen, S., Badeaux, A.I., Jin, Q., et al. (2014). A histone methylation network regulates transgenerational epigenetic memory in C. elegans. Cell Rep. *7*, 113–126.

Hajkova, P., Ancelin, K., Waldmann, T., Lacoste, N., Lange, U.C., Cesari, F., Lee, C., Almouzni, G., Schneider, R., and Surani, M.A. (2008). Chromatin dynamics during epigenetic reprogramming in the mouse germ line. Nature *452*, 877–881.

Heard, E., and Martienssen, R.A. (2014). Transgenerational epigenetic inheritance: myths and mechanisms. Cell *157*, 95–109.

Ho, J.W., Jung, Y.L., Liu, T., Alver, B.H., Lee, S., Ikegami, K., Sohn, K.A., Minoda, A., Tolstorukov, M.Y., Appert, A., et al. (2014). Comparative analysis of metazoan chromatin organization. Nature *512*, 449–452.

Hu, Q., Chen, J., Zhang, J., Xu, C., Yang, S., and Jiang, H. (2016). IOX1, a JMJD2A inhibitor, suppresses the proliferation and migration of vascular smooth muscle cells induced by angiotensin II by regulating the expression of cell cycle-related proteins. Int. J. Mol. Med. *37*, 189–196.

Huber, W., Carey, V.J., Gentleman, R., Anders, S., Carlson, M., Carvalho, B.S., Bravo, H.C., Davis, S., Gatto, L., Girke, T., et al. (2015). Orchestrating high-throughput genomic analysis with Bioconductor. Nat. Methods *12*, 115–121.

Hughes, V. (2014). Epigenetics: The sins of the father. Nature *507*, 22–24.

Iwatani, M., Ikegami, K., Kremenska, Y., Hattori, N., Tanaka, S., Yagi, S., and Shiota, K. (2006). Dimethyl sulfoxide has an impact on epigenetic profile in mouse embryoid body. Stem Cells *24*, 2549–2556.

Juang, J.K., and Liu, H.J. (1987). The effect of DMSO on natural DNA conformation in enhancing transcription. Biochem. Biophys. Res. Commun. *146*, 1458–1464.

Kamath, R.S., and Ahringer, J. (2003). Genome-wide RNAi screening in Caenorhabditis elegans. Methods *30*, 313–321.

Kelly, W.G., and Fire, A. (1998). Chromatin silencing and the maintenance of a functional germline in Caenorhabditis elegans. Development *125*, 2451–2456.

Kelly, W.G., Xu, S., Montgomery, M.K., and Fire, A. (1997). Distinct requirements for somatic and germline expression of a generally expressed Caenorhabditis elegans gene. Genetics *146*, 227–238.

Kim, A., and Dean, A. (2004). Developmental stage differences in chromatin subdomains of the beta-globin locus. Proc. Natl. Acad. Sci. USA *101*, 7028–7033.

Kim, D., Langmead, B., and Salzberg, S.L. (2015). HISAT: a fast spliced aligner with low memory requirements. Nat. Methods *12*, 357–360.

King, O.N., Li, X.S., Sakurai, M., Kawamura, A., Rose, N.R., Ng, S.S., Quinn, A.M., Rai, G., Mott, B.T., Beswick, P., et al. (2010). Quantitative high-throughput screening identifies 8-hydroxyquinolines as cell-active histone demethylase inhibitors. PLoS ONE *5*, e15535.

Kishimoto, S., Uno, M., Okabe, E., Nono, M., and Nishida, E. (2017). Environmental stresses induce transgenerationally inheritable survival advantages via germline-to-soma communication in Caenorhabditis elegans. Nat. Commun. *8*, 14031.

Klosin, A., Casas, E., Hidalgo-Carcedo, C., Vavouri, T., and Lehner, B. (2017). Transgenerational transmission of environmental information in *C. elegans*. Science *356*, 320–323.

Kruidenier, L., Chung, C.W., Cheng, Z., Liddle, J., Che, K., Joberty, G., Bantscheff, M., Bountra, C., Bridges, A., Diallo, H., et al. (2012). A selective jumonji H3K27 demethylase inhibitor modulates the proinflammatory macrophage response. Nature *488*, 404–408.

Leung, D., Du, T., Wagner, U., Xie, W., Lee, A.Y., Goyal, P., Li, Y., Szulwach, K.E., Jin, P., Lorincz, M.C., and Ren, B. (2014). Regulation of DNA methylation turnover at LTR retrotransposons and imprinted loci by the histone methyltransferase Setdb1. Proc. Natl. Acad. Sci. USA *111*, 6690–6695.

Li, H., and Durbin, R. (2009). Fast and accurate short read alignment with Burrows-Wheeler transform. Bioinformatics *25*, 1754–1760.

Liu, T., Rechtsteiner, A., Egelhofer, T.A., Vielle, A., Latorre, I., Cheung, M.S., Ercan, S., Ikegami, K., Jensen, M., Kolasinska-Zwierz, P., et al. (2011). Broad chromosomal domains of histone modification patterns in C. elegans. Genome Res. *21*, 227–236.

Liu, S., Brind'Amour, J., Karimi, M.M., Shirane, K., Bogutz, A., Lefebvre, L., Sasaki, H., Shinkai, Y., and Lorincz, M.C. (2014). Setdb1 is required for germline development and silencing of H3K9me3-marked endogenous retroviruses in primordial germ cells. Genes Dev. *28*, 2041–2055.

Lundby, Z., Camacho, J., and Allard, P. (2016). Fast Functional Germline and Epigenetic Assays in the Nematode Caenorhabditis elegans. Methods Mol. Biol. *1473*, 99–107.

Manikkam, M., Tracey, R., Guerrero-Bosagna, C., and Skinner, M.K. (2013). Plastics derived endocrine disruptors (BPA, DEHP and DBP) induce epigenetic transgenerational inheritance of obesity, reproductive disease and sperm epimutations. PLoS ONE *8*, e55387.

Pasini, D., Cloos, P.A., Walfridsson, J., Olsson, L., Bukowski, J.P., Johansen, J.V., Bak, M., Tommerup, N., Rappsilber, J., and Helin, K. (2010). JARID2 regulates binding of the Polycomb repressive complex 2 to target genes in ES cells. Nature *464*, 306–310.

Peng, J.C., Valouev, A., Swigut, T., Zhang, J., Zhao, Y., Sidow, A., and Wysocka, J. (2009). Jarid2/Jumonji coordinates control of PRC2 enzymatic activity and target gene occupancy in pluripotent cells. Cell *139*, 1290–1302.

Pertea, M., Pertea, G.M., Antonescu, C.M., Chang, T.C., Mendell, J.T., and Salzberg, S.L. (2015). StringTie enables improved reconstruction of a transcriptome from RNA-seq reads. Nat. Biotechnol. *33*, 290–295.

R Core Team (2017). R: A language and environment for statistical computing (R Foundation for Statistical Computing).

Ramírez, F., Dündar, F., Diehl, S., Grüning, B.A., and Manke, T. (2014). deepTools: a flexible platform for exploring deep-sequencing data. Nucleic Acids Res. *42*, W187–W191.

Rechavi, O., Houri-Ze'evi, L., Anava, S., Goh, W.S.S., Kerk, S.Y., Hannon, G.J., and Hobert, O. (2014). Starvation-induced transgenerational inheritance of small RNAs in C. elegans. Cell *158*, 277–287.

Rudgalvyte, M., Peltonen, J., Lakso, M., and Wong, G. (2017). Chronic MeHg exposure modifies the histone H3K4me3 epigenetic landscape in Caenorhabditis elegans. Comp. Biochem. Physiol. C Toxicol. Pharmacol. *191*, 109–116.

Schaner, C.E., and Kelly, W.G. (2006). Germline chromatin. WormBook, 1–14.

Schiller, R., Scozzafava, G., Tumber, A., Wickens, J.R., Bush, J.T., Rai, G., Lejeune, C., Choi, H., Yeh, T.L., Chan, M.C., et al. (2014). A cell-permeable ester derivative of the JmjC histone demethylase inhibitor IOX1. ChemMedChem *9*, 566–571.

Schönfelder, G., Wittfoht, W., Hopp, H., Talsness, C.E., Paul, M., and Chahoud, I. (2002). Parent bisphenol A accumulation in the human maternal-fetal-placental unit. Environ. Health Perspect. *110*, A703–A707.

Seki, Y., Hayashi, K., Itoh, K., Mizugaki, M., Saitou, M., and Matsui, Y. (2005). Extensive and orderly reprogramming of genome-wide chromatin

modifications associated with specification and early development of germ cells in mice. Dev. Biol. *278*, 440–458.

Siklenka, K., Erkek, S., Godmann, M., Lambrot, R., McGraw, S., Lafleur, C., Cohen, T., Xia, J., Suderman, M., Hallett, M., et al. (2015). Disruption of histone methylation in developing sperm impairs offspring health transgenerationally. Science *350*, aab2006.

Singh, S., and Li, S.S. (2012). Epigenetic effects of environmental chemicals bisphenol A and phthalates. Int. J. Mol. Sci. *13*, 10143–10153.

Steinhauser, S., Kurzawa, N., Eils, R., and Herrmann, C. (2016). A comprehensive comparison of tools for differential ChIP-seq analysis. Brief. Bioinform. *17*, 953–966.

Stiernagle, T. (2006). Maintenance of C. elegans. WormBook, 1–11.

Tang, W.W., Kobayashi, T., Irie, N., Dietmann, S., and Surani, M.A. (2016). Specification and epigenetic programming of the human germ line. Nat. Rev. Genet. *17*, 585–600.

Towbin, B.D., González-Aguilera, C., Sack, R., Gaidatzis, D., Kalck, V., Meister, P., Askjaer, P., and Gasser, S.M. (2012). Step-wise methylation of histone H3K9 positions heterochromatin at the nuclear periphery. Cell *150*, 934–947.

Trapphoff, T., Heiligentag, M., El Hajj, N., Haaf, T., and Eichenlaub-Ritter, U. (2013). Chronic exposure to a low concentration of bisphenol A during follicle culture affects the epigenetic status of germinal vesicles and metaphase II oocytes. Fertil. Steril. *100*, 1758–1767.e1.

Vandenberg, L.N., Chahoud, I., Heindel, J.J., Padmanabhan, V., Paumgartten, F.J.R., and Schoenfelder, G. (2010). Urinary, circulating, and tissue biomonitoring studies indicate widespread exposure to bisphenol A. Environ. Health Perspect. *118*, 1055–1070.

Whetstine, J.R., Nottke, A., Lan, F., Huarte, M., Smolikov, S., Chen, Z., Spooner, E., Li, E., Zhang, G., Colaiacovo, M., and Shi, Y. (2006). Reversal of histone lysine trimethylation by the JMJD2 family of histone demethylases. Cell *125*, 467–481.

Wu, C.T., and Morris, J.R. (2001). Genes, genetics, and epigenetics: a correspondence. Science *293*, 1103–1105.

Yang, Y., Fear, J., Hu, J., Haecker, I., Zhou, L., Renne, R., Bloom, D., and McIntyre, L.M. (2014). Leveraging biological replicates to improve analysis in ChIP-seq experiments. Comput. Struct. Biotechnol. J. *9*, e201401002.

Yeo, M., Berglund, K., Hanna, M., Guo, J.U., Kittur, J., Torres, M.D., Abramowitz, J., Busciglio, J., Gao, Y., Birnbaumer, L., and Liedtke, W.B. (2013). Bisphenol A delays the perinatal chloride shift in cortical neurons by epigenetic effects on the Kcc2 promoter. Proc. Natl. Acad. Sci. USA *110*, 4315–4320.

Zhang, Y., Liu, T., Meyer, C.A., Eeckhoute, J., Johnson, D.S., Bernstein, B.E., Nusbaum, C., Myers, R.M., Brown, M., Li, W., and Liu, X.S. (2008). Model-based analysis of ChIP-Seq (MACS). Genome Biol. *9*, R137.

Zhong, S.H., Liu, J.Z., Jin, H., Lin, L., Li, Q., Chen, Y., Yuan, Y.X., Wang, Z.Y., Huang, H., Qi, Y.J., et al. (2013). Warm temperatures induce transgenerational epigenetic release of RNA silencing by inhibiting siRNA biogenesis in Arabidopsis. Proc. Natl. Acad. Sci. USA *110*, 9171–9176.

Cell Reports, Volume *23*

Supplemental Information

The Memory of Environmental Chemical Exposure in *C. elegans* Is Dependent on the Jumonji Demethylases *jmjd-2* and *jmjd-3*/*utx-1*

Jessica Camacho, Lisa Truong, Zeyneb Kurt, Yen-Wei Chen, Marco Morselli, Gerardo Gutierrez, Matteo Pellegrini, Xia Yang, and Patrick Allard

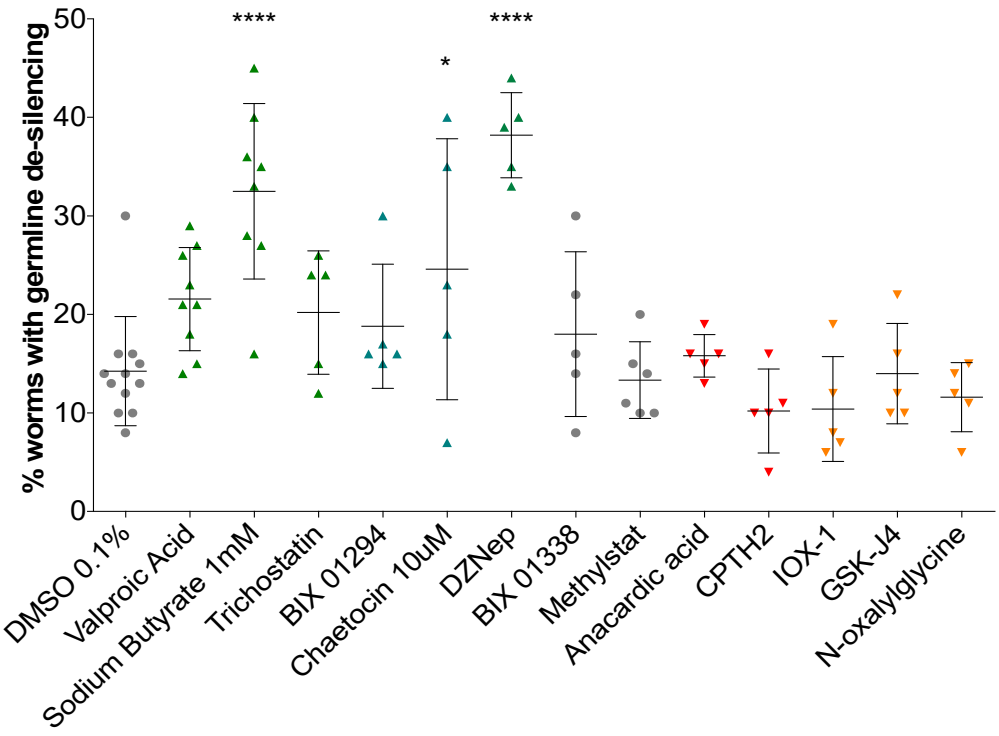

Figure S1: Epigenetic drug inhibitors assessment in P0 nematodes. Related to Figure 1. 13 drug inhibitors were tested for desilencing of the *pkIs1582* array in P0 worms. Chemicals are grouped based on their suspected chromatin effect: active (green), repressive (red) or carrying pleiotropic activity (grey). Unless indicated otherwise, all chemicals were tested at 100 µM. HDAC inhibitors are: Valproic acid, Sodium Butyrate and Trichostatin. Repressive H3K methyltransferase inhibitors are: BIX01294, Chaetocin and DZnep. Non-selective HMT and KDM inhibitors are: BIX 01338 and Methylstat. HAT inhibitors: Anacardic acid and CPTH2. Repressive H3K KDM inhibitors: IOX-1, GSK-J4 and N-oxalylglycine. N=5-9, 25 worms each, *P≤0.05, ****P≤0.0001. One way ANOVA, Sidak correction. All data are represented as mean +/- SEM.

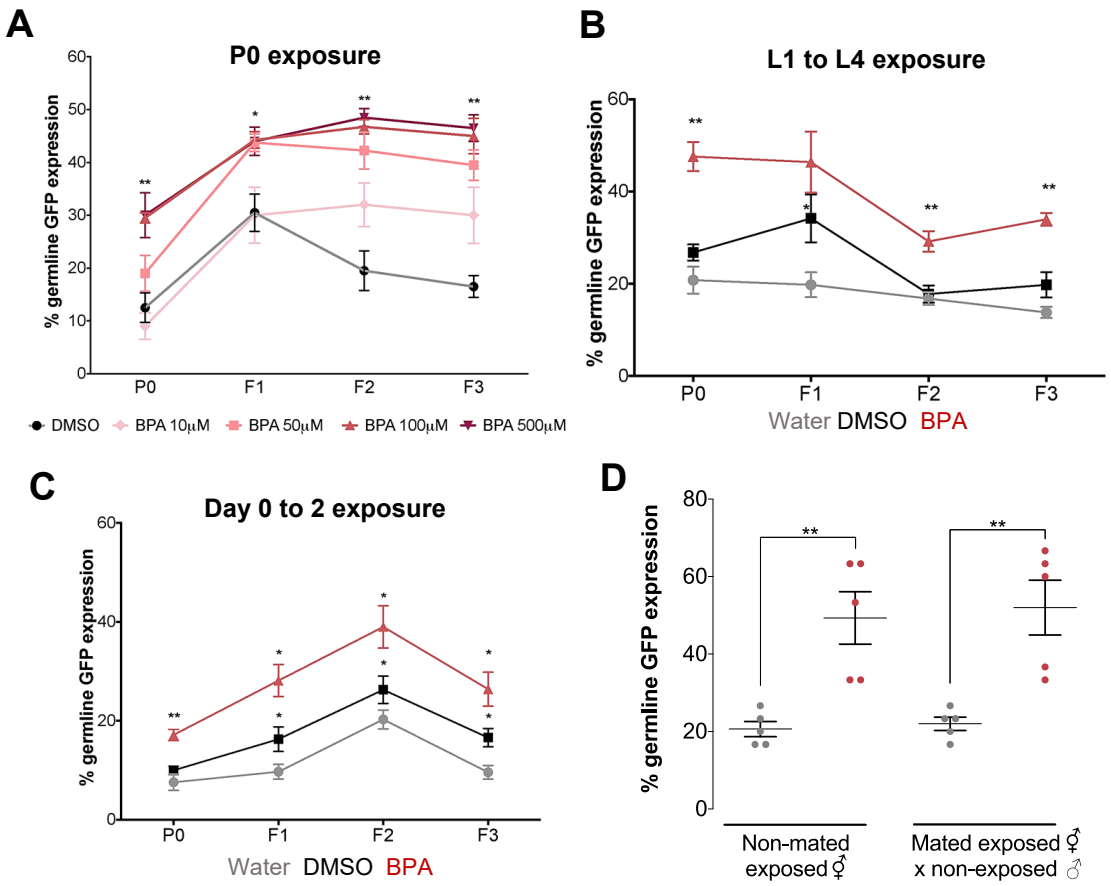

Figure S2: Dose, window and sex dependent germline *pkIs1582* array desilencing. Related to Figure 1. (A) Nematodes were exposed as L4 for 48 hours to BPA at the listed concentrations followed by monitoring of the proportion of worms with desilenced germlines. N=5-9, 25 worms each, *P≤0.05, **P≤0.01. A 100 μM dose was used to test two additional exposure windows, L1 to L4 (B) or Day 1 to Day 2 (C). N=5-9, 25 worms each, *P≤0.05, **P≤0.01. (D) Absence of rescue of ancestral BPA exposure-induced array desilencing in F3 germlines by mating. P0 nematodes were either exposed to DMSO (grey) or BPA (red) and the progeny of GFP-positive P0 worms was either not mated (left) or mated at the F1 generation with unexposed males (right). Expression of the *pkIs1582* integrated array was then monitored in F3 germlines. N=5, 30 worms each **P≤0.01. All data are represented as mean +/- SEM.

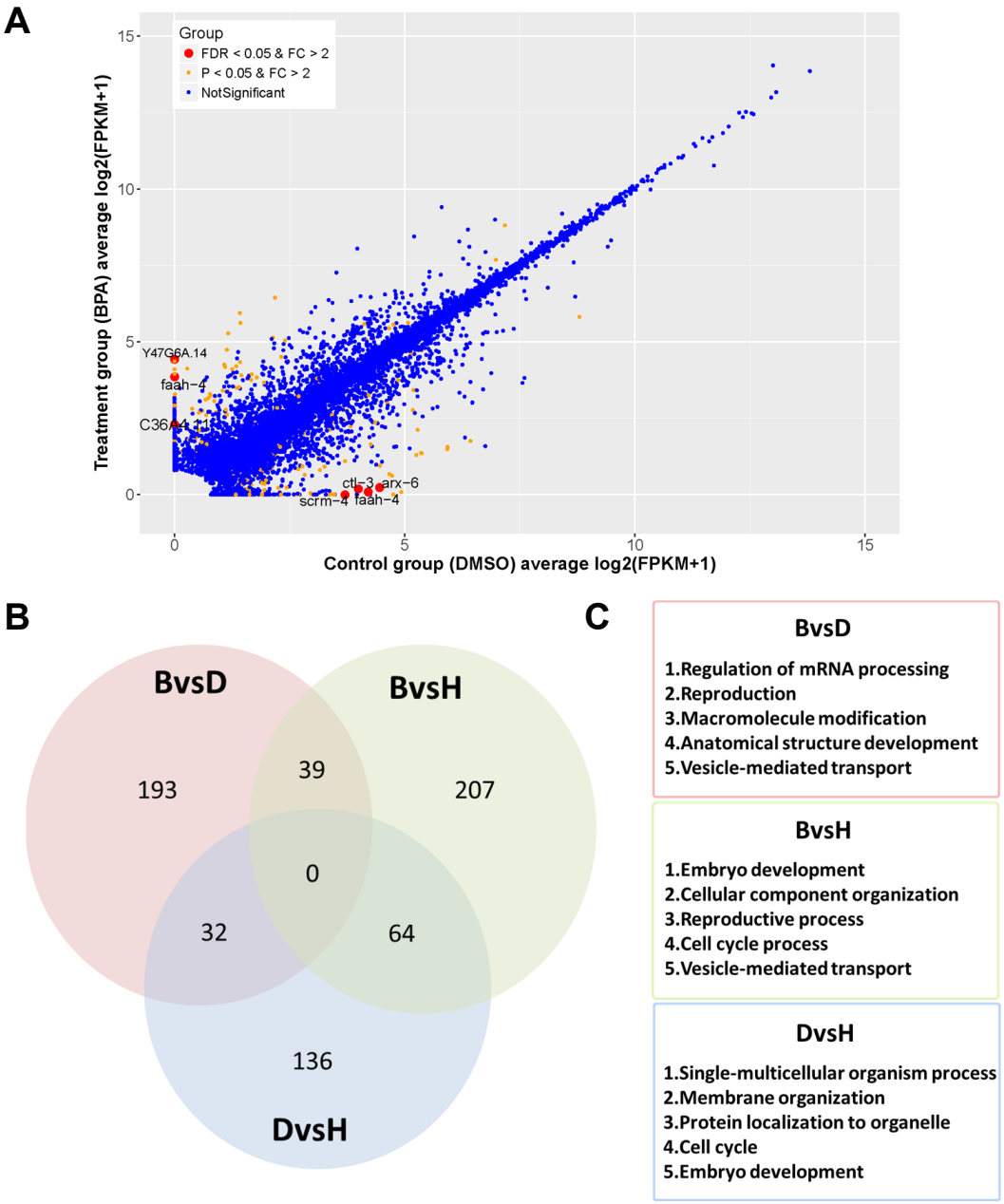

Figure S3: Transgenerational impact of BPA on the germline transcriptome. Related to Figure 2 and 5. A. The pair-wise comparison log2-transformed FKPM obtained by RNA-seq from BPA and DMSO samples. Red circles: FDR<0.05 and fold change >|2|, orange circles P<0.05 and fold change >|2|, blue no significant difference. (B) Venn diagram of transcripts identified in each treatment group. (C) Gene ontology analysis of unique transcripts ≤0.5 or ≥1.5 between all treatment pairs.

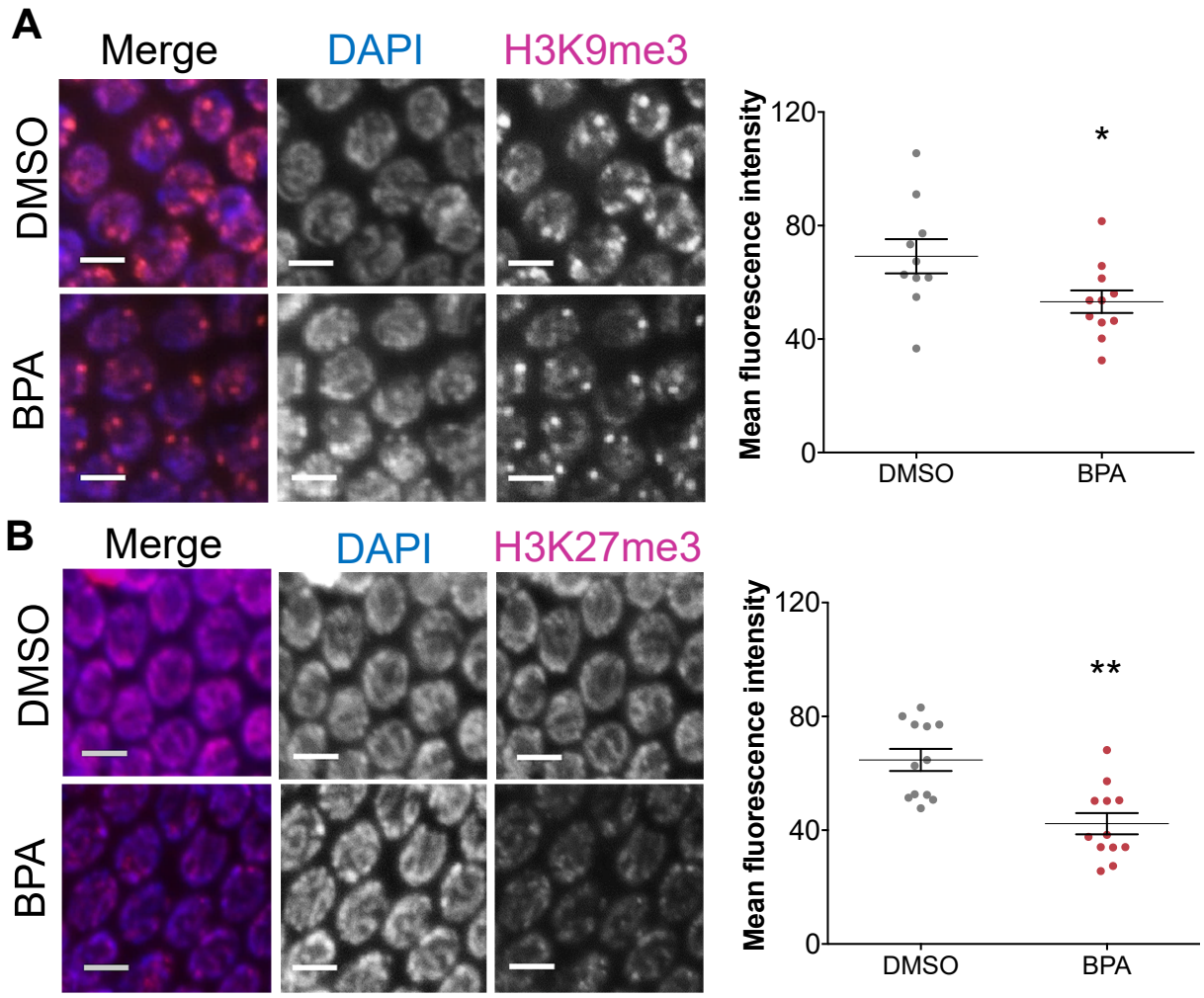

Figure S4: Ancestral BPA exposure decreases H3K9me3 and H3K27me3 levels in F3 germlines carrying an extrachromosomal array. Related to Figure 4. Immunofluorescence images of mid-to-late pachytene germline nuclei from F3 PD7271 (*pha-1(e2123)* III; *ccEx7271*) worms ancestrally exposed to DMSO or BPA and stained for H3K9me3 (A) or H3K27me3 (B). DAPI is represented in blue and the histone mark of interest in magenta in the merge. All images shown were selected representative images of the mean values obtained after quantification of all germline nuclei from that exposure group. The fluorescence intensity quantification is shown on the right panels. N=10-12 worms, 10 nuclei per worm, *P≤0.05, **P≤0.01. All data are represented as mean +/- SEM.

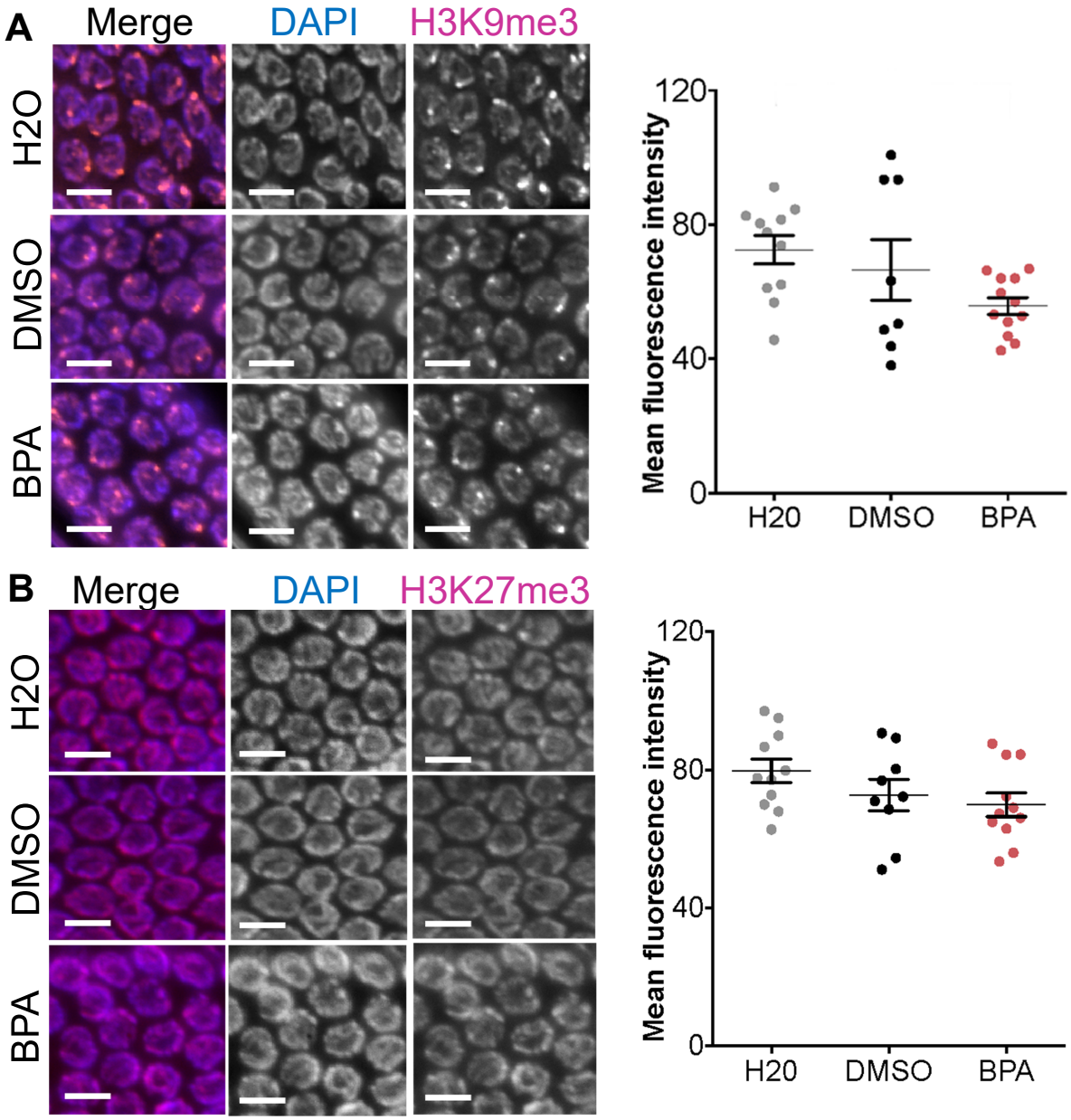

Figure S5: Ancestral BPA exposure does not decrease H3K9me3 and H3K27me3 levels in F7 germlines. Related to Figure 4. Immunofluorescence of mid-to-late pachytene F7 germline nuclei ancestrally exposed and stained for H3K9me3 (A) or H3K27me3 (B). DAPI is blue and the histone marks magenta in the merge. All images were selected representative of the mean values after quantification of all germline nuclei from that exposure group. N=10-12 worms, 10 nuclei quantified per worm. Two-way ANOVA with Sidak correction. All data are represented as mean +/- SEM.

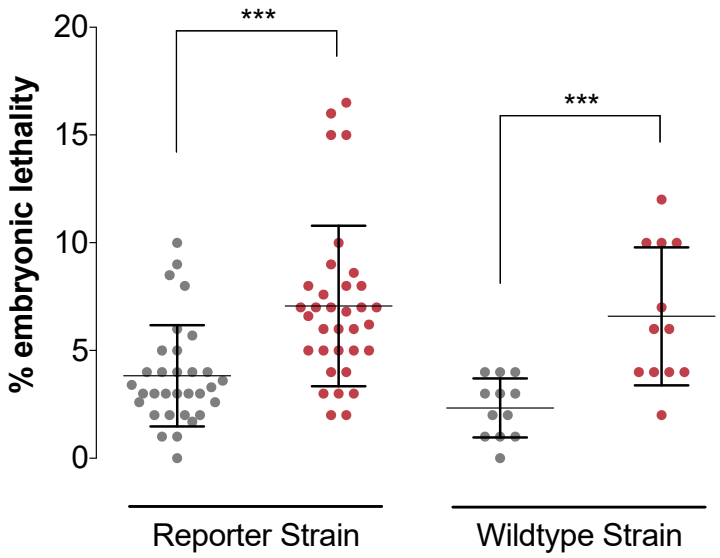

Figure S6: Variation in embryonic lethality phenotype based on genotype and variation in germline desilencing based on mode of inheritance. Related to Figure 6. Embryonic lethality in *pkIs1582* array-carrying NL2507 strain (labeled reporter) and wildtype (N2) *C. elegans* strains at the F3 generation following ancestral DMSO (grey circles) or BPA (red circles) exposure. N=12-30 worms, ***P≤0.001. All data are represented as mean +/- SEM.

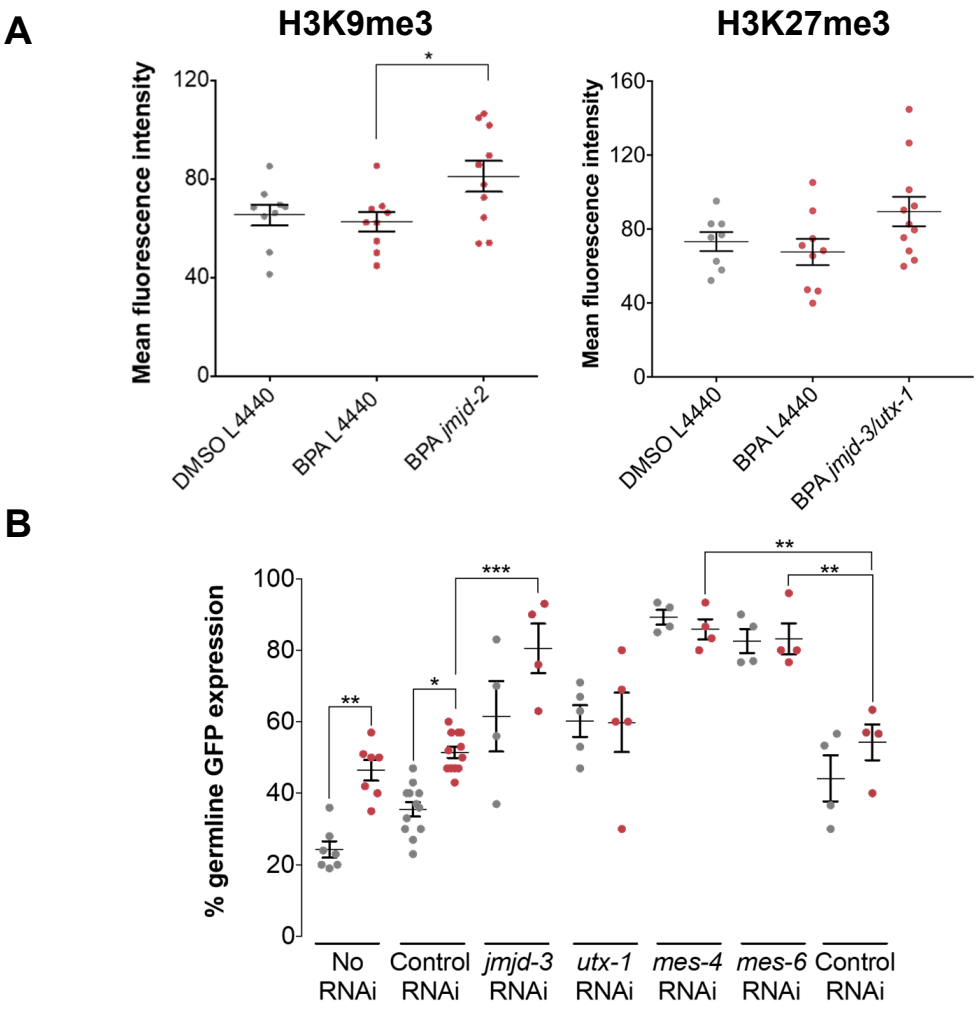

Figure S7: Changes in H3K9me3, H3K27me3, and array desilencing in the F3 generation following RNAi. Related to Figure 7. P0 nematodes were either exposed to DMSO (grey) or BPA (red) and the progeny of GFP-positive P0 worms was then exposed to RNAi. The subsequent F3 generation was then examined for H3K9me3 or H3K27me3 levels by immunofluorescence (A) or expression of the *pkIs1582* integrated array in the germline (B). *mes-4* and *mes-6* RNAi was performed at the F2 to F3 transition to circumvent their maternal sterility phenotype. (A) N=4 repeats, 8-11 gonad per treatment group, 10 nuclei per gonad, *P≤0.05. (B) N=4-7, 30 worms each *P≤0.05, **P≤0.01, ***P≤0.001. Two-way ANOVA. For the *mes* genes, only the comparisons between BPA groups are shown. All data are represented as mean +/- SEM.

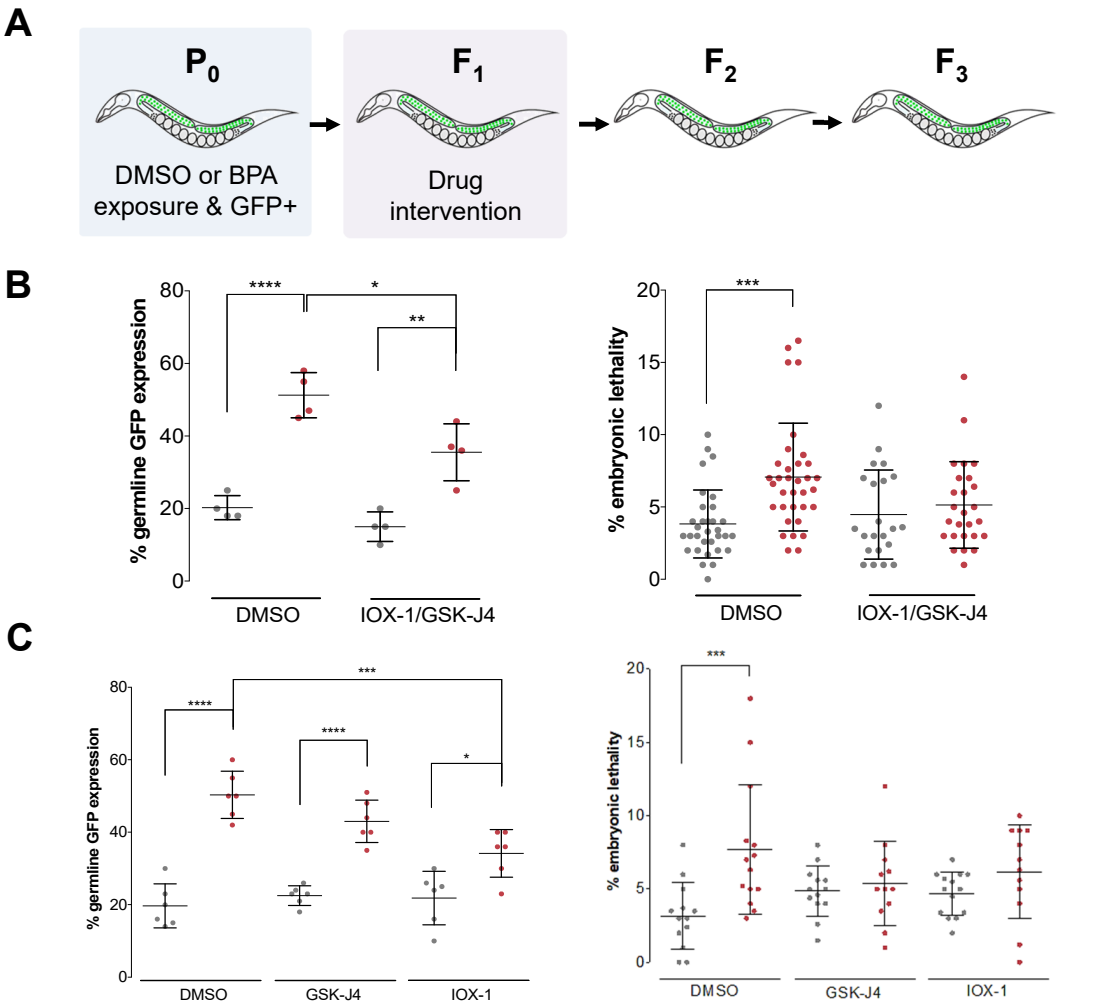

Figure S8: Rescue of F3 germline *pkIs1582* array desilencing and embryonic lethality phenotypes by inhibitor drug exposures. Related to Figure 7. A. Worms exposed to DMSO or BPA and GFP-positive at the P0 are subsequently exposed to DMSO, GSK-J4 and/or IOX-1 as F1s and assayed at the F3 generation. B. Co-treatment with IOX-1 (JMJD-2) and GSK-J4 (JMJD-3) demethylase inhibitors partially rescues the array desilencing and fully rescues BPA-induced embryonic lethality. N=4, 30 worms each desilencing assay and N=10 worms embryonic lethality assay. C. Rescue of BPA-induced transgenerational effects by single exposure at the F1 generation. Array desilencing: N=6, 25-30 worms each. Embryonic lethality: N=12-14,. Grey = DMSO exposed P0s. Red = BPA-exposed P0s. For all panels, * P≤0.05, **P≤0.01 ***P≤0.001, ****P≤0.0001, two-way ANOVA. All data are represented as mean +/- SEM.

Table S.1: RNA-Seq. Related to Figure 2

GeneNames	DAVID_IDs	feature	transcriptNames	FC (BPA/DMSO)	p-val	q-val
F11E6.7	WBGene00008710	transcript	TCONS_00034600	22.91871074	0.020499	0.999966
Y47G6A.14	WBGene00021640	transcript	TCONS_00002975	21.62575318	2.11E-12	2.19E-08
D1044.6	WBGene00017031	transcript	TCONS_00014441	20.56571706	0.0243	0.999966
F36A2.13	NA	transcript	TCONS_00004097	19.13054049	0.021667	0.999966
taf-5	WBGene00006386	transcript	TCONS_00001275	18.11671495	0.026784	0.999966
tag-256	NA	transcript	TCONS_00012700	17.25750344	0.014117	0.999966
pif-1	WBGene00004028	transcript	TCONS_00000085	17.13469793	0.024202	0.999966
F55F10.1	WBGene00018898	transcript	TCONS_00016610	15.39210301	0.023874	0.999966
faah-4	WBGene00013232	transcript	TCONS_00015694	14.52446262	1.60E-07	0.000554
F32B6.3	WBGene00009320	transcript	TCONS_00028295	14.3149513	0.007312	0.999966
sop-3	WBGene00004946	transcript	TCONS_00002859	12.12318748	0.020483	0.999966
syx-5	WBGene00006373	transcript	TCONS_00036844	9.623302077	0.031124	0.999966
C35D10.5	WBGene00016442	transcript	TCONS_00011891	8.979393591	0.026724	0.999966
ufd-2	WBGene00006734	transcript	TCONS_00006885	8.48064623	0.039101	0.999966
sgo-1	WBGene00016381	transcript	TCONS_00027853	8.425925624	0.037215	0.999966
T24H7.2	WBGene00020781	transcript	TCONS_00006424	7.988985762	0.005334	0.999966
Y77E11A.1	NA	transcript	TCONS_00016172	7.691582185	0.024462	0.999966
Y37E11B.5	WBGene00021377	transcript	TCONS_00025723	7.519790865	0.025241	0.999966
fce-2	WBGene00001406	transcript	TCONS_00038558	7.517657054	0.031577	0.999966
epg-4	WBGene00018150	transcript	TCONS_00012348	7.502932937	0.035637	0.999966
Y39B6A.42	WBGene00012700	transcript	TCONS_00042592	7.228606281	0.023899	0.999966
T05E7.3	WBGene00020259	transcript	TCONS_00000935	7.204869304	6.18E-05	0.080179
Y48G8AL.10	WBGene00021689	transcript	TCONS_00002690	7.188244464	0.011635	0.999966
D1044.6	WBGene00017031	transcript	TCONS_00014442	6.224987376	0.044101	0.999966
jmjd-1.2	WBGene00017920	transcript	TCONS_00016665	5.738988397	0.025741	0.999966
ztf-17	WBGene00011639	transcript	TCONS_00009733	5.485929283	0.020772	0.999966
H24K24.3	WBGene00019240	transcript	TCONS_00034779	5.468550758	0.038218	0.999966
W02D3.4	WBGene00020933	transcript	TCONS_00003644	5.396964159	0.032669	0.999966
F42A6.6	WBGene00018328	transcript	TCONS_00025679	5.355162599	0.008547	0.999966
sgo-1	WBGene00016381	transcript	TCONS_00027854	5.341636043	0.018525	0.999966
mpst-7	WBGene00011307	transcript	TCONS_00041423	5.100124078	0.038862	0.999966
F44E2.10	WBGene00018423	transcript	TCONS_00015134	4.938708809	0.037462	0.999966
C36A4.11	WBGene00044167	transcript	TCONS_00025807	4.928874268	1.96E-05	0.029118
uaf-2	WBGene00006698	transcript	TCONS_00034402	4.778134656	0.032316	0.999966
bath-28	WBGene00017461	transcript	TCONS_00008798	4.621857383	0.024052	0.999966
ctl-3	WBGene00013220	transcript	TCONS_00011003	4.559536582	0.010914	0.999966
scrm-4	WBGene00008681	transcript	TCONS_00004719	4.535401797	0.041272	0.999966
W03F8.4	WBGene00020994	transcript	TCONS_00016991	4.471245187	0.038569	0.999966
ucr-2.1	WBGene00012158	transcript	TCONS_00045144	4.4281965	0.009942	0.999966
Y48E1C.1	WBGene00013014	transcript	TCONS_00007914	4.411254194	0.023784	0.999966
sop-2	WBGene00004945	transcript	TCONS_00007750	4.409482026	0.002722	0.999966
B0432.8	WBGene00015189	transcript	TCONS_00008233	4.387580586	0.026096	0.999966
D1005.9	NA	transcript	TCONS_00000320	4.369925663	0.027122	0.999966
F52D2.12	WBGene00219451	transcript	TCONS_00043160	4.318076262	0.046221	0.999966

coq-5	WBGene00000765	transcript	TCONS_00014910	4.240980232	0.036412	0.999966
csnk-1	WBGene00013709	transcript	TCONS_00004458	4.119071132	0.000346	0.338368
Y39G10AR.7	NA	transcript	TCONS_00000273	3.888032354	0.026379	0.999966
met-2	WBGene00019883	transcript	TCONS_00012604	3.867788824	0.025808	0.999966
F44E2.10	WBGene00018423	transcript	TCONS_00015133	3.865045089	0.030498	0.999966
Y52B11A.2	NA	transcript	TCONS_00004602	3.75203157	0.034617	0.999966
F45H11.5	WBGene00009745	transcript	TCONS_00001771	3.472772193	0.047674	0.999966
F49C12.11	WBGene00009880	transcript	TCONS_00028159	3.421527165	0.048823	0.999966
C34B4.2	WBGene00007907	transcript	TCONS_00037196	3.287729156	0.023026	0.999966
tra-3	WBGene00006606	transcript	TCONS_00030400	3.16631588	0.031517	0.999966
.	NA	transcript	TCONS_00034628	3.088758845	0.012577	0.999966
Y50D4A.5	WBGene00021739	transcript	TCONS_00034812	2.974337832	0.010803	0.999966
tag-325	WBGene00008006	transcript	TCONS_00011868	2.832967555	0.040508	0.999966
F43G6.10	WBGene00009662	transcript	TCONS_00007651	2.792606925	0.003777	0.999966
F10C2.5	WBGene00008646	transcript	TCONS_00036930	2.770239069	0.044578	0.999966
epg-4	WBGene00018150	transcript	TCONS_00012359	2.766093442	0.03346	0.999966
C54E4.2	NA	transcript	TCONS_00016261	2.744160211	0.025764	0.999966
F22B3.4	NA	transcript	TCONS_00019293	2.737695156	0.022284	0.999966
mtm-3	WBGene00003476	transcript	TCONS_00014069	2.617072763	0.030481	0.999966
dnj-22	WBGene00001040	transcript	TCONS_00040207	2.387717391	0.04019	0.999966
nucb-1	WBGene00009674	transcript	TCONS_00044819	2.176969149	0.02779	0.999966
T08B2.5	WBGene00020346	transcript	TCONS_00000940	2.082998688	0.013864	0.999966
hpo-24	WBGene00011945	transcript	TCONS_00001692	2.075937495	0.035806	0.999966
T26C11.9	WBGene00194679	transcript	TCONS_00046352	1.95223635	0.007288	0.999966
fox-1	WBGene00001484	transcript	TCONS_00046461	1.922965694	0.032121	0.999966
F57C9.1	WBGene00019008	transcript	TCONS_00000679	1.845940481	0.024263	0.999966
T02G5.4	NA	transcript	TCONS_00006651	1.823718231	0.032603	0.999966
dpf-4	WBGene00001057	transcript	TCONS_00012118	1.815256008	0.025662	0.999966
pqn-59	WBGene00004143	transcript	TCONS_00002598	1.811470083	0.013732	0.999966
sir-2.4	WBGene00004803	transcript	TCONS_00000886	1.747926404	0.015264	0.999966
C35D10.1	WBGene00016439	transcript	TCONS_00011897	1.744733015	0.001331	0.812952
Y73B6BL.29	WBGene00022250	transcript	TCONS_00017983	1.715056004	0.002422	0.999966
aars-1	WBGene00000196	transcript	TCONS_00010515	1.710321348	0.046796	0.999966
set-26	WBGene00013106	transcript	TCONS_00033908	1.627965777	0.031279	0.999966
pgl-3	WBGene00003994	transcript	TCONS_00035342	1.62126183	0.009898	0.999966
.	NA	transcript	TCONS_00010782	1.620146382	0.031022	0.999966
C05D2.10	WBGene00015470	transcript	TCONS_00014452	1.592650276	0.023219	0.999966
Y43E12A.3	WBGene00012795	transcript	TCONS_00019199	1.589986933	0.003535	0.999966
egl-30	WBGene00001196	transcript	TCONS_00000216	1.542385467	0.02562	0.999966
C14A4.3	WBGene00007556	transcript	TCONS_00007379	1.522919077	0.015894	0.999966
CD4.8	WBGene00016993	transcript	TCONS_00039565	1.517044335	0.023906	0.999966
asd-1	WBGene00011279	transcript	TCONS_00011694	1.479331847	0.032117	0.999966
lin-37	WBGene00003022	transcript	TCONS_00014727	1.457347041	0.000824	0.570739
mtm-1	WBGene00003475	transcript	TCONS_00000737	1.43404089	0.047324	0.999966
B0272.3	WBGene00007129	transcript	TCONS_00044660	1.430161988	0.023535	0.999966

Y95D11A.3	WBGene00045434	transcript	TCONS_00001906	1.428964698	0.037743	0.999966
Y92H12BR.3	WBGene00022369	transcript	TCONS_00000160	1.399835725	0.035558	0.999966
F38H4.10	WBGene00009551	transcript	TCONS_00019401	1.396394372	0.00779	0.999966
F10D2.13	NA	transcript	TCONS_00039931	1.355791074	0.026141	0.999966
F10D2.15	NA	transcript	TCONS_00035808	1.341420193	0.026133	0.999966
W01A11.7	WBGene00020912	transcript	TCONS_00039763	1.32786249	0.042122	0.999966
Y45F10D.10	WBGene00012889	transcript	TCONS_00029400	1.319319993	0.032374	0.999966
chin-1	WBGene00015267	transcript	TCONS_00013700	1.317339541	0.016654	0.999966
usp-39	WBGene00017280	transcript	TCONS_00005623	1.315422527	0.034793	0.999966
swah-1	WBGene00007985	transcript	TCONS_00001592	1.310523019	0.004272	0.999966
ife-3	WBGene00002061	transcript	TCONS_00038656	1.293136003	0.038879	0.999966
met-2	WBGene00019883	transcript	TCONS_00012603	1.285540034	0.034932	0.999966
tol-1	WBGene00006593	transcript	TCONS_00000049	1.257417852	0.043807	0.999966
pes-9	WBGene00003982	transcript	TCONS_00041793	1.237161115	0.045108	0.999966
C13C4.4	WBGene00007548	transcript	TCONS_00041195	1.235446018	0.029972	0.999966
R151.8	WBGene00020111	transcript	TCONS_00014782	1.234246148	0.021395	0.999966
C50F4.16	WBGene00008238	transcript	TCONS_00040437	1.220034485	0.047208	0.999966
F53E4.2	WBGene00206516	transcript	TCONS_00037755	1.219397202	0.049769	0.999966
rop-1	WBGene00004405	transcript	TCONS_00040628	1.211875512	0.003898	0.999966
dhps-1	WBGene00012460	transcript	TCONS_00007693	1.191625486	0.0188	0.999966
hcp-1	WBGene00001829	transcript	TCONS_00035704	1.190692714	0.033482	0.999966
nape-2	WBGene00021370	transcript	TCONS_00025747	1.183164676	0.030967	0.999966
rnp-4	WBGene00004387	transcript	TCONS_00011747	1.172567201	0.048033	0.999966
F53F8.5	WBGene00010002	transcript	TCONS_00042840	1.164519548	0.031077	0.999966
ZK858.7	WBGene00014120	transcript	TCONS_00004182	1.159967717	0.018093	0.999966
Y43D4A.4	WBGene00012790	transcript	TCONS_00024769	1.155201963	0.013497	0.999966
rskd-1	WBGene00010096	transcript	TCONS_00041241	1.152642043	0.028376	0.999966
F01D4.5	WBGene00008488	transcript	TCONS_00028466	1.147625545	0.043988	0.999966
mms-19	WBGene00016060	transcript	TCONS_00035459	1.144227692	0.025713	0.999966
K07C5.2	WBGene00010625	transcript	TCONS_00036434	1.139850747	0.015099	0.999966
arf-1.2	WBGene00000182	transcript	TCONS_00012089	1.139338898	0.021533	0.999966
prp-21	WBGene00004188	transcript	TCONS_00005284	1.138573279	0.014038	0.999966
arrd-13	WBGene00011054	transcript	TCONS_00007949	1.136127057	0.008785	0.999966
Y43D4A.3	WBGene00012789	transcript	TCONS_00034040	1.135776908	0.015255	0.999966
gly-4	WBGene00001629	transcript	TCONS_00042715	1.127296623	0.013199	0.999966
ZK1307.9	WBGene00014250	transcript	TCONS_00007222	1.124847571	0.044766	0.999966
T20B12.1	NA	transcript	TCONS_00012405	1.114075053	0.001802	0.999966
K07G5.6	NA	transcript	TCONS_00003738	1.113802215	0.026018	0.999966
vnut-1	WBGene00010758	transcript	TCONS_00008072	1.113355816	0.034025	0.999966
deps-1	WBGene00022034	transcript	TCONS_00000054	1.10627448	0.040388	0.999966
eif-3.I	WBGene00001232	transcript	TCONS_00000295	1.091279722	0.049054	0.999966
F32B4.4	WBGene00009314	transcript	TCONS_00001975	1.08947315	0.02112	0.999966
cpt-2	WBGene00011122	transcript	TCONS_00019248	1.089137826	0.019819	0.999966
henn-1	WBGene00015349	transcript	TCONS_00012564	1.08909032	0.023997	0.999966
ppk-2	WBGene00004088	transcript	TCONS_00011391	1.08639034	0.043162	0.999966

C03C10.4	NA	transcript	TCONS_00014124	1.086205874	0.033953	0.999966
ZK546.5	WBGene00022762	transcript	TCONS_00006095	1.084629637	0.033367	0.999966
ZK856.8	NA	transcript	TCONS_00040600	1.083332679	0.041651	0.999966
haf-2	WBGene00001812	transcript	TCONS_00009621	1.081226915	0.020519	0.999966
thoc-2	WBGene00015813	transcript	TCONS_00012200	1.063021138	0.008136	0.999966
laat-1	WBGene00021546	transcript	TCONS_00008221	0.924758658	0.013392	0.999966
F56B3.2	WBGene00018928	transcript	TCONS_00025383	0.874564218	0.029909	0.999966
.	NA	transcript	TCONS_00045329	0.874536667	0.020491	0.999966
F54D11.3	WBGene00018813	transcript	TCONS_00039391	0.870205793	0.011504	0.999966
C06A5.2	WBGene00015500	transcript	TCONS_00000888	0.867890785	0.045766	0.999966
R02D3.3	WBGene00019821	transcript	TCONS_00025307	0.865761529	0.032531	0.999966
C06A5.3	WBGene00015501	transcript	TCONS_00000885	0.850733069	0.046492	0.999966
par-4	WBGene00003919	transcript	TCONS_00038219	0.849279991	0.032357	0.999966
T15B7.15	WBGene00020527	transcript	TCONS_00039852	0.829102465	0.005034	0.999966
F01F1.15	WBGene00017169	transcript	TCONS_00014502	0.815600584	0.02567	0.999966
R01B10.6	WBGene00019808	transcript	TCONS_00039673	0.80804297	0.016612	0.999966
Y40C5A.4	WBGene00021497	transcript	TCONS_00027734	0.8055999	0.031696	0.999966
kel-8	WBGene00020952	transcript	TCONS_00035055	0.804518187	0.013131	0.999966
clp-6	WBGene00000546	transcript	TCONS_00025474	0.796979102	0.005629	0.999966
oig-4	WBGene00043050	transcript	TCONS_00006779	0.792278748	0.03251	0.999966
gly-14	WBGene00001639	transcript	TCONS_00014000	0.784697604	0.040655	0.999966
tba-4	WBGene00006530	transcript	TCONS_00007437	0.783269993	0.022244	0.999966
H24K24.3	WBGene00019240	transcript	TCONS_00034780	0.778835377	0.033567	0.999966
kin-31	NA	transcript	TCONS_00012669	0.765730916	0.044035	0.999966
Y38F2AR.10	WBGene00021428	transcript	TCONS_00025560	0.76301085	0.04958	0.999966
C07A9.9	WBGene00007405	transcript	TCONS_00015313	0.753842179	0.034148	0.999966
C27F2.1	WBGene00016165	transcript	TCONS_00011926	0.746033626	0.006073	0.999966
.	NA	transcript	TCONS_00046325	0.742973457	0.004007	0.999966
C28D4.10	WBGene00007796	transcript	TCONS_00018914	0.741282489	0.041249	0.999966
F23H11.2	WBGene00017758	transcript	TCONS_00011255	0.739694572	0.041343	0.999966
ZC262.2	WBGene00022579	transcript	TCONS_00012593	0.73729853	0.035898	0.999966
cyn-2	WBGene00000878	transcript	TCONS_00013500	0.736146058	0.014026	0.999966
fzr-1	WBGene00001510	transcript	TCONS_00010122	0.730145636	0.036981	0.999966
ZK795.2	WBGene00014082	transcript	TCONS_00028949	0.727836902	0.03633	0.999966
rpoa-12	WBGene00007616	transcript	TCONS_00041744	0.726742317	0.020541	0.999966
immp-1	WBGene00007021	transcript	TCONS_00013248	0.718953015	0.027641	0.999966
mtrr-1	WBGene00006510	transcript	TCONS_00007152	0.715948735	0.009827	0.999966
C56G2.9	WBGene00016982	transcript	TCONS_00014591	0.714301942	0.036593	0.999966
fbxa-113	WBGene00013757	transcript	TCONS_00038529	0.703369558	0.012578	0.999966
knl-3	WBGene00020392	transcript	TCONS_00034894	0.699350789	0.007381	0.999966
Y39G10AR.32	WBGene00219275	transcript	TCONS_00002797	0.682186142	0.029242	0.999966
rab-39	WBGene00004286	transcript	TCONS_00010052	0.667743504	0.044449	0.999966
F40F9.14	NA	transcript	TCONS_00036326	0.664515698	0.007308	0.999966
nfi-1	WBGene00003592	transcript	TCONS_00006753	0.661512998	0.030067	0.999966
glh-4	WBGene00001601	transcript	TCONS_00000488	0.634619276	0.032161	0.999966

ztf-17	WBGene00011639	transcript	TCONS_00009732	0.621995643	0.01946	0.999966
E02H9.3	WBGene00017101	transcript	TCONS_00011444	0.616669207	0.038718	0.999966
nrd-1	WBGene00017004	transcript	TCONS_00003185	0.609619925	0.010994	0.999966
F13G3.6	WBGene00008766	transcript	TCONS_00003782	0.601508034	0.012804	0.999966
F48F7.6	WBGene00009851	transcript	TCONS_00045500	0.600462993	0.044095	0.999966
ncl-1	WBGene00003559	transcript	TCONS_00012462	0.594957679	0.017765	0.999966
nop-1	WBGene00017774	transcript	TCONS_00012134	0.572447032	0.039582	0.999966
Y52B11A.8	WBGene00013127	transcript	TCONS_00001912	0.566559844	0.005036	0.999966
D2096.12	WBGene00017079	transcript	TCONS_00018628	0.566495517	0.009628	0.999966
T10C6.7	WBGene00011689	transcript	TCONS_00042104	0.564635801	0.020073	0.999966
cec-10	WBGene00022831	transcript	TCONS_00000599	0.561754889	0.041896	0.999966
lst-6	WBGene00016889	transcript	TCONS_00009546	0.558756428	0.032953	0.999966
F25H8.1	WBGene00009131	transcript	TCONS_00028314	0.548196043	0.029995	0.999966
rps-29	WBGene00004498	transcript	TCONS_00011230	0.529290595	0.049658	0.999966
.	NA	transcript	TCONS_00011860	0.519827678	0.014317	0.999966
.	NA	transcript	TCONS_00040790	0.507744641	0.001001	0.650143
C41H7.4	WBGene00016574	transcript	TCONS_00005693	0.506534214	0.045959	0.999966
F53F10.3	WBGene00018765	transcript	TCONS_00000507	0.503856376	0.041637	0.999966
sqrd-1	WBGene00008538	transcript	TCONS_00020591	0.489451128	0.033976	0.999966
tag-325	WBGene00008006	transcript	TCONS_00011863	0.485491478	0.023754	0.999966
pin-2	WBGene00004030	transcript	TCONS_00019608	0.4695527	0.031608	0.999966
T07E3.3	WBGene00020314	transcript	TCONS_00012299	0.460328695	0.003467	0.999966
kal-1	WBGene00002181	transcript	TCONS_00005063	0.452834078	0.023441	0.999966
B0280.17	WBGene00044674	transcript	TCONS_00014745	0.45229781	0.045052	0.999966
D1054.1	WBGene00008370	transcript	TCONS_00040765	0.441249101	0.033316	0.999966
Y54G2A.19	WBGene00021884	transcript	TCONS_00025613	0.420066491	0.022999	0.999966
osta-3	WBGene00012182	transcript	TCONS_00008126	0.417432257	0.048016	0.999966
F21A10.2	NA	transcript	TCONS_00047939	0.396978229	0.046126	0.999966
ZK1127.3	WBGene00022850	transcript	TCONS_00006633	0.395824537	0.029205	0.999966
F56A6.4	NA	transcript	TCONS_00002626	0.392221773	0.013175	0.999966
T05H4.11	WBGene00020274	transcript	TCONS_00039743	0.387241922	0.046329	0.999966
rfp-1	WBGene00007008	transcript	TCONS_00012601	0.379588851	0.005634	0.999966
rfp-1	WBGene00007008	transcript	TCONS_00012600	0.370728287	0.004793	0.999966
K12D12.5	WBGene00010787	transcript	TCONS_00007657	0.366474977	0.036945	0.999966
lin-66	WBGene00001562	transcript	TCONS_00020157	0.34892521	0.031793	0.999966
21ur-2599	NA	transcript	TCONS_00021712	0.34880291	0.014735	0.999966
21ur-9510	NA	transcript	TCONS_00031104	0.347298354	0.014844	0.999966
C06A5.6	WBGene00015504	transcript	TCONS_00003473	0.340469106	0.002592	0.999966
ubc-12	WBGene00006707	transcript	TCONS_00002013	0.337138424	0.024218	0.999966
sop-3	WBGene00004946	transcript	TCONS_00002853	0.330892759	0.035119	0.999966
mib-1	WBGene00012933	transcript	TCONS_00015615	0.32882473	0.018226	0.999966
Y73B3A.3	NA	transcript	TCONS_00046119	0.322853511	0.030521	0.999966
F10E7.2	WBGene00017344	transcript	TCONS_00006665	0.3195963	0.04689	0.999966
D2005.4	WBGene00008399	transcript	TCONS_00001257	0.292242944	0.031216	0.999966
mtm-3	WBGene00003476	transcript	TCONS_00014064	0.285715248	0.038985	0.999966

F11A10.5	WBGene00008686	transcript	TCONS_00019464	0.276162192	0.014348	0.999966
dlst-1	WBGene00020950	transcript	TCONS_00039818	0.275751858	0.03353	0.999966
F52D2.12	WBGene00219451	transcript	TCONS_00043161	0.267729713	0.045361	0.999966
ucr-2.1	WBGene00012158	transcript	TCONS_00045143	0.267069649	0.000379	0.338368
adr-2	WBGene00000080	transcript	TCONS_00014784	0.26369516	0.023349	0.999966
C13F10.6	WBGene00015745	transcript	TCONS_00039951	0.249431115	0.039032	0.999966
zip-1	WBGene00006986	transcript	TCONS_00013306	0.24419306	0.000391	0.338368
F27B3.5	NA	transcript	TCONS_00014635	0.219705085	0.029906	0.999966
dnj-25	WBGene00001043	transcript	TCONS_00042847	0.217036217	0.028272	0.999966
R08D7.5	WBGene00011145	transcript	TCONS_00012727	0.201236113	0.025693	0.999966
selb-1	NA	transcript	TCONS_00002221	0.196565959	0.013954	0.999966
set-26	WBGene00013106	transcript	TCONS_00033909	0.195379591	0.026328	0.999966
B0205.6	WBGene00015021	transcript	TCONS_00001866	0.187884937	0.049898	0.999966
fut-3	WBGene00006402	transcript	TCONS_00009207	0.163474947	0.032707	0.999966
emc-5	WBGene00195248	transcript	TCONS_00007585	0.163066383	0.024427	0.999966
math-33	WBGene00010406	transcript	TCONS_00036629	0.161994309	0.035765	0.999966
dpf-4	WBGene00001057	transcript	TCONS_00012115	0.154170485	0.022565	0.999966
sdz-27	WBGene00011124	transcript	TCONS_00019251	0.132836757	0.025735	0.999966
zig-7	WBGene00006984	transcript	TCONS_00000668	0.126111675	0.017533	0.999966
ptc-1	WBGene00004208	transcript	TCONS_00006855	0.125948211	0.027702	0.999966
F42A6.6	WBGene00018328	transcript	TCONS_00025681	0.116357956	0.030007	0.999966
crn-3	WBGene00000796	transcript	TCONS_00007385	0.111815052	0.045284	0.999966
Y48G8AL.10	WBGene00021689	transcript	TCONS_00002691	0.097467723	0.024067	0.999966
Y45F10D.7	WBGene00012887	transcript	TCONS_00020036	0.094399161	0.028954	0.999966
arp-11	WBGene00016793	transcript	TCONS_00027876	0.089729687	0.01539	0.999966
Y47G6A.14	WBGene00021640	transcript	TCONS_00002974	0.087148884	0.000613	0.45509
scrm-4	WBGene00008681	transcript	TCONS_00004716	0.076845336	3.75E-06	0.009735
ctl-3	WBGene00013220	transcript	TCONS_00011007	0.071959993	1.77E-05	0.029118
F32B6.3	WBGene00009320	transcript	TCONS_00028296	0.064267428	0.022443	0.999966
R05D3.2	WBGene00019877	transcript	TCONS_00012605	0.062601546	0.026092	0.999966
ZK418.5	WBGene00022734	transcript	TCONS_00014729	0.062560955	0.000207	0.239352
F55F10.1	WBGene00018898	transcript	TCONS_00016611	0.061576426	0.024748	0.999966
faah-4	WBGene00013232	transcript	TCONS_00015695	0.057956971	6.46E-09	3.35E-05
C14C11.2	WBGene00015766	transcript	TCONS_00035491	0.057951613	0.045849	0.999966
arx-6	WBGene00000204	transcript	TCONS_00011898	0.053914916	7.58E-06	0.015754
M05D6.2	WBGene00010875	transcript	TCONS_00006972	0.048176434	0.000476	0.380518
T24H7.2	WBGene00020781	transcript	TCONS_00006429	0.045977222	0.024317	0.999966
acdh-3	WBGene00019433	transcript	TCONS_00003586	0.039078117	0.03097	0.999966
F36A2.13	NA	transcript	TCONS_00004098	0.037068928	0.024054	0.999966
sup-17	WBGene00006324	transcript	TCONS_00001442	0.034755212	0.025715	0.999966

Table S2: Differentially expressed reproduction genes. Related to Figure S3.

RNA-seq identification of 61 genes differentially expressed between BPA and DMSO and belonging to the GO term "reproduction" GO:0000003.

F55F10.1, NFI-1, FOX-1, IFE-3, ARF-1.2, SGO-1, Y47G6A.14, TBA-4, EIF-3.I, B0205.6, E02H9.3, USP-39, R151.8, CSNK-1, THOC-2, AARS-1, HCP-1, DEPS-1, SOP-2, SOP-3, FZR-1, MET-2, C14C11.2, B0280.17, NOP-1, DNJ-22, Y45F10D.7, SYX-5, SIR-2.4, RNP-4, RPS-29, C06A5.3, PTC-1, KEL-8, TRA-3, F32B6.3, DLST-1, Y95D11A.3, KAL-1, F23H11.2, T08B2.5, LIN-66, LIN-37, RFP-1, R02D3.3, Y43E12A.3, UBC-12, KNL-3, MTM-3, RPOA-12, ZK858.7, UAF-2, F53E4.2, EGL-30, F11A10.5, UFD-2, W03F8.4, PQN-59, ARP-11, PRP-21, GLH-4

Table S3: Broad peak counts. Related to Figure 2 and S3.

Count of all identified broad peaks by MACS2 broad peak function

	H3K9me3	H3K27me3
water	3,740	19,810
DMSO	4,951	21,741
BPA	4,888	19,019

Table S4: ChIP-seq GO analysis. Related to Figure 2.

GO analysis of genes associated with a loss of H3K27me3

GO biological process complete	Reference gene list	Uploaded gene list	Expected gene count	Upload fold enrichment	P-value	FDR
Cellular response to unfolded protein (GO:0034620)	77	9	1.9	4.74	2.25E-04	2.58E-02
Steroid hormone mediated signaling pathway (GO:0043401)	280	19	6.91	2.75	1.27E-04	1.84E-02
Intracellular transport (GO:0046907)	382	22	9.43	2.33	3.98E-04	4.21E-02
Regulation of transcription, DNA-templated (GO:0006355)	935	47	23.08	2.04	8.54E-06	2.04E-03
Ion transport (GO:0006811)	724	35	17.87	1.96	2.47E-04	2.77E-02
Transmembrane transport (GO:0055085)	855	41	21.1	1.94	8.12E-05	1.35E-02
Organelle organization (GO:0006996)	1,150	50	28.38	1.76	1.94E-04	2.32E-02
Cellular macromolecule metabolic process (GO:0044260)	2,565	93	63.3	1.47	1.81E-04	2.27E-02
Nitrogen compound metabolic process (GO:0006807)	3,679	131	90.8	1.44	1.05E-05	2.30E-03

Table S5: Histone PTM quantitation. Related to Figure 2 and Figure 4.

Histone PTM level change following DMSO or BPA exposure following Luminex based multiplex quantitation assay

	H3K9me1	H3K9me2	H3K9me3	H3K27me2	H3K27me3	H3K36me3
DMSO	0.44 (6.2E-5)	0.11 (1.2E-4)	0.25 (9E-3)	0.13 (9.5E-3)	0.28 (2E-3)	0.28 (9.1E-4)
BPA	0.31 (9.9E-4)	0.08 (5.5E-3)	0.19 (1.9E-3)	0.06 (3.5E-3)	0.20 (8.7E-3)	0.31 (5.3E-3)
% change	-30.37	-33.41	-24.71	-56.27	-29.07	+8.40

CHAPTER 3

Transgenerational germline dysfunction caused by BPA exposure in *C. elegans*

Summary

BPA has been shown to alter the germline epigenome and cause reproductive dysfunction both directly at the F1 as well as transgenerationally at the F3 (Camacho *et al.,* 2018). Our aim is to further characterize the transgenerational effects of BPA on the germline machinery and identify the perturbations that cause the reproductive defects we had previously observed such increased embryonic lethality and germline apoptosis (Camacho *et al.,* 2018). Previous studies have shown that germline mechanisms can be directly perturbed by BPA exposure (Chen *et al.,* 2016; Allard and Colaiacovo, 2010). However, little is known about how BPA exposure can transgenerationally impair germline machinery and how these perturbations are inherited across generations. Here, our work focuses on characterizing the transgenerational effects of BPA exposure on checkpoint mechanisms and chromosome dynamics, while exploring the role epigenetics plays in the inheritance of these effects across generations.

Introduction

In sexually reproducing organisms, germ cell development is vital for the faithful transmission of the genome and epigenome across generations (Saitou, 2021). Haploid gametes are produced through the process of meiosis, a specialized cell division program that successfully generates germ cells that contain half of the original amount of genetic information (Hillers *et al.*, 2017). This process is highly regulated and controlled to ensure that gametes produced are viable and do not contain errors that may be passed on to future generations. During meiosis, chromosomes undergo homologous pairing, synapsis, and recombination during prophase I to ensure proper chromosome inheritance in gametes (Gerton and Hawley, 2005; Whitby M, 2005; Rog and Dernburg, 2013). Homologous pairing allows for homologous chromosomes to find each other which is vital for down-stream processes (MacQueen *et al.,* 2001). Once chromosomes have found their homologs, synapsis occurs in which the

synaptonemal complex (SC), a protein complex that physically tethers paired homologous chromosomes together during pachytene, is formed (Zickler and Kleckner, 2015; Bohr *et al*., 2016). This stabilizes pairing between homologs and results in the parallel orientation of each homologous pair from end to end, a prerequisite for crossover (CO) formation (Hillers *et al.*, 2017; MacQueen *et al.,* 2001). Recombination allows for the exchange of genetic material between homologous chromosomes and increasing genetic diversity during sexual reproduction (Gerton and Hawley, 2005; Whitby M, 2005). Thus, all three processes are tightly regulated and errors will lead to the activation of specific germline checkpoints that result in apoptosis (Pucci *et al.,* 2000; Gartner *et al*., 2008; Fausett *et al.,* 2021; Bhalla and Dernburg, 2005).

Environmental toxicant exposures can directly or indirectly affect the fidelity of these meiotic processes, with the possibility of effects being inherited across generations. Recent studies have shown that germ cell development is affected by different environmental toxicants, resulting in a decrease in germ cell health and number (Holm *et al.,* 2016; Mylchreest *et al.,* 2002; Uzumcu *et al.,* 2004; Anway *et al.,* 2005). BPA specifically has also been shown to affect these meiotic processes in models such as mice, monkey, as well as *C. elegans* (Susiarjo *et al.,* 2007; Hunt *et al.,* 2012; Allard and Colaiacovo, 2010). In addition, we had observed an increase in embryonic lethality and germline apoptosis as a result of BPA exposure, both directly at the F1 and transgenerationally at the F3 (Camacho *et al*., 2018). Therefore, we were interested in investigating how BPA affects these germline mechanisms and whether these effects are inherited across generations. In this chapter, we will exam BPA's transgenerational effects on germline function, with a focus on the synapsis and meiotic recombination processes.

Results

BPA intergenerationally and transgenerationally impairs chromosome segregation

In our previous work, BPA has been shown to cause reproductive dysfunction both directly at the F1 as well as transgenerationally at the F3. Specifically, we observed a significant

increase in embryonic lethality in BPA groups when compared to DMSO and water controls both at the F1 and F3. Embryonic lethality is reflective of a worm's progeny viability and increases suggest germline perturbations. One possibility for the observed increased embryonic lethality could be due to chromosomal missegregation in gametes which leads to embryos with an abnormal number of chromosomes or aneuploidies. To explore this possibility, we utilized a GFP tagged reporter strain *Pxol-1::gfp* (TY2441) that allows us to visualize the occurrence of aneuploidy in early embryos. In *C. elegans*, sex determination is defined by two X chromosomes resulting in hermaphrodite fate. However, in rare cases, missegregation of the X can result in embryos with just one X chromosome, leading to a male fate. Xol-1 is responsible for male development and turns on in male embryos (Kelly *et al.,* 2000; Allard *et al.,* 2013).

Thus, the observation of GFP+ embryos in xol-1::GFP worms post BPA exposure would suggest that BPA exposure causes missegregation of the X chromosome and aneuploidy in embryos. We exposed xol-1::GFP worms to BPA for 48 hours as previously described and assessed the incidence of GFP+ embryos both directly at the F1 and transgenerationally at the F3. We observed an increase, although not significantly, in the percentage of worms with at least one GPF+ embryo in the BPA treated groups as compared to the DMSO and water controls (Figure 1A and 1B: N=11, 30 worms per repeat, Two-way ANOVA with Bonferroni correction, *P<0.05). In addition, we also observed an increase in number of GFP+ embryos per worm in the BPA treated groups. This suggests that not only are there more individuals whose germline mechanisms are being perturbed by BPA exposure, but also that perturbations are more severe within individuals.

BPA does not transgenerationally increases apoptosis by perturbing the DNA damage checkpoint

In addition to BPA exposure transgenerationally increasing embryonic lethality, we also previously observed BPA exposure directly and transgenerationally increasing another metric

for germline dysfunction, apoptosis, which we validated with acridine orange staining of wild-type N2 at the F3 (Figure 2A, 2B: N=12, 22 worms per repeat, Two-way ANOVA with Bonferroni correction, ****P<0.0001). Apoptosis in the germline is a checkpoint response to errors in the meiotic process (Gartner *et al*., 2008; Fausett *et al.,* 2021; Bhalla and Dernburg, 2005). In *C. elegans*, increased germline apoptosis suggests either activation of the synapsis checkpoint or the DNA damage checkpoint (Gartner *et al*., 2008; Fausett *et al.,* 2021; Gartner *et al.,* 2000; Bhalla and Dernburg, 2005). In order to understand whether BPA exposure affects either or both checkpoint mechanisms, we used mutants for genes crucial for each checkpoint. First, we investigated whether the increase in apoptosis could be due to an activation of the DNA damage checkpoint. By exposing mutants of the DNA damage checkpoint genes to BPA, we analyzed whether or not BPA exposure continues to increase apoptosis at the F3. If BPA-induced increase in apoptosis persists, that suggests that BPA's effects are not mediate through the DNA damage checkpoint; however, if BPA's transgenerational apoptotic increase is abrogated, that would then suggest that BPA's effects are mediated through the DNA damage checkpoint.

We tested mutants for two different DNA damage checkpoint mechanism genes, *spo-11* and *cep-1*. SPO-11 is a conserved enzyme that begins the recombination process by introducing double-strand breaks (DSBs) (Dernburg *et al.,* 1998). SPO-11's activity is tightly regulated to ensure that breaks are induced in a specific manner that controls for number, timing, and distribution of DSBs (Hillers *et al.*, 2017). These breaks are then resected into single-stranded DNA and repaired through homologous recombination with the formation of six obligate crossovers (CO) per nucleus (Lemmens and Tijsterman, 2011). Failure at any step of this process results in activation of the DNA damage checkpoint and apoptosis (Gartner *et al.,* 2000). Here, we utilized mutant worms homozygous for the *spo-11* deletion which display an array of phenotypes indicating errors of meiotic chromosome segregation, but specifically, they lack *spo-11* dependent apoptosis (Dernburg *et al.,* 1998). We exposed a *spo-11* balanced strain

(AV157) to BPA at P0, and performed acridine orange staining at the F3 to assess for changes in the number of apoptotic nuclei per gonad. This strain carries a balancer that contains a pharyngeal GFP and a homozygous lethal mutation which allows us to distinguish between *spo-11* homozygotes and heterozygotes. Maintenance of the heterozygotes will result in a quarter of the population being *spo-11* homozygotes, a half being heterozygotes (which we will use as a control), and the last quarter will not survive. Staining with acridine orange to visualize apoptotic nuclei in the germline of the F3 *spo-11* homozygous mutants revealed that apoptosis induced by transgenerational BPA exposure was not rescued in homozygous mutants compared to heterozygotes (Figure 2C and 2D: N=6, 22 worms per repeat, Two-way ANOVA with Bonferroni correction, *P<0.05, **P<0.01, ****P<0.0001). This suggests that BPA's transgenerational increase in apoptosis is not mediated through the DNA damage checkpoint.

To further confirm that BPA's transgenerational apoptotic increase is not due to an activation of the DNA damage checkpoint, we repeated the apoptosis assay using a different DNA damage checkpoint mutant, *cep-1*. The *C. elegans* homolog of the p53 tumor suppressor, *cep-1*, has been shown to be required for regulating apoptosis in response to DNA damage and meiotic recombination failure in the germline (Schumacher *et al.,* 2001). Similarly to *spo-11*, exposure of a *cep-1* balanced strain (CV63) acridine orange staining in F3 *cep-1* homozygous mutants showed that the BPA-induced transgenerational increase in number of apoptotic nuclei per gonad was not rescued in homozygous mutants compared to heterozygotes (Figure 2E: N=8, 22 worms per repeat, Two-way ANOVA with Bonferroni correction, *P<0.05, **P<0.01, ***P<0.001, ****P<0.0001). This further supports the notion that BPA's transgenerational increase in apoptosis is not mediated through the DNA damage checkpoint.

BPA transgenerationally increases apoptosis by perturbing the synapsis checkpoint, not the DNA damage checkpoint

Since *spo-11* and *cep-1* mutants failed to rescue BPA's transgenerational apoptotic effects, we next explored whether the increased germline apoptosis could be from the activation of the synapsis checkpoint. Similarly to the *spo-11* and *cep-1* experiments, by exposing mutants of the synapsis checkpoint genes to BPA, we analyzed whether or not BPA exposure continues to increase apoptosis at the F3. If BPA-induced increase in apoptosis persists, that suggests that BPA's effects are not mediate through the synapsis checkpoint; however, if BPA's transgenerational apoptotic increase is abrogated, then that would suggest that BPA's effects are mediated through the synapsis checkpoint. PCH-2 has been shown to be required for the activation of apoptosis due to synaptic failure (Bhalla and Dernburg, 2005). To this end, we exposed *pch-2* mutants (CA388) to BPA and monitored germline apoptosis at the F3. Acridine orange staining in F3 *pch-2* homozygous mutants showed that the BPA-induced transgenerational increase in number of apoptotic nuclei per gonad was successfully rescued in homozygous mutants compared to heterozygotes (Figure 2F and 2G: N=6, 22 worms per repeat, Two-way ANOVA with Bonferroni correction, ****P<0.0001). This suggests that BPA exposure transgenerationally increases apoptosis through the activation of the synapsis checkpoint at the F3.

Aberrant synapsis induced by transgenerational BPA exposure correlates with decreased reproductive function

Since BPA's transgenerational increase in apoptosis was induced by the activation of the synapsis checkpoint, we next explored which parts of synapsis might be perturbed by transgenerational BPA exposure. A hallmark of synapsis is the formation of the synaptonemal complex (SC) which consists of four different SYP proteins (SYP-1, SYP-2, SYP-3, SYP-4) that make the central region and four HORMA-domain proteins (HIM-3, HTP-1, HTP-2, HTP-3) that comprise the axial elements between paired homologous chromosomes (Schild-Prufert *et al*., 2011). This protein structure functions to physically tether the homologs together and is required

for proper chromosome segregation (Hillers *et al.*, 2017; MacQueen *et al.,* 2001). Studies have shown that SC components including SYP-3, HTP-3, HIM-3, and HTP-1 are required for functional synapsis checkpoint and that proper SC assembly is monitored by the synapsis checkpoint (Bohr *et al*., 2016). Therefore, we hypothesized that activation of the synapsis checkpoint by ancestral BPA exposure could be in response to errors in SC assembly. We visualized the SC using a SYP-3::GFP strain (CA1218) that was transgenerationally exposed to BPA and observed SYP-3 aggregates which we characterized into two groups: punctae and halo at the F3 (Figure 3A: N=3, 4-6 worms per repeat). Analysis of the incidence of each SYP-3 group (normal, punctae, or halo) indicated that F3 worms that were ancestrally exposed to BPA had a higher incidence of germlines that contained punctae SYP-3 aggregates as compared to water or DMSO (Figure 3B: N=3, 4-6 worms per repeat). Additionally, fertility analysis of these characterized worms showed a correlation between embryonic lethality and aggregate state (Figure 3B: N=3, 4-6 worms per repeat). Together, this suggests that ancestral BPA exposure causes an abnormal aggregation of SYP-3, one of the SYP proteins that is crucial for the formation of the SC, which may be what is triggering the synapsis checkpoint and resulting in an increase in apoptosis. Furthermore, this aggregation also correlates with increased embryonic lethality which we had previously observed at the F3 due to ancestral BPA exposure (Camacho *et al*., 2018).

BPA's transgenerational increase in apoptosis is mediated through *jmjd-1.2*

Previously, we had shown that ancestral BPA exposure decreases H3K9me3 and H3K27me3 levels in the F3 germline and that *jmjd-2* and *jmjd-3/utx-1* demethylases are required for the BPA-induced transgenerational increase in embryonic lethality and desilencing effects (Camacho *et al*., 2018). Therefore, we were interested in exploring whether BPA's transgenerational increase in apoptosis is also mediated through histone modifications. Previously, we had identified through RNA-seq of extracted germlines that ancestral BPA

exposure causes a significant up-regulation of the histone demethylase *jmjd-1.2* (Camacho *et al*., 2018). It has also been previously shown that JMJD-1.2 controls multiple histone post-translation modifications including histone 3 lysine 9, lysine 23, and lysine 27 di-methylation (H3K9/K23/K27me2) in meiotic cells (Myers *et al.*, 2018). To explore the possible role of *jmjd-1.2* in mediating BPA's effects, we exposed the *jmjd-1.2* mutant (FX03713) to BPA and compared it to BPA's apoptotic effects in wild-type N2 worms. Exposure of N2 worms to BPA caused both an intergenerational at F1 and transgenerational at F3 increase in number of apoptotic nuclei per gonad. Interestingly, ancestral BPA exposure fails to increase apoptosis in jmjd-1.2 mutants both at the F1 and the F3 (Figure 4A and 4B: N=6, 20 worms each, Two-way ANOVA with Bonferroni correction, ****P<0.0001). Upon analysis of another metric for reproductive function, embryonic lethality, we identify a similar trend with BPA transgenerationally increasing embryonic lethality in wild-type worms, but failing to do so in *jmjd-1.2* mutants (Figure 4C: N=3, 2-3 worms each, Two-way ANOVA with Bonferroni correction, *P<0.05, ***P<0.001). Together, this suggests that BPA-induced reproductive dysfunction is transgenerationally inherited through histone modifications.

Conclusions and future directions

BPA exposure has been shown previously to affect fertility both directly at the F1 as well as transgenerationally at the F3 (Camacho *et al.*, 2018). While we had identified histone modifications to be the mechanism of inheritance of these transgenerational reproductive effects, how BPA affects germline mechanisms is unknown. Increases in embryonic lethality suggests possible chromosomal errors in embryos. This led us to explore chromosome mis-segregation using the xol-1::GFP worms through which we identified a higher incidence of F3 worms containing embryos with aneuploidies in those that were ancestrally exposed to BPA as compared to DMSO or water (Figure 1A). Interestingly, we also observed an increase in the incidence of embryos containing aneuploidies per worm in the BPA treated groups (Figure 1B).

This suggests that not only are there more individuals whose germline mechanisms are being perturbed by ancestral BPA exposure, but also that perturbations are more severe within individuals themselves.

Since we had previously shown that ancestral BPA exposure caused an apoptotic increase transgenerationally at the F3, we next explored the basis for this increase. In *C. elegans*, increase in apoptosis can be due to an activation of the synapsis or DNA damage checkpoints. Here, we identify BPA's transgenerational apoptotic increase to be due to an activation of the synapsis checkpoint, not the DNA damage checkpoint (Figure 2). We further analyzed a component of the synaptonemal complex and saw not only that ancestral BPA exposure cause an abnormal aggregation of SYP-3, but also that the SYP-3 aggregates correlated with increased embryonic lethality (Figure 3A and 3B). Moving forward, we propose to take a closer look at other components of the SC including SYP-1, SYP-2, and SYP-4, to identify whether aggregation is unique to SYP-3 or if there is a general aggregation of SC proteins. In addition, we would be interested in exploring the identity of these SYP-3 aggregates. Interestingly, studies have shown that the SC has liquid crystalline properties and can form polycomplexes, three-dimensional lattices that recapitulate the structure of SCs but do not associate closely with chromosomes (Goldstein P., 1987; Rog et al., 2017). Due to their similarities, we hypothesize that the SYP-3 aggregates we observed due to ancestral BPA exposure are actually polycomplexes. Since studies have shown that polycomplexes can be dissolved by 1,6-hexanediol, we propose to test our hypothesize by exposing our F3 worms to 1,6-hexanediol in order to see whether SYP-3 aggregates rapidly dissolve as well. If they do, this would suggest that BPA transgenerationally induces polycomplex formation at the F3.

Lastly, since we had shown that ancestral BPA exposure decreases H3K9me3 and H3K27me3 levels in the F3 germline and that *jmjd-2* and *jmjd-3/utx-1* demethylases are required for the BPA-induced transgenerational increase in embryonic lethality and desilencing effects (Camacho *et al.*, 2018), we were interested in exploring whether BPA's

transgenerational increase in apoptosis is also mediated through histone modifications. Using a *jmjd-1.2* mutant, we discovered that BPA's transgenerational increase in both apoptosis and embryonic lethality are mediated through histone modifications. However, since JMJD-1.2 controls multiple histone post-translation modifications including histone 3 lysine 9, lysine 23, and lysine 27 di-methylation (H3K9/K23/K27me2) in meiotic cells (Myers *et al.*, 2018), it would be interesting to explore the possible interactions between each of these histone marks with components of the SC. To do this, we propose to use immunofluorescence to visualize the colocalization of these histone marks with different SYP proteins. We hypothesize that these histone marks may function as signals for proper SC loading between homologous chromosomes. However, because BPA exposure has been shown to disrupt histone modifications, we hypothesize that this in turn disrupts SC formation and results in polycomplexes.

Together, our findings being to tell a story about the potential mechanism by which BPA induces transgenerational reproductive dysfunction and a model begins to appear. We observed that BPA exposure transgenerationally impairs SC formation and induces SYP aggregation at the F3. This aggregation triggers the synapsis checkpoint which then increases germline apoptosis. However, not all of the nuclei with SC errors are caught by the synapsis checkpoint which results in embryos with aneuploidies, since it has been shown that synapsis is vital to ensure proper chromosome segregation in gametes. This in turn manifests as increased embryonic lethality. Since it has been previously shown that gametes inherit not only the genome but also the epigenome from the parents and we had previously shown that BPA's transgenerational effects are mediated through histone demethylase activity, it is possible that there might be a connection between histone marks and SC formation. This would suggest that BPA's transgenerational effects are due to a reduction and redistribution of histone modifications at the P0 that is inherited across generations. This in turn impairs SC formation and results in the observed reproductive dysfunction. Thus, assessment of the influence of

epigenetic marks on SC proteins will be vital in our understanding of how BPA induces transgenerational reproductive defects.

Experimental Procedures

Culture conditions and strains

Standard methods of culturing and handling of *C. elegans* were followed (Stiernagle T. 2006). Worms were maintained on nematode growth medium (NGM) plates streaked with OP50 E. coli. Strains used in this chapter were obtained from the *C. elegans* Genetics Center (CGC) and others include the following: TY2441 (yls34 (Pxol-1::GFP+rol-6 (pRF4)), AV157 (spo-11 (me44)/nT1 [unc-?(n754) let-? qls50] (IV;V)), CV63 (cep-1 (Ig12501) I / hT2 (gIs48) I;III), CA388 (pch-2 (tm1458) II), CA1218 (ieSiII[EmGFP-SYP-3; C6-UAC-119]; syp-3 (OK758)), FX03713 (jmjd-1.2 (tm3713)).

Chemical exposure protocol

The exposure was performed as described in Lundby *et al.,* 2016. BPA was obtained from Sigma Aldrich and dissolved in DMSO to a stock concentration of 100mM. Worms were synchronized by bleaching an adult population of either strains, plating the eggs, and allowing the population to reach L4 larval stage (50-52 hours). L4 worms were then exposed for 48 hours. After 48 hours, they 20 P0 adult hermaphrodites were transferred to new NGM plates to lay F1 eggs for 2 hours. Populations were maintained as per the conditions of each specific strain and adult F1 and F3 hermaphrodites were analyzed.

Chromosome missegregation/aneuploidy assay

TY2441 (Pxol-1::GFP) worms were synchronized and exposed at P0 to 100uM BPA following protocol above. L4 larvae worms were isolated and analysis was performed 16-20 hours post-L4 at F1 and F3 generations after direct exposures at P0. Worms were scored for GFP positive embryo expression using a Nikon H600L microscope at 40X magnification.

Apoptosis assay

Apoptosis assay was performed by Acridine Orange staining on synchronized adult hermaphrodites collected at 20-24 hours post-L4 at F1 and F3 generations after direct exposures at P0 as previously described (Allard and Colaiacovo, 2011; Chen *et al.,* 2016).

SYP-3::GFP aggregation status analysis

CA1218 (syp-3 (OK758)) worms were synchronized and exposed at P0 to 100uM BPA following protocol above. F3 worms were selected at L4 stage and placed overnight at 20°C. They were then collected at 24 hours post-L4 stage and dissected in 15µl of M9. Excess liquid was removed and 15µl of Hoechst 33342 (12.3 mg/mL) was added to a final concentration of 5µg/ml. Slides are covered with a cover slip and placed in a dark box to settle for about 20-25 min while prepping the second slide. They were then imaged on an Eclipse Ni-E microscope (Nikon) and a cooled CCD camera (model CoolSNAP HQ, Photometrics) controlled by the NIS Elements AR system (Nikon).

Embryonic lethality assessment

After the 48-hour exposure, P0 worms were maintained until the F3. F3 L4s were singled out and moved into individual 33mm plates. Embryonic lethality was performed by monitoring the number of embryos produced each day and the subsequent larvae hatched from these embryos for each individual worm starting from L4 through the end of its reproductive lifespan. Embryonic lethality is calculated by the number of embryos that fail to hatch over the total number of embryos multiplied by 100. This was monitored for 72 hours post L4, after which the day 3 hermaphrodite were analyzed for SYP-3 aggregate status following the protocol described above.

Statistical Analyses

For multi-group comparisons, two-way ANOVA with Bonferroni correction was used.

Figure 1

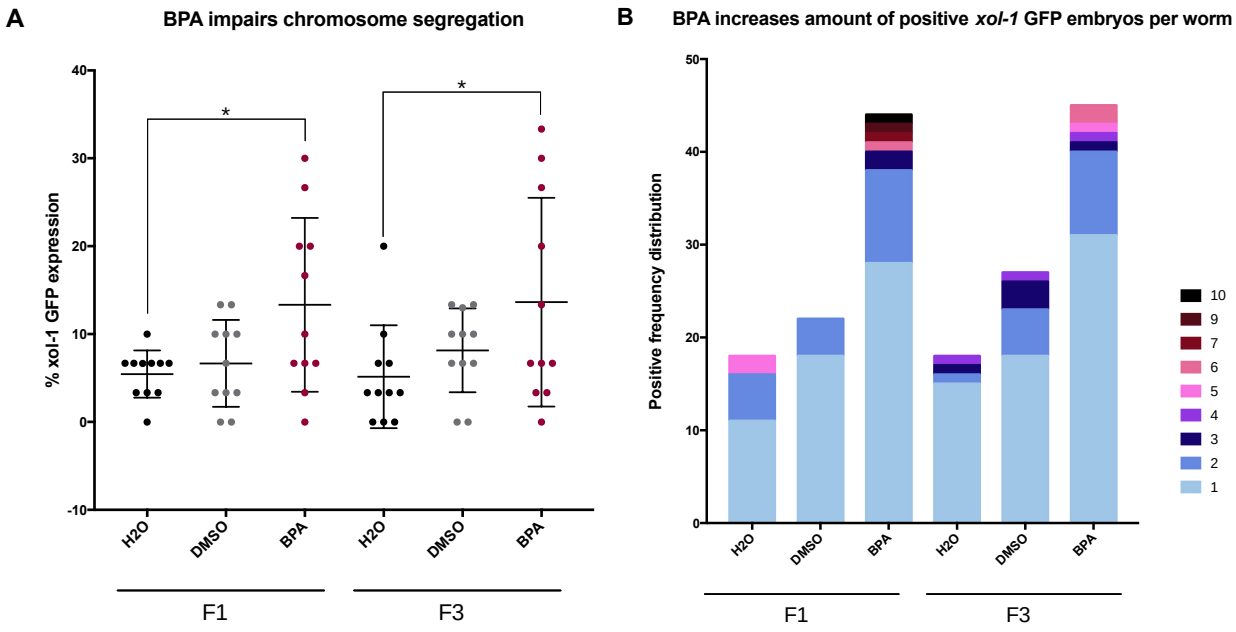

Figure 1: BPA exposure impairs chromosome segregation and induces aneuploidies at both the F1 and F3

P0 hermaphrodites were exposed to water (black), DMSO (grey), or BPA (red). Out of 30 total worms per repeat, the percent (%) of worms with at least 1 GFP+ embryo was recorded at F1 and F3 (a). Number of GFP+ embryos per worm was also recorded at F1 and F3 (b). N=11, 30 worms per repeat. Two-way ANOVA with Bonferroni correction. *P<0.05

Figure 2

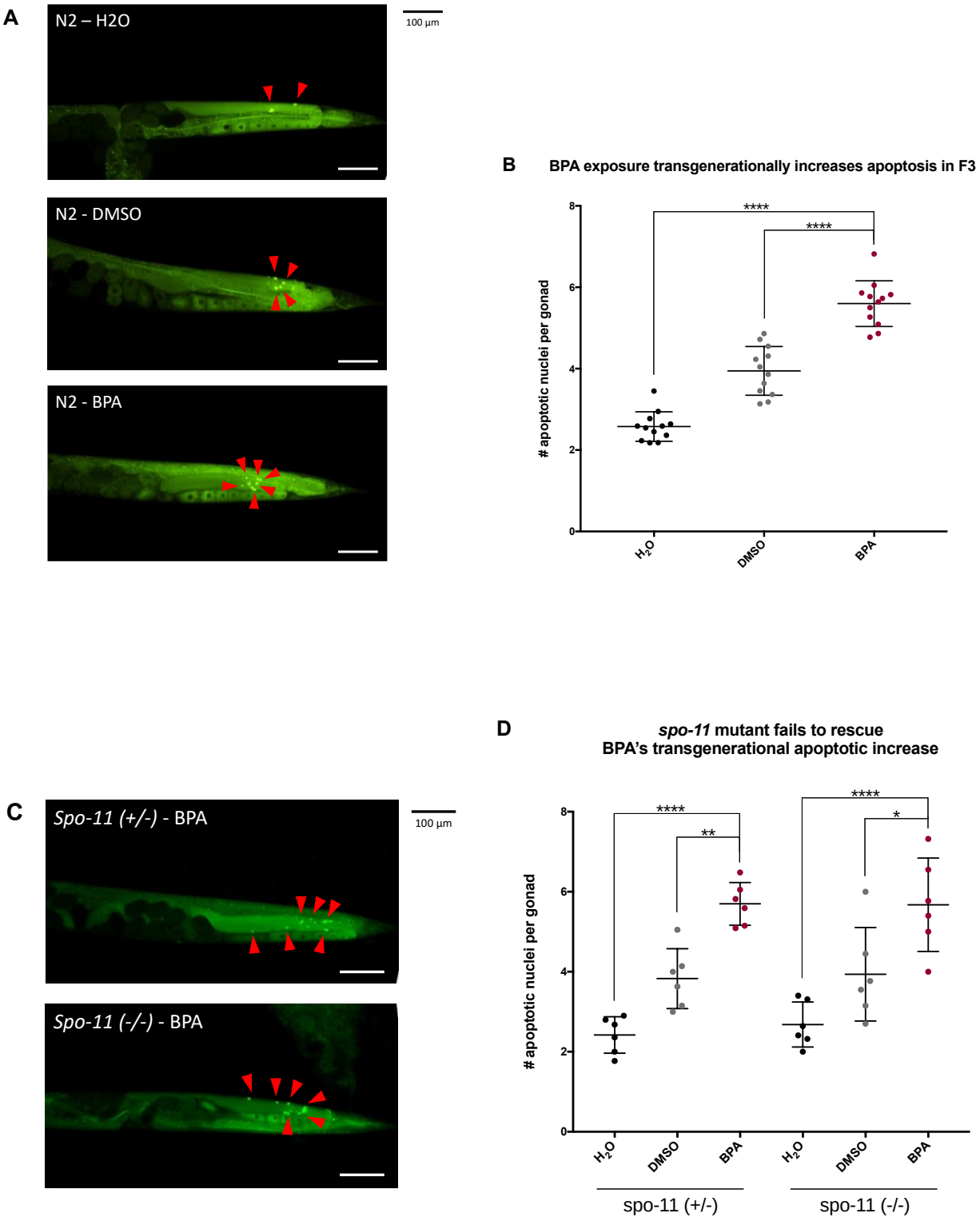
A
N2 – H2O
100 µm
N2 - DMSO
N2 - BPA
B
BPA exposure transgenerationally increases apoptosis in F3
apoptotic nuclei per gonad
****
****
H2O
DMSO
BPA
C
Spo-11 (+/-) - BPA
100 µm
Spo-11 (-/-) - BPA
D
spo-11 mutant fails to rescue
BPA's transgenerational apoptotic increase
apoptotic nuclei per gonad
****
**
****
*
H2O
DMSO
BPA
H2O
DMSO
BPA
spo-11 (+/-)
spo-11 (-/-)

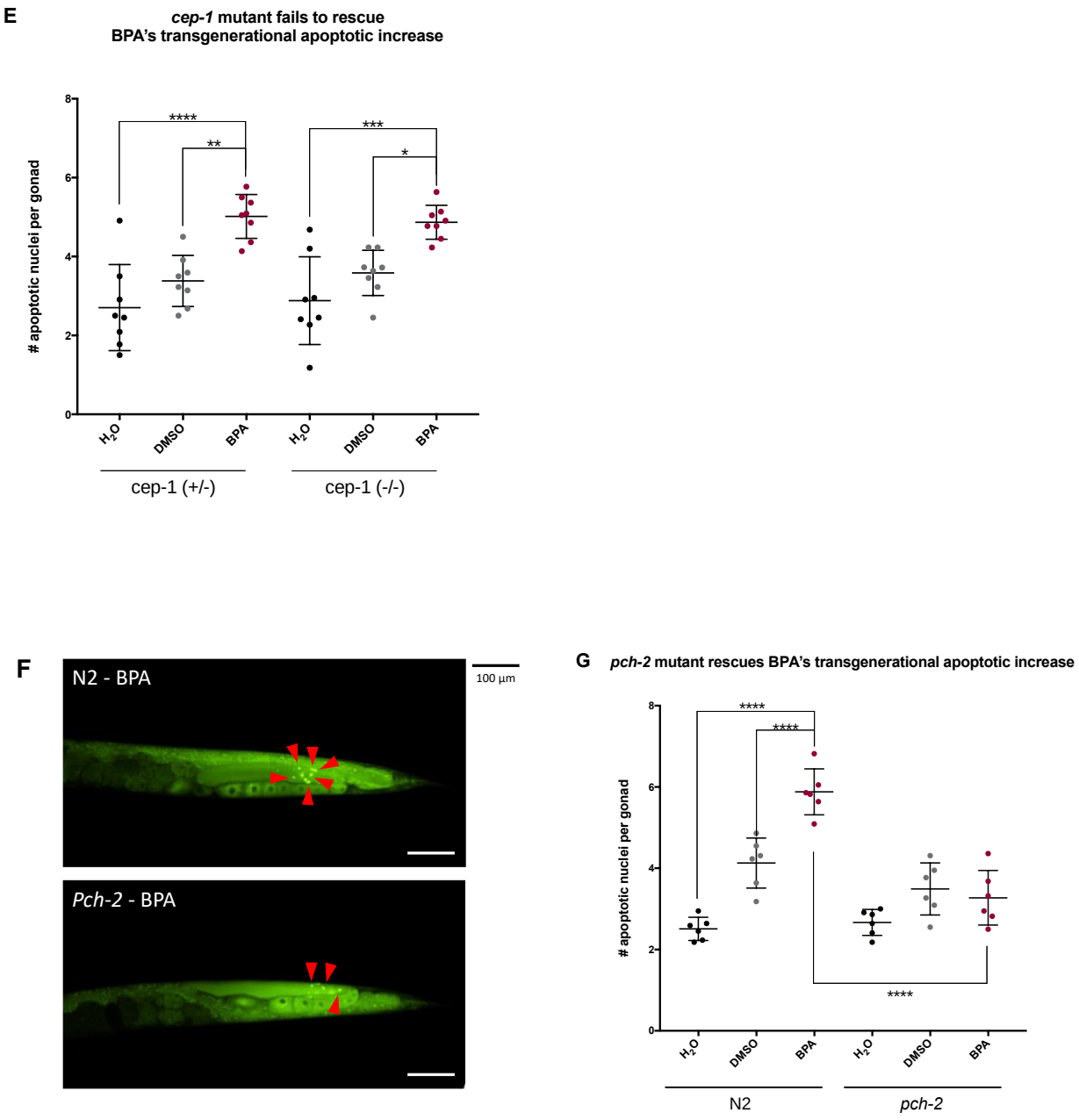

Figure 2: BPA transgenerationally increases apoptosis by perturbing the synapsis checkpoint, not the DNA damage checkpoint

P0 hermaphrodites were exposed to water (black), DMSO (grey), or BPA (red). Number of apoptotic nuclei per gonadal arm was assessed at F3 for wild-type N2 (a-b), DNA damage checkpoint mutants *spo-11* (c-d) and *cep-1* (e), and synapsis checkpoint mutant *pch-2* (f-g). N=6-12, 22 worms per repeat. Two-way ANOVA with Bonferroni correction.
*P<0.05, **P<0.01, ***P<0.001, ****P<0.0001

Figure 3

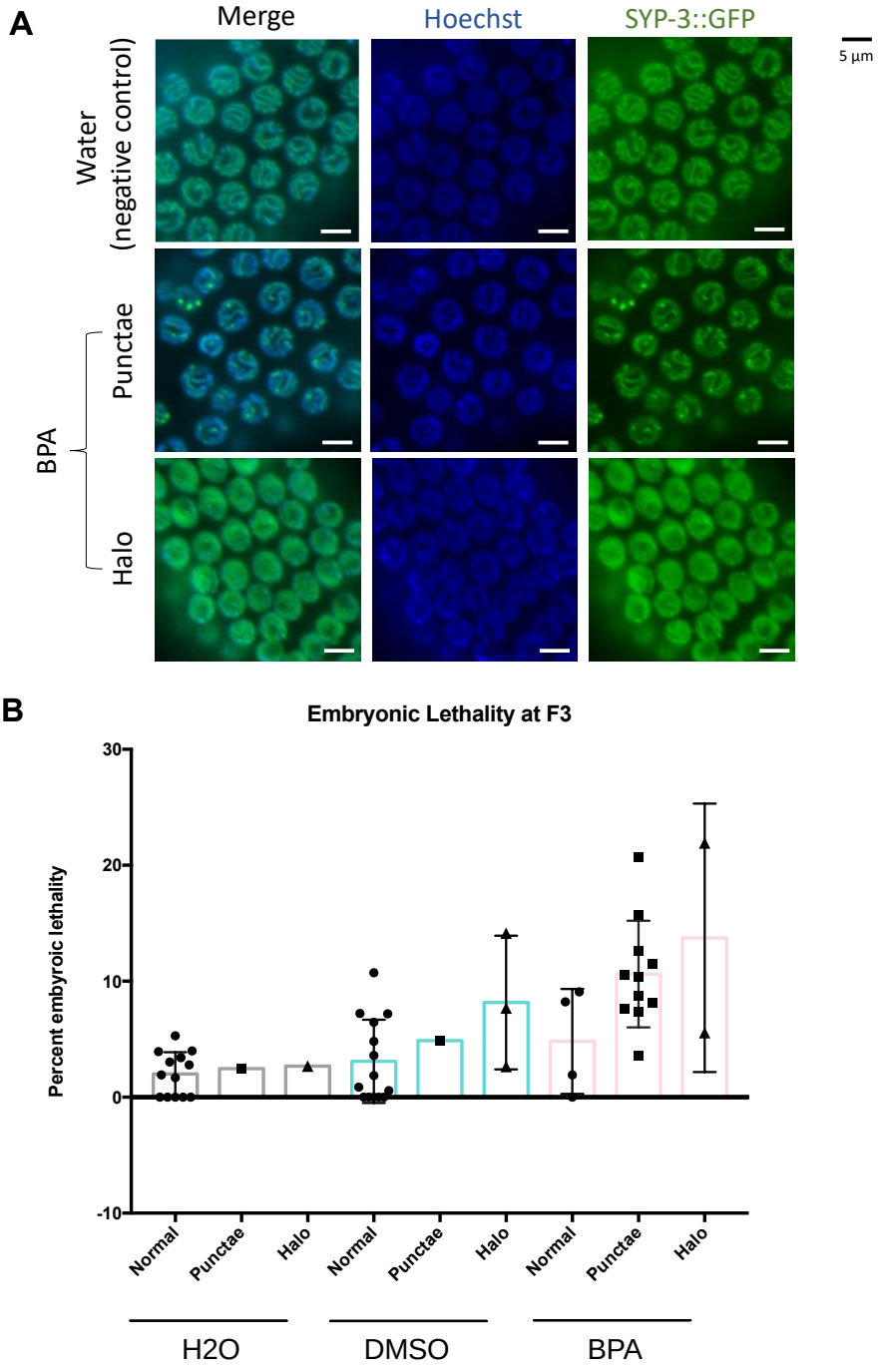

Figure 3: Aberrant synapsis induced by transgenerational BPA exposure correlates with decreased reproductive function

P0 hermaphrodites were exposed to water (grey), DMSO (blue), or BPA (pink). SYP-3::GFP expression was visualized at F3 (a). Percent embryonic lethality per worm was measured at F3 and the corresponding SYP-3::GFP status was assessed (b). N=4, 3-6 worms per repeat.

Figure 4

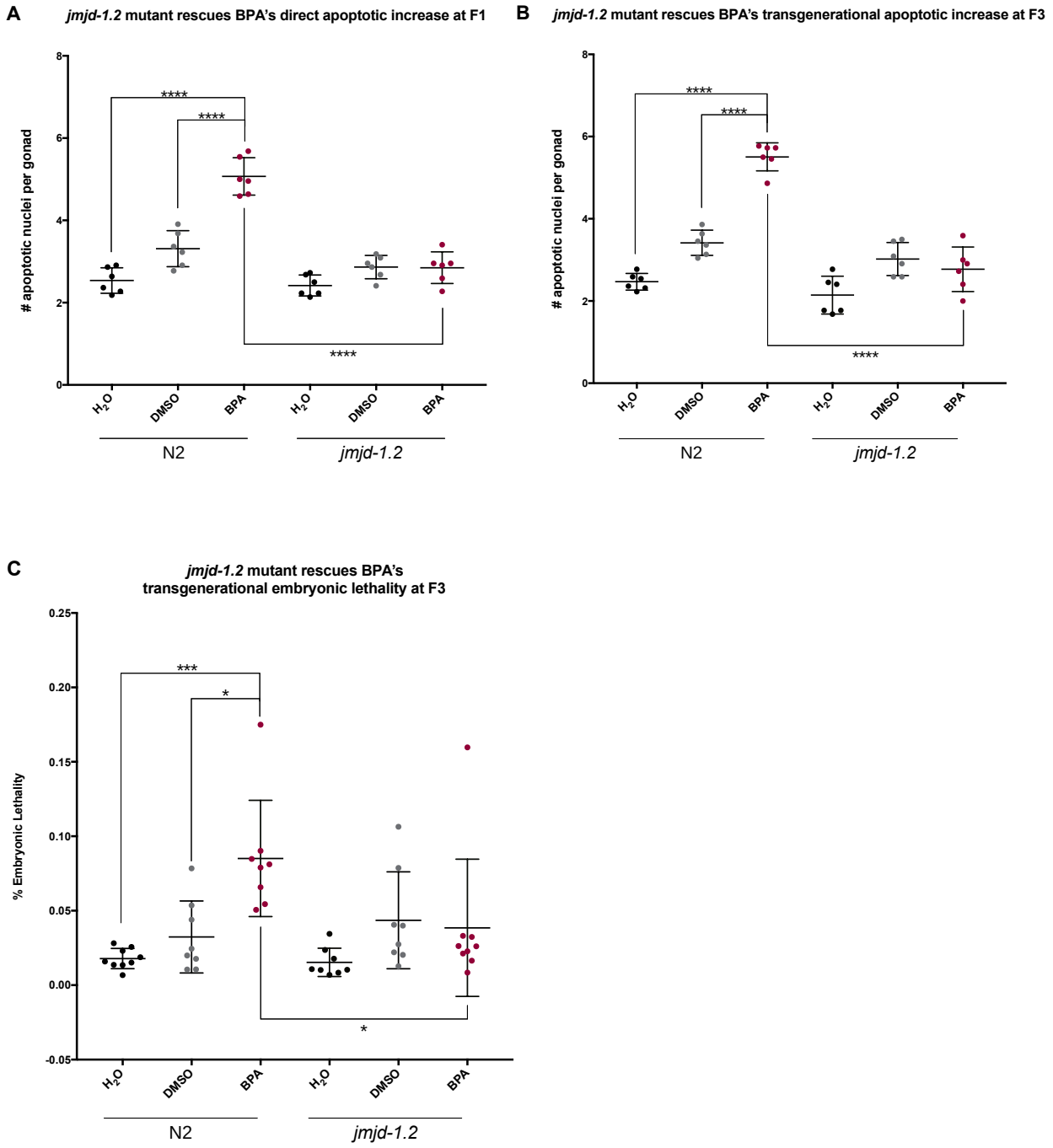

Figure 4: BPA's apoptotic increase and embryonic lethality is rescued by *jmjd-1.2*

P0 hermaphrodites were exposed to water (black), DMSO (grey), or BPA (red). Number of apoptotic nuclei per gonadal arm was assessed at F1 (a) or F3 (b). N=6, 22 worms per repeat. Percent embryonic lethality per worm was measured for F3 (c). N=3, 2-3 worms pre repeat. Two-way ANOVA with Bonferroni correction. *P<0.05, **P<0.01, ***P<0.001, ****P<0.0001

References

Allard, P., & Colaiácovo, M. P. (2010). Bisphenol A impairs the double-strand break repair machinery in the germline and causes chromosome abnormalities. *Proceedings of the National Academy of Sciences of the United States of America*, *107*(47), 20405–20410. https://doi.org/10.1073/PNAS.1010386107

Allard, P., & Colaiácovo, M. P. (2011). Mechanistic insights into the action of Bisphenol A on the germline using C. elegans. *Cell Cycle (Georgetown, Tex.)*, *10*(2), 183–184. https://doi.org/10.4161/CC.10.2.14478

Allard, P., Kleinstreuer, N. C., Knudsen, T. B., & Colaiácovo, M. P. (2013). A C. elegans screening platform for the rapid assessment of chemical disruption of germline function. *Environmental Health Perspectives*, *121*(6), 717–724. https://doi.org/10.1289/EHP.1206301

Anway, M. D., Cupp, A. S., Uzumcu, N., & Skinner, M. K. (2005). Epigenetic transgenerational actions of endocrine disruptors and male fertility. *Science (New York, N.Y.)*, *308*(5727), 1466–1469. https://doi.org/10.1126/SCIENCE.1108190

Bhalla, N., & Dernburg, A. F. (2005). Cell biology: A conserved checkpoint monitors meiotic chromosome synapsis in Caenorhabditis elegans. *Science*, *310*(5754), 1683–1686. https://doi.org/10.1126/SCIENCE.1117468/SUPPL_FILE/BHALLA_SOM.PDF

Bohr, T., Ashley, G., Eggleston, E., Firestone, K., & Bhalla, N. (2016). Synaptonemal complex components are required for meiotic checkpoint function in caenorhabditis elegans. *Genetics*, *204*(3), 987–997. https://doi.org/10.1534/GENETICS.116.191494/-/DC1

Camacho, J., Truong, L., Kurt, Z., Chen, Y. W., Morselli, M., Gutierrez, G., Pellegrini, M., Yang, X., & Allard, P. (2018). The Memory of Environmental Chemical Exposure in C. elegans Is Dependent on the Jumonji Demethylases jmjd-2 and jmjd-3/utx-1. *Cell Reports*, *23*(8), 2392–2404. https://doi.org/10.1016/j.celrep.2018.04.078

Chen, Y., Shu, L., Qiu, Z., Lee, D. Y., Settle, S. J., Que Hee, S., Telesca, D., Yang, X., & Allard, P. (2016). Exposure to the BPA-Substitute Bisphenol S Causes Unique Alterations of Germline Function. *PLOS Genetics*, *12*(7), e1006223. https://doi.org/10.1371/JOURNAL.PGEN.1006223

Dernburg, A. F., McDonald, K., Moulder, G., Barstead, R., Dresser, M., & Villeneuve, A. M. (1998). Meiotic recombination in C. elegans initiates by a conserved mechanism and is dispensable for homologous chromosome synapsis. *Cell*, *94*(3), 387–398. https://doi.org/10.1016/S0092-8674(00)81481-6

Fausett, S., Poullet, N., Gimond, C., Vielle, A., Bellone, M., & Braendle, C. (2021). Germ cell apoptosis is critical to maintain Caenorhabditis elegans offspring viability in stressful environments. *PLOS ONE*, *16*(12), e0260573. https://doi.org/10.1371/JOURNAL.PONE.0260573

Gartner, A., Boag, P. R., & Blackwell, T. K. (2008). Germline survival and apoptosis. *WormBook : The Online Review of C. Elegans Biology*, 1–20. https://doi.org/10.1895/WORMBOOK.1.145.1

Gartner, A., Milstein, S., Ahmed, S., Hodgkin, J., & Hengartner, M. O. (2000). A Conserved Checkpoint Pathway Mediates DNA Damage–Induced Apoptosis and Cell Cycle Arrest in C. elegans. *Molecular Cell*, *5*(3), 435–443. https://doi.org/10.1016/S1097-2765(00)80438-4

Gerton, J. L., & Hawley, R. S. (2005). Homologous chromosome interactions in meiosis: diversity amidst conservation. *Nature Reviews. Genetics*, *6*(6), 477–487. https://doi.org/10.1038/NRG1614

Goldstein, P. (1987). Multiple synaptonemal complexes (polycomplexes): origin, structure and function. *Cell Biology International Reports*, *11*(11), 759–796. https://doi.org/10.1016/0309-1651(87)90157-3

Holm, J. B., Mazaud-Guittot, S., Danneskiold-Samsøe, N. B., Chalmey, C., Jensen, B., Nørregård, M. M., Hansen, C. H., Styrishave, B., Svingen, T., Vinggaard, A. M., Koch, H. M., Bowles, J., Koopman, P., Jégou, B., Kristiansen, K., & Kristensen, D. M. (2016). Intrauterine Exposure to Paracetamol and Aniline Impairs Female Reproductive Development by Reducing Follicle Reserves and Fertility. *Toxicological Sciences : An Official Journal of the Society of Toxicology*, *150*(1), 178–189. https://doi.org/10.1093/TOXSCI/KFV332

Hunt, P. A., Lawson, C., Gieske, M., Murdoch, B., Smith, H., Marre, A., Hassold, T., & VandeVoort, C. A. (2012). Bisphenol A alters early oogenesis and follicle formation in the fetal ovary of the rhesus monkey. *Proceedings of the National Academy of Sciences of the United States of America*, *109*(43), 17525–17530. https://doi.org/10.1073/PNAS.1207854109

Kelly, K. O., Dernburg, A. F., Stanfield, G. M., & Villeneuve, A. M. (2000). *Caenorhabditis elegans msh-5 Is Required for Both Normal and Radiation-Induced Meiotic Crossing Over but Not for Completion of Meiosis*.

KJ, H., V, J., E, M.-P., & JL, Y. (2017). Meiosis. *WormBook : The Online Review of C. Elegans Biology*, *2017*(3700), 433–434. https://doi.org/10.1895/WORMBOOK.1.178.1

Klosin, A., Casas, E., Hidalgo-Carcedo, C., Vavouri, T., & Lehner, B. (2017). Transgenerational transmission of environmental information in C. elegans. *Science (New York, N.Y.)*, *356*(6335), 320–323. https://doi.org/10.1126/SCIENCE.AAH6412

Lemmens, B. B. L. G., & Tijsterman, M. (2011). DNA double-strand break repair in Caenorhabditis elegans. *Chromosoma*, *120*(1), 1. https://doi.org/10.1007/S00412-010-0296-3

Lundby, Z., Camacho, J., & Allard, P. (2016). Fast Functional Germline and Epigenetic Assays in the Nematode Caenorhabditis elegans. *Methods in Molecular Biology (Clifton, N.J.)*, *1473*, 99–107. https://doi.org/10.1007/978-1-4939-6346-1_11

MacQueen, A. J., & Villeneuve, A. M. (2001). Nuclear reorganization and homologous chromosome pairing during meiotic prophase require C. elegans chk-2. *Genes & Development*, *15*(13), 1674–1687. https://doi.org/10.1101/GAD.902601

Myers, T. R., Amendola, P. G., Lussi, Y. C., & Salcini, A. E. (2018). JMJD-1.2 controls multiple histone post-translational modifications in germ cells and protects the genome from replication stress. *Scientific Reports 2018 8:1*, *8*(1), 1–11. https://doi.org/10.1038/s41598-018-21914-9

Mylchreest, E., Sar, M., Wallace, D. G., & Foster, P. M. D. (2002). Fetal testosterone insufficiency and abnormal proliferation of Leydig cells and gonocytes in rats exposed to di(n-butyl) phthalate. *Reproductive Toxicology (Elmsford, N.Y.)*, *16*(1), 19–28. https://doi.org/10.1016/S0890-6238(01)00201-5

Pucci, B., Kasten, M., & Giordano, A. (2000). Cell Cycle and Apoptosis. *Neoplasia (New York, N.Y.)*, *2*(4), 291. https://doi.org/10.1038/SJ.NEO.7900101

Rog, O., & Dernburg, A. F. (2013). Chromosome pairing and synapsis during C. elegans meiosis. *Current Opinion in Cell Biology*, *25*(3), 349. https://doi.org/10.1016/J.CEB.2013.03.003

Rog, O., Köhler, S., & Dernburg, A. F. (2017). The synaptonemal complex has liquid crystalline properties and spatially regulates meiotic recombination factors. *ELife*, *6*. https://doi.org/10.7554/ELIFE.21455

Saitou, M. (2021). Mammalian Germ Cell Development: From Mechanism to In Vitro Reconstitution. *Stem Cell Reports*, *16*(4), 669. https://doi.org/10.1016/J.STEMCR.2021.01.008

Schild-Prüfert, K., Saito, T. T., Smolikov, S., Gu, Y., Hincapie, M., Hill, D. E., Vidal, M., McDonald, K., & Colaiácovo, M. P. (2011). Organization of the Synaptonemal Complex During Meiosis in Caenorhabditis elegans. *Genetics*, *189*(2), 411–421. https://doi.org/10.1534/GENETICS.111.132431

Schumacher, B., Hofmann, K., Boulton, S., & Gartner, A. (2001). The C. elegans homolog of the p53 tumor suppressor is required for DNA damage-induced apoptosis. *Current Biology : CB*, *11*(21), 1722–1727. https://doi.org/10.1016/S0960-9822(01)00534-6

Stiernagle, T. (2006). Maintenance of C. elegans. *WormBook : The Online Review of C. Elegans Biology*, 1–11. https://doi.org/10.1895/WORMBOOK.1.101.1

Susiarjo, M., Hassold, T. J., Freeman, E., & Hunt, P. A. (2007). Bisphenol A exposure in utero disrupts early oogenesis in the mouse. *PLoS Genetics*, *3*(1), 0063–0070. https://doi.org/10.1371/JOURNAL.PGEN.0030005

Uzumcu, M., Suzuki, H., & Skinner, M. K. (2004). Effect of the anti-androgenic endocrine disruptor vinclozolin on embryonic testis cord formation and postnatal testis development and function. *Reproductive Toxicology (Elmsford, N.Y.)*, *18*(6), 765–774. https://doi.org/10.1016/J.REPROTOX.2004.05.008

Whitby, M. C. (2005). Making crossovers during meiosis. *Biochemical Society Transactions*, *33*(Pt 6), 1451–1455. https://doi.org/10.1042/BST20051451

Zickler, D., & Kleckner, N. (2015). Recombination, Pairing, and Synapsis of Homologs during Meiosis. *Cold Spring Harbor Perspectives in Biology*, *7*(6), 1–28. https://doi.org/10.1101/CSHPERSPECT.A016626

CHAPTER 4

Single-nucleus resolution mapping of the adult *C. elegans* and its application to elucidate inter- and trans-generational response to alcohol exposure

Introduction

In mammals, *in utero* exposure to alcohol is associated with an array of well-characterized morphological, neurological, and reproductive deficits in F1 progeny that are grouped as symptoms of Fetal Alcohol Syndrome Disorders (FASD) (Ungerer *et al*., 2013). The plurality of the conditions associated with FASD reflects the variety of organ systems and processes showing structural and functional anomalies following prenatal alcohol exposure, such as the reproductive system, the central nervous system, craniofacial morphogenesis, the heart, kidney, liver, and gastrointestinal system (reviewed in Caputo *et al.,* 2016; La Vignera *et al*., 2013). However, while *in utero* alcohol exposure clearly impacts the function of multiple organ systems, a comprehensive understanding of all organs, tissues, and cell types that are the most affected by alcohol remains lacking (Dguzeh et al., 2018; Obad *et al.,* 2018).

In addition to impacting the health of the F1 progeny, mounting evidence in various model systems, such as mice, rats, *Drosophila*, and *C. elegans*, indicates that at least some exposure-related adverse reproductive and neurobehavioral features also extend beyond the F1 and are detectable in F3 progeny (Nizhnikov *et al.,* 2016; Gangisetty *et al.,* 2022; Bozler *et al*., 2019). For instance, a rat model of late gestational ethanol exposure demonstrated that not only F1, but also F2 and F3, individuals show an average 50% increase in ethanol intake (Nizhnikov *et al.,* 2016). Moreover, preconception exposure is sufficient to cause increased alcohol intake in the offspring, together with signs of spatial learning and memory deficits (Hollander *et al*., 2019). Notably, the impact of ethanol on alcohol and substance use across several generations is observed in the broader context of several established multi- and transgenerational models in which various cognitive, behavioral, or physical endpoints are altered (reviewed in Lam *et al.,* 2000; Yohn *et al*., 2005).

C. elegans is a simplified but highly advantageous model for studying the effects of alcohol and is the most used invertebrate species for modeling FASD (reviewed in Benjamini and Hochberg, 1995). Direct exposure to ethanol causes a variety of dose- and duration-dependent

outcomes similar to those elicited in mammals such as growth and fertility impairments, neuro-depressive effects, increased alcohol preference and disinhibition, withdrawal, all supported by the involvement of similar cellular and neurological pathways (Lacar et al., 2016; Benjamini and Hochberg, 1995). Ethanol's metabolism is also remarkably conserved (Alaimo *et al*., 2012) with *C. elegans* metabolizing ethanol through a two-step process in which ethanol is first metabolized by alcohol dehydrogenase (ADH) into acetaldehyde, which subsequently is metabolized by aldehyde dehydrogenase (ALDH) into acetate, similarly to humans. In addition, its reproductive system, with two gonads opening into a common uterus where embryos initiate their development, provides a window for *in utero* exposure to alcohol.

Recently, the combination of single-cell RNA sequencing (scRNA-seq) technologies and the tractability of the model organism *C. elegans*, with its well-established differentiation lineages and timing, has enabled the layering of transcriptional data with developmental events at both embryonic and larval (L2) stages (Cao *et al*., 2017; Packer et al., 2019). This has led to the identification of gene expression changes that track the development of 502 preterminal and terminal cell types in embryos (Packer et al., 2019) and the characterization of 27 distinct cell types at larval stages (Cao *et al*., 2017). Furthermore, we and others have shown that *C. elegans* is also a powerful model for the study of multigenerational and transgenerational responses to environmental stimuli (Camacho *et al.*, 2018; Weinhouse *et al.,* 2018; Kelley W, 2014; Kishimoto *et al.,* 2017; Klosin *et al.,* 2017). However, single cell transcriptomic approaches have yet to be applied to the characterization of environmental exposures, including alcohol, at the whole organism level and across generations.

Here, we used a single nucleus approach to maximize the isolation of diverse cell types, including neuronal cell types with long processes as well as syncytial organs such as the germline, followed by RNA-seq. We applied this approach to examine the transcriptional impact of parental (P0) exposure to physiologically relevant doses of ethanol on the F1 offspring (intergenerational exposure) as well as on the F3 generation (transgenerational exposure). We

show that mechanical extraction and isolation of adult *C. elegans* nuclei followed by snRNA-seq identifies a large number of distinct cell types that resolve into both known and novel functional categories. We also demonstrate that this powerful method can provide insights into the effect of intergenerational ethanol exposure at tissue-, cell-, and nucleus-specific resolution and identify the cells, and molecular pathways that are most impacted by such an exposure.

Results

Single-nucleus preparation and snRNA-seq

Intact nuclei were isolated from adult *fog-1(q253) C. elegans* raised at the restrictive temperature of 25°C (Barton and Kimble, 1990). Since the focus of our study was on the characterization of adult tissue's response to ethanol, this sperm-defective strain was used to prevent self-fertilization and the crowding of our snRNA-seq data with embryonic cell types (see material and methods section). Briefly, worms were synchronized using 10µm filters and allowed to grow to day one of adulthood before mechanical nuclear extraction (Figure 1A). Nuclei concentration was determined using flow cytometry and nuclear integrity was assessed by high-resolution microscopy (Figure S1A). Single nucleus RNA-seq library preparation was performed using the 10X Genomics Chromium system followed by 50 PE sequencing on the Illumina Novaseq 6000 platform. In total, we generated transcriptomic data for 81,267 nuclei, each with more than 500 transcripts derived from 31 groups collected in 5 distinct batches. On average, 2,181 unique molecular identifiers (UMIs) and 992 genes were detected per nucleus with high sequencing depth (90.3% average sequencing depth) (Figure 1B, Figure S1B).

snRNA-seq reads were demultiplexed and aligned to the ENSEMBL ce10 *C. elegans* transcriptome to generate gene expression matrices using CellRanger (10x Genomics) (see material and methods). To mitigate the inclusion of empty droplets and to correct for ambient RNA contamination, we applied DIEM (Alvarez et al., 2020) and SoupX (Young and Behjati, 2020) respectively. DIEM or Debris Identification using Expectation Maximization identifies

empty droplets through modeling semi-supervised expectation maximization and outperforms other methods in snRNA-seq. Since DIEM only filters for empty droplets and does not correct for the expression of the remaining droplets, we combined DIEM with SoupX which removes ambient RNA contaminations by quantifying the extent of ambient mRNA contamination levels and purifying the cell-specific signal from the mixture of cellular and exogenous mRNAs. Using these stringent parameters, we retained transcriptomic data from 41,750 droplets representing an average of 1627 UMIs and 1007 genes per nucleus. A total of 31 discrete clusters were identified following batch/group effect correction by canonical correlation analysis (CCA) in Seurat v3 followed by Louvain clustering algorithm (Stuart *et al*., 2019; Waltman *et al.,* 2013). Log-normalized expression levels in t-SNE (t-distributed stochastic neighbor embedding) plot projections were used to visualize cell clusters in two dimensions and dot heatmap were used to visualize marker expression across different cell types.

To facilitate unbiased cluster identification, gene enrichment (FDR<0.05, $\log_2$FC>0) for each cluster was used to mine the Enrichment Analysis module of Wormbase (Angeles-Albores et al., 2016) which encompasses Tissue Enrichment Analysis (TEA), Phenotype Enrichment Analysis (PEA), and Gene Ontology Enrichment Analysis (GEA). We further refined cluster identity by mining cell type-specific markers from the literature as well as making use of the Nematode Expression Pattern Database. Examples of putative clusters are shown in (Figure 1C) and cluster specific enrichment analysis, top 20 up-regulated and down-regulated genes, as well as examples of genes that are both cluster specific and tissue specific according to the RNA *in situ* database is collated in our dashboard. Our clustering method revealed the identification of a large variety of cell identities including all major cell types and their support cells: germline, neurons, muscle cells, epithelial cells, intestinal cells, and sheath cells.

SnRNA-seq reveals broad impacts of intergenerational exposure to ethanol

We first applied snRNA-seq to identify the transcriptional changes of a 48-hour (L4 to end of day 1 of adulthood) parental exposure to two concentrations of ethanol (0.05% and 0.5%) compared to water control on the F1 adult progeny. Theses doses were chosen to capture both low levels of ethanol easily reached in human populations and in pregnant women in particular (Dejong *et al.,* 2019). We first compared cell type proportion in the F1 following parental ethanol exposure and observed that broadly similar cell type distributions were observed across all treatment conditions (Figure 2A). However, we observed a significant number of Differentially Expressed Genes (DEGs) with an FDR<0.05 between treatment conditions. Upon comparison of the 0.05% ethanol exposure condition to water at the F1, we identified a total of 1,223 DEGs, including 583 uniformly up-regulated DEGs, 520 uniformly down-regulated DEGs, and 120 DEGs that were differentially up- or down-regulated in cluster specific ways (i.e. up-regulated in some clusters but down-regulated in other clusters). Surprisingly, compared to 0.05%, exposure to the higher ethanol concentration of 0.5% resulted in fewer DEGs identified at the F1 with a total of 948 DEGs, including 430 uniformly up-regulated DEGs, 407 uniformly down-regulated DEGs, and 111 up- and down-regulated DEGs. A detailed Venn diagram shows 152 DEGs were shared across all conditions and can be seen in Figure 2B.

Gene Ontology analysis of all DEGs revealed the enrichment of some functional categories that align with alcohol metabolism such as the GO categories “carboxylic acid metabolic process” and “oxidoreductase activity, acting on the aldehyde or oxo group of donors, NAD or NADP as acceptor” driven by the presence in our DEG list of several aldehyde dehydrogenases, which catalyze the second step of ethanol metabolism from acetaldehyde into acetate, in both exposure groups as compared to water at the F1 (Table 1). Other GO categories that are shared across all exposure conditions at F1 include “small molecule biosynthetic process” largely enriched in fatty acid biosynthetic process genes and “defense

response". Interestingly, there is a large representation of GO categories that involve reproduction such as "embryo development ending in birth or egg hatching", "gamete generation", "cellular process involved in reproduction in multicellular organism", and "germ cell development" that is shared between both exposure conditions at the F1 with many of them being shared across generations with the F3 as well (Table 1). Together, these results suggest that both concentrations of ethanol at the F1 have effects on various crucial metabolic and developmental pathways, with many of these effects being in reproductive pathways suggesting a multi-generational effect of ethanol exposure.

SnRNA-seq reveals tissue-specific DEGs from intergenerational exposure to ethanol

Followed by analysis conducted on DEGs across all clusters, we conducted cluster-specific DEG analysis to investigate cell type specific effects at the F1. As previously mentioned, cluster-specific analysis did not reveal significant changes in cell type proportions for either treatment doses at both the F1 and F3 generations (Figure 2A). However, cluster-resolved DEG analysis clearly identifies distinct transcriptional responses to parental ethanol exposure between cell types. While some genes were consistently up-regulated (*atp-6, nduo-6*) or down-regulated (*vit-5*) across all clusters between ethanol and water treatments, most DEGs showed cell type-specific restriction as highlighted by the low overlap of the top DEGs per cluster (Figure S3). To rank order the clusters by sensitivity of the F1 to ethanol exposure, we employed a Euclidean distance analysis (Arneson *et al*., 2018; Liu *et la.,* 2020), which estimates the degree of global transcriptomic shifts between exposure and control groups (see Material and Methods). Several clusters (1, 12, 15, 23) with a strong germline identity showed some of the largest degree of transcriptomic shifts at the F1 generation under the 0.5% ethanol exposure condition (Figure 3A). Cluster 1 shows a gene signature suggestive of mid-pachytene; cluster 12 of transition zone or early-pachytene; cluster 15 of late-pachytene; cluster 23 of mitotic zone. Other clusters that appears most affected includes clusters related to muscle function such as

cluster 2 (body wall musculature) and cluster 17 (striated muscle cells). The degree of transcriptomic shift was much less pronounced following 0.05% ethanol exposure compared to 0.5% ethanol, suggestive of a dose-dependent transcriptomic response across cell types.

Next, we were interested in exploring the impact of ancestral ethanol exposure on ethanol metabolism. While most DEGs are shown to be cell type-specific, genes implicated in ethanol metabolism may show a more uniform response across clusters. Thus, we investigated the expression of genes involved in ethanol metabolism, including 2 distinct alcohol dehydrogenases (*sodh-1*, *hphd-1*) and 5 aldehyde dehydrogenases (*alh-3, -4, -8, -9, -13*), whose expression was detected in our datasets to be differentially expressed (Figure S2). Contrary to our expectations, of the 7 genes examined, only 5 showed significant consistent changes in expression (FDR < 0.05) and did so in a cluster-dependent fashion at the F1. For example, *sodh-1* was up-regulated in cluster 13 and cluster 18 under the 0.05% exposure condition, but was down-regulated in cluster 2 and cluster 27 at 0.5% in the F1 (Figure S2). Notably, some of the cell types showing the highest increase in ethanol metabolism genes (cluster 4, 13, 22) were also the cell types that were the least sensitive to ethanol and the cell types showing the highest decrease in ethanol metabolism genes (clusters 2 and 17) were also the cell types that were the most sensitive to ethanol, suggesting that upregulation of ethanol metabolism does protect a tissue from the intergenerational impact of ethanol exposure (Figure S2 and 3A).

We further inspected top DEGs across cell types in order to identify the top responsive genes under each ethanol condition (Figure 3B). Analysis identified ribosomal related genes (*rrn-3.1*, *rpl-10*, *rrn-2.1*), cytochrome related genes (*ctc-2*, *ctc-3*, *ctb-1*, *ctc-1*), and vitellogenin related genes (*vit-2*, *vit-3*, *vit-6*, *vit-1*) were among the most commonly altered genes across different cell types in both exposure conditions. Interestingly, majority of genes were down-regulated across clusters under the 0.05% ethanol treatment group with cluster 6 which shows a gene signature suggestive of hypodermis being down-regulated for all three gene classes. On

the contrary, majority of genes are up-regulated across clusters under the 0.5% ethanol treatment group, with cytochrome related genes being uniformly up-regulated across clusters, while ribosomal related genes and vitellogenin related genes are either up- or down-regulated depending on the cluster. Upon closer analysis of germline specific clusters, cluster 1 (mid-pachytene) was down-regulated in ribosomal and vitellogenin related genes but up-regulated in cytochrome related genes; cluster 12 (early-pachytene) was down-regulated ribosomal and vitellogenin related genes; cluster 15 (late-pachytene) was up-regulated in ribosomal related genes. Together, top DEG analysis showed that parental 0.5% ethanol exposure mainly up-regulated major pathways both in the germline and other somatic tissues at the F1 while 0.05% ethanol exposure mainly down-regulated these pathways, suggesting that ethanol's effects are strongly dose-dependent.

SnRNA-seq reveals tissue-specific pathway changes due to intergenerational exposure to ethanol

Despite the low overlap in their top DEGs, we next interrogated the cluster-resolved F1 data to identify whether there might be an overlap in pathway enrichment between different clusters (Figure 3C and 3D and summarized table in Table 1). Gene Ontology (GO) analysis conducted for both biological pathway (GOBP) in Figure 3C and molecular function (GOMF) in Figure 3D revealed a strong overlap of molecular pathways related to ribosomal and lipid function. Interestingly, GOBP also identified biological pathways involved in lifespan and aging that were down-regulated in cluster 6 (hypodermis) at the F1 but were up-regulated in clusters 15 (germline) and 17 (striated muscle) (Figure 3C). Since germline clusters displayed the largest degrees of global transcriptomic shifts between exposure and control groups in our Euclidean Distance analysis with the two most sensitive clusters displaying germline identity (Figure 3A), we examined whether reproduction-related phenotypes were significantly over-represented in our dataset. By mapping our data to the Wormbase phenotype gene database,

we discovered that several of the top shared phenotypes across clusters with the largest degrees of global transcriptomic shifts including four clusters with strong germline identities (clusters 1, 12, 15, 23) were related to reproductive function (Figure 3E).

To validate that this trend was not due to the fact that there was a higher proportion of germline related annotations in the Wormbase phenotype gene database, we took the top Wormbase phenotype annotations, plotted the proportions of each annotation from our dataset of all enriched pathways in red, and compared it to the proportions of each annotation from the Wormbase phenotype gene database in blue (Figure 3F). The results indicated that our dataset had a significantly higher proportion of phenotypes related to the reproductive system between both treatment groups. This suggests that the observed trend was not due to the higher proportion of germline related annotations in the Wormbase phenotype gene database, but instead that ethanol exposure significantly impacts reproduction-related phenotypes directly at the F1 (Figure 3F).

SnRNA-seq reveals broad impacts of transgenerational exposure to ethanol

To capture the transgenerational effect of an ancestral ethanol exposure, we performed a similar 48-hour parental (P0) exposure to two concentrations of ethanol (0.05% and 0.5%) and collected adult progeny for snRNA-seq at the F3 generation (Figure 4). Similarly to the F1, comparison of cell type proportions in the F3 following ancestral ethanol exposure revealed similar cell type distributions across all treatment conditions (Figure 2A). In addition, we observed a significant number of Differentially Expressed Genes (DEGs) with an FDR<0.05 between treatment conditions when compared to water at the F3. Upon comparison of the 0.05% ethanol exposure condition with water, we observed a total of 798 DEGs, including 366 uniformly up-regulated DEGs, 369 uniformly down-regulated DEGs, and 63 DEGs that were differentially up- or down-regulated in cluster specific ways (i.e. up-regulated in some clusters but down-regulated in other clusters). Interestingly at the F3, exposure to the higher ethanol

concentration of 0.5% resulted in more DEGs identified, with a total of 918 DEGs, including 402 uniformly up-regulated DEGs, 422 uniformly down-regulated DEGs, and 94 DEGs that were differentially up- or down-regulated in cluster specific ways. A detailed Venn diagram summarizing this can be seen in Figure 2B.

Gene Ontology analysis at the F3 of all DEGs revealed the enrichment of some functional categories that align with alcohol metabolism such as the GO categories “carboxylic acid metabolic process”, “drug metabolic process”, and “small molecule catabolic process” driven by the presence in our DEG list of alcohol dehydrogenase genes, *sodh-1* and *hphd-1*, which catalyze the first step of ethanol metabolism from ethanol to acetaldehyde, as well as aldehyde dehydrogenase genes, *alh-8* and *alh-13*, which catalyzes the second step of ethanol metabolism from acetaldehyde into acetate, in both exposure groups as compared to water at the F3 (Table 1). Other GO categories that are shared across all exposure conditions at F3 include “defense response”, “actin cytoskeleton organization”, and “aging”. However, unlike at the F1, there is much less GO categories that involve reproduction at the F3 with the 0.5% exposure condition including GO categories such as “embryo development ending in birth or egg hatching”, “sexual reproduction”, “cellular process involved in reproduction in multicellular organism”, and “oogenesis” whereas the 0.05% exposure condition included none (Table 1). Together, these results suggest that both concentrations of ethanol at the F3 have effects on various crucial metabolic and developmental pathways, while only the higher concentration of ethanol persists in having transgenerational reproductive effects.

SnRNA-seq reveals tissue-specific DEGs from transgenerational ethanol exposure

Next, we conducted cluster specific DEG analysis to investigate ethanol’s cell type specific effects at the F3. Cluster-resolved DEG analysis clearly indicated distinct transcriptional responses to ancestral ethanol exposure between cell types. Interestingly, while majority of the DEGs found at the F1 were up-regulated, in comparison, majority of the DEGs found at the F3

were down-regulated, especially for the 0.5% ethanol exposure condition. While some genes were consistently up-regulated (*tts-1*) and others were down-regulated (*rrn-3.1*, *hsp-16.2*) across all cluster between both ethanol conditions when compared to water, most DEGs were cell type specific as highlighted by the low overlap of the top DEGs per cluster (Figure S4). Similarly to the F1, we next rank ordered the F3 clusters by sensitivity to ethanol exposure using Euclidean distance analysis (Lopez *et al.,* 2018; Arneson *et al.,* 2018). Again, several clusters (1, 12, 15) with a strong germline identity showed some of the largest degree of transcriptomic shifts at the F3 from an ancestral 0.5% ethanol exposure and in the case of cluster 1, from the 0.05% ethanol exposure condition as well (Figure 4A). Interestingly, Cluster 12 which is suggestive of early-pachytene, Cluster 1 which is suggestive of mid-pachytene, and cluster 15 which is suggestive of late-pachytene into early diplotene consistently show the largest degree of transcriptomic changes for both exposure conditions at the F1 and F3. Together, this suggests that both direct and transgenerational ethanol exposure affects the transcriptome of pachytene-staged germline nuclei. This is a crucial since pachytene encompasses some of the most important germline programs including synaptonemal complex (SC) formation, double-strand break (DSBs) formation, and recombination, which are vital processes for germ cell development. Failure in any of these processes will trigger checkpoint mechanisms that lead to programmed cell death and any errors that bypass these checkpoints will result in inviable embryos and decreased fertility. We further explore these reproductive endpoints later (Figure 7). Other clusters that appeared most affected includes body wall musculature (cluster 2), intestine (clusters 0, 5, 8), and sheath cells (clusters 20 and 25). Again, the degree of transcriptomic shift was much less pronounced following 0.05% ethanol exposure compared to 0.5% ethanol, suggesting a dose-dependent transcriptomic response across cell types.

Since most DEGs are cell type specific at the F3 and ethanol metabolism genes were also cluster dependent at the F1, we next investigated ethanol metabolism genes at the F3. Of the 2 distinct alcohol dehydrogenases (*sodh-1*, *hphd-1*) and 5 aldehyde dehydrogenases (*alh-3,*

-4, -8, -9, -13), whose expression was detected in our datasets to be differentially expressed, only 3 showed significant changes in expression (FDR < 0.05) in a cluster-dependent manner at the F3 (figure S2). This time, *sodh-1* was down-regulated in cluster 13 for the 0.05% exposure condition but was up-regulated in cluster 18 for the 0.5% exposure condition. Similarly to F1, the cell types showing the highest increase in ethanol metabolism genes (clusters 14 and 18) corresponded with the cell types that were the least sensitive to ethanol and one of the cell types showing the highest decrease in ethanol metabolism genes (cluster 1) corresponded with the cell type that was the most sensitive to ethanol, suggesting that upregulation of ethanol metabolism does protect a tissue from the transgenerational impact of exposure as well (Figure S2 and 4A).

We inspected the top DEGs across cell types in order to identify the top responsive genes under each ethanol condition (Figure 4B). Similarly to F1, analysis identified ribosomal related genes (*rrn-3.1*) and cytochrome related genes (*ctc-1*, *ctc-2*, *ctc-3*, *ctb-1*) were among the most commonly altered genes across different cell types in both exposure conditions. In addition, collagen related genes (col-119, col-124, col-181, col-20) were also identified to be down-regulated in the majority of cell types. As compared to F1, the directionality of these DEGs reversed, with majority of genes being up-regulated across clusters under the 0.05% ethanol treatment group but down-regulated across clusters under the 0.50% ethanol treatment group. Upon closer analysis of germline specific clusters, cluster 1 (mid-pachytene) is down-regulated for all three gene classes at both ethanol exposure conditions while cluster 12 (early-pachytene) and cluster 15 (late-pachytene) are both down-regulated for majority of genes at the 0.50% ethanol condition. Together with the F1 DEG analysis, this suggests that the pachytene region of the germline is most sensitive to both intergenerational and transgenerational ethanol exposure, carrying significant implication for ethanol's multigenerational reproductive effects that we will explore later (Figure 7).

SnRNA-seq reveals tissue-specific pathway changes due to transgenerational exposure to ethanol

Pathway analysis with gene ontology (GO) analysis conducted for both biological pathway (GOBP) in Figure 4C and molecular function (GOMF) in Figure 4D revealed a strong overlap of molecular pathways related to cytoskeleton and muscle development and function. In comparison to F1 which was mostly comprised of pathways related to ribosomal and lipid function, pathway analysis at the F3 consists mostly of somatic growth and development. Similarly to F1, since germline clusters displayed the largest degrees of global transcriptomic shifts between exposure and control groups in our Euclidean Distance analysis with the top most sensitive cluster displaying germline identity (Figure 4A), we examined whether reproduction-related phenotypes were significantly over-represented in our dataset at the F3 as well. By mapping our data to the Wormbase phenotype gene database, we discovered that several of the top shared phenotypes across clusters with the largest degrees of global transcriptomic shifts were related to reproductive function, although not as many as in F1 (Figure 4E). In addition to reproductive phenotypes, we also identified phenotypes that are involve in body morphology and movement. This correlates well with the GO analysis which identified biological pathways that involve cytoskeletal and muscle development and function (Figure 4C). While reproductive phenotypes are present in our comparative analysis, it does not comprise the entirety of the top shared phenotypes identified at F3. In addition, a comparison of the proportion of each top Wormbase phenotype annotation between our dataset of all enriched pathways and the Wormbase phenotype gene database revealed that our dataset at the F3 also had a significantly higher proportion of reproductive phenotypes for both treatment groups as compared to the Wormbase database (Figure 4F). Together, this suggests that ethanol's reproductive effects may last until the F3, but is stronger at the F1 as compared to the F3.

Ethanol elicits both shared and unique responses across generations

In order to investigate whether effects from ethanol exposure persists across generations, we performed DEG and pathway analysis comparing F1 and F3 for the same concentrations. For the parental exposure of 0.05%, top DEGs analysis between F1 and F3 revealed that cluster 0 (intestine) and cluster 6 (hypodermis) were impacted by ethanol exposure at both generations with ribosomal related genes (*rrn-3.1*, rrn-3.1) being down-regulated for both clusters while collagen related genes (*col-119*, *col-160*, *col-19*, *col-20*) were uniformly down-regulated by cluster 6 at F1 but were uniformly up-regulated in cluster 0 at F3. Interestingly, germline clusters were also identified with cluster 1 (mid-pachytene) containing genes that are strongly differentially expressed at the F1 while cluster 15 (late-pachytene) contained the top DEGs at F3 (Figure 5A). This suggests that different regions of the germline may be more sensitive to ethanol exposure at different generations.

Gene Ontology (GO) analysis conducted for both biological pathway (GOBP) in Figure 5B and molecular function (GOMF) in Figure 5C comparing the two generations revealed that there was no biological pathways and only two molecular functions shared between the two generations, structural molecule activity and structural constituent of cuticle. By mapping our data to the Wormbase phenotype gene database, we discovered that several of the top shared phenotypes across generations were related to reproductive function (Figure 5D). However, ethanol's down-regulation of these phenotypes were much stronger in the F1 than in the F3 and were identified in non-germline clusters. This suggests that 0.05% ethanol exposure may cause DEGs and changes in pathways that are unique to each generation, with changes in reproductive pathways not being conserved across generations.

Next we were interested in whether effects from 0.50% ethanol exposure persists across generations. We performed DEG analysis comparing F1 and F3 and showed that the top DEGs were shared across multiple cell types between the F1 and F3 generations. Majority of the genes identified were composed of cytochrome related genes (*ctc-1*, *ctc-2*, *ctc-3*, *ctb-1*),

vitellogenin related genes (*vit-1*, *vit-2*, vit-6), and collagen related genes (*col-124*, *col-98*, *col-119*, *col122*) in both germline and non-germline clusters. Interestingly, DEGs were mostly up-regulated in the F1 while the same DEGs were down-regulated at the F3 (Figured 5E). This suggests that there may be an initial transcriptomic response to ethanol exposure at the F1 which then gets remedied by a reversal at the F3.

Gene Ontology (GO) analysis conducted for both biological pathway (GOBP) in Figure 5F and molecular function (GOMF) in Figure 5G comparing the two generations revealed highly different pathway enrichment between the two generations. GOPB analysis identified pathways related to ribosomes, lipids, and peptides, with majority of the pathways being down-regulated in cluster 12 (early-pachytene) but up-regulated in cluster 15 (late-pachytene) at the F1, but down-regulated in cluster 1 (mid-pachytene) at the F3. More pathways were identified to be differentially expressed across both germline and non-germline clusters at the F1 than at the F3, suggesting that ethanol's effects are stronger at the F1 (Figure 5F). Similarly, GO analysis on molecular function identified the majority of altered functions both for germline and non-germline clusters at the F1 to be related to ribosomes, lipids, and RNA function, while the majority of altered functions at the F3 were related to cuticle, actin, and cytoskeleton (Figure 5G). By mapping our data to the Wormbase phenotype gene database, we discovered that most of the top shared phenotypes across generations were related to reproductive function (Figure 5H). Comparisons at the F1 revealed that both germline, including clusters 1 (mid-pachytene), cluster 15 (late-pachytene) and cluster 23 (mitotic zone), as well as non-germline clusters were mostly up-regulated for reproductive phenotypes except for cluster 12 (early-pachytene) which was uniformly down-regulated. Interestingly, cluster 1 (mid-pachytene) was up-regulated for reproductive phenotypes at the F1 but down-regulated at the F3. Together, this suggests that while the higher concentration of ethanol resulted in more shared DEGs, pathways, and phenotypes, it appears that there were still persistent generation-specific effects.

Both inter- and transgenerational snRNA-seq results validated using smFISH and reproductive assays

Lastly, we validated the snRNA-seq data by performing single molecule fluorescence *in situ* hybridization (smFISH) followed by fluorescence quantification using FISH-Quant v3 (Lee *et al*., 2017; Mueller *et al.*, 2013) to validate the changes in gene expression at both the F1 and F3 due to ancestral ethanol exposure. For F1, we identified *tra-2* which is involved in reproduction and sex-determination in oocytes (Ellis et al., 2007) to be down-regulated in the mitotic zone of the *C. elegans* germline from parental 0.50% ethanol exposure at the F1. We designed and ordered *tra-2* specific probes from Stellaris and performed smFISH on dissected *C. elegans* germlines (Lee *et al*., 2017). Slides were imaged on the Leica SP8 confocal microscope and representative images can be seen in Figured 6A. Both nuclear and cytoplasmic *tra-2* foci can be seen in the mitotic zone of the water condition and consistent with our snRNA-seq data, the *tra-2* expression level decreases in the 0.50% ethanol condition. We further quantified the number of *tra-2* foci using FISH-Quant v3, which revealed a significant decrease in the number of *tra-2* smFISH spots per germline nucleus in F1 ancestrally exposed to 0.50% ethanol as compared to water (Figure 6B).

Next, we also validated the snRNA-seq data at the F3. We identified *mex-3* which is involved in anterior cell fate specification in embryos with mutations leading to embryonic lethality (Mennatallah *et al.,* 2021) to be up-regulated in the mid- to late-pachytene of the *C. elegans* germline from ancestral 0.50% ethanol exposure at the F3. Similarly to F1, we performed smFISH on dissected *C. elegans* germlines using *mex-3* probes that were designed and ordered from Stellaris (Lee *et al*., 2017). Slides were imaged on the Leica SP8 confocal microscope and representative images can be seen in Figured 6C. Interestingly, while both nuclear and cytoplasmic *mex-3* foci can be seen in the water condition, we were able to identify 1-2 significantly brighter *mex-3* foci per germline nucleus which we suspect to be active transcription sites. Consistent with our snRNA-seq data, the *mex-3* expression level appears to

increase in the 0.50% ethanol condition. We further quantified the number of *mex-3* foci using FISH-Quant v3 (Mueller *et al.*, 2013), which revealed a significant increase in the number of *mex-3* smFISH spots per germline nucleus in the F3 ancestrally exposed to 0.50% ethanol as compared to water (Figure 6D).

Additionally, clusters representing different stages of pachytene including cluster 12 for early-pachytene, cluster 1 for mid-pachytene, and cluster 15 for late-pachytene consistently show the largest degree of transcriptomic shifts through Euclidean Distance analysis for both exposure conditions at the F1 and F3. In addition, DEG analysis and phenotype analysis at both F1 and F3 also identified clusters 1, 12, and 15 to have the largest changes in genes and pathways as a result of ethanol exposure. Together, this suggests that the pachytene region of the germline is the most sensitive to ethanol exposure and both direct and transgenerational ethanol exposure affects the transcriptome of pachytene-staged germline nuclei. This is a crucial since pachytene encompasses some of the most important germline programs including synaptonemal complex (SC) formation, double-strand break (DSBs) formation, and recombination, which are vital processes for proper germ cell development. Failure in any of these processes will trigger checkpoint mechanisms that lead to programmed cell death and any errors that bypass these checkpoints will result in inviable embryos and aneuploidies. Therefore, we next characterized the reproductive effects of ancestral ethanol exposure by looking at three metrics for germline health: apoptosis, aneuploidy, and embryonic lethality. We measured apoptosis through acridine orange staining and observed a significant increase in the number of apoptotic nuclei per gonad in both the F1 and F3 who were ancestrally exposed to either ethanol concentrations (Figure 7A). Next, we monitored aneuploidy through the high incidence of male (XO) embryos caused by mis-segregation of the X-chromosome and identified a significant increase in the incidence of male embryos marked by expression of xol-1::gfp for both ethanol concentrations at both the F1 and F3 (Figure 7B) (Kelly *et al.,* 2000; Allard *et al.,* 2013). Lastly, we observed an increase in embryonic lethality between both ethanol

conditions and water control at both F1 and F3 (Figure 7C). Together, these results indicate a profound impact of intergenerational and transgenerational alcohol exposure on reproduction.

Conclusions and discussion

We have developed a single-nucleus RNA-seq approach in the adult *C. elegans* nematode that identifies a large number of known cell types while providing in-depth transcriptional information about them and can be applied to achieve a nuanced understanding of physiological responses to environmental cues.

Our methods generates robust numbers of genes per nucleus, even when compared to mammalian studies (Selewa *et al*., 2020). Additionally, single-cell and single-nucleus sequencing are very well correlated and single-nucleus sequencing has the advantage of removing confounding transcripts from the mitochondrial genome (Cao *et al.,* 2017).

While it can be further adapted to capture small RNAs, the current approach readily provides valuable insights into their regulation. For example, we observed high and prevalent expression of small RNA regulatory factors implicated in the biogenesis of a variety of 26 and 22G small RNA classes such as *rde-8, rde-10, rde-1, rde-4, nrde-1, nrde-4,* which are highly expressed in the late pachytene cluster and *nrde-3*, which is enriched in the oocyte cluster.

Genes implicated in the regulation of histone post-translational modifications were also detected, such as *mes-4* which is highly expressed in the mitotic zone and the oocyte clusters. Thus, while future development will be focused on adapting this method for single-nucleus ATAC-seq, Cut & Run, or ChIP-seq, snRNA-seq provides information about epigenetic pathways by examining the transcriptional changes of their enzymatic regulators.

Our approach has several limitations. By working in a *fog-1* mutant background, we were not able to identify sperm cells, a necessary trade-off to avoid the production of embryos. It is possible that *fog-1's* absence alters the transcriptional landscape of the germline. However, *fog-1(q253)* was chosen specifically because of the normal morphology and staging of the

hermaphrodite germline in *fog-1* mutants (Barton and Kimble, 1990) which we validated by DAPI staining and clustering analysis.

Nonetheless, we were successful in functionally validating some findings of our ethanol studies through experimental means, such as the apoptosis phenotypes, showing that both transcriptional readouts and functional testing align at least in some contexts. These results demonstrate that both low and high dose of ethanol at the parental generation has a significant impact on the offspring's oocyte function and embryonic viability and extends transgenerationally through the F3. Direct ethanol exposure has been known to cause aneuploidy in mammals for many years (Kaufman *et al.,* 1984; Hunt P, 1987; Kaufman M, 1983), however the underlying molecular mechanisms at play and whether these effects extend to the F1's germline have remained uncertain. Here, we show that several key factors crucial for proper chromosome dynamics and segregation are significantly downregulated in the F1's and F3's oocytes. However, many other impacts of ethanol remain to be validated. For example, prenatal exposure to alcohol dramatically increases the production of autophagosome and autophagic activity in human and mouse cortical brain microvessels (Girault *et al.,* 2017). In our dataset, autophagy and autophagosome production were the rare pathways to be upregulated €n ethanol exposed F1, specifically in the uterine epithelium. These results therefore suggest that the connection between autophagy and FASD should be explored further in a variety of tissues.

Together, snRNA-seq of the adult *C. elegans* represents a powerful method for the comprehensive identification of cell types in the nematode and for probing the transcriptional impact of physiological and environmental changes.

Experimental Procedures

Culture conditions and strains

Worms were maintained on standard nematode growth medium (NGM) plates streaked with single colony Harvard OP50 *E. coli*. All experiments were grown at 20°C up until the generation right before sequencing during which they were moved at the L1 stage to 25°C and grown until day 2 of adulthood (i.e. 48 hours at 25°C). The JK560 (*fog-1(q253) I.*), wild-type N2, and TY2441 (Pxol-1::gfp*; rol-6(pRF4)*) strains used in this study were obtained from the *C. elegans* Genetics Center (CGC). This strain was chosen due to its defect in the last step of spermatogenesis. These mutants were observed to have a fully developed germline but not fertilized embryos at 25°C.

C. elegans exposures and expansions

Worms were synchronized using a 10µm nylon mesh filter (NY1102500 EDM Millipore and SX00025000 EDM Millipore) which only allowed L1 staged worms to pass. The L1 worms were washed twice with M9 and centrifuged at 100g for 1 minute. These pellets were plated on fresh OP50-seeded NGM plates and transferred to 25°C. Worms were grown for 62 hours at 25°C and washed 5 times with M9. Between each wash, adult worms were centrifuged at 1300g for 1 minute to remove bacteria. After washing, worms were placed in 1mL of M9 in a 1.5mL low retention microcentrifuge tube and incubated in a rotator at 20°C for 30 minutes to remove residual OP50 from the worms' gut. These microcentrifuge tubes were then set upright and the worms were allowed to settle by gravity for 5 minutes. The M9 supernatant was discarded and the final compact worm pellet volume was adjusted to 30µL.

Single-nucleus dissociation

All reagents except for Triton-X100, PBS-BSA 1%, and inhibitors were prepared the night before and all low retention 1.5mL microcentrifuge tubes were clearly labeled. The bench space and equipment used in this protocol were thoroughly sanitized with 70% ethanol and cleaned

with RNaseZAP (AM9780 Fisher) before starting the dissociation. Reagents were prepared using Rnase free water (BP2484100 Fisher). The FA lysis buffer was made using the following reagents: 50mM HEPES/NaOH pH 7.5, 1mM EDTA, 0.1% Triton X-100, 150mM NaCl, Protease inhibitor 0.5X (Roche 11697498001), Rnase inhibitor 0.2U/μL (Thermo Fisher 10777019), and Rnase free water and stored at 4°C or on ice. BSA was prepared to a final concentration of 1% in pH 7.4 1X PBS (AM9624 Thermo Fisher) using RNAse free water and RNAse free PBS. This solution was filtered using a 0.22μm pressure filter (Thermo Scientific 03-377-26, Fisher SLGP033RS).

All equipment and reagents were moved to a 4°C cold room and subsequent steps were performed at 4°C.Homogenizers were stored pre-chilled at -20°C when not in use and moved to the 4°C room before starting the extraction. Each Wheaton 1.5mL Dounce homogenizers (Z378623-1EA Sigma) was cleaned using 70% ethanol, RNaseZAP, and Rnase free water. Homogenizers were rinsed twice with ethanol, twice with RNaseZAP, and 5 times with 1-2mL of Rnase free water.

The compact 30μL pellet of adult *C. Elegans* was transferred to the Dounce homogenizer and 400μL of ice cold FA buffer was used to rinse any remaining worms from the 1.5mL low bind microcentrifuge tube and 1000μL low bind pipette tip and added to the homogenizer. Worms were homogenized with 10 strokes of the Dounce homogenizer using a corkscrew motion with a B (tight) pestle. Homogenized worms were transferred to a new low bind 1.5ml microcentrifuge tube and centrifuged at 100g for 1 minute to pellet debris. The supernatant containing the dissociated nuclei was removed using a 1000μL low bind tip and transferred to a fresh low bind 1.5mL microcentrifuge tube labeled pooled nuclei. 300μL of FA buffer was added to the debris remaining in the first microcentrifuge tube and homogenized using 10 strokes in a corkscrew fashion with an Eppendorf Dounce homogenizer. The newly homogenized sample was then centrifuged at 100g for 1 minute to pellet debris. The supernatant containing the newly dissociated nuclei was pooled with the previously dissociated nuclei and the previous steps with

the Eppendorf Dounce homogenizer were repeated once more to further homogenize the sample. In total, worms were homogenized with 30 strokes: 10 strokes with the 1.5mL Wheaton Dounce homogenizer and 20 strokes with the Eppendorf Dounce homogenizer. Between each homogenization step, debris was pelleted at 100g for 1 minute and the supernatant containing the dissociated nuclei was removed and added to a single 1.5mL microcentrifuge tube labeled pooled nuclei. Dissociated nuclei were removed after each set of 10 homogenization strokes to prevent overdigestion of nuclei.

After homogenization, the pooled supernatant containing the dissociated nuclei was centrifuged at 100g for 1 minute to pellet any remaining or accidentally transferred debris. The top 900µL of supernatant containing nuclei was transferred to a clean low bind 1.5mL microcentrifuge tube, being careful not to disturb the debris pellet. These pooled nuclei were pelleted at 500g for 4 minutes. After pelleting, approximately 800µL of FA buffer was removed, being careful not to disrupt the nuclei pellet, and the pelleted nuclei were resuspended with 1000µL of PBS-BSA 1%. The nuclei were again centrifuged at 500g for 4 minutes and 1000µL of the PBS-BSA 1% supernatant was removed. Lastly, the nuclei pellet was resuspended in 750-850µL of PBS-BSA 1% (final volume was determined by examining the size of the nuclei pellet). After resuspension, the nuclei were filtered using a 40µm Flowmi tip filter (BAH136800040-50EA Sigma Aldrich). Filtered nuclei were transferred to a 1.5mL low retention microcentrifuge tube for FACS sorting or 10X sequencing.

FACS/FLOW

The BD Analyzer Celesta plate reader at the UCLA BSCRC flow cytometry core was used to assess nuclei concentration. 150µL aliquots of filtered nuclei samples were stained with DAPI to determine concentration. Flow cytometry was done using the Violet 405nm 50mW laser with the slowest flow rate to obtain accurate counts. Nuclei concentration was determined to be within 700 to 1200 nuclei per microliter. If concentration was too high, filtered nuclei sample was

diluted with PBS-1% BSA. A flat bottom clear 96-well plate was used to assess nuclei concentration.

Library Preparation and sequencing

Library preparation was performed by UCLA Technology Center for Genomics & Bioinformatics. Nuclei were isolated into single droplets and barcoded using the 10X Chromium Next GEM single cell 3' reagent kit. We sequenced using 50bp long paired end reads with the NovaSeq 6000.

Single-nuclei transcriptional analysis

snRNA-seq reads were demultiplexed and aligned to the ENSEMBL ce10 *C. elegans* transcriptome to generate gene expression matrices using CellRanger (10x Genomics). The reference transcriptome was converted to accommodate pre-mRNA alignment by replacing “transcript” to “exon” in annotation GTF file. We first filtered the matrices to exclude low-quality cells or potential doublets using the following criteria: 1) gene number less than 500 or more than 8000, 2) unique molecular identifier (UMI) count less than 500 or more than 40000, 3) mitochondrial RNA percentage > 5% per cell, and 4) ribosomal RNA >20% per cell. After preprocessing, 8727, 4623 and 4871 cells were retained in unexposed, water treatment and 0.05% ethanol treatment groups, respectively.

Identification of cell clusters

R Seurat 3.1.5 (1) package was used for normalization, cell type identification, marker identification and batch effect correction of snRNA-seq data using all 9 sample groups. snRNA-seq data was log-normalized. The top 2000 variable genes were selected as representative features, followed by correcting gene expression with UMI counts, mitochondrial gene percentage and ribosomal RNA percentage for further clustering analysis. Canonical correlation analysis (CCA) was applied across different batches and treatment conditions to mitigate batch

effects in cluster identification. Cell clusters were identified from Louvain algorithm (2). We included all treatment groups for unsupervised clustering since increased cell numbers was shown to increase power in identifying smaller cell types (3). Cluster specific genes were detected by Wilcoxon Rank Sum test (4). To reduce biases from treatment in finding markers, only unexposed cells were included unless unexposed groups consist of less than 20% of the cluster of interest. Furthermore, for each cluster, the gene had to be expressed in at least 25% of the cells of the given cluster and there had to be at least a 0.25 log fold change in gene expression compared to other cells. Cell cluster identity was determined based on the overlap between highly expressed genes in each cluster with known cell type marker genes obtained from literature (Dashboard). Log-normalized expression levels in t-SNE (t-distributed stochastic neighbor embedding) plot projections were used to visualize cell clusters in two dimensions and dot heatmap were used to visualize marker expression across different cell types. While tSNE clusters were created using all 9 samples, marker genes enriched for each cluster were identified using only the unexposed samples to avoid confounding ethanol effects.

Differential gene expression and pathway analyses

Log-normalized gene counts were used in differential gene expression analysis. Differential gene analysis between water and ethanol treatment samples was conducted by Wilcoxon Rank Sum test to identify DEGs. To be considered in the analysis, the gene had to be expressed in at least 10% of the single nuclei from one of the two groups for that cell type and there had to be at least a 0.05 log fold change in gene expression between the groups. A lower threshold was used to account for subtle effects from low concentration ethanol treatment. Multiple testing correction was done using the Benjamini–Hochberg method to estimate FDR.

The DEGs were then subject to pathway annotation analysis. Because of low ethanol dose and a limited numbers of nuclei captured for certain cell types, using a stringent FDR cutoff yielded few DEGs which limits the statistical power for downstream pathway analysis. Previous

studies (5) showed that pathway enrichment analysis is less sensitive to random noise because the random chance to have multiple genes from the same pathway being DEGs is low, making a less stringent DEG P value cutoff feasible for pathway analysis. For this reason, we used DEGs with a P value < 0.01 for consideration in pathway enrichment analysis. Gene ontology analysis was conducted using clusterprofiler package (6) with *C. elegans* gene ontology biological pathway (GOBP) and molecular function (GOMF) database (7). Enrichment P values were corrected by Benjamini–Hochberg method and FDR < 0.05 were considered significant. For significantly enriched pathways, fold changes were calculated by averaging the fold changes of the pathway genes between treatment and control nuclei.

Euclidean distance-based measurement of cell type sensitivity

To identify cell types that are sensitive to ethanol treatment, the Euclidean distance metric was used (8). For each cell type, expression distance between nuclei of water and ethanol treatment groups were squared and summed, followed by taking the square root. In order to avoid potential biases caused by genes that are either highly expressed or non-expressed, expression values were normalized to z-scores and only the top 1,000 expressed genes were used. To account for variabilities in expression characteristics per each cell type, null distributions for individual cell types were calculated based on permutated treatment labels for 1000 times. P values were calculated between the observed Euclidean distance and the null distribution for each cell type and adjusted with the Benjamini & Hochberg method.

To visualize the differences between water and ethanol treated nuclei for individual cell types, the fold change (FC) in the Euclidean distance of ethanol treatment group compared with water treatment group in each cell type was normalized by dividing the empirical Euclidean distance by the median Euclidean distance of the null distribution per cell type. The log10(FC) vs. -log10(adjusted p value) of each cell type was then plotted to visualize and rank the vulnerable cell types in ethanol treatment.

Embryonic lethality assessment and *xol-1::gfp* analysis

After the 48-hour exposure, wild-type N2 P0 worms were allowed to lay F1 eggs overnight. F1 L4s were singled out and moved into individual 33mm plates. Embryonic lethality was performed on N2 by monitoring the number of embryos produced each day and the subsequent larvae hatched from these embryos for each individual worm starting from L4 through the end of its reproductive lifespan. Embryonic lethality is calculated by the number of embryos that fail to hatch over the total number of embryos multiplied by 100. Pxol-1::GFP analysis was done by fluorescent microscopy. Day 1 adults (24-hours post L4) were scored for the occurrence of GFP+ embryos (expressing Pxol-1::gfp). The proportion of xol-1::GFP+ was calculated by dividing the amount of worms with at least 1 GFP+ embryo by the total number of worms analyzed (30 worms) multiplied by 100.

Apoptosis assay

Apoptosis assay was performed on wild-type N2 by Acridine Orange staining on synchronized adult hermaphrodites collected at 20-24 hours post-L4 at F1 and F3 generations after direct exposures at P0 as previously described (Allard and Colaiacovo, 2011; Chen *et al.,* 2016).

Single molecule fluorescence *in situ* hybridization (smFISH) assay

Single molecule fluorescence *in situ* hybridization (smFISH) was performed using *C. elegans* specific protocol developed by the Kimble Lab (Lee *et al*., 2017). Probes were designed and ordered through Stellaris. Slides were imaged on the Leica SP8 confocal microscope. Fluorescence images were quantified using FISH-Quant v3 (Mueller *et al.*, 2013).

Statistical Analysis

Unless otherwise mentioned, statistical analysis was conducted by R/3.5.1 (R Core Team, 2020). For reproductive assays, one-way ANOVA with Bonferroni correction was used.

Figure 1

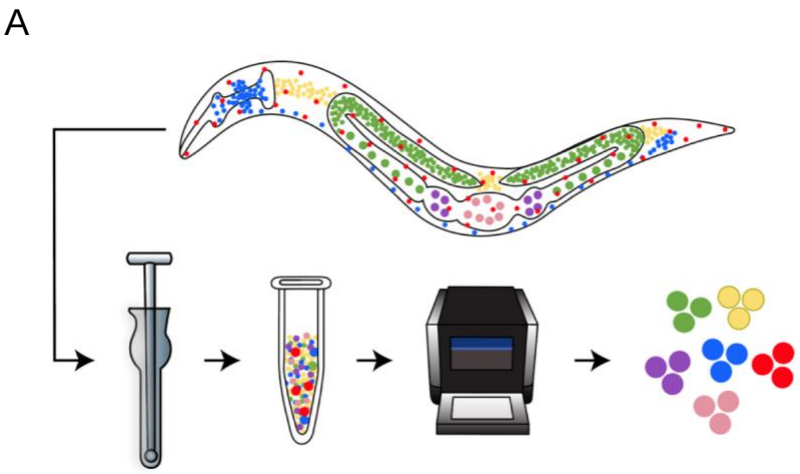
A

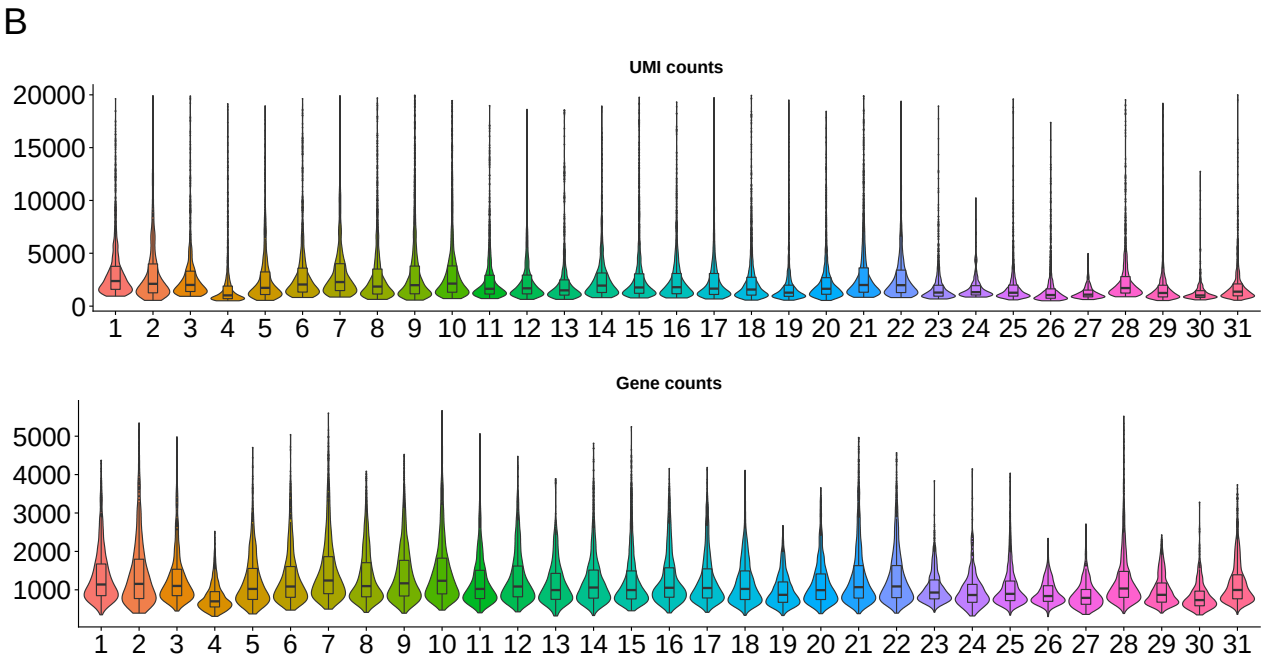
B
UMI counts
20000
15000
10000
5000
0
1 2 3 4 5 6 7 8 9 10 11 12 13 14 15 16 17 18 19 20 21 22 23 24 25 26 27 28 29 30 31
Gene counts
5000
4000
3000
2000
1000
1 2 3 4 5 6 7 8 9 10 11 12 13 14 15 16 17 18 19 20 21 22 23 24 25 26 27 28 29 30 31

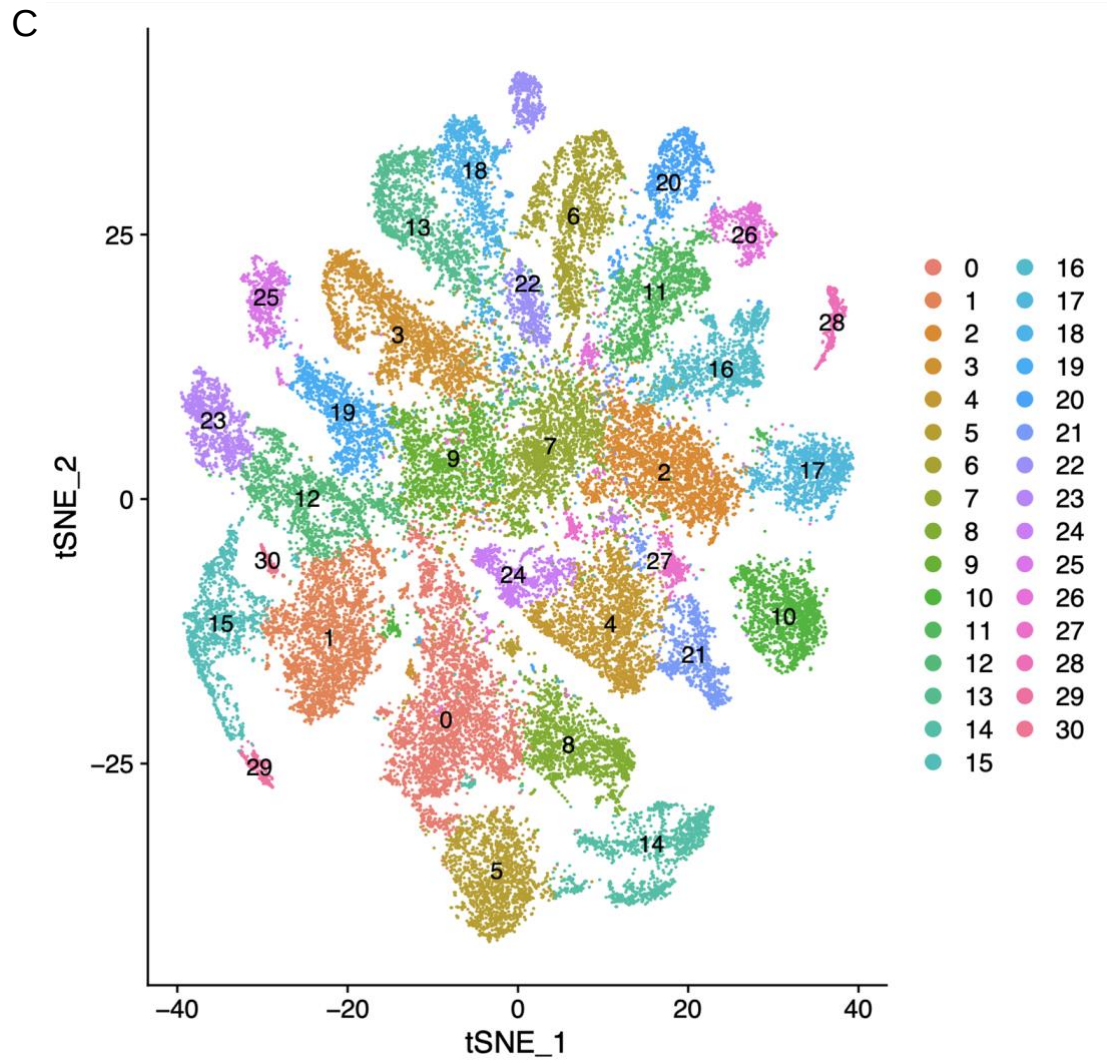

Figure 1: snRNA-seq identifies distinct cell and functional categories in the *C. elegans* adult hermaphrodite.
(A). Experimental flow for single-nucleus isolation and snRNA-seq. (B). Violin and boxplot of UMI (unique molecular identifier) and gene counts per cell in each sample across 31 single-nuclei samples. (C). t-distributed stochastic neighbor embedding (t-SNE) plot of cells from all the samples with clustering through unsupervised Louvain clustering.

Figure 2

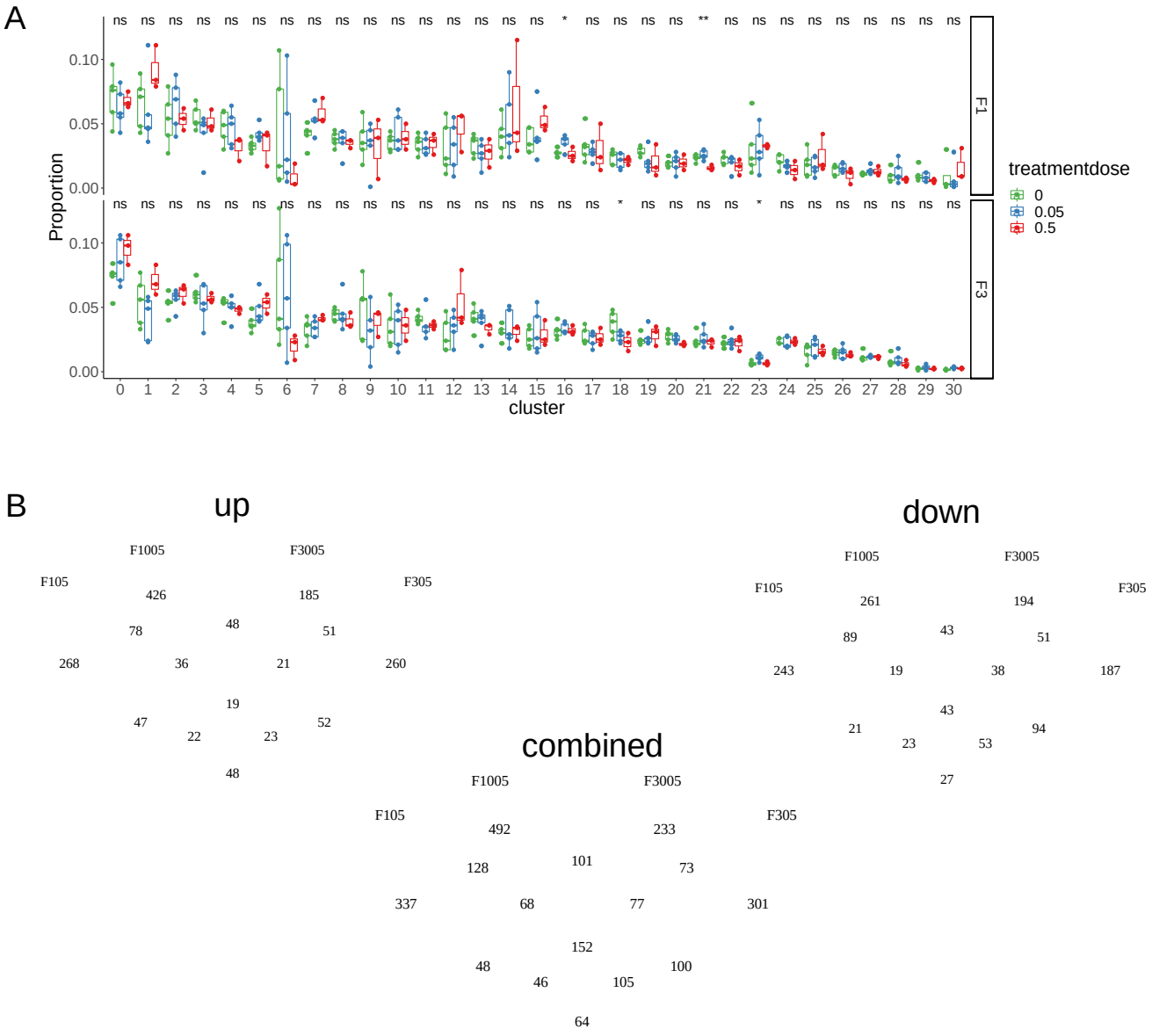

Figure 2: F1 and F3 analysis reveals proportions and DEGs shared between different treatment conditions

(A) Proportion distribution plot of all F1 and F3 samples colored by different treatment dose, each dot represents one sample. X-axis indicates cluster number assigned by Louvain clustering and Y-axis indicates cells of that cluster divided by all cells from that specific sample. All conditions were non-significant based on post-hoc Tukey statistic. (B) Venn diagram based on the union of DEGs across all the cell types, separated by Up-regulated DEGs only (left), Downregulated genes only (right), and all DEGs (middle). F105 indicates 0.5% ethanol for the F1 generation. F1005 indicates 0.05% ethanol for the F1 generation. F305 indicates 0.5% ethanol for the F3 generation. F3005 indicates 0.05% ethanol for the F3 generation.

Figure 3

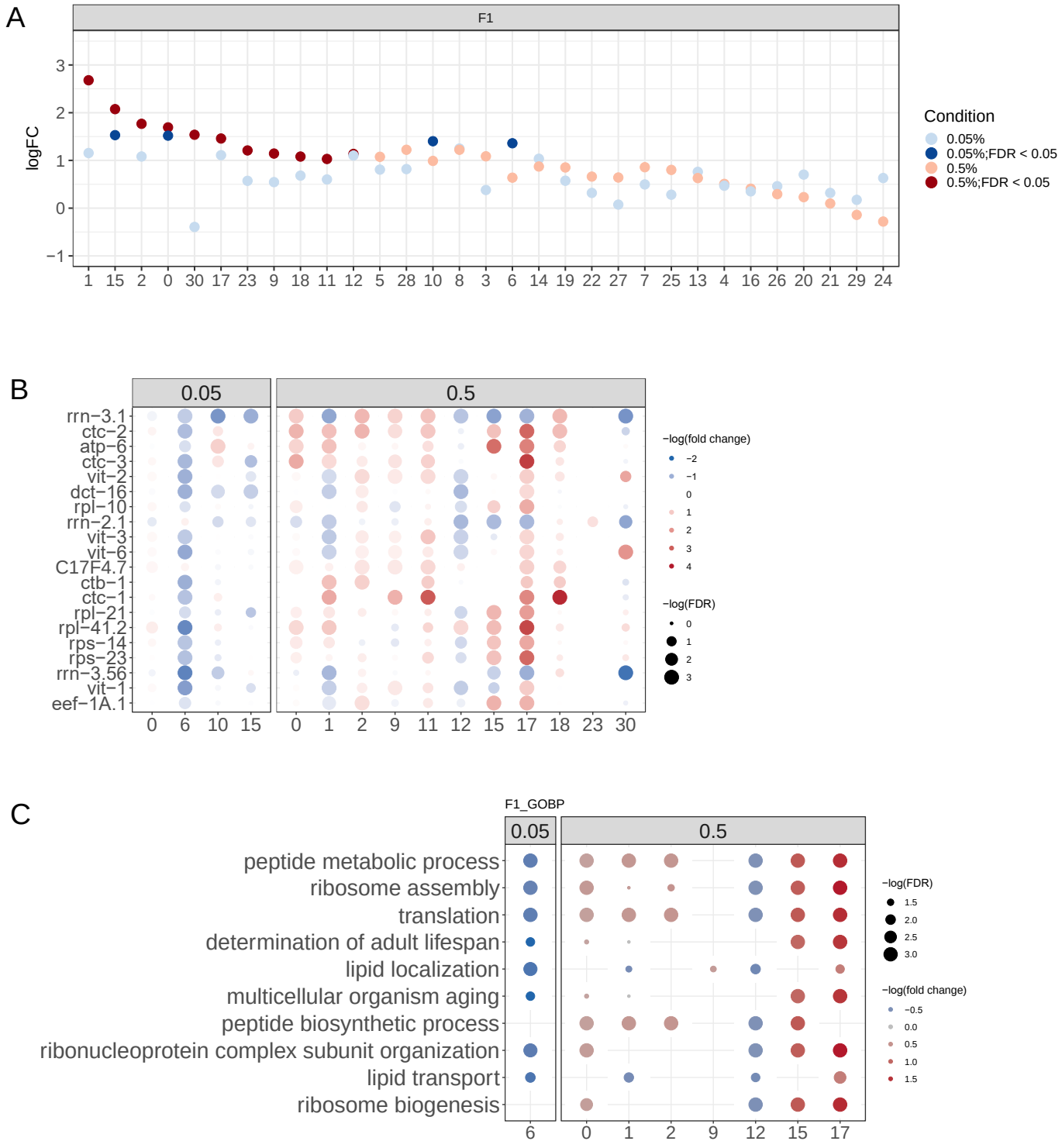
A
F1
logFC
3
2
1
0
−1
1 15 2 0 30 17 23 9 18 11 12 5 28 10 8 3 6 14 19 22 27 7 25 13 4 16 26 20 21 29 24
Condition
0.05%
0.05%;FDR < 0.05
0.5%
0.5%;FDR < 0.05
B
0.05
0.5
rrn−3.1
ctc−2
atp−6
ctc−3
vit−2
dct−16
rpl−10
rrn−2.1
vit−3
vit−6
C17F4.7
ctb−1
ctc−1
rpl−21
rpl−41.2
rps−14
rps−23
rrn−3.56
vit−1
eef−1A.1
0 6 10 15
0 1 2 9 11 12 15 17 18 23 30
−log(fold change)
−2
−1
0
1
2
3
4
−log(FDR)
0
1
2
3
C
F1_GOBP
0.05
0.5
peptide metabolic process
ribosome assembly
translation
determination of adult lifespan
lipid localization
multicellular organism aging
peptide biosynthetic process
ribonucleoprotein complex subunit organization
lipid transport
ribosome biogenesis
6
0 1 2 9 12 15 17
−log(FDR)
1.5
2.0
2.5
3.0
−log(fold change)
−0.5
0.0
0.5
1.0
1.5

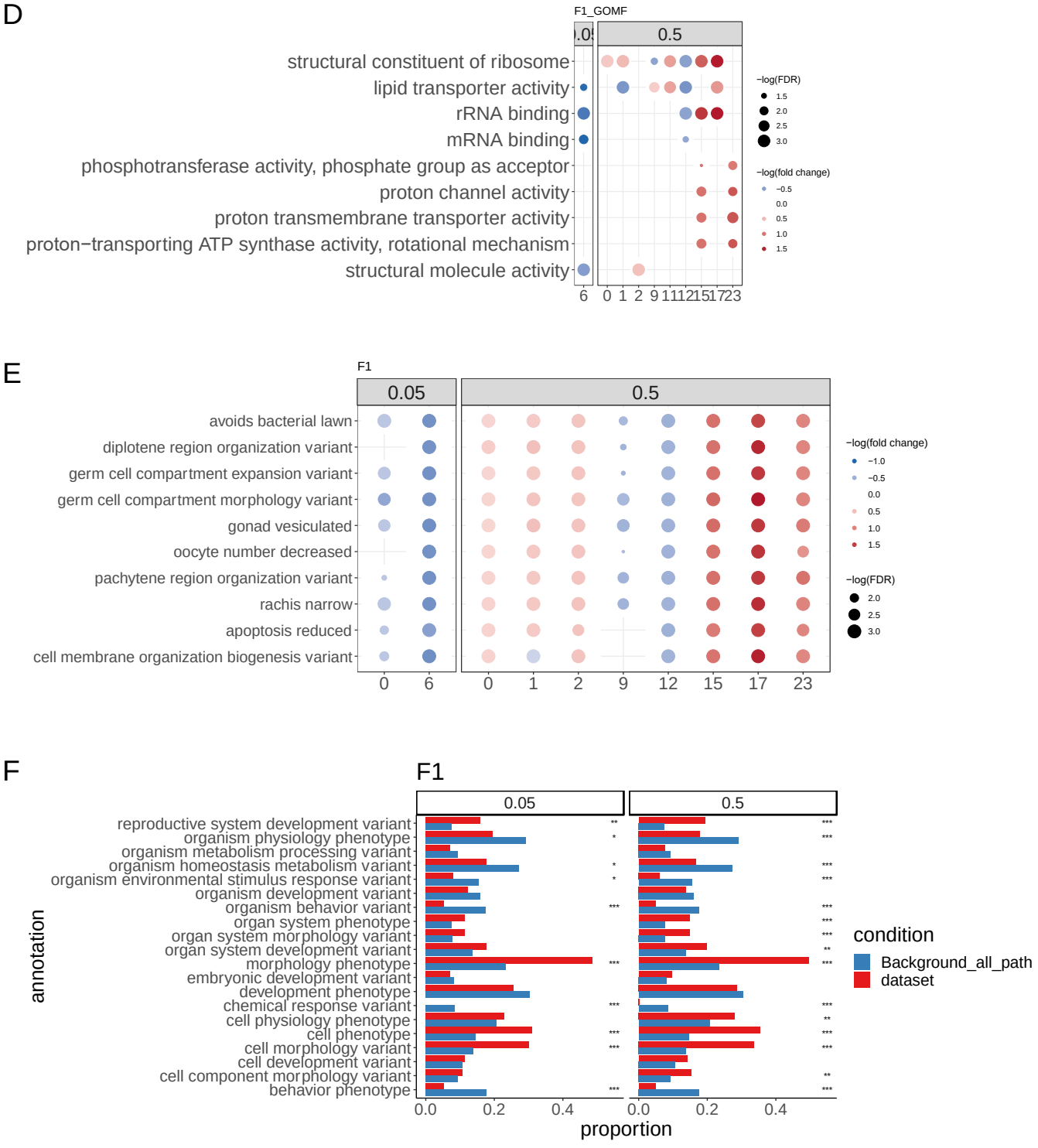

Figure 3: Cluster-specific analysis of ethanol's intergenerational effects (F1)
(A) Euclidean distance analysis of all cell clusters. X-axis indicates cluster number and y-axis indicates log fold change compared to Euclidean distance obtained by permuting treatment labels. Significance was assessed based on comparing Euclidean distance against 1000 random permutated labels. (B) Dot heatmap of top shared DEGs across cell types with

significantly altered Euclidean distance metric. Dot size corresponded to -log(FDR) and dot color corresponded to -log(fold change) retrieved by differential gene analysis, only significant DEGs were plotted. (C) Dot heatmap of top shared gene ontology biological pathway (GOBP) pathways across cell types with significantly altered Euclidean distance metric. Dot size corresponded to -log(FDR) obtained from enrichment analysis and dot color corresponded -log(median fold change) of overlapping genes in each pathway. (D) Dot heatmap of top shared gene ontology molecular function (GOMF) pathways across cell types with significantly altered Euclidean distance metric. Dot size corresponded to -log(FDR) obtained from enrichment analysis and dot color corresponded -log(median fold change) of overlapping genes in each pathway. € Dot heatmap of top shared wormbase phenotype across cell types with significantly altered Euclidean distance metric. Dot size corresponded to -log(FDR) obtained from enrichment analysis and dot color corresponded -log(median fold change) of overlapping genes in each pathway. (F) Bar graph showing the proportion of top wormbase phenotype annotations from all enriched pathways (“dataset”) and wormbase phenotype database (“Background_all_path”). For each wormbase phenotype from original database we retrieved corresponding wormbase phenotype annotations by querying EBI OLS API, followed by selecting top 20 shared phenotypes. Annotations from first level (nematode phenotype, physiology phenotype and anatomical phenotype) since these terms were too general to make interpretations. Proportion were calculated based on proportion of annotations among all enriched pathways (“dataset”) and wormbase phenotype database (“Background_all_path”). Fisher exact test was used to compare proportions between two conditions in each annotation category.

Figure 4

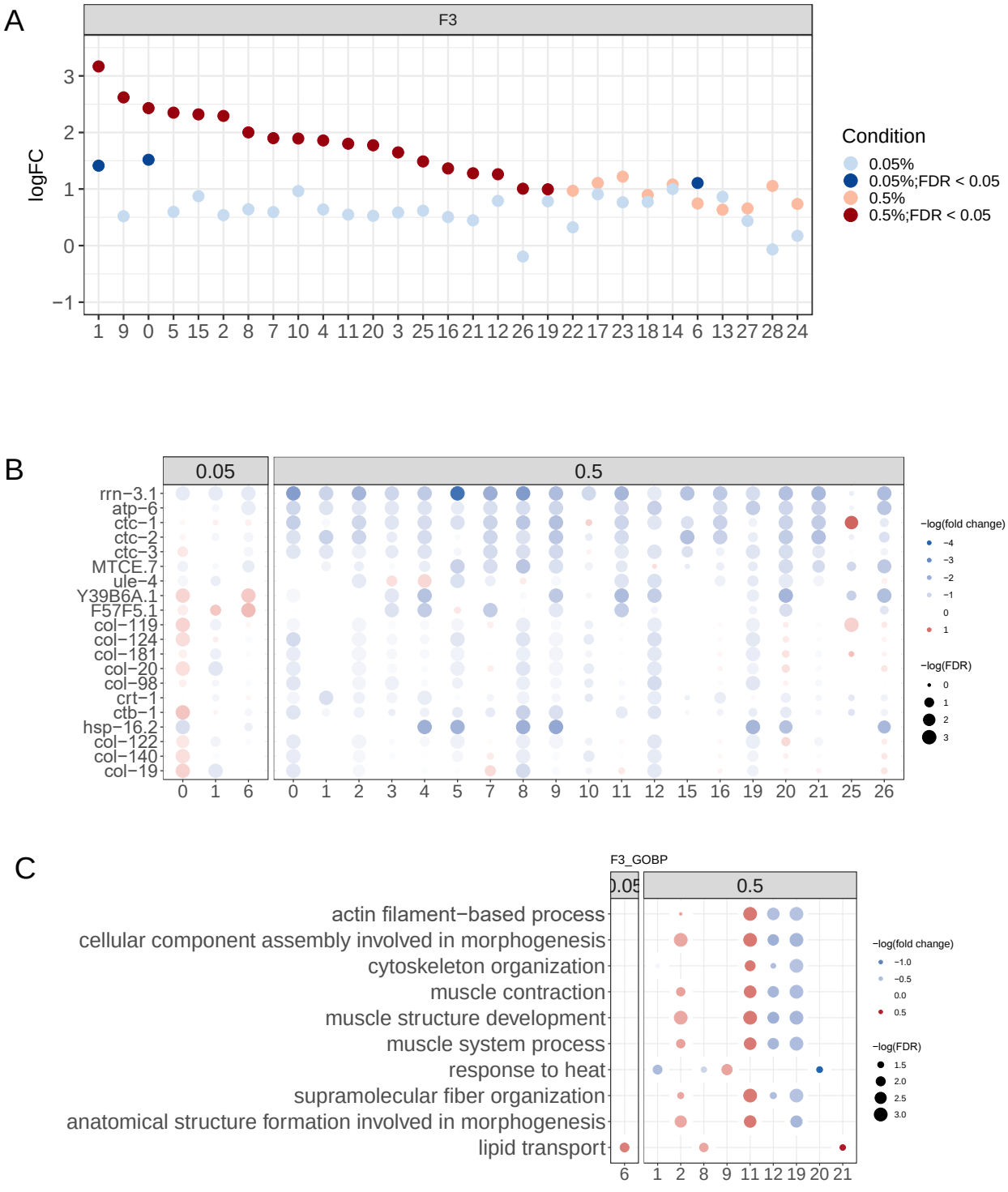
A
F3
logFC
3
2
1
0
−1
1 9 0 5 15 2 8 7 10 4 11 20 3 25 16 21 12 26 19 22 17 23 18 14 6 13 27 28 24
Condition
0.05%
0.05%;FDR < 0.05
0.5%
0.5%;FDR < 0.05
B
0.05
0.5
rrn−3.1
atp−6
ctc−1
ctc−2
ctc−3
MTCE.7
ule−4
Y39B6A.1
F57F5.1
col−119
col−124
col−181
col−20
col−98
crt−1
ctb−1
hsp−16.2
col−122
col−140
col−19
0 1 6
0 1 2 3 4 5 7 8 9 10 11 12 15 16 19 20 21 25 26
−log(fold change)
−4
−3
−2
−1
0
1
−log(FDR)
0
1
2
3
C
F3_GOBP
0.05
0.5
actin filament−based process
cellular component assembly involved in morphogenesis
cytoskeleton organization
muscle contraction
muscle structure development
muscle system process
response to heat
supramolecular fiber organization
anatomical structure formation involved in morphogenesis
lipid transport
6
1 2 8 9 11 12 19 20 21
−log(fold change)
−1.0
−0.5
0.0
0.5
−log(FDR)
1.5
2.0
2.5
3.0

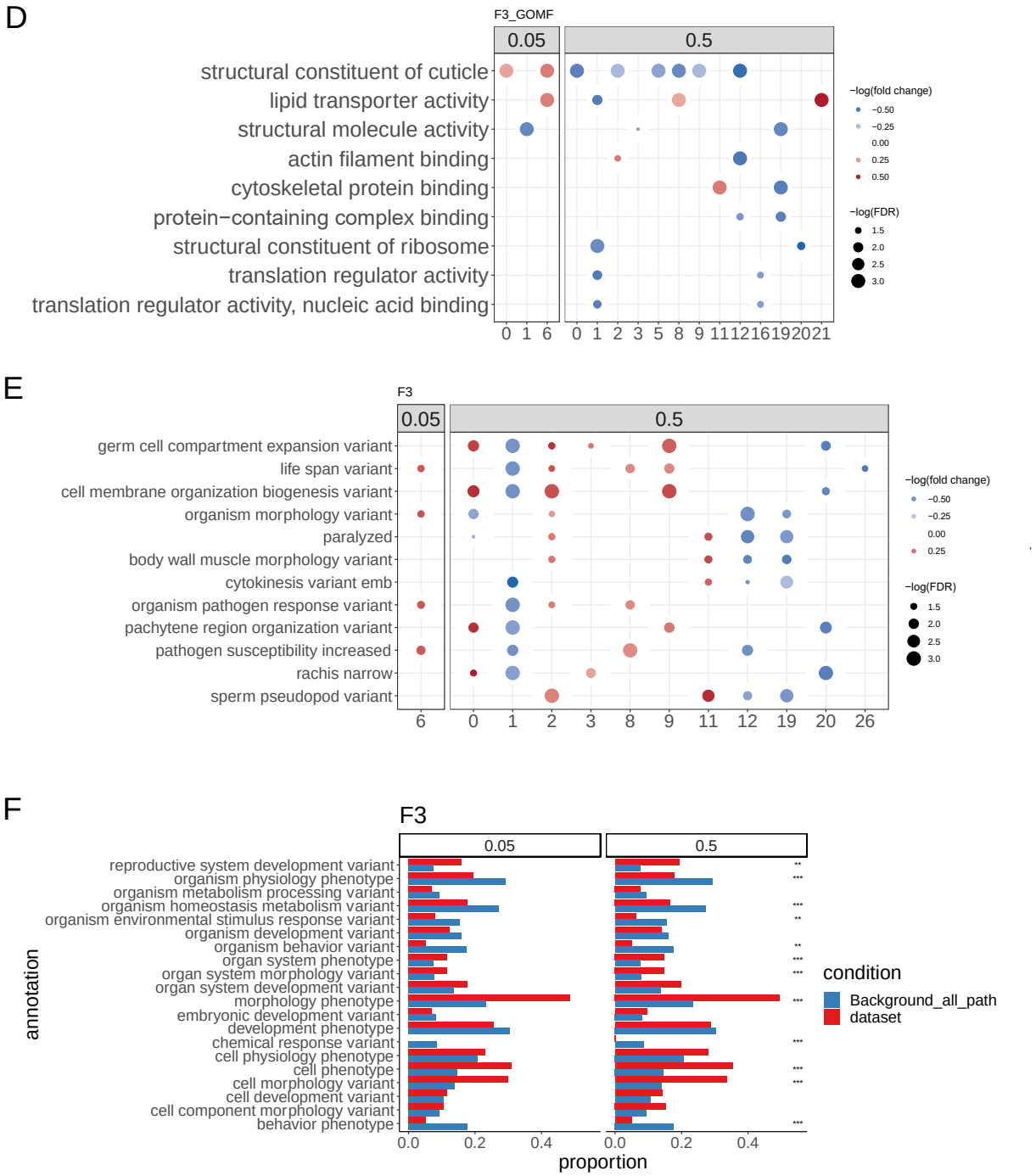

Figure 4. Cluster-specific analysis of ethanol's transgenerational effects (F3)
(A). Euclidean distance sensitivity analysis of all the cell clusters. X-axis indicates cluster number and y-axis indicates log fold change compared to Euclidean distance obtained by permuting treatment labels. Significance was assessed based on comparing Euclidean distance against 1000 random permutated labels. (B). Dot heatmap of top shared DEGs across cell types with significantly altered Euclidean distance metric. Dot size corresponded to -log(FDR) and dot color corresponded to -log(fold change) retrieved by differential gene analysis, only significant

DEGs were plotted. (C). Dot heatmap of top shared gene ontology biological pathway (GOBP) pathways across cell types with significantly altered Euclidean distance metric. Dot size corresponded to -log(FDR) obtained from enrichment analysis and dot color corresponded -log(median fold change) of overlapping genes in each pathway. (D). Dot heatmap of top shared gene ontology molecular function (GOMF) pathways across cell types with significantly altered Euclidean distance metric. Dot size corresponded to -log(FDR) obtained from enrichment analysis and dot color corresponded -log(median fold change) of overlapping genes in each pathway. €. Dot heatmap of top shared wormbase phenotype across cell types with significantly altered Euclidean distance metric. Dot size corresponded to -log(FDR) obtained from enrichment analysis and dot color corresponded -log(median fold change) of overlapping genes in each pathway. (F). Bar plot showing the proportion of top wormbase phenotype annotations from all enriched pathways ("dataset") and wormbase phenotype database ("Background_all_path"). For each wormbase phenotype from original database we retrieved corresponding wormbase phenotype annotations by querying EBI OLS API, followed by selecting top 20 shared phenotypes. Annotations from first level (nematode phenotype, physiology phenotype and anatomical phenotype) since these terms were too general to make interpretations. Proportion were calculated based on proportion of annotations among all enriched pathways ("dataset") and wormbase phenotype database ("Background_all_path"). Fisher exact test was used to compare proportions between two conditions in each annotation category.

Figure 5

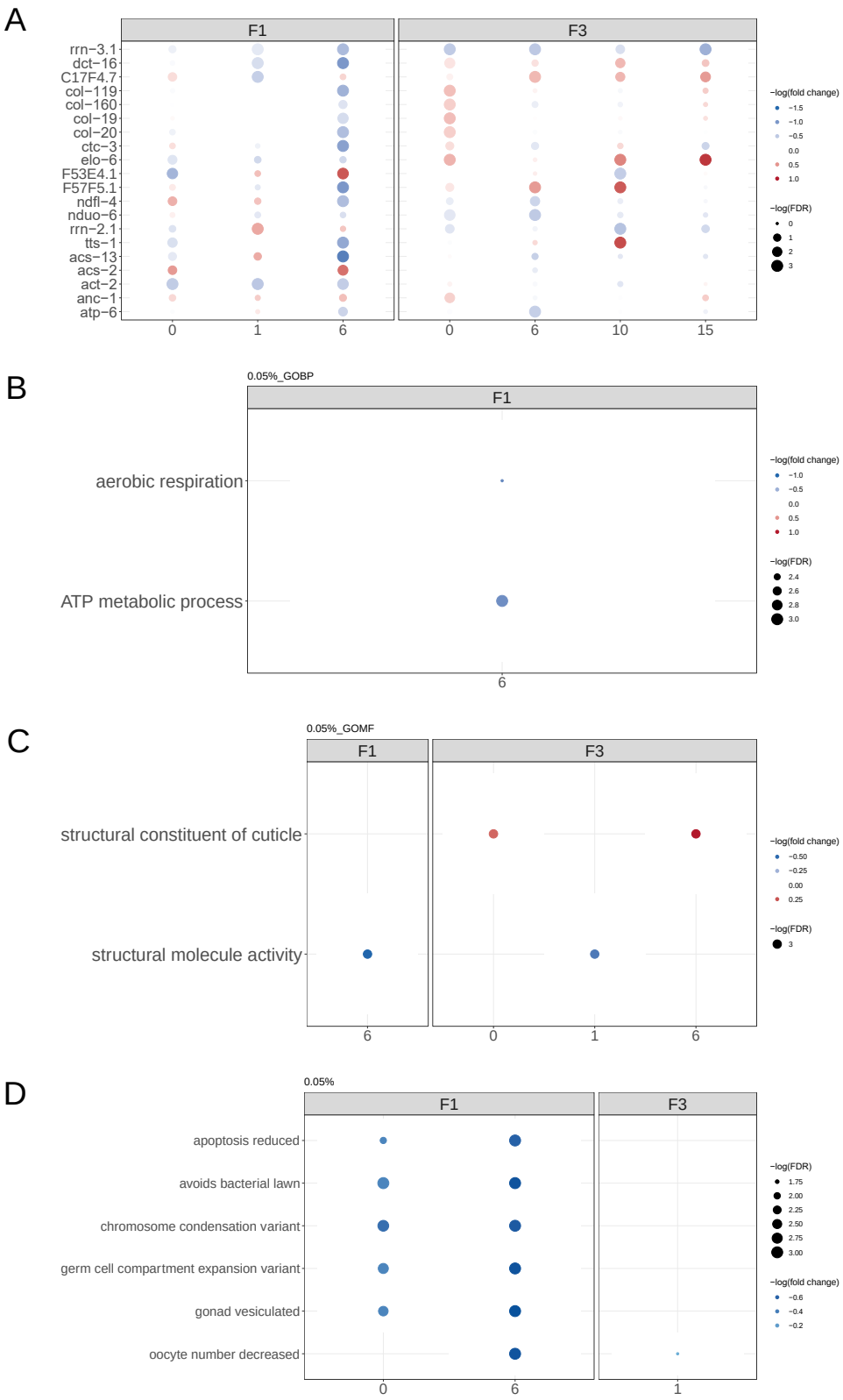
A
F1
F3
rrn−3.1
dct−16
C17F4.7
col−119
col−160
col−19
col−20
ctc−3
elo−6
F53E4.1
F57F5.1
ndfl−4
nduo−6
rrn−2.1
tts−1
acs−13
acs−2
act−2
anc−1
atp−6
0
1
6
0
6
10
15
−log(fold change)
−log(FDR)
B
0.05%_GOBP
F1
aerobic respiration
ATP metabolic process
6
−log(fold change)
−log(FDR)
C
0.05%_GOMF
F1
F3
structural constituent of cuticle
structural molecule activity
6
0
1
6
−log(fold change)
−log(FDR)
D
0.05%
F1
F3
apoptosis reduced
avoids bacterial lawn
chromosome condensation variant
germ cell compartment expansion variant
gonad vesiculated
oocyte number decreased
0
6
1
−log(FDR)
−log(fold change)

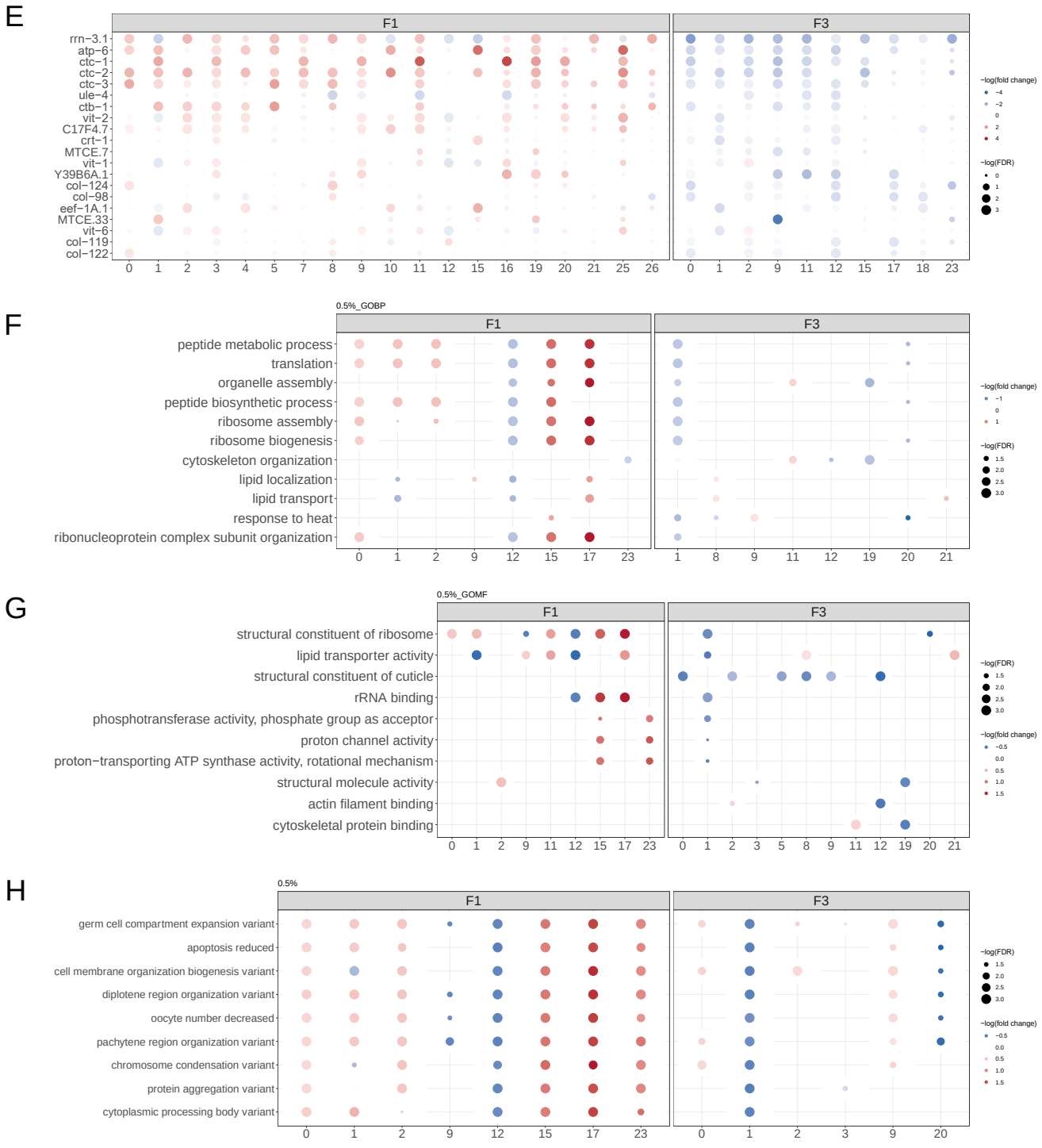

Figure 5: Cross generation comparison of ethanol exposure effects.
Cross generation comparison of 0.05% ethanol exposure were shown in (A) top shared DEGs, (B) top shared GOBP, (C) top shared GOMF pathways, (D) top shared wormbase phenotypes among cell types with significant sensitivity. Cross generation comparison of 0.5% ethanol exposure were shown in (E) top shared DEGs, (F) top shared GOBP, (G) top shared GOMF pathways, (H) top shared wormbase phenotypes among cell types with significant sensitivity.

Figure 6

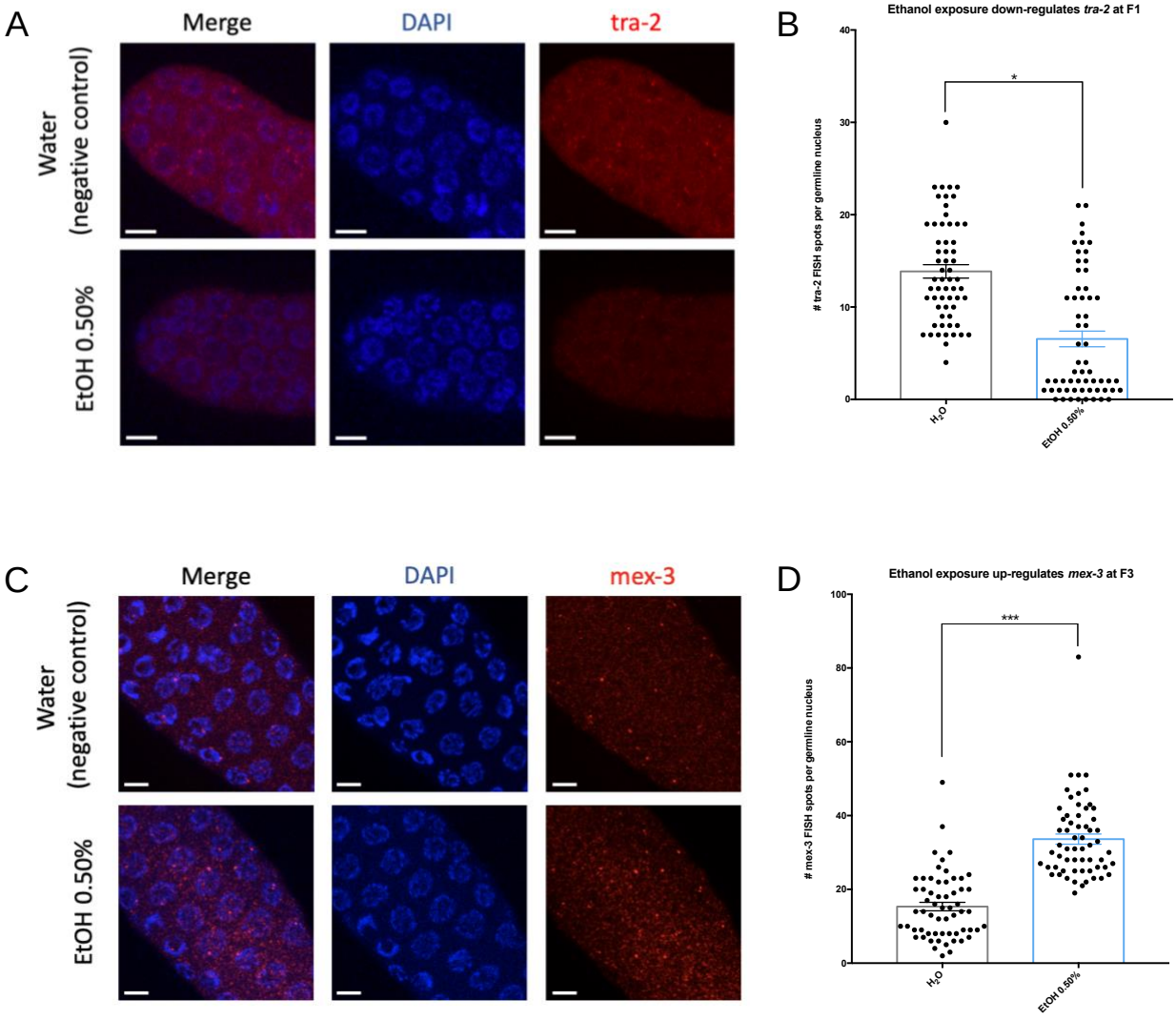

Figure 6: Validation of snRNA-seq results using smFISH
Validation of snRNA-seq data through single molecule fluorescence *in situ* hybridization (smFISH). Slides were imaged on the Leica SP8 confocal microscope (A,C), followed by fluorescence quantification using FISH-Quant v3 (B,D). Probe for *tra-2* was generated by Stellaris and used to validate F1 snRNA-seq results (A-B). Probe for *mex-3* was generated by Stellaris and used to validate F3 snRNA-seq results (C-D). Scale bar 5 µm. N=3, 2 worms per repeat, 10 nuclei per germline. *P<0.05, ***P<0.001.

Figure 7

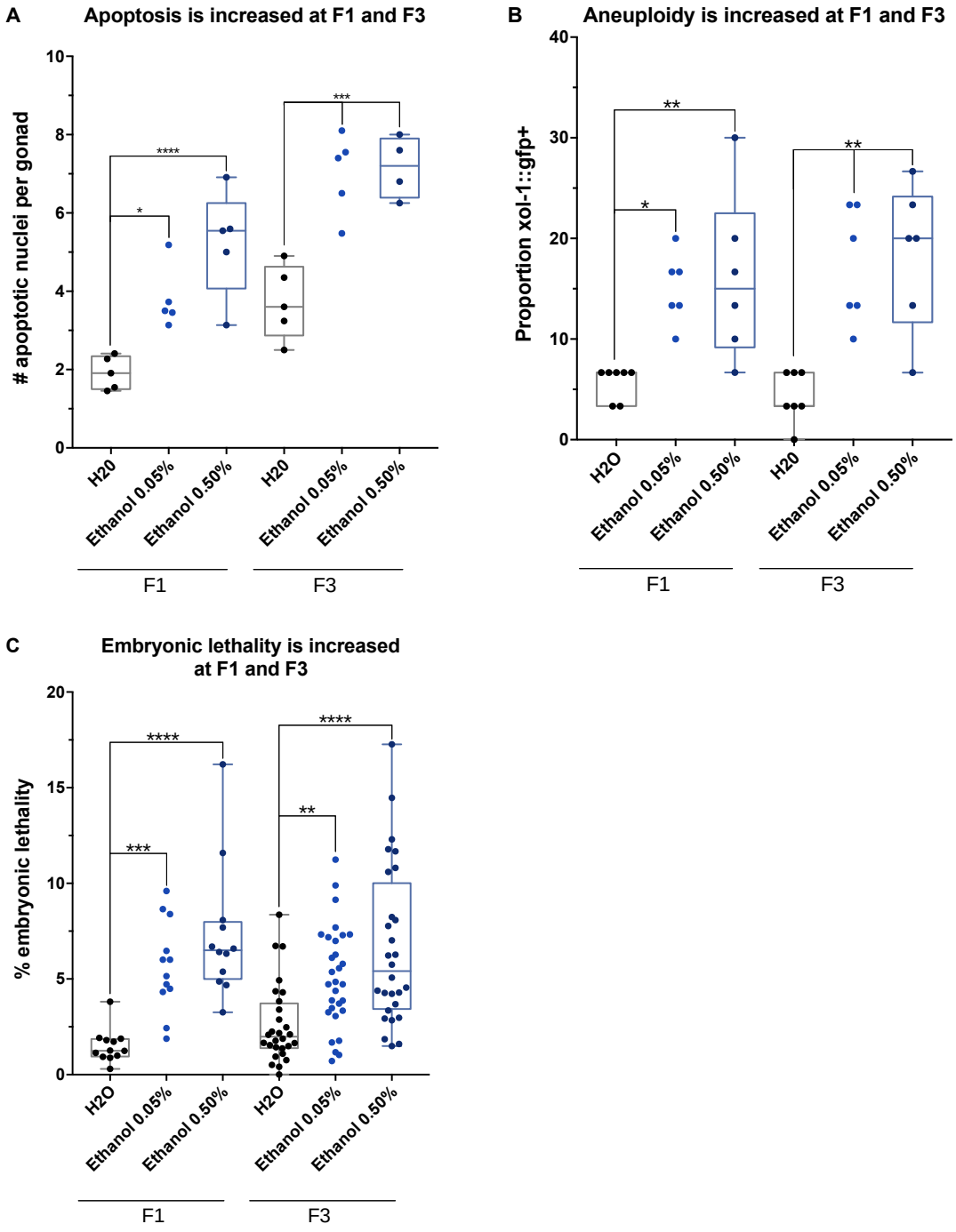

Figure 7: Ethanol exposure causes reproductive dysfunction both at F1 and F3
P0 hermaphrodites were exposed to water (black), 0.05% ethanol (light blue), or 0.50% ethanol (dark blue). Number of apoptotic nuclei per gonadal arm was assessed for N2, N=4-5, 22 worms per repeat (A). Out of 30 total worms per repeat, the percent (%) of worms with at least 1 GFP+ embryo was recorded, N=6, 30 worms per repeat (B). Percent embryonic lethality per worm was measured for N2, N=4-10, 2-3 worms per repeat (C). One-way ANOVA with Bonferroni correction. *P<0.05, **P<0.01, ***P<0.001, ****P<0.0001

Figure S1

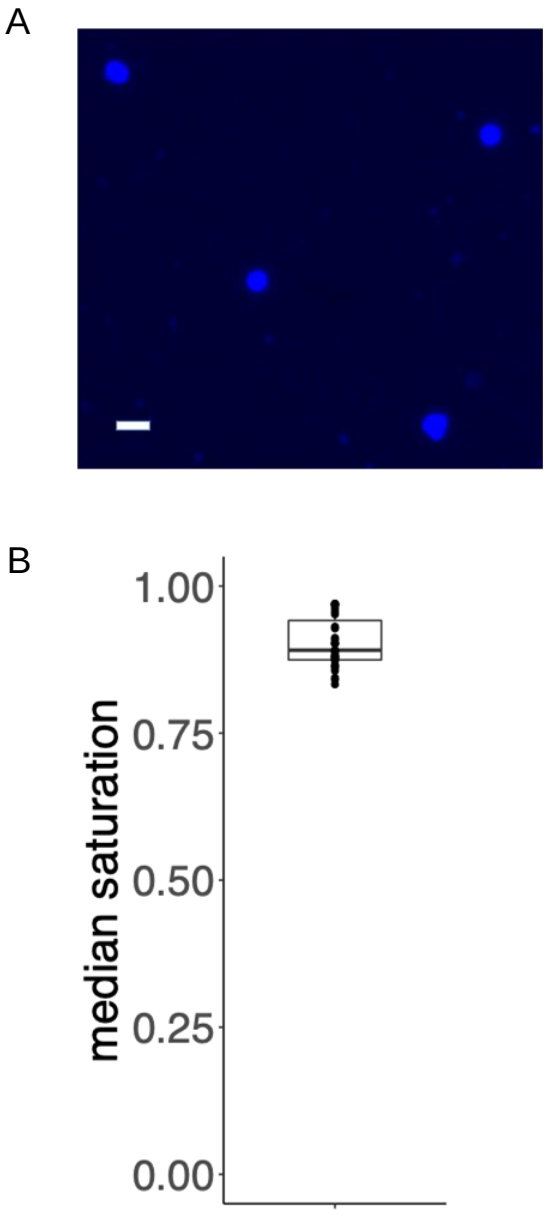

Figure S1: Single-nucleus extraction and sequencing
(A). High resolution fluorescent microscopy image of DAPI stained dissociated nuclei showing intact appearance. Scale bar is 10μM. (B). Boxplot of median saturation value across all 31 samples. Median saturation is derived from Cellranger. Median saturation is defined by how many genes can be detected with the median read number of the cell compared to cells with highest reads number. An average saturation of 90.3% was achieved indicating a high read depth.

Figure S2

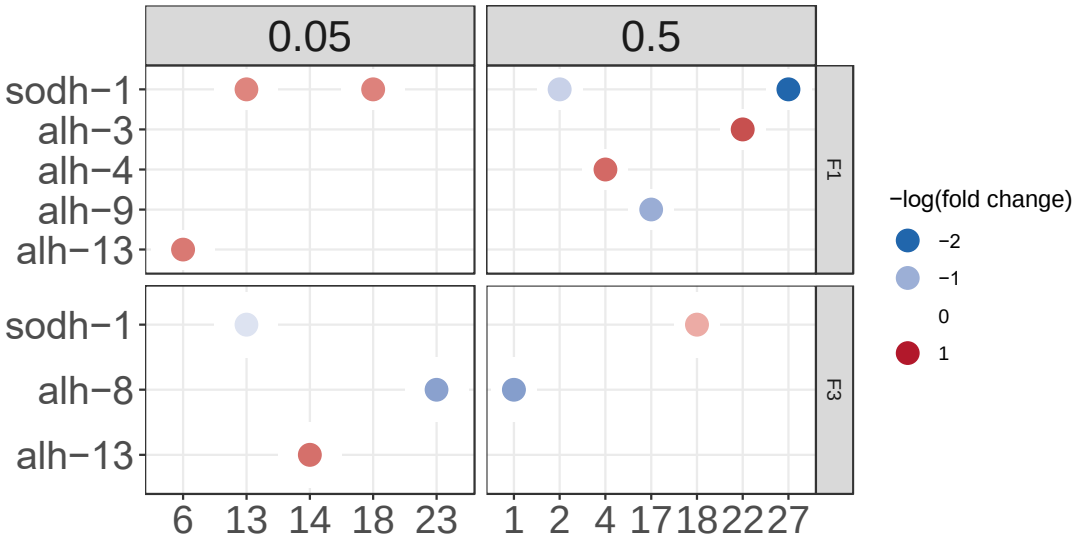

Figure S2: Cluster-specific DEGs related to ethanol metabolism at F1 and F3
Dot heatmap of ethanol metabolism related genes across different clusters, separated by exposure dose and generation. Only DEGs with an FDR < 5% were plotted. Color indicates –log10(fold change).

Figure S3

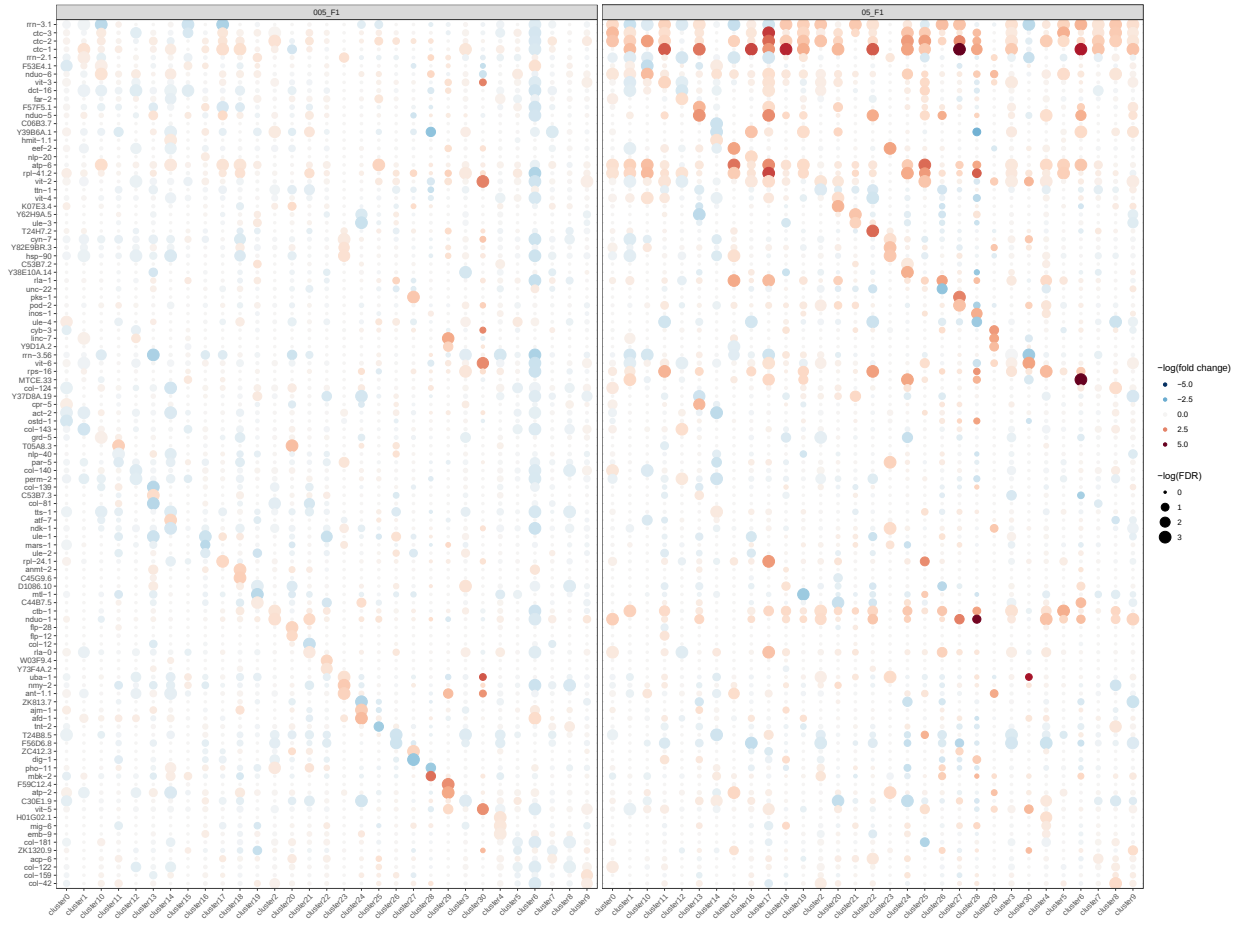

Figures S3: Dot heatmap of top 3 differential expressed genes across clusters in F1. X-axis indicates different clusters representing different tissues and Y-axis indicates top 3 differentially expressed genes after ethanol treatment across clusters ranked by monocle based FDR. The plot is further separated by different ethanol doses (0.05% on the left and 0.5% on the right). The size of the dot is correlated to –log(FDR) of differential expression p-value and the color represents direction and scale of fold change with upregulation is shown in red and downregulation is shown in blue.

Figures S4

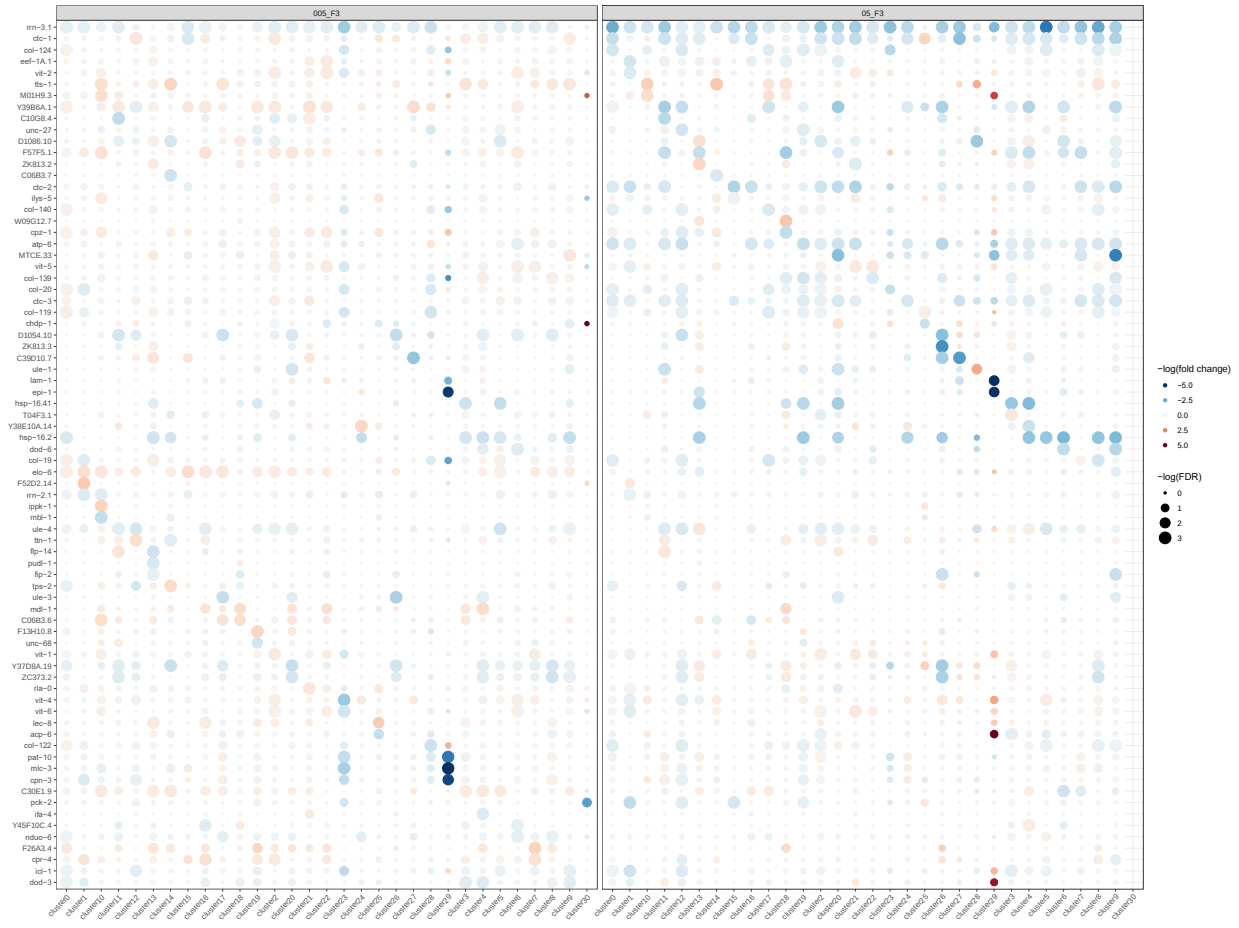

Figure S4: Dot heatmap of top 3 differential expressed genes across clusters in F3
X-axis indicates different clusters representing different tissues and Y-axis indicates the top 3 differentially expressed genes after ethanol treatment across clusters ranked by monocle based FDR. The plot is further separated by different ethanol doses (0.05% on the left and 0.5% on the right). The size of the dot is correlated to –log(FDR) of differential expression p-value and the color represents direction and scale of fold change with upregulation is shown in red and downregulation is shown in blue.

Table 1

Pathways	conditions
peptide metabolic process	F105,F305,F1005,F3005
carboxylic acid metabolic process	F105,F305,F1005,F3005
small molecule biosynthetic process	F105,F305,F1005,F3005
defense response	F105,F305,F1005,F3005
embryo development ending in birth or egg hatching	F105,F305,F1005
aging	F105,F1005,F3005
ribosome assembly	F105,F305,F1005
cytoskeleton organization	F105,F305,F3005
multi-organism process	F105,F305,F1005
ribose phosphate metabolic process	F105,F305,F1005
cellular process involved in reproduction in multicellular organism	F105,F305,F1005
protein catabolic process	F105,F1005,F3005
response to heat	F105,F305,F1005
phosphotransferase activity, phosphate group as acceptor	F105,F305,F1005
threonine-type peptidase activity	F105,F305,F1005
unfolded protein binding	F105,F305,F1005
structural molecule activity	F305,F1005,F3005
calcium ion binding	F305,F1005,F3005

Table 1: Shared pathways identified through DEG analysis across both exposures and generations

Table of selected highly shared pathways identified by the union of all cell type specific DEGs across our four conditions. F105 indicates 0.5% ethanol exposure at the F1 generation. F1005 indicates 0.05% ethanol exposure at the F1 generation. F305 indicates 0.5% ethanol exposure at the F3 generation. F3005 indicates 0.05% ethanol exposure at the F3 generation.

t-SNE showing cell type 1

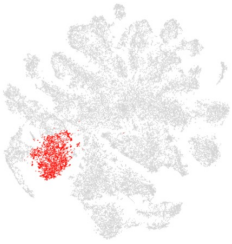

Top 20 enriched genes

	p_val	avg_log2FC	pct.1	pct.2	p_val_adj
linc-7	2.79E-277	2.8461492	0.564	0.188	1.31E-272
mix-1	0	2.64656064	0.79	0.264	0
set-24	0	2.64356758	0.552	0.08	0
Y57A10A.31	0	2.59424002	0.593	0.132	0
such-1	0	2.4308028	0.533	0.104	0
Y57A10A.1	0	2.42585518	0.478	0.051	0
xpc-1	0	2.42568406	0.648	0.187	0
mdt-17	0	2.4250593	0.466	0.096	0
H06I04.3	0	2.41221422	0.683	0.237	0
F52D2.14	4.74E-224	2.40706998	0.253	0.041	2.22E-219
fcd-2	0	2.36277275	0.555	0.121	0
npp-8	0	2.36057674	0.642	0.21	0
T05F1.2	2.97E-245	2.3525074	0.619	0.257	1.39E-240
chk-2	0	2.33130698	0.39	0.028	0
lea-1	0	2.31164841	0.877	0.531	0
gcn-1	1.62E-286	2.30627886	0.645	0.264	7.60E-282
F53H1.4	0	2.241348	0.645	0.206	0
Y48G8AL.5	0	2.23551318	0.541	0.131	0
Y79H2A.3	0	2.20657813	0.631	0.214	0
attf-6	0	2.20258992	0.511	0.135	0

Top 20 depleted genes

	p_val	avg_log2FC	pct.1	pct.2	p_val_adj
ule-4	1.52E-67	-3.32952	0.285	0.52	7.15E-63
D1086.10	4.67E-54	-3.1766948	0.191	0.404	2.19E-49
pat-10	1.34E-236	-3.1255073	0.28	0.731	6.29E-232
lev-11	1.23E-263	-3.0455223	0.27	0.753	5.75E-259
act-4	6.72E-265	-3.0262073	0.242	0.746	3.15E-260
far-2	1.18E-250	-3.016277	0.392	0.787	5.55E-246
dig-1	1.67E-33	-2.9673044	0.088	0.246	7.84E-29
cpn-3	6.78E-221	-2.9104893	0.254	0.706	3.18E-216
mlc-3	1.43E-233	-2.8939846	0.235	0.708	6.69E-229
ttr-16	3.64E-214	-2.8665463	0.199	0.669	1.71E-209
unc-54	5.17E-218	-2.8490946	0.257	0.707	2.42E-213
lbp-2	2.38E-190	-2.8031531	0.225	0.655	1.11E-185
unc-27	1.07E-210	-2.7971513	0.24	0.69	5.03E-206
F46H5.3	1.07E-301	-2.7703362	0.34	0.827	5.01E-297
nlp-77	2.54E-214	-2.7427856	0.304	0.726	1.19E-209
unc-87	6.95E-217	-2.7392701	0.171	0.654	3.26E-212
unc-15	1.51E-212	-2.7286407	0.213	0.671	7.08E-208
col-95	2.76E-155	-2.7143854	0.212	0.61	1.30E-150
perm-4	1.63E-120	-2.6835737	0.257	0.597	7.65E-116
col-140	6.81E-223	-2.5844856	0.365	0.758	3.19E-218

Tissue enrichment | -log10 Q-values

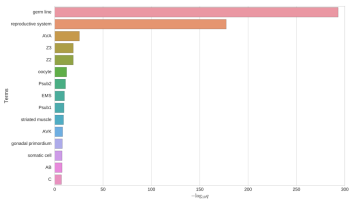

GO enrichment | -log10 Q-values

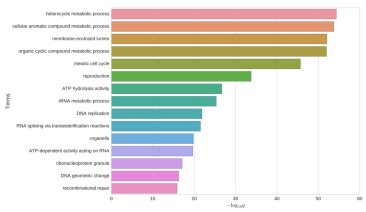

Phenotype enrichment | -log10 Q-values

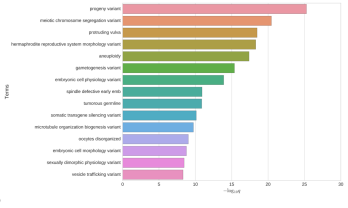

such-1 (suppressor of spindle checkpoint defect)

clone	cluster	chromosome	cosmid	CDS	gene	size
133c4	CELE03479	3	Y66D12A	Y66D12A.17		1.97

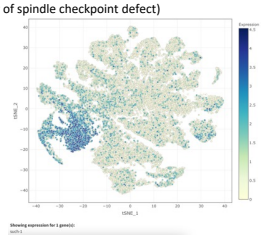

xpc-1 (enable DNA damage binding activity in response to

clone	cluster	chromosome	cosmid	CDS	gene	size
116e7	CELE03226	4	Y7H8.12C	Y7H8.12C.2		1.46

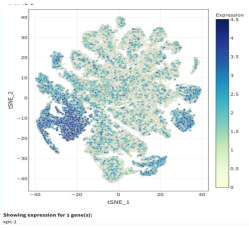

t-SNE showing cell type 2

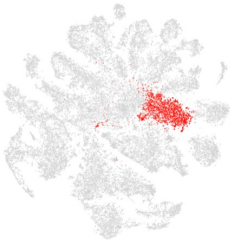

Top 20 enriched genes

	p_val	avg_log2FC	pct.1	pct.2	p_val_adj
unc-27	0	2.51261312	0.992	0.647	0
unc-54	0	2.35277309	0.997	0.665	0
F37H8.5	0	2.35062914	0.911	0.428	0
tnt-2	0	2.33913036	0.981	0.58	0
lbp-2	0	2.30163363	0.982	0.611	0
cpn-3	0	2.23614211	0.992	0.663	0
unc-15	0	2.21255302	0.988	0.626	0
unc-87	0	2.2004755	0.989	0.607	0
clik-1	0	2.19257175	0.986	0.658	0
ttr-25	0	2.18420317	0.84	0.384	0
ttr-16	0	2.1791393	0.992	0.624	0
pat-10	0	2.15411398	0.997	0.69	0
lec-5	0	2.13330611	0.89	0.439	0
act-1	0	2.11696419	0.999	0.76	0
R13H4.2	0	2.11351016	0.883	0.407	0
mup-2	0	2.08212893	0.943	0.538	0
lev-11	0	2.06259183	0.997	0.711	0
myo-3	0	2.05768003	0.87	0.413	0
act-4	0	2.05004295	0.996	0.702	0

Top 20 depleted genes

	p_val	avg_log2FC	pct.1	pct.2	p_val_adj
ule-3	5.58E-18	-2.7243192	0.146	0.248	2.62E-13
D1054.10	4.77E-25	-2.6661453	0.197	0.328	2.24E-20
ule-4	5.11E-14	-2.5256237	0.449	0.51	2.40E-09
D1086.10	6.78E-11	-2.5136821	0.334	0.396	3.18E-06
ZK813.7	7.39E-15	-2.4653669	0.14	0.228	3.47E-10
Y37D8A.19	1.26E-25	-2.4334874	0.232	0.364	5.92E-21
Y62H9A.5	1.06E-21	-2.4331092	0.169	0.287	4.98E-17
Y46H3C.7	4.76E-12	-2.3137245	0.06	0.127	2.23E-07
ule-5	8.38E-20	-2.3087491	0.223	0.333	3.93E-15
ZK813.3	9.36E-17	-2.2143448	0.146	0.246	4.39E-12
ZK813.1	9.74E-16	-2.2066885	0.119	0.209	4.57E-11
ZC373.2	1.85E-19	-2.1305956	0.228	0.339	8.66E-15
C39D10.7	6.15E-16	-2.0528625	0.192	0.288	2.89E-11
ZK813.2	2.64E-20	-2.0403526	0.187	0.295	1.24E-15
C10G8.4	3.34E-11	-2.0156747	0.273	0.347	1.57E-06
F55B11.2	1.24E-22	-1.8482166	0.097	0.212	5.80E-18
C30E1.9	2.24E-43	-1.8151273	0.313	0.493	1.05E-38
W02D9.7	1.82E-16	-1.7365146	0.149	0.246	8.55E-12
fipr-2	5.14E-15	-1.7134813	0.111	0.2	2.41E-10

Tissue enrichment | -log10 Q-values

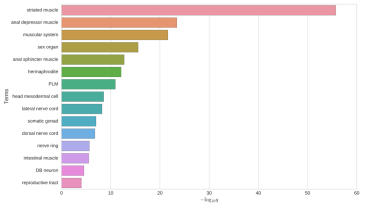

GO enrichment | -log10 Q-values

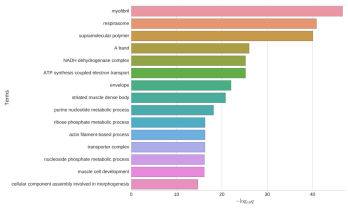

Phenotype enrichment | -log10 Q-values

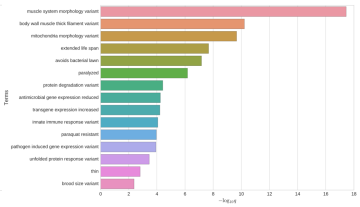

myo-3 (cytoskeletal motor activity)

clone	cluster	chromosome	cosmid	CDS	gene	size
39865	CELK00030	3	K12F2	K12F2.1	myo-3	1.94

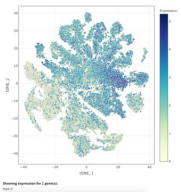

unc-27 (troponin c binding activity, locomotion)

cluster	chromosome	cosmid	CDS	gene
CELK01572	X	ZK721	9	unc-27

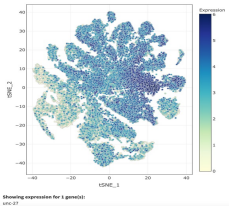

t-SNE showing cell type 3

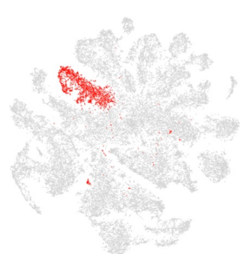

Top 20 enriched genes

	p_val	avg_log2FC	pct.1	pct.2	p_val_adj
ule-3	0	5.53196666	0.943	0.2	0
ZK813.7	0	5.35917056	0.917	0.182	0
D1054.10	0	5.24724634	0.987	0.281	0
ZK813.3	0	5.11824728	0.944	0.199	0
ZK813.1	0	5.11695215	0.901	0.163	0
Y62H9A.5	0	5.00096792	0.955	0.241	0
Y37D8A.19	0	4.96385168	0.985	0.32	0
ule-5	0	4.88593002	0.978	0.289	0
ZC373.2	0	4.82725502	0.982	0.294	0
Y57G11B.5	0	4.6462841	0.876	0.139	0
F55B11.2	0	4.6248496	0.883	0.166	0
F55B11.3	0	4.53398409	0.846	0.12	0
W02D9.7	0	4.50938141	0.889	0.202	0
F57C2.4	0	4.46009522	0.938	0.201	0
Y62H9A.4	0	4.26011605	0.874	0.156	0
Y62H9A.3	0	4.23553124	0.81	0.114	0
F53H4.2	0	3.94550278	0.78	0.14	0
F17E9.4	0	3.68168104	0.816	0.147	0
D1086.11	0	3.3350133	0.567	0.047	0
W02D9.6	0	3.31209428	0.607	0.072	0

Top 20 depleted genes

	p_val	avg_log2FC	pct.1	pct.2	p_val_adj
dig-1	3.51E-10	-2.9252217	0.168	0.241	1.64E-05
ttn-1	8.26E-13	-1.4457523	0.399	0.473	3.87E-08
spsb-1	9.84E-15	-1.2982337	0.203	0.293	4.61E-10
crh-1	3.92E-15	-1.1897702	0.179	0.267	1.84E-10
F53H2.3	4.96E-11	-1.173763	0.135	0.205	2.33E-06
lys-7	2.64E-08	-1.1636346	0.269	0.33	0.00123679
ddo-2	8.82E-10	-1.1633019	0.254	0.322	4.13E-05
Y105E8A.25	4.02E-15	-1.1468382	0.263	0.35	1.88E-10
sos-1	5.14E-17	-1.0759648	0.143	0.237	2.41E-12
mix-1	7.93E-14	-1.0676817	0.216	0.297	3.72E-09
ced-1	1.79E-23	-1.0378924	0.258	0.381	8.41E-19
tos-1	4.37E-19	-1.0219256	0.407	0.503	2.05E-14
daf-2	3.70E-15	-1.0164055	0.119	0.205	1.73E-10
mnk-1	1.30E-11	-0.9814214	0.137	0.21	6.11E-07
F53E4.1	9.30E-12	-0.9698191	0.202	0.282	4.36E-07
unc-22	3.44E-10	-0.9627772	0.276	0.344	1.61E-05
1-Jun	7.95E-07	-0.9303412	0.096	0.144	0.03727813
col-162	8.18E-07	-0.9114224	0.073	0.118	0.03837362
elpc-2	2.85E-10	-0.8936066	0.136	0.2	1.34E-05
C02E7.7	6.85E-07	-0.8918021	0.063	0.108	0.03212916

Tissue enrichment | -log10 Q-values

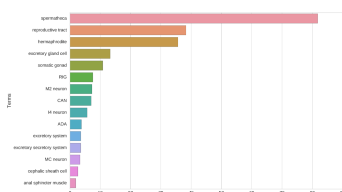

GO enrichment | -log10 Q-values

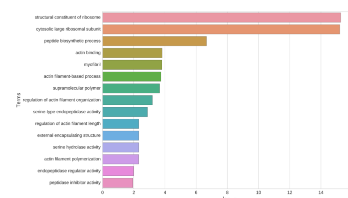

Phenotype enrichment | -log10 Q-values

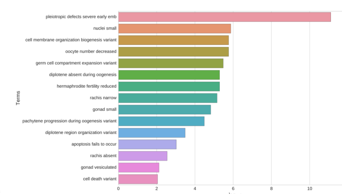

ule-3 (uterine lumen, hypodermis)

clone	cluster	chromosome	cosmid	CDS	gene	size
278e3	CELK02153	5	D1054	D1054.11		1.23

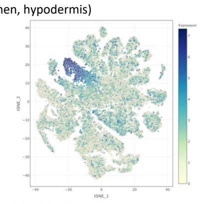

Y62H9AA.5 (spermatheca)

clone	cluster	chromosome	cosmid	CDS	gene	size
560a10	CELK02705	x	Y62H9A	Y62H9A.5		0.84

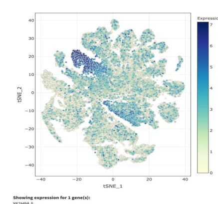

t-SNE showing cell type 4

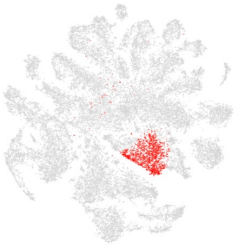

Top 20 enriched genes

	p_val	avg_log2FC	pct.1	pct.2	p_val_adj
D1086.10	0	4.69156497	0.985	0.36	0
C35B1.4	0	4.23538542	0.836	0.229	0
Y22D7AR.10	0	4.08597529	0.927	0.259	0
ule-4	0	4.00805606	0.993	0.481	0
ZK813.2	0	3.86467499	0.896	0.256	0
Y45F10C.4	0	3.84203999	0.825	0.194	0
C10G8.4	0	3.71029704	0.897	0.313	0
F30A10.13	0	3.65922406	0.741	0.116	0
T12B5.15	0	3.61403938	0.7	0.161	0
Y43B11AR.1	0	3.44459617	0.82	0.138	0
F30A10.14	0	3.35881613	0.693	0.113	0
ttr-2	0	3.34558089	0.95	0.437	0
abf-2	0	3.28478792	0.466	0.098	0
nas-20	0	3.19213102	0.526	0.09	0
ule-2	0	3.10882655	0.859	0.263	0
K10C2.8	0	3.02523171	0.641	0.114	0
F17H10.2	0	2.57116443	0.678	0.127	0
ifa-1	0	2.56981153	0.698	0.167	0
K10C2.7	0	2.56414417	0.499	0.04	0
H01G02.1	0	2.4752212	0.457	0.086	0

Top 20 depleted genes

	p_val	avg_log2FC	pct.1	pct.2	p_val_adj
crh-1	6.58E-27	-1.4559612	0.134	0.269	3.08E-22
spsb-1	3.61E-17	-1.37875	0.19	0.294	1.69E-12
Y105E8A.25	5.53E-25	-1.3025727	0.221	0.352	2.59E-20
F53H2.3	1.34E-11	-1.2233709	0.13	0.205	6.27E-07
F57F5.1	1.06E-23	-1.2160887	0.396	0.505	4.96E-19
sos-1	3.47E-24	-1.2081503	0.114	0.238	1.63E-19
mix-1	7.32E-24	-1.1974038	0.169	0.3	3.43E-19
afd-1	1.65E-23	-1.1973247	0.214	0.343	7.72E-19
daf-2	5.75E-22	-1.1632197	0.093	0.206	2.70E-17
1-Jun	2.66E-13	-1.1246379	0.069	0.145	1.25E-08
ddo-2	3.22E-09	-1.1239299	0.25	0.322	0.00015106
mnk-1	4.23E-18	-1.0912991	0.107	0.211	1.98E-13
elpc-2	1.78E-20	-1.0684162	0.093	0.202	8.37E-16
aakg-1	1.78E-18	-1.0602111	0.11	0.213	8.37E-14
plg-1	1.14E-13	-1.050763	0.143	0.23	5.36E-09
tos-1	5.21E-15	-1.019243	0.423	0.502	2.44E-10
vit-2	4.48E-18	-1.0115699	0.706	0.725	2.10E-13
lys-2	5.48E-17	-1.0064367	0.39	0.478	2.57E-12
C23H5.8	6.11E-15	-1.0052236	0.372	0.457	2.87E-10
asp-3	4.05E-22	-1.0000237	0.511	0.596	1.90E-17

Tissue enrichment | -log10 Q-values

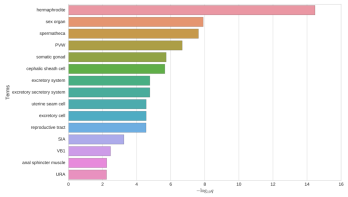

GO enrichment | -log10 Q-values

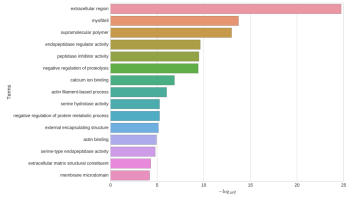

Phenotype enrichment | -log10 Q-values

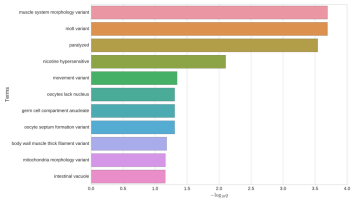

ifa-1 (intermediate filament expressed in several structures including egg laying apparatus)

clone	cluster	chromosome	countid	CDS	gene	size
2315	CEL.K00958	X	F30B2	F30B2.1a	ifa-1	0.95

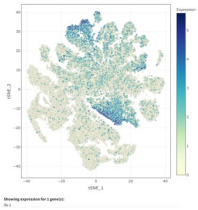

C35B1.4 (enriched in cephalic sheath cell, neurons, hypodermis)*

clone	cluster	chromosome	countid	CDS	gene	size
53945	CEL.K06648	4	C35B1	C35B1.4		0.59

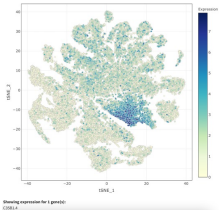

t-SNE showing cell type 5

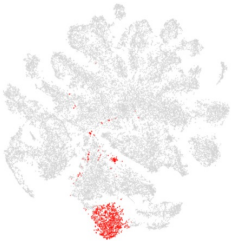

Top 20 enriched genes

	p_val	avg_log2FC	pct.1	pct.2	p_val_adj
pho-11	0	3.29863936	0.925	0.345	0
Y39B6A.1	7.09E-271	3.12430316	0.857	0.412	3.33E-266
irg-7	0	3.0944596	0.928	0.332	0
B0035.13	0	2.73722258	0.789	0.186	0
T15B7.1	0	2.64635729	0.785	0.19	0
clec-48	0	2.5804716	0.821	0.249	0
C17F4.7	1.26E-259	2.31138011	0.96	0.702	5.93E-255
T25C12.3	2.37E-277	2.14591607	0.809	0.352	1.11E-272
asp-14	6.23E-266	2.07244978	0.687	0.22	2.92E-261
ZK6.11	7.79E-196	1.99431006	0.771	0.392	3.66E-191
elo-6	1.19E-240	1.89115393	0.911	0.536	5.59E-236
asp-5	4.11E-239	1.88841255	0.897	0.489	1.93E-234
F53A9.8	3.68E-250	1.88357533	0.606	0.172	1.72E-245
F19C7.1	9.48E-245	1.86857115	0.829	0.417	4.45E-240
mtl-1	7.60E-74	1.82874675	0.545	0.296	3.56E-69
clec-50	6.06E-252	1.82190629	0.936	0.553	2.84E-247
asp-2	1.24E-256	1.81738524	0.932	0.554	5.84E-252
Y34B4A.6	8.63E-257	1.80575958	0.855	0.416	4.05E-252
clec-47	6.57E-210	1.79353628	0.535	0.151	3.08E-205
drd-5	0	1.78454448	0.496	0.082	0

Top 20 depleted genes

	p_val	avg_log2FC	pct.1	pct.2	p_val_adj
dig-1	2.51E-30	-3.415744	0.072	0.244	1.18E-25
ule-4	2.36E-24	-2.550801	0.37	0.512	1.10E-19
ZK813.7	2.89E-16	-2.496447	0.112	0.227	1.35E-11
ule-3	5.23E-15	-2.463883	0.131	0.246	2.45E-10
D1086.10	7.40E-23	-2.444667	0.247	0.398	3.47E-18
ZC513.7	1.03E-38	-2.142376	0.218	0.438	4.81E-34
C10G8.4	2.04E-14	-2.111001	0.231	0.347	9.59E-10
D1054.10	3.61E-10	-1.986445	0.23	0.324	1.70E-05
ZK813.1	4.72E-12	-1.975437	0.112	0.208	2.21E-07
ZK813.3	4.37E-10	-1.974798	0.156	0.244	2.05E-05
ule-2	7.62E-18	-1.973331	0.164	0.299	3.57E-13
ule-5	2.19E-11	-1.973291	0.233	0.331	1.03E-06
fasn-1	3.24E-14	-1.957954	0.165	0.28	1.52E-09
fipr-2	7.02E-17	-1.952572	0.086	0.199	3.29E-12
Y62H9A.5	6.72E-13	-1.945464	0.179	0.285	3.15E-08
ZK813.2	1.02E-17	-1.926902	0.166	0.294	4.77E-13
ttn-1	5.63E-31	-1.874718	0.293	0.476	2.64E-26
Y37D8A.19	1.29E-09	-1.866362	0.273	0.36	6.05E-05
ule-1	6.23E-09	-1.827216	0.184	0.267	0.0002922
ZC373.2	6.75E-09	-1.791299	0.253	0.336	0.0003165

Tissue enrichment | -log10 Q-values

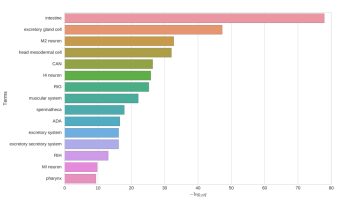

GO enrichment | -log10 Q-values

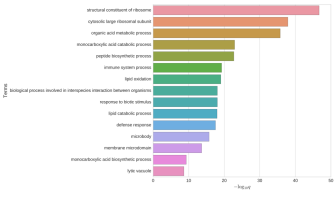

Phenotype enrichment | -log10 Q-values

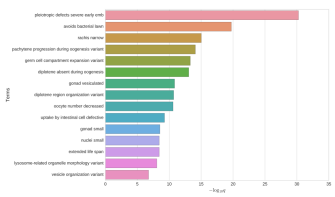

hmit-1.1 (intestinal symporter)

clone	cluster	chromosome	cosmid	CDS	gene	size
822h03	CELK09241	5		Y51A2D	Y51A2D.4	2,07

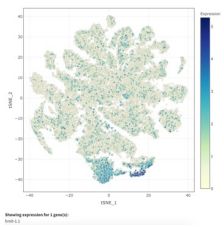

Y39B6A.1 (predicted to be in nucleolus/nucleoplasm)*

clone	cluster	chromosome	cosmid	CDS	gene	size
100c8	CELK02853	5		Y39B6A	Y39B6A.1	1,25

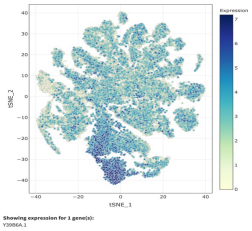

t-SNE showing cell type 6

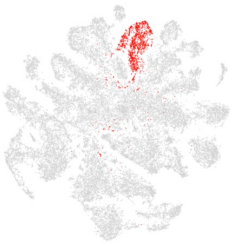

Top 20 enriched genes

	p_val	avg_log2FC	pct.1	pct.2	p_val_adj
F41F3.3	0	4.449515	0.749	0.067	0
col-77	0	4.3392538	0.769	0.087	0
dpy-13	0	4.145277	0.713	0.076	0
dpy-4	0	4.1100631	0.739	0.079	0
col-71	0	4.0777486	0.702	0.079	0
col-125	0	3.9988999	0.815	0.12	0
C02E7.6	0	3.9922095	0.739	0.094	0
col-38	0	3.9770409	0.683	0.074	0
F53F1.4	0	3.9102241	0.803	0.18	0
Y48G8AL.12	0	3.9013868	0.676	0.062	0
col-73	0	3.8400754	0.696	0.07	0
bli-6	0	3.8038908	0.807	0.129	0
col-161	0	3.7997899	0.741	0.098	0
col-175	0	3.7903889	0.633	0.052	0
col-107	0	3.7595114	0.732	0.079	0
col-138	0	3.739299	0.627	0.059	0
col-162	0	3.6847322	0.672	0.086	0
C02E7.7	0	3.6801433	0.643	0.076	0
ram-2	0	3.6073646	0.865	0.226	0
col-14	0	3.560494	0.708	0.051	0

Top 20 depleted genes

	p_val	avg_log2FC	pct.1	pct.2	p_val_adj
dig-1	2.17E-08	-2.1578555	0.318	0.233	0.0010179
ule-1	1.52E-26	-2.0047118	0.126	0.271	7.13E-22
C10G8.4	1.93E-11	-1.9180115	0.264	0.347	9.06E-07
C39D10.7	7.11E-15	-1.907543	0.185	0.288	3.33E-10
vit-5	5.23E-98	-1.85104	0.577	0.774	2.45E-93
Y62H9A.5	9.84E-20	-1.6864584	0.163	0.287	4.61E-15
ule-3	3.46E-09	-1.6826192	0.17	0.246	0.0001622
vit-2	7.90E-78	-1.6602462	0.55	0.733	3.71E-73
T21C9.13	5.32E-18	-1.6488545	0.062	0.158	2.49E-13
col-95	8.51E-53	-1.6478596	0.405	0.598	3.99E-48
clec-87	3.81E-39	-1.6052114	0.183	0.377	1.79E-34
Y22D7AR.10	1.60E-11	-1.5674783	0.214	0.298	7.49E-07
vit-6	3.75E-76	-1.5588859	0.597	0.763	1.76E-71
F56D6.8	2.93E-29	-1.5506839	0.079	0.219	1.37E-24
ule-2	1.61E-08	-1.5339991	0.225	0.297	0.000756
ule-5	9.54E-11	-1.4958015	0.247	0.331	4.48E-06
T24B8.5	2.37E-15	-1.4932008	0.328	0.412	1.11E-10
ZK813.1	1.28E-16	-1.4378633	0.105	0.209	5.98E-12
F56D6.9	1.67E-27	-1.4338885	0.123	0.265	7.81E-23
vit-3	3.93E-58	-1.4144058	0.567	0.72	1.84E-53

Tissue enrichment | -log10 Q-values

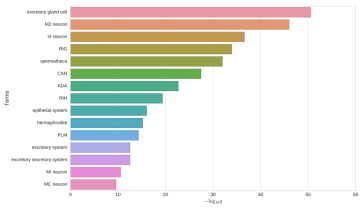

GO enrichment | -log10 Q-values

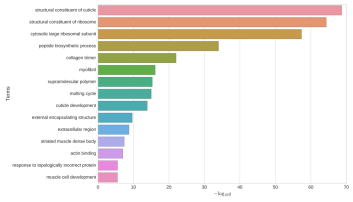

Phenotype enrichment | -log10 Q-values

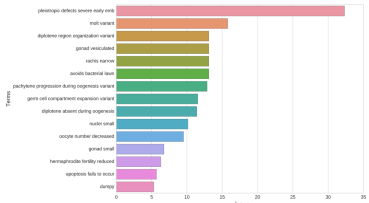

dpy-5 (cuticle development)

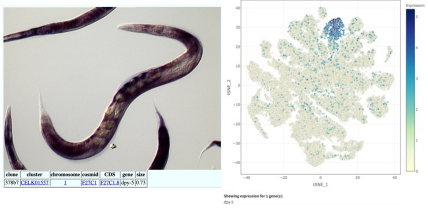

clone	cluster	chromosome	cosmid	CDS	gene	size
57867	CEL.639.537	I	F22C1	F22C1.8	dpy-5	5173

sqt-3 (cuticle development)

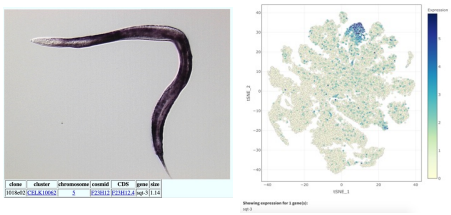

clone	cluster	chromosome	cosmid	CDS	gene	size
1016e02	CEL.K.10062	X	F23H12	F23H12.4	sqt-3	1.14

t-SNE showing cell type 7

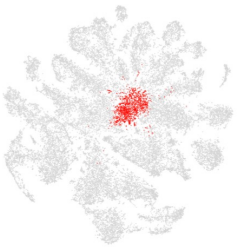

Top 20 enriched genes

	p_val	avg_log2FC	pct.1	pct.2	p_val_adj
grd-3	1.72E-158	2.37200642	0.776	0.419	8.09E-154
grd-5	8.85E-155	2.2833273	0.796	0.45	4.15E-150
col-95	1.37E-231	2.22281109	0.942	0.574	6.43E-227
col-103	4.46E-284	2.05943165	0.98	0.624	2.09E-279
col-42	1.52E-284	2.05906452	0.965	0.594	7.11E-280
col-98	7.94E-296	2.03754652	0.984	0.622	3.72E-291
D1086.3	4.47E-154	2.01044005	0.693	0.34	2.10E-149
col-119	0	1.9486887	0.998	0.719	0
col-101	1.87E-299	1.9321734	0.978	0.705	8.76E-295
F15E6.3	2.58E-103	1.92641576	0.54	0.246	1.21E-98
brp-1	5.97E-229	1.91297689	0.93	0.537	2.80E-224
H39E23.3	1.50E-58	1.89606716	0.2	0.061	7.03E-54
osm-11	5.70E-169	1.88990853	0.722	0.339	2.67E-164
col-143	6.96E-293	1.85958865	0.991	0.737	3.26E-288
col-8	5.27E-268	1.83289202	0.968	0.632	2.47E-263
F56D6.9	1.90E-83	1.83251154	0.515	0.247	8.93E-79
dct-8	4.47E-108	1.82923756	0.44	0.16	2.10E-103
F56D6.8	1.08E-79	1.79915976	0.452	0.202	5.07E-75
col-106	8.37E-293	1.79407149	0.989	0.672	3.93E-288
col-140	0	1.78407051	0.998	0.727	0

Top 20 depleted genes

	p_val	avg_log2FC	pct.1	pct.2	p_val_adj
D1086.10	3.71E-11	-2.5933411	0.313	0.396	1.74E-06
ule-4	2.11E-07	-2.4563715	0.488	0.508	0.00990206
D1054.10	1.82E-10	-2.4090505	0.237	0.324	8.52E-06
ule-5	2.58E-08	-1.9182479	0.252	0.33	0.00120943
ZK813.2	8.94E-17	-1.9072577	0.173	0.294	4.19E-12
Y37D8A.19	8.29E-07	-1.8344605	0.29	0.359	0.03886863
fipr-2	8.39E-11	-1.673803	0.112	0.198	3.93E-06
T21C9.13	6.91E-11	-1.6038851	0.075	0.156	3.24E-06
F55B11.2	2.32E-08	-1.5857711	0.135	0.209	0.00108911
W02D9.7	9.26E-10	-1.5803547	0.158	0.244	4.34E-05
C53B7.3	2.33E-11	-1.503996	0.162	0.256	1.09E-06
F57C2.4	5.19E-07	-1.4784079	0.178	0.245	0.02435468
C49G7.3	1.50E-09	-1.4349223	0.108	0.188	7.04E-05
F55B11.3	3.79E-07	-1.3736901	0.1	0.164	0.01776466
Y45F10C.4	2.01E-13	-1.3289441	0.126	0.231	9.41E-09
Y105E8A.25	8.38E-24	-1.3263241	0.193	0.351	3.93E-19
D1086.7	1.42E-10	-1.3262246	0.146	0.237	6.66E-06
T20G5.8	8.25E-08	-1.319649	0.106	0.174	0.0038719
Y62H9A.4	9.84E-09	-1.3189104	0.124	0.2	0.00046158
Y39B6A.1	1.73E-14	-1.2559505	0.32	0.434	8.10E-10

Tissue enrichment | -log10 Q-values

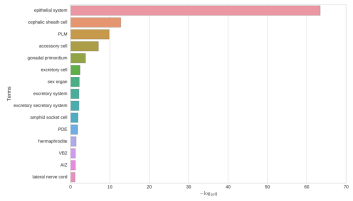

GO enrichment | -log10 Q-values

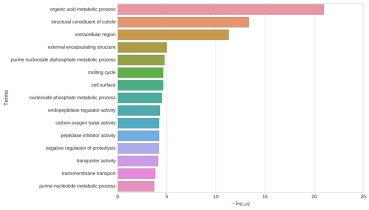

Phenotype enrichment | -log10 Q-values

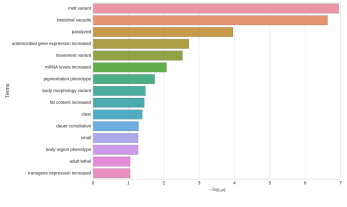

dct-8 (enriched in hypodermis and somatic gonad precursors)

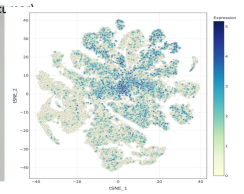

clone	cluster	chromosome	cosmid	CDS	gene	size
577c1	CELK06826	4	F56D6			1.64

W01F3.2 (predicted to enable metalloendopepidase activity, collagen catabolic processes)

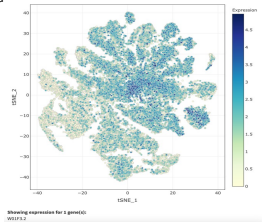

cluster	chromosome	cosmid	CDS	gene
CELK03787	5	W01F3	W01F3.2	x

t-SNE showing cell type 8

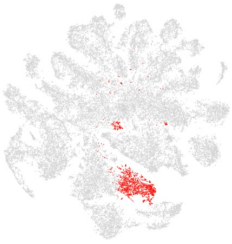

Top 20 enriched genes

	p_val	avg_log2FC	pct.1	pct.2	p_val_adj
lys-7	0	4.0594949	0.963	0.298	0
F55G11.4	0	3.70860887	0.759	0.191	0
C14C6.5	0	3.40609692	0.871	0.219	0
F01D5.5	0	3.21148937	0.704	0.104	0
dod-19	0	3.10116108	0.905	0.344	0
F13D12.6	0	3.08995782	0.953	0.365	0
spp-2	0	2.86771753	0.858	0.283	0
tag-10	0	2.82908937	0.718	0.12	0
T24B8.5	0	2.71803449	0.895	0.387	0
C14C6.2	0	2.67714794	0.668	0.082	0
clec-41	0	2.63464402	0.754	0.178	0
T01D3.6	0	2.56268599	0.778	0.197	0
C50F7.5	0	2.54477688	0.504	0.08	0
cpr-1	0	2.52352544	0.938	0.431	0
F52E1.14	0	2.46028867	0.847	0.337	0
Y43C5A.2	0	2.42181632	0.729	0.208	0
lys-1	0	2.40233128	0.961	0.553	0
lys-8	0	2.32468153	0.928	0.455	0
spp-14	0	2.31550767	0.956	0.587	0
F01D5.1	0	2.31320803	0.652	0.134	0

Top 20 depleted genes

	p_val	avg_log2FC	pct.1	pct.2	p_val_adj
dig-1	2.02E-15	-2.8017102	0.128	0.242	9.48E-11
ule-3	9.65E-11	-1.9787025	0.158	0.246	4.52E-06
ule-4	8.31E-15	-1.9074952	0.415	0.511	3.90E-10
ZC513.7	6.49E-26	-1.8628847	0.271	0.436	3.04E-21
fasn-1	1.88E-13	-1.8489222	0.176	0.28	8.81E-09
C10G8.4	1.16E-11	-1.805678	0.252	0.347	5.44E-07
D1054.10	4.28E-07	-1.7656258	0.253	0.324	0.02006366
ule-1	8.13E-11	-1.7613421	0.178	0.268	3.81E-06
C39D10.7	3.83E-08	-1.7500612	0.211	0.286	0.00179501
ule-2	1.37E-14	-1.7229286	0.184	0.298	6.43E-10
Y62H9A.5	3.28E-09	-1.677695	0.204	0.284	0.00015397
ZK813.1	5.11E-08	-1.6555386	0.136	0.207	0.00239575
D1086.10	7.27E-14	-1.5848056	0.284	0.397	3.41E-09
inos-1	2.85E-14	-1.5581579	0.045	0.132	1.34E-09
Y22D7AR.10	2.06E-10	-1.5114018	0.21	0.297	9.65E-06
T21C9.13	2.02E-09	-1.5102531	0.085	0.156	9.46E-05
Y37D8A.19	1.09E-07	-1.5046894	0.288	0.36	0.00512857
ule-5	6.96E-08	-1.4536947	0.258	0.33	0.00326462
ttn-1	1.11E-14	-1.4025093	0.367	0.473	5.20E-10
crh-1	1.68E-20	-1.3867873	0.14	0.267	7.89E-16

Tissue enrichment | -log10 Q-values

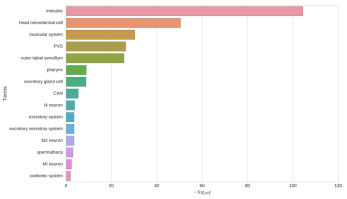

GO enrichment | -log10 Q-values

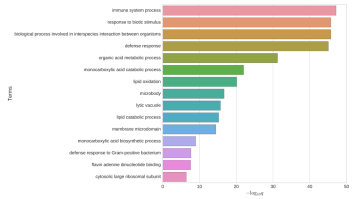

Phenotype enrichment | -log10 Q-values

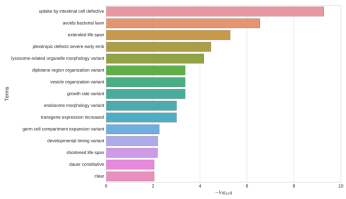

lys-7 (defense response, expressed in head neurons, intestine, rectal gland)

clone	cluster	chromosome	cosmid	CDS	gene	size
361@23	CEL:K02118	5	C02A12		lys-7	0.63

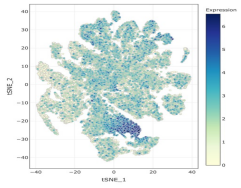

Showing expression for 1 gene(s):
lys-7

dod-19 (innate immune response)*

clone	cluster	chromosome	cosmid	CDS	gene	size
703@2	CEL:K08434	5	ZK6	ZK6.10		3.71

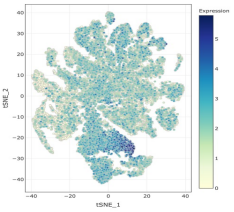

Showing expression for 1 gene(s):
dod-19

t-SNE showing cell type 9

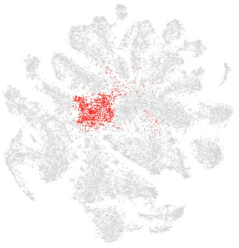

Top 20 enriched genes

	p_val	avg_log2FC	pct.1	pct.2	p_val_adj
cey-2	8.14E-131	1.14445315	0.669	0.311	3.82E-126
cpg-1	4.24E-141	1.11774305	0.681	0.309	1.99E-136
cpg-2	1.23E-135	1.07027514	0.729	0.363	5.76E-131
cbd-1	2.32E-143	1.06625001	0.699	0.316	1.09E-138
sip-1	3.27E-131	1.02858936	0.784	0.428	1.53E-126
rmd-1	9.58E-96	1.00273309	0.579	0.288	4.49E-91
clec-87	6.67E-148	0.99947049	0.731	0.35	3.13E-143
mesp-1	1.08E-88	0.94704534	0.428	0.176	5.08E-84
gln-6	5.85E-102	0.94194277	0.515	0.219	2.75E-97
W05F2.3	3.47E-103	0.9211276	0.581	0.271	1.63E-98
cpg-3	1.70E-92	0.86340233	0.661	0.352	8.00E-88
ran-1	1.47E-75	0.85027519	0.592	0.324	6.88E-71
nasp-2	2.18E-87	0.84774327	0.567	0.274	1.02E-82
rnr-2	3.86E-98	0.845464	0.47	0.191	1.81E-93
cgh-1	4.50E-84	0.84188692	0.693	0.411	2.11E-79
clec-91	2.62E-73	0.81629824	0.466	0.22	1.23E-68
rpl-11.1	3.46E-78	0.80981696	0.587	0.303	1.62E-73
M28.5	4.17E-68	0.79616773	0.415	0.186	1.96E-63
clec-88	6.91E-83	0.77826019	0.427	0.178	3.24E-78
hil-4	3.42E-83	0.77802478	0.598	0.298	1.60E-78

Top 20 depleted genes

	p_val	avg_log2FC	pct.1	pct.2	p_val_adj
C30E1.9	8.11E-14	-1.4485576	0.401	0.487	3.80E-09
F53H2.3	7.03E-18	-1.4376546	0.098	0.206	3.30E-13
Y105E8A.25	4.84E-25	-1.4312299	0.213	0.351	2.27E-20
crh-1	1.75E-20	-1.4079217	0.145	0.267	8.22E-16
D1054.10	2.71E-14	-1.3622332	0.464	0.314	1.27E-09
D1086.10	1.27E-13	-1.3463393	0.544	0.385	5.94E-09
spsb-1	1.18E-12	-1.2972569	0.2	0.292	5.54E-08
ZK813.7	1.25E-20	-1.2869616	0.366	0.216	5.86E-16
sos-1	4.23E-24	-1.2383515	0.102	0.238	1.98E-19
tos-1	3.12E-16	-1.2051101	0.417	0.502	1.46E-11
anc-1	2.12E-30	-1.2044106	0.6	0.694	9.95E-26
ZK813.1	8.79E-15	-1.2003792	0.321	0.199	4.12E-10
aakg-1	2.84E-20	-1.1985001	0.096	0.213	1.33E-15
mnk-1	1.87E-18	-1.192513	0.099	0.21	8.79E-14
Y62H9A.5	3.14E-13	-1.1890592	0.407	0.275	1.47E-08
ule-4	7.80E-30	-1.1852717	0.728	0.497	3.66E-25
daf-2	1.75E-16	-1.1571312	0.102	0.205	8.19E-12
ule-5	8.36E-17	-1.1499111	0.482	0.32	3.92E-12
afd-1	4.09E-12	-1.1379935	0.255	0.34	1.92E-07
ell-1	8.14E-19	-1.1126796	0.288	0.403	3.82E-14

Tissue enrichment | -log10 Q-values

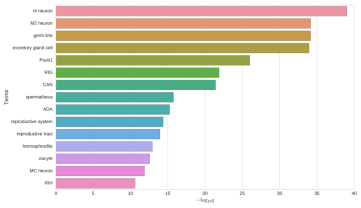

GO enrichment | -log10 Q-values

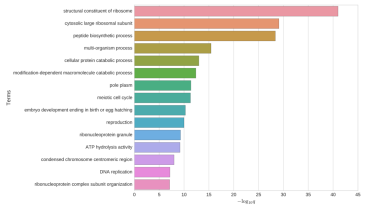

Phenotype enrichment | -log10 Q-values

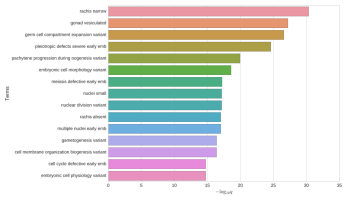

rnr-2 (ribonucleotide diphosphate reductase activity, involved in embryo development)

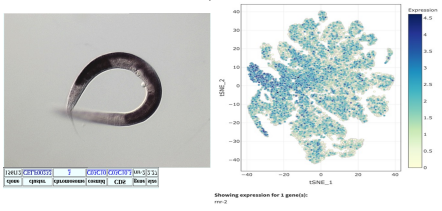

cluster	chromosome	cosmid	CDS	gene
CELK02665	I	F46F11	F46F11.2	cey-2

Showing expression for 1 gene(s):
rnr-2

cey-2 (ribonucleoprotein complex in nucleus in germ cells)

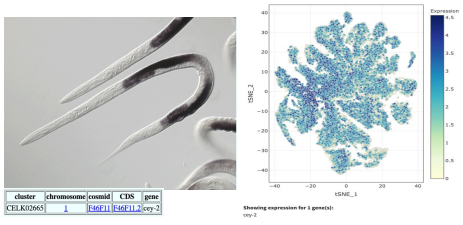

Showing expression for 1 gene(s):
cey-2

t-SNE showing cell type 10

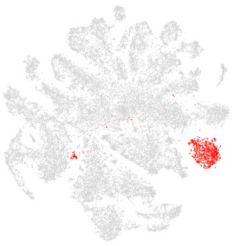

Top 20 enriched genes

	p_val	avg_log2FC	pct.1	pct.2	p_val_adj
spsb-1	0	3.48086164	0.894	0.266	0
D2023.1	1.96E-277	3.1846028	0.428	0.075	9.21E-273
crh-1	0	3.12326781	0.848	0.24	0
Y37A1A.2	0	3.05464434	0.45	0.069	0
C15A11.7	1.84E-214	2.94361625	0.39	0.078	8.65E-210
F23F12.12	4.62E-183	2.93421689	0.755	0.417	2.17E-178
F16C3.2	7.50E-273	2.75324784	0.473	0.095	3.52E-268
afd-1	0	2.73694822	0.855	0.317	0
T12A2.1	0	2.73264997	0.531	0.091	0
fkh-7	1.45E-296	2.68763878	0.642	0.167	6.79E-292
ist-1	1.84E-272	2.65253224	0.453	0.084	8.63E-268
Y17G7B.10	1.41E-198	2.64500738	0.615	0.223	6.60E-194
mnk-1	0	2.61023332	0.724	0.186	0
ell-1	5.30E-253	2.60624036	0.82	0.383	2.48E-248
linc-72	0	2.5929721	0.364	0.031	0
sms-3	2.72E-269	2.54123223	0.564	0.138	1.28E-264
daf-2	0	2.5182282	0.703	0.182	0
C30E1.9	7.63E-287	2.49428335	0.927	0.467	3.58E-282
lmd-3	6.82E-239	2.46861555	0.808	0.392	3.20E-234
lim-9	5.50E-198	2.4685942	0.612	0.219	2.58E-193

Top 20 depleted genes

	p_val	avg_log2FC	pct.1	pct.2	p_val_adj
ule-4	5.69E-10	-2.3953821	0.439	0.509	2.67E-05
pat-10	6.54E-90	-2.2979457	0.473	0.715	3.07E-85
C10G8.4	1.67E-14	-2.2961586	0.226	0.347	7.84E-10
perm-4	2.63E-43	-2.276476	0.375	0.586	1.24E-38
lev-11	3.32E-110	-2.275305	0.438	0.737	1.56E-105
D1086.10	1.52E-08	-2.2750585	0.325	0.395	0.00071474
far-2	8.08E-98	-2.2374198	0.579	0.773	3.79E-93
act-4	2.33E-99	-2.2255171	0.462	0.728	1.10E-94
lbp-2	2.64E-78	-2.2120837	0.369	0.641	1.24E-73
ttr-16	1.39E-78	-2.1985425	0.393	0.653	6.54E-74
ZK813.2	1.66E-24	-2.1542344	0.13	0.295	7.76E-20
cpn-3	9.73E-77	-2.069591	0.455	0.69	4.57E-72
mlc-2	1.10E-88	-2.0602468	0.346	0.646	5.18E-84
mlc-3	1.73E-82	-2.0109373	0.424	0.691	8.11E-78
ule-2	7.07E-10	-2.0104303	0.206	0.297	3.32E-05
act-1	6.49E-93	-2.0009527	0.553	0.781	3.04E-88
tnt-2	8.44E-72	-1.9978179	0.339	0.611	3.96E-67
unc-87	2.64E-84	-1.9953146	0.32	0.639	1.24E-79
unc-27	3.47E-68	-1.96237	0.447	0.674	1.63E-63
act-3	3.50E-104	-1.9411241	0.497	0.783	1.64E-99

Tissue enrichment | -log10 Q-values

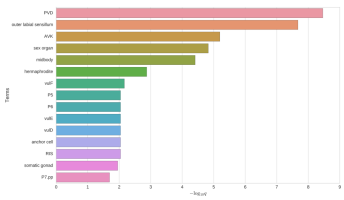

GO enrichment | -log10 Q-values

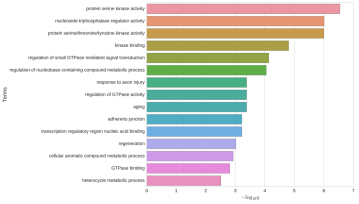

Phenotype enrichment | -log10 Q-values

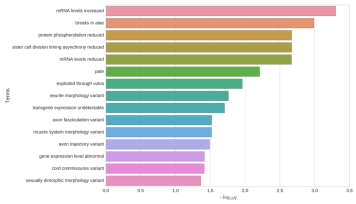

afd-1 (actin binding protein, Parkinson's disease)

cluster	chromosome	cosmid	CDS	gene
CELK01975	1	W02F11	W02F11.6	x

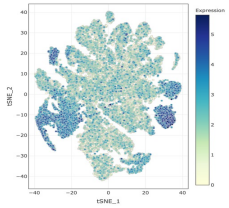

Showing expression for 1 gene(s):
afd-1

spsb-1 (protein catabolic processes, ubiquitin ligase complex)*

cluster	chromosome	cosmid	CDS	gene
CELK02377	2	Y46E12BL	Y46E12BL.4	x

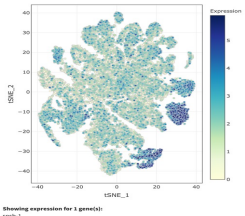

Showing expression for 1 gene(s):
spsb-1

t-SNE showing cell type 11

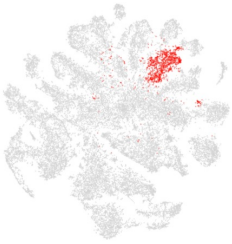

Top 20 enriched genes

	p_val	avg_log2FC	pct.1	pct.2	p_val_adj
pdf-1	1.14E-263	3.15792657	0.493	0.109	5.37E-259
flp-11	9.30E-97	2.88892322	0.22	0.05	4.36E-92
pgal-1	0	2.65560862	0.637	0.136	0
sbt-1	0	2.59544926	0.743	0.204	0
flp-1	2.89E-33	2.58795689	0.136	0.045	1.36E-28
egl-3	0	2.58001703	0.596	0.118	0
egl-21	0	2.57536604	0.707	0.195	0
flp-14	1.71E-166	2.55395872	0.425	0.116	8.04E-162
flp-9	1.12E-284	2.46279816	0.516	0.113	5.25E-280
nlp-6	1.69E-112	2.38301882	0.213	0.043	7.92E-108
pghm-1	0	2.35901892	0.575	0.104	0
nlp-21	1.13E-295	2.35357859	0.449	0.081	5.28E-291
ida-1	0	2.3037682	0.54	0.091	0
T27C4.1	0	2.2822674	0.602	0.121	0
nlp-49	6.03E-82	2.19388208	0.199	0.048	2.83E-77
flp-19	8.36E-104	2.18585826	0.201	0.041	3.92E-99
flp-28	1.09E-59	2.11679099	0.294	0.113	5.11E-55
cla-1	3.17E-258	2.1069887	0.304	0.041	1.49E-253
flp-12	5.62E-77	2.08639834	0.245	0.072	2.64E-72
unc-25	1.54E-110	2.06484427	0.222	0.047	7.24E-106

Top 20 depleted genes

	p_val	avg_log2FC	pct.1	pct.2	p_val_adj
dig-1	8.14E-21	-1.7349397	0.375	0.231	3.82E-16
pos-1	3.06E-12	-1.1794904	0.119	0.214	1.43E-07
clec-87	4.19E-08	-1.1481222	0.297	0.37	0.0019661
Y105E8A.25	7.81E-16	-1.0939968	0.23	0.35	3.66E-11
spn-4	5.96E-10	-1.0274175	0.139	0.224	2.80E-05
C05C10.5	1.48E-07	-0.9652952	0.113	0.18	0.00691876
ipla-1	1.86E-09	-0.9564141	0.272	0.352	8.70E-05
plg-1	7.81E-09	-0.949854	0.153	0.228	0.00036647
afd-1	5.70E-12	-0.9290684	0.242	0.34	2.68E-07
hil-5	1.75E-10	-0.898671	0.149	0.238	8.19E-06
ced-1	1.74E-12	-0.8920637	0.28	0.378	8.18E-08
npp-8	7.59E-13	-0.8548046	0.138	0.237	3.56E-08
patr-1	6.23E-07	-0.8203308	0.139	0.204	0.02923966
F53H1.4	8.71E-12	-0.81501	0.139	0.234	4.09E-07
C23H5.8	3.11E-07	-0.8111844	0.396	0.455	0.01457872
vit-6	2.87E-09	-0.8095996	0.752	0.755	0.00013463
vit-2	1.27E-09	-0.802357	0.699	0.725	5.97E-05
vit-3	1.68E-11	-0.8020149	0.669	0.714	7.87E-07
F57F5.1	1.61E-08	-0.788964	0.439	0.502	0.00075311
vit-5	1.95E-09	-0.786694	0.757	0.764	9.13E-05

Tissue enrichment | -log10 Q-values

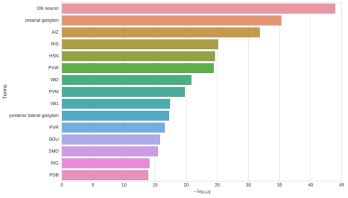

GO enrichment | -log10 Q-values

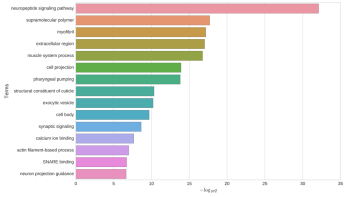

Phenotype enrichment | -log10 Q-values

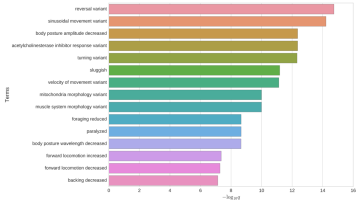

egl-3 (FBXO binding, locomotion, expressed in axons)

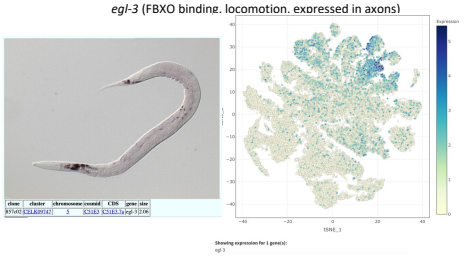

sbt-1 (peptidase activity, muscle contraction, expressed in neurons)

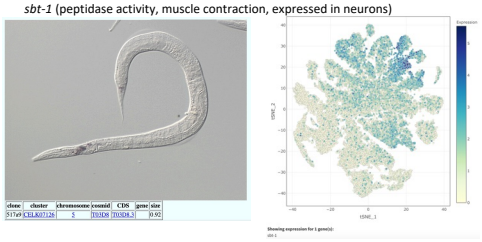

t-SNE showing cell type 12

Top 20 enriched genes

	p_val	avg_log2FC	pct.1	pct.2	p_val_adj
T21C9.13	4.82E-208	2.4510172	0.575	0.141	2.26E-203
clec-87	6.98E-187	2.38901326	0.805	0.354	3.27E-182
pos-1	3.32E-210	2.33671855	0.678	0.197	1.56E-205
C05C10.5	2.87E-183	2.30531624	0.586	0.166	1.35E-178
spn-4	4.68E-199	2.1976582	0.678	0.208	2.20E-194
F14H3.6	4.56E-194	2.09675757	0.483	0.104	2.14E-189
cpg-2	1.87E-134	2.00619924	0.751	0.369	8.76E-130
cpg-1	1.64E-134	2.00164692	0.707	0.315	7.71E-130
gyg-2	3.77E-167	1.99890985	0.625	0.206	1.77E-162
cey-3	3.90E-160	1.99649716	0.688	0.261	1.83E-155
patr-1	1.26E-119	1.98802883	0.537	0.192	5.91E-115
chs-1	4.11E-147	1.97655156	0.597	0.203	1.93E-142
hil-5	3.66E-167	1.97308027	0.653	0.222	1.72E-162
mex-5	5.85E-151	1.94497216	0.664	0.254	2.74E-146
oma-2	2.80E-161	1.93810121	0.639	0.22	1.31E-156
puf-5	5.57E-158	1.93576749	0.649	0.23	2.61E-153
cyb-3	1.18E-162	1.89649281	0.632	0.208	5.55E-158
cbd-1	1.99E-137	1.8950696	0.722	0.321	9.33E-133
hil-4	1.58E-158	1.87890268	0.739	0.299	7.43E-154
era-1	4.78E-133	1.87052723	0.48	0.14	2.24E-128

Top 20 depleted genes

	p_val	avg_log2FC	pct.1	pct.2	p_val_adj
dig-1	3.36E-26	-3.5631672	0.056	0.242	1.57E-21
ttn-1	3.59E-64	-3.0264135	0.119	0.479	1.68E-59
D1086.10	6.65E-33	-2.8301514	0.163	0.399	3.12E-28
ule-4	1.26E-45	-2.7514809	0.22	0.515	5.90E-41
act-4	6.95E-115	-2.4636351	0.273	0.731	3.26E-110
nlp-77	2.04E-100	-2.4192281	0.312	0.715	9.55E-96
C10G8.4	8.07E-25	-2.4138488	0.149	0.349	3.78E-20
C30E1.9	1.81E-65	-2.3884692	0.127	0.493	8.48E-61
ule-2	6.93E-28	-2.3755741	0.093	0.299	3.25E-23
ule-3	7.81E-10	-2.3588929	0.139	0.245	3.66E-05
col-95	3.55E-66	-2.3486214	0.244	0.598	1.66E-61
ttr-16	1.59E-89	-2.3221053	0.239	0.656	7.44E-85
D1054.10	1.39E-13	-2.2894495	0.186	0.325	6.50E-09
unc-54	1.71E-90	-2.2856174	0.3	0.694	8.00E-86
ZC513.7	9.11E-36	-2.2806017	0.185	0.436	4.27E-31
pat-10	7.01E-97	-2.2675325	0.303	0.718	3.29E-92
anc-1	2.31E-100	-2.2157306	0.251	0.702	1.08E-95
cpn-3	4.92E-88	-2.1972421	0.308	0.692	2.31E-83
ttr-2	1.42E-46	-2.1843719	0.176	0.471	6.67E-42
acp-6	2.93E-70	-2.1766639	0.18	0.556	1.37E-65

Tissue enrichment | -log10 Q-values

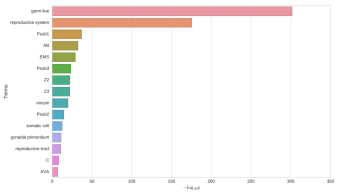

GO enrichment | -log10 Q-values

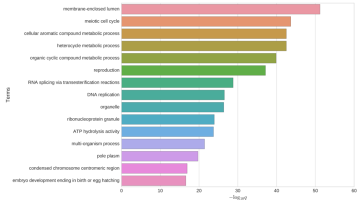

Phenotype enrichment | -log10 Q-values

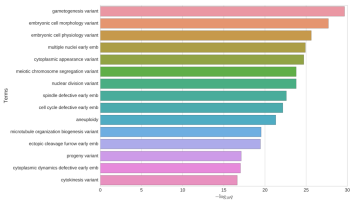

glp-1 (RNA pol II transcription, gene regulation, germ cells and nervous system)

clone	cluster	chromosome	cosmid	CDS	gene	size
SJ12	CELK00212	X	JH2A9	JH2A9.0	glp-1	2.85

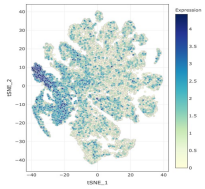

Showing expression for 1 gene(s):
glp-1

pos-1 (embryonic fate specification)

cluster	chromosome	cosmid	CDS	gene
CELK01662	X	F52H1	1x	pos-1

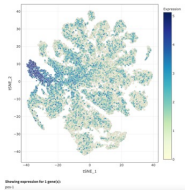

t-SNE showing cell type 13

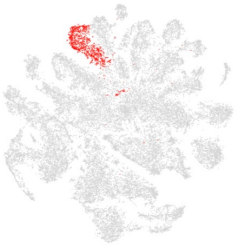

Top 20 enriched genes

	p_val	avg_log2FC	pct.1	pct.2	p_val_adj
C49G7.3	0	4.76498013	0.911	0.157	0
T20G5.8	0	4.48679784	0.896	0.143	0
dod-6	0	4.32944692	0.94	0.26	0
C45G9.6	0	4.07980917	0.772	0.107	0
F15A4.6	0	4.06762594	0.826	0.107	0
scl-5	0	3.58833138	0.647	0.05	0
ZK596.1	0	3.51535406	0.703	0.06	0
fip-2	0	3.46578445	0.638	0.13	0
fipr-1	0	3.40325944	0.726	0.113	0
F41G3.10	0	3.29428648	0.665	0.055	0
fipr-5	0	3.20836232	0.502	0.075	0
msrp-7	0	3.15755235	0.587	0.04	0
ttr-21	0	2.97396129	0.674	0.099	0
R06F6.14	0	2.89970209	0.573	0.046	0
pqn-75	0	2.86196876	0.528	0.037	0
abf-5	0	2.76422695	0.556	0.06	0
myo-1	0	2.72050712	0.664	0.13	0
fipr-9	0	2.69876417	0.411	0.052	0
myo-2	0	2.68324963	0.645	0.133	0
ttr-26	2.25E-307	2.67652747	0.644	0.163	1.06E-302

Top 20 depleted genes

	p_val	avg_log2FC	pct.1	pct.2	p_val_adj
mix-1	2.90E-17	-1.260283	0.175	0.297	1.36E-12
afd-1	5.34E-15	-1.2392402	0.23	0.341	2.51E-10
elpc-2	1.70E-16	-1.131765	0.089	0.201	8.00E-12
F57F5.1	3.78E-15	-1.1203366	0.403	0.503	1.77E-10
daf-2	1.37E-10	-1.0981456	0.12	0.204	6.45E-06
sos-1	5.00E-13	-1.0970272	0.136	0.235	2.34E-08
plg-1	1.12E-13	-1.0809637	0.124	0.229	5.25E-09
lpd-3	2.40E-13	-1.0697997	0.238	0.336	1.13E-08
npp-8	2.83E-21	-1.0691297	0.099	0.238	1.33E-16
crh-1	4.52E-08	-1.0595862	0.193	0.264	0.00211953
Y105E8A.25	4.47E-09	-1.0572706	0.274	0.348	0.00020988
H06I04.3	2.59E-16	-1.0357275	0.149	0.266	1.21E-11
mnk-1	5.56E-08	-0.9994211	0.138	0.208	0.002606
F53H1.4	1.74E-17	-0.9896699	0.111	0.235	8.18E-13
ceh-100	9.07E-15	-0.9589538	0.134	0.244	4.26E-10
ipla-1	1.58E-09	-0.9479123	0.272	0.352	7.40E-05
golg-4	5.87E-13	-0.9314871	0.167	0.268	2.75E-08
aakg-1	4.62E-08	-0.9294196	0.14	0.211	0.00216874
pos-1	6.68E-07	-0.913956	0.143	0.213	0.03134372
klp-12	2.49E-11	-0.9089067	0.292	0.377	1.17E-06

Tissue enrichment | -log10 Q-values

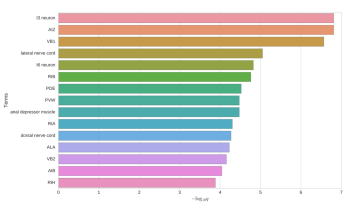

GO enrichment | -log10 Q-values

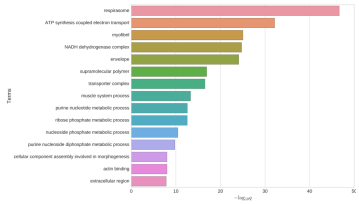

Phenotype enrichment | -log10 Q-values

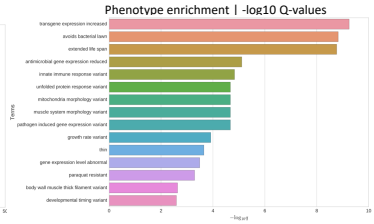

phat-3 (germline, intestine, mechanosensory neurons)

clone	cluster	chromosome	cosmid	CDS	gene	size
27269	CELK03835	5	C49G7	C49G7.4		1.23

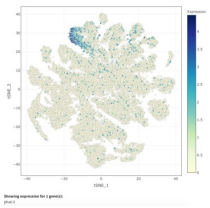

F15A4.6 (predicted to encode protein in pharyngeal gland cells)*

clone	cluster	chromosome	cosmid	CDS	gene	size
N1911	CELK03833	2	F15A4	F15A4.6		1.01

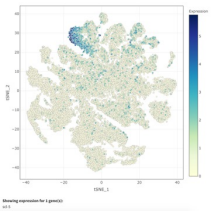

t-SNE showing cell type 14

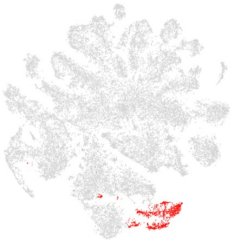

Top 20 enriched genes

	p_val	avg_log2FC	pct.1	pct.2	p_val_adj
ddo-2	0	3.9754197	0.9	0.299	0
C52D10.3	0	3.92693037	0.646	0.073	0
1-Jun	0	3.8267561	0.844	0.119	0
C23H5.8	0	3.34288879	0.965	0.436	0
ipla-1	7.61E-241	3.27978183	0.823	0.334	3.57E-236
fkh-7	0	3.11782257	0.749	0.166	0
F53H2.3	0	3.1177772	0.798	0.182	0
pals-24	0	3.08561474	0.476	0.051	0
fat-6	1.96E-229	2.92262566	0.912	0.539	9.19E-225
Y105C5A.15	0	2.91868665	0.737	0.116	0
F19B2.5	0	2.86278305	0.681	0.125	0
dhs-3	0	2.82789468	0.886	0.295	0
mnk-1	0	2.74638539	0.794	0.187	0
spsb-1	9.17E-271	2.70029077	0.806	0.272	4.30E-266
ZK228.4	0	2.68464437	0.555	0.071	0
Y105E8A.25	1.83E-273	2.66687103	0.854	0.329	8.60E-269
R193.2	6.47E-226	2.66437263	0.505	0.11	3.03E-221
math-27	0	2.65024879	0.695	0.038	0
ugt-29	0	2.63283628	0.598	0.086	0
ugt-26	5.54E-156	2.63214985	0.561	0.178	2.60E-151

Top 20 depleted genes

	p_val	avg_log2FC	pct.1	pct.2	p_val_adj
dig-1	7.81E-27	-3.4443488	0.063	0.243	3.66E-22
ule-4	1.72E-24	-2.6602656	0.345	0.512	8.05E-20
ule-3	2.78E-09	-2.6090091	0.154	0.245	0.00013018
ZK813.7	3.68E-13	-2.5801459	0.116	0.226	1.72E-08
D1086.10	4.32E-18	-2.5625027	0.257	0.397	2.02E-13
perm-4	1.77E-62	-2.5587253	0.288	0.588	8.32E-58
ZC513.7	6.52E-48	-2.4508518	0.166	0.438	3.06E-43
far-2	1.78E-105	-2.4113742	0.504	0.774	8.35E-101
C10G8.4	1.49E-21	-2.3593901	0.183	0.348	7.00E-17
C39D10.7	2.49E-14	-2.3292463	0.165	0.287	1.17E-09
act-4	2.79E-101	-2.2656725	0.405	0.728	1.31E-96
ZK813.3	3.74E-12	-2.2340126	0.133	0.244	1.75E-07
Y62H9A.5	4.64E-08	-2.2233081	0.2	0.284	0.00217621
far-1	1.92E-67	-2.2072894	0.368	0.64	9.02E-63
ule-2	2.92E-19	-2.1965398	0.146	0.298	1.37E-14
lbp-2	5.60E-62	-2.1440925	0.401	0.639	2.62E-57
pat-10	1.32E-77	-2.1339196	0.467	0.714	6.18E-73
ZK813.2	3.81E-20	-2.1324268	0.142	0.294	1.79E-15
fasn-1	2.82E-22	-2.1258283	0.117	0.281	1.32E-17
unc-27	1.33E-75	-2.0966367	0.391	0.675	6.22E-71

Tissue enrichment | -log10 Q-values

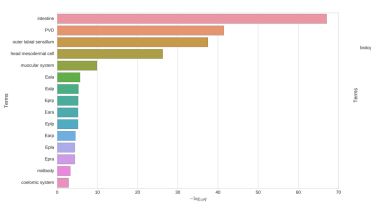

GO enrichment | -log10 Q-values

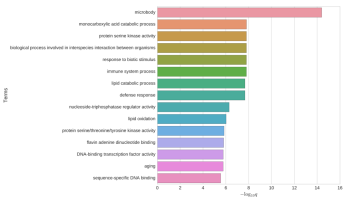

Phenotype enrichment | -log10 Q-values

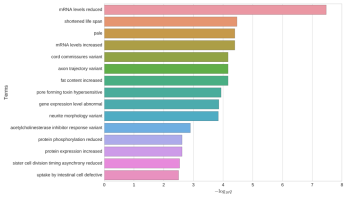

hmit-1.1 (intestinal symporter)

cluster	cluster	chromosome	cosmid	CDS	gene	size
K2843	CELK00541	5	Y51A2D	Y51A2D.6		2.07

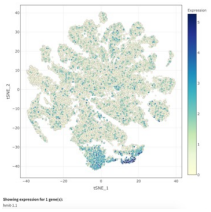

spsb-1 (protein catabolic processes, ubiquitin ligase complex)*

cluster	chromosome	cosmid	CDS	gene
CELK02377	2	Y46E12BL	Y46E12BL.4	x

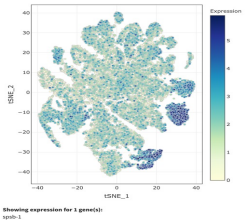

t-SNE showing cell type 15

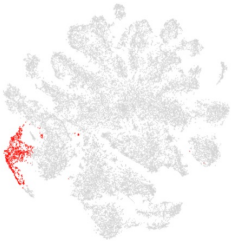

Top 20 enriched genes

	p_val	avg_log2FC	pct.1	pct.2	p_val_adj
Y46H3C.7	0	6.15006878	0.93	0.099	0
Y9D1A.2	0	5.52199185	0.877	0.069	0
Y51H7C.15	0	4.42494133	0.757	0.033	0
F59C12.4	0	3.74340812	0.515	0.046	0
Y46H3C.5	0	2.92288937	0.508	0.019	0
elf-1	0	2.78345415	0.526	0.042	0
egl-1	0	2.38028235	0.371	0.037	0
mix-1	2.05E-268	2.30741333	0.81	0.277	9.63E-264
F29G9.1	0	2.25867831	0.392	0.01	0
spat-3	6.90E-237	2.1926356	0.569	0.132	3.24E-232
Y32H12A.8	1.42E-188	2.18849146	0.624	0.197	6.64E-184
Y9D1A.1	0	2.17054062	0.312	0.009	0
kni-2	1.22E-211	2.06610802	0.564	0.142	5.71E-207
afd-1	5.78E-195	2.00796476	0.786	0.323	2.71E-190
Y17D7C.3	2.57E-297	1.95416135	0.462	0.068	1.21E-292
ssl-1	1.86E-186	1.91506025	0.603	0.177	8.72E-182
F53H1.4	7.39E-187	1.90292189	0.658	0.217	3.47E-182
daf-19	1.68E-213	1.89315279	0.417	0.075	7.88E-209
xnp-1	6.57E-159	1.88359903	0.709	0.301	3.08E-154
uvs-1	1.28E-208	1.87663107	0.459	0.092	5.99E-204

Top 20 depleted genes

	p_val	avg_log2FC	pct.1	pct.2	p_val_adj
pat-10	2.21E-137	-3.091701	0.225	0.721	1.04E-132
ule-4	4.90E-47	-3.0434865	0.24	0.515	2.30E-42
dig-1	1.18E-17	-3.033376	0.093	0.242	5.53E-13
lev-11	1.94E-148	-3.0173882	0.232	0.742	9.08E-144
D1086.10	9.02E-33	-3.0136596	0.172	0.399	4.23E-28
act-4	9.93E-146	-3.0041424	0.212	0.734	4.66E-141
far-2	3.40E-147	-2.9022608	0.31	0.78	1.59E-142
unc-54	6.06E-119	-2.8991705	0.237	0.696	2.84E-114
cpn-3	5.16E-122	-2.8383992	0.239	0.695	2.42E-117
unc-27	7.07E-121	-2.7958162	0.208	0.68	3.32E-116
nlp-77	1.23E-123	-2.7903966	0.266	0.717	5.76E-119
mlc-3	4.08E-127	-2.7852102	0.216	0.696	1.92E-122
ttr-16	9.06E-112	-2.7733748	0.208	0.657	4.25E-107
F46H5.3	3.15E-161	-2.7082589	0.33	0.815	1.48E-156
unc-15	4.65E-112	-2.6995118	0.216	0.659	2.18E-107
col-119	1.85E-127	-2.6820211	0.299	0.742	8.69E-123
col-181	4.10E-128	-2.6567225	0.291	0.738	1.93E-123
Y37D8A.19	1.26E-25	-2.6532443	0.168	0.362	5.90E-21
unc-87	5.37E-112	-2.6204657	0.186	0.641	2.52E-107
ZK813.7	1.00E-16	-2.6156693	0.09	0.227	4.70E-12

Tissue enrichment | -log10 Q-values

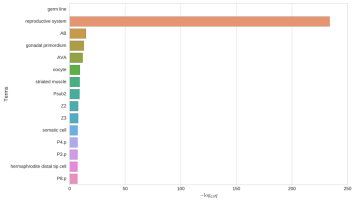

GO enrichment | -log10 Q-values

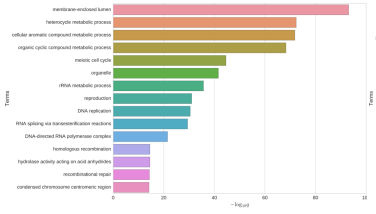

Phenotype enrichment | -log10 Q-values

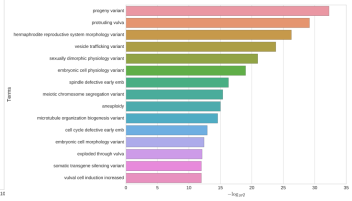

Y9D1A.1 (germline, interneuron enriched)

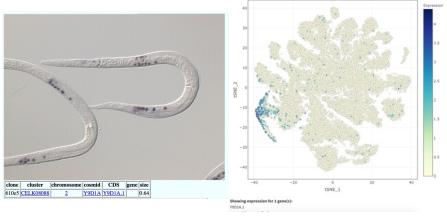

clone	cluster	chromosome	countd	CDS	gene	size
fc16e5	CEL.K00088	2		Y9D1A	Y9D1A.1	0.64

elf-1 (DNA binding factor in gonad development, expressed in neurons)

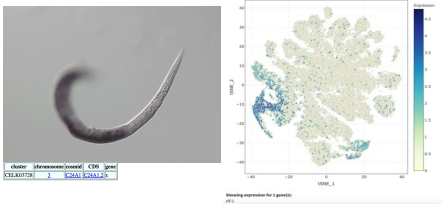

cluster	chromosome	countd	CDS	gene
CEL.K0728	2		C24A1	C24A1.2

t-SNE showing cell type 16

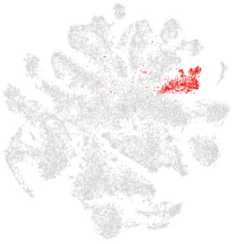

Top 20 enriched genes

	p_val	avg_log2FC	pct.1	pct.2	p_val_adj
nlp-20	0	3.38587624	0.455	0.05	0
C02F5.14	0	3.05523726	0.554	0.077	0
pah-1	0	2.81978947	0.846	0.224	0
haly-1	0	2.67644923	0.752	0.17	0
Y51H4A.7	0	2.65518573	0.653	0.095	0
col-118	2.49E-173	2.58170994	0.53	0.145	1.17E-168
col-34	4.57E-269	2.51585999	0.455	0.072	2.14E-264
nlp-12	8.33E-165	2.30297016	0.287	0.044	3.91E-160
col-153	1.29E-248	2.3028854	0.371	0.051	6.07E-244
F55H12.4	8.07E-241	2.17031807	0.891	0.383	3.78E-236
mec-17	1.51E-111	2.15966739	0.282	0.06	7.08E-107
acp-6	4.69E-195	2.09288874	0.943	0.533	2.20E-190
F20A1.1	3.10E-142	2.0512075	0.548	0.174	1.45E-137
nlp-77	4.14E-227	2.01281701	0.997	0.694	1.94E-222
mec-7	3.48E-103	1.96252335	0.222	0.04	1.63E-98
Y47D7A.6	8.39E-155	1.95789023	0.264	0.04	3.94E-150
T23B12.8	7.87E-291	1.93687575	0.373	0.044	3.69E-286
Y46H3A.4	0	1.88512427	0.277	0.021	0
cnc-10	1.60E-195	1.8530118	0.389	0.069	7.50E-191
ttr-10	1.39E-303	1.83922593	0.361	0.039	6.50E-299

Top 20 depleted genes

	p_val	avg_log2FC	pct.1	pct.2	p_val_adj
dig-1	9.70E-13	-2.0217388	0.368	0.233	4.55E-08
F57F5.1	1.26E-29	-1.4958071	0.301	0.505	5.89E-25
vit-5	5.26E-29	-1.4383023	0.687	0.766	2.47E-24
vit-2	3.14E-30	-1.4135271	0.598	0.728	1.47E-25
vit-3	2.31E-28	-1.3640309	0.603	0.716	1.09E-23
vit-1	1.69E-26	-1.3615896	0.559	0.679	7.92E-22
cpr-1	3.58E-19	-1.3498833	0.305	0.457	1.68E-14
F53H2.3	2.88E-08	-1.306804	0.123	0.203	0.00135151
T24B8.5	3.44E-09	-1.2997323	0.318	0.411	0.00016118
lys-2	9.90E-21	-1.2887652	0.326	0.478	4.64E-16
C23H5.8	1.65E-15	-1.2802881	0.337	0.456	7.73E-11
lys-7	8.30E-07	-1.2728533	0.251	0.328	0.03894275
mlx-1	1.34E-13	-1.2703497	0.177	0.296	6.30E-09
vit-4	4.83E-17	-1.2605453	0.6	0.684	2.27E-12
Y105E8A.25	3.23E-09	-1.2412627	0.266	0.347	0.00015146
vit-6	2.51E-22	-1.23215	0.699	0.757	1.18E-17
daf-2	2.91E-13	-1.2258175	0.092	0.204	1.36E-08
clec-87	4.45E-07	-1.2085648	0.295	0.369	0.02087809
pos-1	5.60E-08	-1.2041826	0.13	0.213	0.00262603
lys-1	2.76E-17	-1.1659088	0.485	0.573	1.30E-12

Tissue enrichment | -log10 Q-values

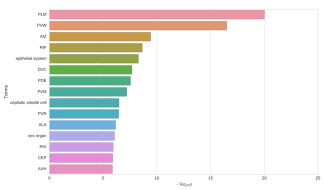

GO enrichment | -log10 Q-values

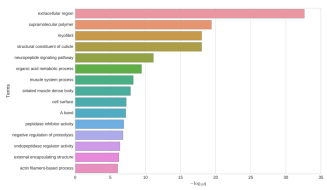

Phenotype enrichment | -log10 Q-values

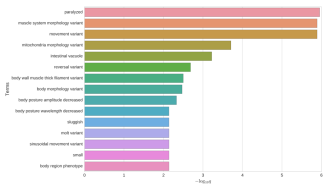

nlp-20 (neuropeptide signaling expressed in head neurons)

cluster	chromosome	cosmid	CDS	gene
CELK04101	4	F45E4	k	nlp-20

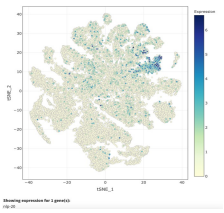

F55H12.4 (expressed in anus, hypodermis, pharynx)*

cluster	chromosome	cosmid	CDS	gene
CELK10501	1	F55H12	F55H12.4	k

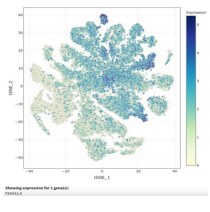

t-SNE showing cell type 17

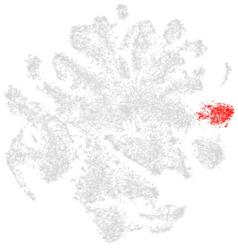

Top 20 enriched genes

	p_val	avg_log2FC	pct.1	pct.2	p_val_adj
ttn-1	0	4.71043392	0.997	0.454	0
ndnf-1	0	3.86345479	0.668	0.08	0
pde-4	0	3.65561682	0.843	0.171	0
unc-22	0	3.49590736	0.933	0.323	0
cpna-2	1.20E-307	3.16785947	0.926	0.38	5.63E-303
M04G7.3	0	3.00944881	0.54	0.052	0
C32E12.4	0	2.82390468	0.68	0.137	0
unc-68	3.90E-264	2.6685098	0.811	0.281	1.83E-259
Y47H10A.4	0	2.653438	0.411	0.033	0
him-4	1.78E-145	2.609877	0.657	0.271	8.37E-141
unc-89	6.19E-256	2.59746611	0.917	0.424	2.90E-251
unc-49	0	2.59683984	0.539	0.074	0
unc-103	0	2.56775832	0.509	0.06	0
T13H5.1	5.27E-286	2.55410525	0.608	0.126	2.47E-281
prk-1	9.63E-206	2.55329927	0.647	0.196	4.52E-201
tnt-3	2.38E-190	2.55167952	0.695	0.246	1.12E-185
kin-1	1.83E-235	2.52008987	0.676	0.192	8.60E-231
C30E1.9	1.38E-243	2.499007	0.943	0.47	6.46E-239
W05F2.4	2.27E-242	2.4930021	0.651	0.174	1.06E-237
ketn-1	1.23E-192	2.44618878	0.842	0.397	5.77E-188

Top 20 depleted genes

	p_val	avg_log2FC	pct.1	pct.2	p_val_adj
ule-2	6.54E-07	-2.0044753	0.215	0.296	0.03067617
ZK813.2	3.80E-09	-1.6817148	0.193	0.292	0.00017805
T20G5.8	2.78E-13	-1.6650378	0.064	0.175	1.30E-08
dod-6	7.60E-12	-1.6223984	0.165	0.289	3.56E-07
fipr-2	1.83E-08	-1.6200748	0.11	0.197	0.00085739
nlp-77	6.99E-38	-1.6092246	0.573	0.707	3.28E-33
C49G7.3	3.11E-09	-1.603107	0.095	0.188	0.00014586
T21C9.13	4.32E-09	-1.5734879	0.069	0.155	0.00020264
clec-87	6.65E-14	-1.5470366	0.239	0.37	3.12E-09
Y22D7AR.10	1.32E-10	-1.5246077	0.179	0.297	6.20E-06
ttr-2	1.06E-10	-1.5077988	0.356	0.466	4.96E-06
ZC513.7	6.16E-07	-1.4791371	0.339	0.432	0.02887184
myo-1	2.34E-08	-1.3284302	0.072	0.153	0.00109781
acp-6	2.67E-18	-1.3073254	0.422	0.549	1.25E-13
fipr-1	8.82E-10	-1.296676	0.052	0.138	4.14E-05
spn-4	4.41E-15	-1.274259	0.091	0.225	2.07E-10
col-95	8.96E-12	-1.2364756	0.509	0.591	4.20E-07
C45G9.6	1.08E-07	-1.2274516	0.06	0.134	0.00504972
pos-1	3.89E-11	-1.2127919	0.103	0.213	1.82E-06
C05C10.5	1.02E-08	-1.1876856	0.093	0.18	0.00047721

Tissue enrichment | -log10 Q-values

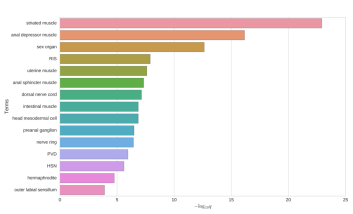

GO enrichment | -log10 Q-values

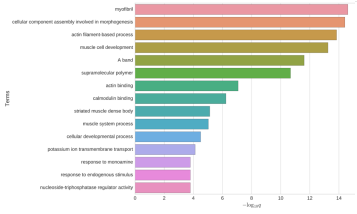

Phenotype enrichment | -log10 Q-values

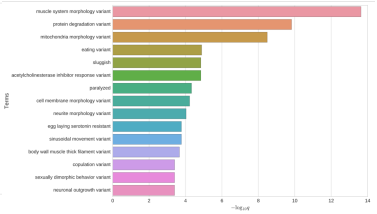

ttn-1 (actin and myosin binding)

cluster	chromosome	cosmid	CDS	gene
CELK04252	X	M04H8		

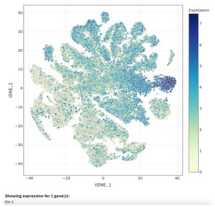

pde-4 (G protein coupled activity, neurons)*

cluster	chromosome	cosmid	CDS	gene
CELK03451	2	R153	R153.1	x

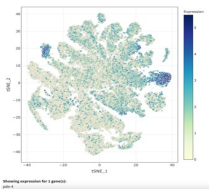

t-SNE showing cell type 18

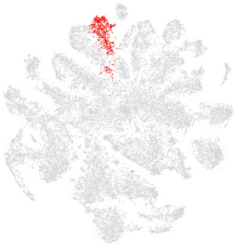

Top 20 enriched genes

	p_val	avg_log2FC	pct.1	pct.2	p_val_adj
fipr-2	0	4.24298534	0.874	0.174	0
Y73F4A.2	0	4.08631311	0.779	0.083	0
myo-1	0	3.75760284	0.841	0.129	0
T03F1.11	0	3.7259048	0.886	0.143	0
myo-2	0	3.71661903	0.879	0.13	0
F41E6.15	0	3.64043414	0.818	0.122	0
tnt-4	0	3.38733634	0.739	0.072	0
C53B7.3	0	3.36929307	0.882	0.233	0
gpx-3	0	3.32405266	0.665	0.062	0
F35B12.3	0	3.19616538	0.775	0.089	0
hsp-12.2	0	3.19423322	0.787	0.13	0
tnc-2	0	3.13992367	0.76	0.104	0
tni-4	0	3.08797734	0.816	0.162	0
C45E5.4	0	3.02575579	0.464	0.035	0
abf-6	0	3.00805583	0.63	0.07	0
fipr-1	0	3.00647639	0.615	0.121	0
ttr-21	0	2.94070591	0.726	0.102	0
marg-1	0	2.90635956	0.51	0.033	0
ttr-27	0	2.90170531	0.66	0.077	0
myo-5	0	2.68708692	0.63	0.098	0

Top 20 depleted genes

	p_val	avg_log2FC	pct.1	pct.2	p_val_adj
F53H2.3	3.64E-13	-1.4527763	0.093	0.204	1.71E-08
afd-1	1.26E-14	-1.2849631	0.211	0.34	5.92E-10
Y39B6A.1	8.86E-07	-1.223081	0.354	0.432	0.04153365
Y105E8A.25	1.19E-14	-1.2145742	0.222	0.349	5.60E-10
mix-1	2.12E-10	-1.1284448	0.195	0.296	9.93E-06
F57F5.1	8.53E-16	-1.1220463	0.382	0.503	4.00E-11
F53H1.4	2.90E-16	-1.0922292	0.101	0.234	1.36E-11
vit-2	2.51E-11	-1.0774401	0.726	0.724	1.18E-06
sos-1	5.85E-14	-1.0709941	0.114	0.235	2.74E-09
daf-2	3.81E-08	-1.0644315	0.124	0.203	0.00178525
spat-2	1.24E-15	-1.0411305	0.193	0.325	5.80E-11
plg-1	6.50E-09	-1.0209548	0.138	0.228	0.00030495
vit-5	5.91E-11	-1.0201046	0.765	0.764	2.77E-06
crh-1	2.18E-09	-1.013326	0.169	0.265	0.00010211
vit-6	3.36E-09	-0.9862497	0.781	0.754	0.00015777
ced-1	2.84E-12	-0.9835985	0.264	0.377	1.33E-07
lpd-3	3.27E-13	-0.9772606	0.213	0.336	1.53E-08
apx-1	1.58E-10	-0.960731	0.055	0.143	7.43E-06
npa-1	1.30E-16	-0.9534892	0.502	0.596	6.09E-12
vit-3	5.24E-09	-0.9480677	0.707	0.712	0.00024579

Tissue enrichment | -log10 Q-values

Nothing found on tissue analysis

GO enrichment | -log10 Q-values

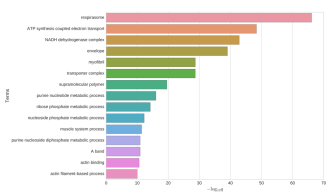

Phenotype enrichment | -log10 Q-values

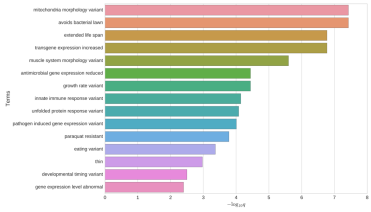

tni-4 (troponin binding, pharyngeal pumping)

clone	cluster	chromosome	cosmid	CDS	gene	size
328a10	CEL.K05276	II	W03F8		tni-4	0.96

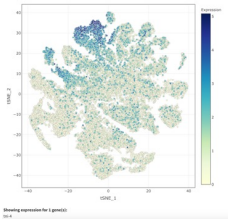

tnt-4 (larval development, tropomyosin binding activity)

clone	cluster	chromosome	cosmid	CDS	gene	size
K.PAY6	CEL.E03221	X	T04B1	T04B1.2	tnt-4	1.11

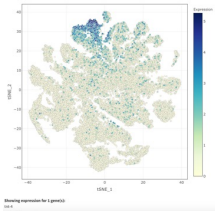

t-SNE showing cell type 19

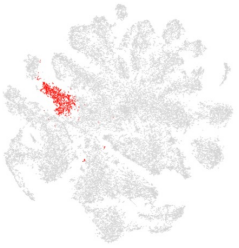

Top 20 enriched genes

	p_val	avg_log2FC	pct.1	pct.2	p_val_adj
T04G9.7	0	3.89920734	0.971	0.365	0
perm-4	0	3.89342678	1	0.567	0
C39D10.7	0	3.73402905	0.977	0.264	0
tbh-1	0	3.70462896	0.923	0.199	0
C44B7.5	1.68E-157	3.59594683	0.71	0.296	7.90E-153
skpo-1	0	3.57449359	0.914	0.204	0
F48E3.4	0	3.54587511	0.908	0.228	0
B0513.4	0	3.3118748	0.847	0.207	0
perm-2	3.47E-285	3.17875693	0.998	0.687	1.63E-280
inx-8	0	3.17547075	0.784	0.149	0
sdz-27	0	3.16140111	0.86	0.245	0
ddo-3	0	2.78148639	0.692	0.125	0
fasn-1	2.90E-253	2.6233437	0.8	0.262	1.36E-248
F41C3.5	6.60E-220	2.57541678	0.941	0.524	3.10E-215
C17G1.2	0	2.54993391	0.644	0.081	0
cle-1	2.13E-252	2.46666479	0.674	0.168	9.99E-248
cht-3	1.97E-118	2.41511485	0.709	0.338	9.22E-114
W09C3.7	0	2.35509598	0.642	0.105	0
Y32F6A.5	6.30E-170	2.09865379	0.851	0.432	2.96E-165
Y38E10A.14	2.20E-129	2.08652542	0.628	0.232	1.03E-124

Top 20 depleted genes

	p_val	avg_log2FC	pct.1	pct.2	p_val_adj
dig-1	9.17E-09	-3.0593139	0.142	0.24	0.00043018
ttn-1	2.74E-10	-1.7852621	0.387	0.471	1.29E-05
crh-1	3.58E-19	-1.5974024	0.108	0.266	1.68E-14
spsb-1	1.01E-14	-1.5258619	0.155	0.292	4.72E-10
C30E1.9	2.58E-15	-1.4824084	0.347	0.487	1.21E-10
tos-1	2.42E-20	-1.3574729	0.342	0.502	1.14E-15
ttr-2	1.64E-09	-1.3464398	0.369	0.466	7.71E-05
col-12	4.00E-10	-1.2316612	0.149	0.257	1.88E-05
ram-2	2.27E-09	-1.2309732	0.158	0.261	0.00010626
acp-6	2.18E-13	-1.2260347	0.451	0.548	1.02E-08
1-Jun	6.83E-11	-1.2147543	0.049	0.144	3.20E-06
daf-2	5.14E-11	-1.1847657	0.099	0.203	2.41E-06
sos-1	5.17E-13	-1.1688857	0.113	0.235	2.43E-08
fkh-7	3.06E-12	-1.1639645	0.076	0.187	1.43E-07
T28D6.3	9.92E-08	-1.1620953	0.151	0.238	0.00465501
F53H2.3	1.81E-07	-1.1276952	0.121	0.203	0.00849378
nlp-77	5.26E-17	-1.1017946	0.649	0.705	2.47E-12
ddo-2	4.36E-07	-1.0950375	0.236	0.32	0.02043326
col-155	5.41E-07	-1.0827854	0.122	0.201	0.0253796
T04F3.1	8.39E-12	-1.0557274	0.183	0.312	3.93E-07

Tissue enrichment | -log10 Q-values

Nothing found on tissue analysis

GO enrichment | -log10 Q-values

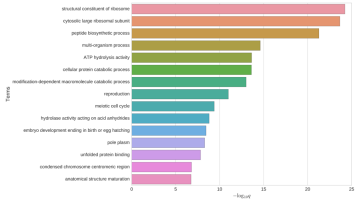

Phenotype enrichment | -log10 Q-values

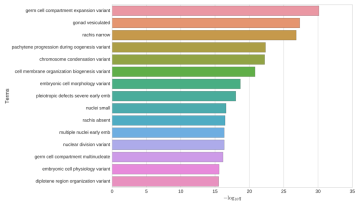

tbh-1 (beta hydroxylase activity, located in synapse)

clone	cluster	chromosome	cosmid	CDS	gene	size
54349	CEL.K07299	X	X13N06	X13N06.6	tbh-1	1.12

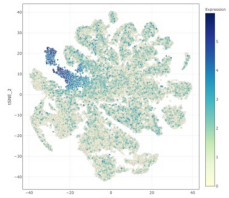

C39D10.7 (chitin binding activity, expressed in germline)*

clone	cluster	chromosome	cosmid	CDS	gene	size
43x10	CEL.K00008	X	C39D10	C39D10.7		0.71

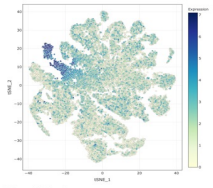

t-SNE showing cell type 20

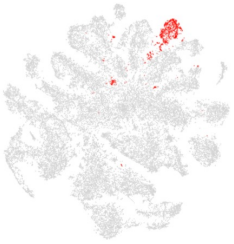

Top 20 enriched genes

	p_val	avg_log2FC	pct.1	pct.2	p_val_adj
F53F4.13	0	4.0027797	0.922	0.182	0
F20A1.1	0	3.9822104	0.915	0.167	0
T02B11.3	0	3.82711022	0.899	0.131	0
far-8	0	3.53357811	0.813	0.103	0
F20A1.10	0	3.36043654	0.642	0.094	0
R11D1.3	0	3.25926067	0.732	0.065	0
F35B12.9	0	3.05471114	0.66	0.064	0
R102.2	6.63E-221	2.854265	0.547	0.109	3.11E-216
C33G8.4	0	2.80403476	0.668	0.076	0
F40F8.4	0	2.7879273	0.646	0.06	0
ZK822.4	0	2.59163118	0.62	0.057	0
Y69A2AR.22	0	2.58024445	0.606	0.052	0
F14D7.10	0	2.55719265	0.543	0.06	0
F59A7.2	0	2.52169293	0.547	0.055	0
tag-209	0	2.5049903	0.588	0.061	0
F14D7.7	2.28E-293	2.27685081	0.483	0.064	1.07E-288
K01A6.8	0	2.23840573	0.471	0.03	0
Y42G9A.2	0	2.16989085	0.487	0.04	0
F59A7.5	0	2.1248598	0.461	0.035	0
F07C6.3	0	2.08387698	0.479	0.031	0

Top 20 depleted genes

	p_val	avg_log2FC	pct.1	pct.2	p_val_adj
dig-1	1.56E-10	-1.9855564	0.368	0.234	7.31E-06
afd-1	1.95E-09	-1.2546251	0.241	0.339	9.12E-05
Y105E8A.25	5.78E-08	-1.1795545	0.264	0.347	0.00271109
mix-1	2.93E-09	-1.1506557	0.193	0.295	0.00013747
sos-1	2.40E-09	-1.1266752	0.133	0.234	0.0001126
F57F5.1	1.08E-10	-1.1006425	0.404	0.502	5.08E-06
klp-12	4.49E-08	-1.0225981	0.298	0.375	0.00210585
F53H1.4	3.64E-08	-0.9829643	0.139	0.232	0.001709
apx-1	1.23E-08	-0.9389229	0.056	0.142	0.00057833
golg-4	5.56E-08	-0.9294097	0.175	0.267	0.00260799
unc-40	8.38E-09	-0.9106337	0.099	0.196	0.00039286
npp-8	2.10E-08	-0.8990429	0.139	0.236	0.00098298
Y57A10A.31	3.38E-09	-0.8771811	0.066	0.159	0.00015854
attf-6	1.69E-09	-0.8768652	0.064	0.157	7.92E-05
xpc-1	3.91E-08	-0.8762269	0.121	0.215	0.0018354
Y53F4B.21	3.61E-08	-0.8582019	0.052	0.132	0.00169348
Y48G8AL.5	1.07E-07	-0.8387539	0.074	0.156	0.00503567
ceh-100	5.20E-08	-0.8343194	0.149	0.242	0.00243906
lea-1	6.27E-07	-0.7774685	0.479	0.552	0.02942488
sqv-6	8.92E-07	-0.7504222	0.038	0.102	0.04181791

Tissue enrichment | -log10 Q-values

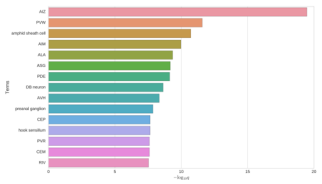

GO enrichment | -log10 Q-values

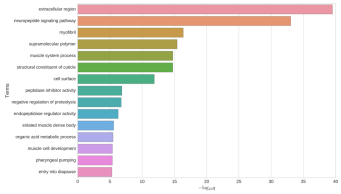

Phenotype enrichment | -log10 Q-values

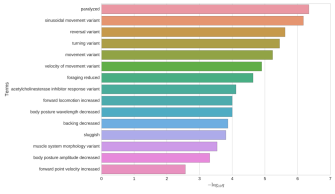

T02B11.3 (expressed in amphid sheath cell)

clone	cluster	chromosome	cosmid	CDS	gene	size
30761	CEL.K05391	5	T02B11	T02B11.3		0.77

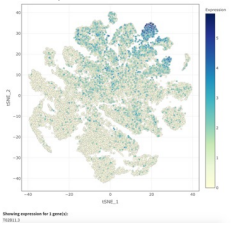

Showing expression for 1 gene(s):
T02B11.3

F53F4.13 (expressed in amphid sheath cell, unknown domain)

clone	cluster	chromosome	cosmid	CDS	gene	size
72807	CEL.K04786	5		F53F4	F53F4.13	0.95

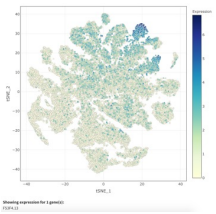

Showing expression for 1 gene(s):
F53F4.13

t-SNE showing cell type 21

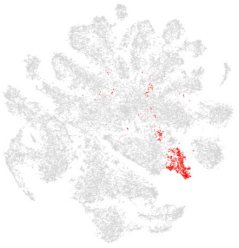

Top 20 enriched genes

	p_val	avg_log2FC	pct.1	pct.2	p_val_adj
fipr-13	0	4.09801999	0.786	0.101	0
col-155	0	4.03167096	0.92	0.182	0
col-96	0	3.71423829	0.887	0.208	0
col-166	0	3.44090176	0.846	0.188	0
nas-37	0	3.30584965	0.639	0.058	0
col-118	0	3.26232385	0.743	0.142	0
hsp-43	1.90E-178	2.6812599	0.715	0.23	8.91E-174
Y105C5B.5	3.56E-173	2.53049404	0.893	0.434	1.67E-168
acp-6	4.27E-177	2.51770205	0.949	0.536	2.00E-172
F13D12.3	1.22E-184	2.35840307	0.63	0.17	5.72E-180
hsp-12.3	5.25E-106	2.12185877	0.439	0.123	2.46E-101
F42A8.1	6.73E-139	2.08036413	0.708	0.266	3.15E-134
Y43C5A.3	9.71E-129	2.05158343	0.528	0.155	4.55E-124
far-3	5.90E-82	2.00067362	0.563	0.227	2.77E-77
cht-3	1.23E-101	1.98297365	0.731	0.339	5.78E-97
F45E4.5	9.70E-164	1.96733219	0.357	0.058	4.55E-159
nlp-77	2.20E-160	1.91667965	0.99	0.696	1.03E-155
col-141	1.13E-263	1.9144458	0.31	0.027	5.31E-259
K07C11.7	1.65E-120	1.88810073	0.522	0.156	7.74E-116
col-142	2.24E-149	1.82949433	0.936	0.573	1.05E-144

Top 20 depleted genes

	p_val	avg_log2FC	pct.1	pct.2	p_val_adj
dig-1	1.48E-07	-2.1262216	0.353	0.234	0.00693907
F53H2.3	1.96E-07	-1.2280449	0.115	0.203	0.00919183
mix-1	7.71E-10	-1.1270753	0.183	0.296	3.62E-05
ipla-1	8.24E-08	-0.9886066	0.257	0.352	0.00386426
cpr-1	1.49E-09	-0.9807509	0.347	0.455	7.01E-05
dct-16	2.23E-15	-0.9685919	0.715	0.763	1.05E-10
sos-1	4.81E-09	-0.9529103	0.129	0.234	0.00022559
H06I04.3	3.81E-12	-0.9406015	0.133	0.265	1.79E-07
npp-8	1.57E-09	-0.935673	0.127	0.236	7.36E-05
lpd-3	4.23E-09	-0.8951715	0.226	0.335	0.00019824
lys-2	5.79E-07	-0.8929382	0.409	0.475	0.02716372
crh-1	3.12E-07	-0.8856172	0.17	0.264	0.01464534
Y119D3B.21	2.87E-10	-0.8745702	0.604	0.66	1.35E-05
sql-1	1.89E-08	-0.8708044	0.133	0.232	0.0008851
vit-2	1.03E-08	-0.8630216	0.678	0.725	0.00048082
mdt-26	6.32E-07	-0.859684	0.158	0.244	0.02962771
Y79H2A.3	1.91E-07	-0.8571863	0.144	0.239	0.00895627
asp-3	8.77E-09	-0.8566837	0.515	0.594	0.00041158
F57F5.1	4.75E-08	-0.8506876	0.4	0.502	0.00222874
fib-1	1.24E-09	-0.8498251	0.185	0.299	5.84E-05

Tissue enrichment | -log10 Q-values

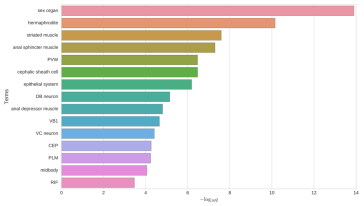

GO enrichment | -log10 Q-values

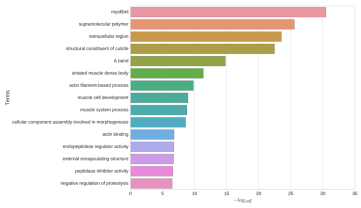

Phenotype enrichment | -log10 Q-values

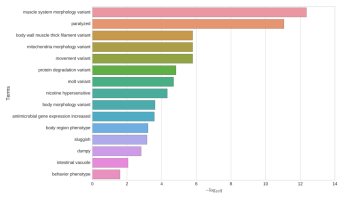

hsp-43 (hermaphrodite gonad)

cluster	chromosome	cosmid	CDS	gene
CELK05633	X	C14F11	C14F11.5	hsp-43

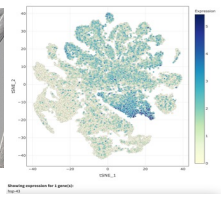

nas-37 (collagen and cuticle development, expressed in intestine, epithelial, rectal gland)*

cluster	chromosome	cosmid	CDS	gene
CELK04079	X	C17G1	C17G1.6	nas-37

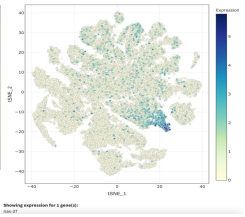

t-SNE showing cell type 22

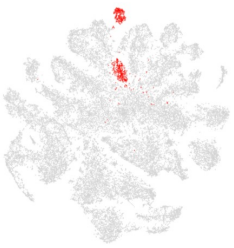

Top 20 enriched genes

	p_val	avg_log2FC	pct.1	pct.2	p_val_adj
T28D6.3	0	3.91335063	0.936	0.22	0
ZK669.3	3.32E-285	2.66178642	0.691	0.136	1.56E-280
gst-41	9.84E-274	2.57465492	0.338	0.03	4.62E-269
B0238.12	1.14E-170	2.39212287	0.375	0.059	5.33E-166
abf-6	1.65E-204	2.30638666	0.471	0.078	7.72E-200
acp-6	2.74E-183	2.17380794	0.963	0.536	1.29E-178
ZC443.1	0	2.11871188	0.447	0.038	0
tni-3	3.53E-114	2.04566023	0.629	0.225	1.66E-109
F55H12.4	1.23E-97	2.03481537	0.765	0.39	5.77E-93
nlp-77	1.39E-190	2.010419	0.998	0.697	6.53E-186
acs-3	1.40E-102	1.97707573	0.18	0.022	6.59E-98
T26C5.4	1.74E-191	1.95778926	0.465	0.081	8.14E-187
D1086.1	1.70E-116	1.95346603	0.518	0.149	7.98E-112
vap-2	1.03E-219	1.93097021	0.522	0.091	4.85E-215
col-150	2.93E-167	1.8655416	0.572	0.136	1.37E-162
del-6	1.13E-121	1.84253629	0.735	0.316	5.30E-117
Y73F4A.2	1.29E-160	1.83960282	0.478	0.096	6.07E-156
tag-290	1.43E-147	1.82229644	0.373	0.065	6.70E-143
C45B2.1	7.11E-114	1.77727406	0.846	0.43	3.33E-109
Y113G7A.16	0	1.74637826	0.287	0.014	0

Top 20 depleted genes

	p_val	avg_log2FC	pct.1	pct.2	p_val_adj
F53H2.3	1.51E-07	-1.3168283	0.112	0.203	0.0070754
F57F5.1	7.75E-15	-1.2806699	0.353	0.503	3.63E-10
vit-2	1.89E-15	-1.2784977	0.673	0.725	8.86E-11
mix-1	1.44E-08	-1.1876436	0.191	0.295	0.00067357
afd-1	2.74E-07	-1.1640927	0.25	0.338	0.0128373
daf-2	7.47E-11	-1.1464714	0.086	0.203	3.50E-06
elpc-2	1.31E-11	-1.1291539	0.079	0.199	6.16E-07
vit-3	6.37E-13	-1.1086278	0.638	0.714	2.99E-08
aakg-1	8.90E-08	-1.1070908	0.118	0.21	0.00417221
Y79H2A.3	2.17E-08	-1.0841757	0.14	0.239	0.00101978
F53H1.4	6.62E-10	-1.080703	0.121	0.232	3.11E-05
vit-1	1.89E-10	-1.0753422	0.61	0.677	8.87E-06
vit-6	1.89E-11	-1.0661482	0.721	0.756	8.85E-07
cpr-1	8.06E-09	-1.0544938	0.342	0.455	0.00037797
sos-1	5.31E-07	-1.0541899	0.147	0.233	0.02492856
npp-8	9.75E-12	-1.0412026	0.107	0.236	4.58E-07
vit-5	2.41E-09	-1.0344991	0.741	0.764	0.00011301
lpd-3	1.84E-09	-1.0333984	0.224	0.334	8.61E-05
C17F4.7	6.95E-08	-1.0279658	0.702	0.712	0.00326113
cpr-6	8.78E-12	-1.0100447	0.632	0.681	4.12E-07

Tissue enrichment | -log10 Q-values

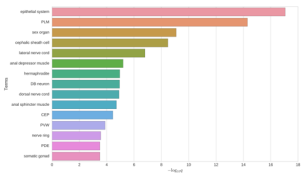

GO enrichment | -log10 Q-values

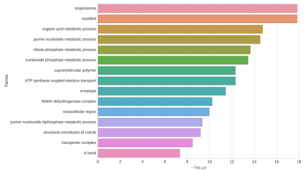

Phenotype enrichment | -log10 Q-values

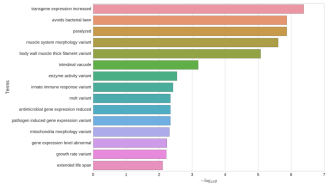

ZK669.3 (oxidoreductase activity in extracellular region)

cluster	chromosome	cosmid	CDS	gene
CELK05728	2	ZK669	ZK669.4	

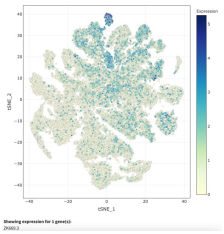

B0238.12 (endopeptidase activity in extracellular region)

cluster	chromosome	cosmid	CDS	gene
CELK09505	5	B0238	B0238.12	

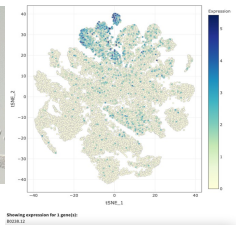

t-SNE showing cell type 23

Top 20 enriched genes

	p_val	avg_log2FC	pct.1	pct.2	p_val_adj
T21C9.13	0	5.07789238	0.964	0.132	0
F14H3.6	0	4.1271477	0.916	0.094	0
C05C10.5	0	4.11788199	0.918	0.158	0
pos-1	0	4.11616973	0.962	0.191	0
F08F3.6	0	4.06865345	0.89	0.085	0
spn-4	0	3.98897048	0.951	0.202	0
patr-1	0	3.90285022	0.922	0.183	0
mom-2	0	3.87843379	0.882	0.105	0
C37C3.9	0	3.86279559	0.894	0.114	0
T12G3.6	0	3.75388201	0.899	0.11	0
T10B11.8	0	3.71742132	0.753	0.072	0
mtk-1	0	3.71654974	0.798	0.151	0
tmem-131	0	3.7144092	0.869	0.197	0
rbr-2	0	3.70569234	0.816	0.185	0
clec-87	0	3.68817575	0.977	0.351	0
Y4C6A.3	0	3.6619247	0.802	0.056	0
neg-1	0	3.62277969	0.781	0.082	0
era-1	0	3.60817646	0.882	0.13	0
C13F10.7	0	3.59369398	0.791	0.081	0
zif-1	0	3.58539126	0.857	0.084	0

Top 20 depleted genes

	p_val	avg_log2FC	pct.1	pct.2	p_val_adj
ule-4	1.64E-92	-5.2174366	0.038	0.519	7.67E-88
far-2	2.67E-191	-4.9787011	0.08	0.784	1.25E-186
col-122	1.08E-182	-4.8207586	0.051	0.756	5.06E-178
col-119	9.43E-178	-4.72203	0.053	0.747	4.42E-173
col-101	1.96E-170	-4.6967788	0.067	0.733	9.18E-166
act-4	3.07E-175	-4.6217209	0.048	0.736	1.44E-170
col-140	7.43E-180	-4.6023819	0.059	0.755	3.49E-175
col-181	4.42E-176	-4.5743292	0.049	0.742	2.08E-171
col-184	6.51E-169	-4.4634474	0.04	0.719	3.05E-164
unc-54	8.33E-157	-4.46105	0.051	0.699	3.91E-152
col-124	3.38E-166	-4.3704093	0.048	0.723	1.59E-161
col-20	5.79E-171	-4.332734	0.059	0.739	2.72E-166
lev-11	2.82E-178	-4.3296425	0.042	0.744	1.32E-173
D1086.10	3.64E-63	-4.3175522	0.03	0.402	1.71E-58
col-95	9.42E-119	-4.2974024	0.051	0.602	4.42E-114
pat-10	1.09E-167	-4.2782809	0.038	0.724	5.09E-163
col-80	3.57E-175	-4.2730347	0.07	0.751	1.67E-170
nlp-77	4.94E-162	-4.2670336	0.072	0.72	2.32E-157
cpn-3	1.19E-154	-4.2597754	0.061	0.697	5.56E-150
col-143	2.31E-180	-4.2557594	0.078	0.764	1.08E-175

Tissue enrichment | -log10 Q-values

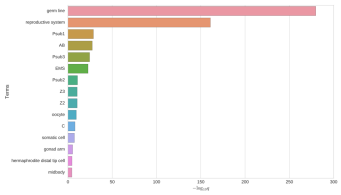

GO enrichment | -log10 Q-values

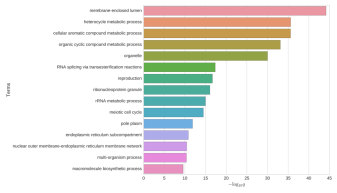

Phenotype enrichment | -log10 Q-values

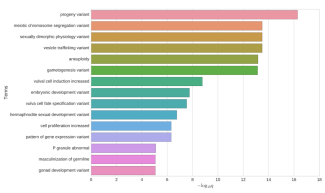

gld-1 (metabolic processes, oocyte development, reproductive processes regulation)

clone	cluster	chromosome	cosmid	CDS	gene	size
44-B4	CEL:K03NR	I	T23G11	T23G11.3	gld-1	2.29

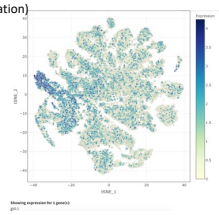

glp-1(RNA pol II, gene expression regulation, in germline and neurons)

clone	cluster	chromosome	cosmid	CDS	gene	size
5d13	CEL:K06212	I	F02A9	F02A9.6	glp-1	2.43

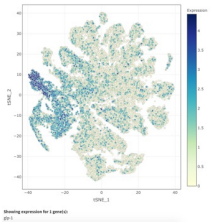

t-SNE showing cell type 24

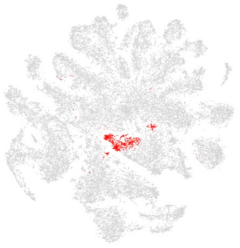

Top 20 enriched genes

	p_val	avg_log2FC	pct.1	pct.2	p_val_adj
ule-1	0	5.06501145	0.874	0.25	0
ule-2	0	4.40636231	0.914	0.28	0
D1086.7	0	4.32192192	0.899	0.219	0
C08A9.10	0	3.75268209	0.804	0.136	0
K11D12.13	1.40E-209	3.5461727	0.626	0.143	6.54E-205
F09E10.1	0	3.50895164	0.599	0.081	0
Y48G1C.13	0	3.48193198	0.632	0.083	0
C46C2.5	1.08E-298	3.40809568	0.599	0.094	5.06E-294
F59A6.12	0	3.3948197	0.727	0.084	0
ule-4	6.68E-231	3.34343654	0.954	0.497	3.13E-226
C10G8.4	2.87E-122	3.32627956	0.744	0.334	1.35E-117
C30G7.4	0	3.27786374	0.698	0.071	0
Y106G6D.8	1.38E-238	3.08765547	0.762	0.208	6.48E-234
ttr-34	1.97E-295	2.92212669	0.705	0.135	9.24E-291
hex-1	4.38E-128	2.78020561	0.553	0.166	2.06E-123
Y51H7C.1	3.65E-251	2.67086809	0.518	0.08	1.71E-246
K10C2.8	7.48E-99	2.56086893	0.454	0.134	3.51E-94
F08F1.4	6.81E-164	2.55133084	0.612	0.173	3.19E-159
T25D3.3	0	2.54687445	0.474	0.037	0
ttr-2	3.28E-109	2.53731675	0.826	0.455	1.54E-104

Top 20 depleted genes

	p_val	avg_log2FC	pct.1	pct.2	p_val_adj
crh-1	2.35E-09	-1.152779	0.145	0.264	0.00011017
spsb-1	6.99E-08	-1.1264596	0.181	0.291	0.0032786
F53E4.1	3.91E-09	-1.0097246	0.161	0.28	0.0001832
daf-2	6.08E-09	-0.947104	0.095	0.203	0.00028526
elpc-2	3.17E-08	-0.9275282	0.099	0.199	0.00148886
lmd-3	2.44E-09	-0.9272528	0.297	0.41	0.00011433
afd-1	6.38E-07	-0.9037204	0.24	0.339	0.0299427
H06I04.3	2.63E-07	-0.8065096	0.167	0.264	0.01235367
tni-4	3.82E-07	-0.7926128	0.093	0.184	0.01790638
C35B1.2	8.25E-09	-0.7859282	0.101	0.209	0.00038703
ceh-100	3.09E-07	-0.7592855	0.145	0.242	0.01447461
rsks-1	1.47E-07	-0.7558131	0.137	0.237	0.00688257
unc-40	3.42E-08	-0.7512286	0.095	0.196	0.00160331
sql-1	8.52E-09	-0.7492299	0.121	0.232	0.00039943
Y105C5A.15	3.70E-08	-0.7432723	0.048	0.137	0.00173431
F58B3.6	1.48E-11	-0.742568	0.11	0.24	6.92E-07
Y48G8AL.5	1.85E-07	-0.738407	0.068	0.155	0.00869343
egl-4	8.59E-11	-0.7326871	0.35	0.482	4.03E-06
F16A11.1	2.39E-07	-0.730184	0.148	0.243	0.01119518
W07E11.1	1.70E-07	-0.7196724	0.205	0.304	0.00798622

Tissue enrichment | -log10 Q-values

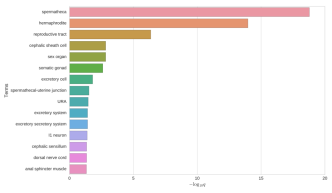

GO enrichment | -log10 Q-values

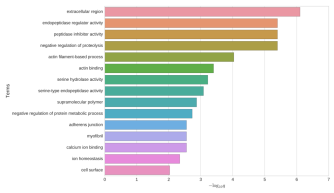

Phenotype enrichment | -log10 Q-values

Nothing found on phenotype analysis

ule-1 (uterine lumen, chitin binding activity in ECM)

clone	cluster	chromosome	cosmid	CDS	gene	size
570b7	CEL.IG3006	I	W03F11	W03F11.1		1.00

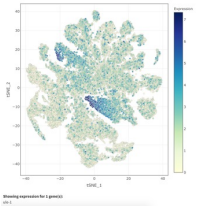

*pes-23 (transmembrane transporter)**

clone	cluster	chromosome	cosmid	CDS	gene	size
550g9	CEL.F01450	X	F14B8	F14B8.3	pes-23	3.79

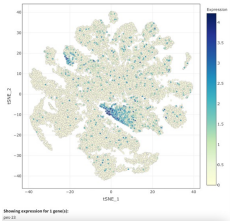

t-SNE showing cell type 25

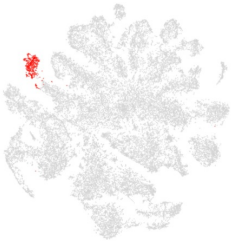

Top 20 enriched genes

	p_val	avg_log2FC	pct.1	pct.2	p_val_adj
fasn-1	0	5.84270177	0.982	0.265	0
C39D10.7	8.09E-300	5.09991577	0.985	0.272	3.79E-295
ZC513.7	9.50E-223	4.72135562	0.982	0.42	4.46E-218
B0545.4	0	4.67893158	0.772	0.041	0
irk-1	0	4.18698545	0.723	0.014	0
abts-4	0	4.12604164	0.754	0.07	0
tbh-1	3.29E-273	3.99128796	0.888	0.207	1.54E-268
aak-1	0	3.86598673	0.86	0.155	0
skpo-1	4.83E-240	3.75765996	0.86	0.213	2.27E-235
frm-1	1.24E-174	3.75278549	0.936	0.436	5.82E-170
F45B8.5	0	3.54379944	0.663	0.015	0
Y105C5A.25	0	3.36408584	0.672	0.033	0
C44B7.5	1.76E-66	3.36197696	0.641	0.302	8.27E-62
W04A4.2	1.24E-293	3.33351245	0.535	0.056	5.82E-289
Y38E10A.14	1.04E-106	3.29254218	0.663	0.236	4.88E-102
W09C3.7	0	3.24707631	0.787	0.108	0
lim-7	0	3.22596324	0.578	0.024	0
C04G2.14	0	3.18178109	0.48	0.04	0
perm-4	7.25E-159	3.14982192	0.994	0.572	3.40E-154
anc-1	5.69E-170	3.08059504	0.994	0.685	2.67E-165

Top 20 depleted genes

	p_val	avg_log2FC	pct.1	pct.2	p_val_adj
ule-4	5.03E-14	-2.8176448	0.347	0.509	2.36E-09
D1086.10	4.79E-12	-2.7534585	0.231	0.395	2.25E-07
nlp-77	1.86E-57	-2.4992579	0.325	0.709	8.72E-53
lbp-2	1.99E-42	-2.4948408	0.322	0.636	9.34E-38
ttr-16	3.24E-40	-2.4426892	0.368	0.648	1.52E-35
ule-2	9.60E-08	-2.359075	0.176	0.295	0.00450282
cpn-3	6.90E-41	-2.2887364	0.419	0.685	3.24E-36
col-95	4.48E-30	-2.2716506	0.298	0.593	2.10E-25
col-140	1.21E-54	-2.2649531	0.419	0.742	5.65E-50
C35B1.4	1.44E-12	-2.2265026	0.097	0.263	6.78E-08
C10G8.4	1.27E-07	-2.2191065	0.231	0.345	0.00597648
col-119	1.91E-49	-2.217853	0.438	0.734	8.97E-45
col-122	8.48E-52	-2.1939011	0.426	0.743	3.98E-47
col-184	1.32E-46	-2.1271967	0.413	0.706	6.20E-42
col-20	1.30E-49	-2.1167704	0.377	0.728	6.12E-45
col-181	2.34E-46	-2.1116332	0.453	0.729	1.10E-41
tnt-2	1.92E-36	-2.105879	0.31	0.606	9.01E-32
col-101	1.10E-43	-2.0968267	0.429	0.721	5.16E-39
fipr-2	2.66E-12	-2.0924108	0.046	0.197	1.25E-07
col-80	1.81E-50	-2.079209	0.416	0.739	8.48E-46

Tissue enrichment | -log10 Q-values

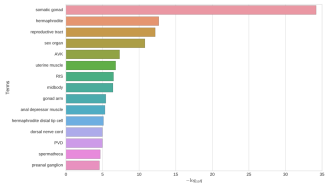

GO enrichment | -log10 Q-values

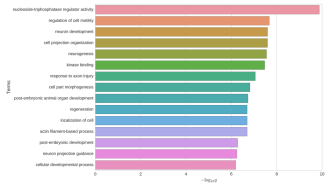

Phenotype enrichment | -log10 Q-values

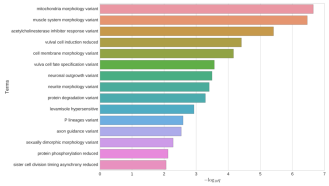

C39D10.7 (chitin binding activity in germline)

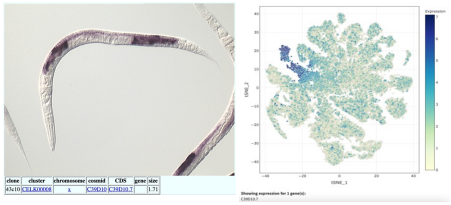

clone	cluster	chromosome	cosmid	CDS	gene	size
AN10	C2L4A8KR	X	C39D10	C39D10.7		1-71

*tbh-1 (*beta hydroxylase activity, located in synapse)*

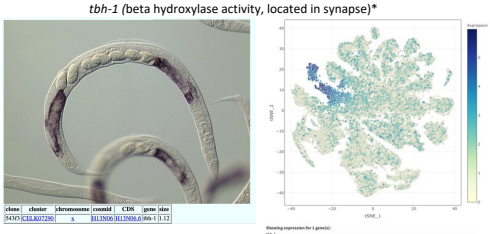

clone	cluster	chromosome	cosmid	CDS	gene	size
9430	C2L4J7Z6	X	H12N06	H12N06.6	tbh-1	1-12

t-SNE showing cell type 26

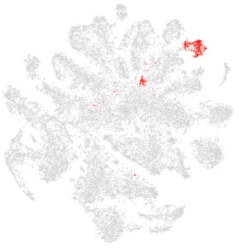

Top 20 enriched genes

	p_val	avg_log2FC	pct.1	pct.2	p_val_adj
nspc-4	0	4.83083584	0.897	0.111	0
nspc-7	0	4.48240695	0.836	0.086	0
nspc-14	0	4.31236431	0.805	0.071	0
nspc-20	0	4.21284414	0.775	0.07	0
nspc-9	0	3.91972667	0.763	0.059	0
nspc-10	0	3.5758342	0.69	0.047	0
nspc-1	0	3.55081748	0.684	0.038	0
nspc-13	0	3.29167112	0.626	0.03	0
nspc-3	0	2.23152161	0.45	0.019	0
flp-1	1.87E-52	2.13844162	0.225	0.046	8.77E-48
nlp-49	7.24E-81	1.88416721	0.286	0.05	3.40E-76
lips-15	6.71E-65	1.69913496	0.465	0.147	3.15E-60
nspc-5	0	1.55568815	0.249	0.008	0
D1086.3	2.43E-50	1.47985337	0.696	0.348	1.14E-45
flp-11	3.56E-26	1.43407009	0.188	0.055	1.67E-21
F56D6.8	3.06E-28	1.41220853	0.441	0.209	1.44E-23
F36D1.7	1.39E-139	1.38164486	0.292	0.033	6.54E-135
hmit-1.2	4.51E-76	1.34085027	0.207	0.029	2.11E-71
F56D6.9	1.73E-22	1.23794153	0.474	0.254	8.13E-18
dct-8	1.15E-32	1.19908386	0.407	0.168	5.41E-28

Top 20 depleted genes

	p_val	avg_log2FC	pct.1	pct.2	p_val_adj
H06I04.3	6.44E-08	-1.0927223	0.149	0.263	0.00301887
lipl-7	1.39E-07	0.25088682	0.213	0.117	0.00650119
nape-2	7.27E-07	0.25152394	0.146	0.074	0.03411702
K01C8.1	3.84E-07	0.25392687	0.356	0.23	0.01802796
R09B5.11	5.94E-07	0.25517123	0.185	0.101	0.02786719
C06B3.6	6.96E-08	0.25715037	0.438	0.296	0.00326424
cyp-34A4	8.94E-08	0.25740227	0.155	0.075	0.00419203
F36A2.3	5.52E-07	0.2654605	0.237	0.137	0.02590107
K09G1.1	1.62E-07	0.26592074	0.502	0.356	0.00759409
grd-10	9.03E-09	0.26722876	0.35	0.211	0.00042343
kdp-1	8.41E-07	0.26798393	0.599	0.446	0.03944543
vap-2	3.80E-08	0.2697477	0.191	0.099	0.00178416
tag-196	3.45E-08	0.26981926	0.401	0.26	0.00161692
F43H9.4	2.34E-07	0.27071288	0.225	0.128	0.010996
act-2	9.45E-07	0.2723172	0.839	0.72	0.04434558
egl-3	1.93E-09	0.28143663	0.252	0.135	9.07E-05
got-1.2	2.99E-08	0.28204974	0.462	0.314	0.00140163
C39E9.8	2.94E-10	0.28285206	0.578	0.412	1.38E-05
F53F4.10	9.79E-07	0.28576074	0.508	0.375	0.04590945
T10H9.8	2.14E-07	0.2873615	0.164	0.083	0.01005265

Tissue enrichment | -log10 Q-values

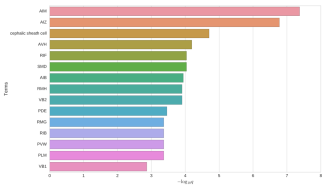

GO enrichment | -log10 Q-values

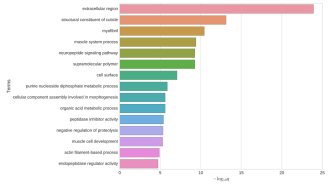

Phenotype enrichment | -log10 Q-values

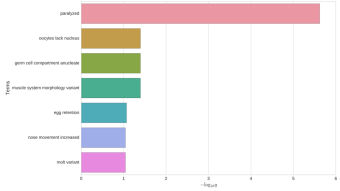

dct-8 (enriched in hypodermis and somatic gonad precu

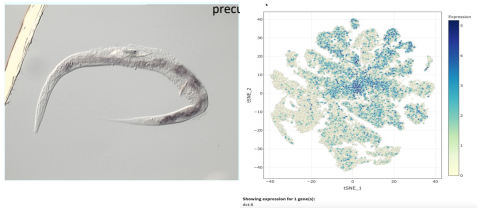

*nspc-7 (enriched in excretory gland cell)**

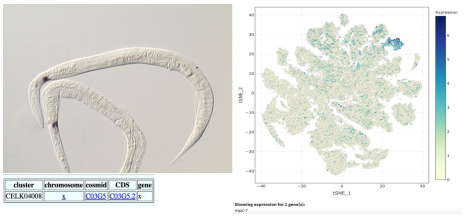

cluster	chromosome	cosmid	CDS	gene
CEL.K04008	X	C03G5	C03G5.2	lx

t-SNE showing cell type 27

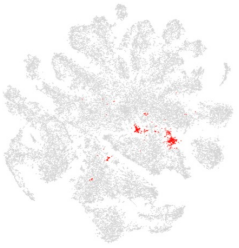

Top 20 enriched genes

	p_val	avg_log2FC	pct.1	pct.2	p_val_adj
pks-1	8.89E-89	4.0228231	0.342	0.052	4.17E-84
acbp-6	1.03E-86	3.74026067	0.406	0.077	4.84E-82
F22F4.5	2.99E-167	3.71888228	0.41	0.042	1.40E-162
C53B7.2	2.65E-102	3.71641946	0.603	0.146	1.24E-97
cht-3	3.36E-67	3.25922289	0.761	0.344	1.58E-62
Y71H2B.1	1.10E-151	3.07514599	0.397	0.043	5.15E-147
C53B7.3	4.34E-58	2.84432466	0.645	0.248	2.03E-53
lbp-3	1.76E-60	2.68080243	0.679	0.288	8.24E-56
K10C2.12	2.94E-107	2.37296349	0.303	0.034	1.38E-102
bgal-1	6.02E-61	2.32577319	0.509	0.152	2.82E-56
pod-2	5.45E-11	2.31473403	0.679	0.547	2.56E-06
C09D4.2	1.72E-71	2.22813074	0.59	0.182	8.08E-67
hsp-12.3	2.43E-46	2.19630957	0.423	0.127	1.14E-41
mig-6	5.25E-66	2.11583586	0.786	0.362	2.46E-61
ost-1	6.55E-40	1.96370231	0.863	0.616	3.07E-35
lbp-1	5.88E-38	1.94751109	0.62	0.293	2.76E-33
ZC412.3	4.07E-41	1.90713406	0.521	0.203	1.91E-36
let-2	3.73E-41	1.90557376	0.838	0.572	1.75E-36
timp-1	7.54E-56	1.85244889	0.5	0.152	3.54E-51
acs-1	6.59E-19	1.78451102	0.632	0.404	3.09E-14

Top 20 depleted genes

	p_val	avg_log2FC	pct.1	pct.2	p_val_adj
dig-1	1.12E-13	-1.268791	0.436	0.235	5.26E-09
ule-4	1.93E-16	-0.3599361	0.752	0.504	9.04E-12
ZK813.2	8.17E-07	-0.3408854	0.449	0.288	0.03832419
Y22D7AR.10	2.80E-07	-0.3006009	0.457	0.291	0.01313691
dpf-1	2.83E-10	0.27956127	0.111	0.034	1.33E-05
sgcb-1	2.03E-08	0.29524916	0.141	0.056	0.00095125
D1086.7	2.10E-09	0.31563778	0.393	0.232	9.87E-05
twk-24	6.28E-07	0.32437312	0.103	0.039	0.02944204
W01F3.2	2.24E-07	0.32908288	0.538	0.363	0.0105118
col-122	9.98E-08	0.34294622	0.897	0.736	0.00468078
F48E3.8	6.69E-12	0.34343288	0.103	0.028	3.14E-07
F14F9.5	2.57E-07	0.34608299	0.111	0.042	0.01206204
zmp-4	8.24E-07	0.34889801	0.226	0.121	0.03865012
ttr-15	1.01E-09	0.35317955	0.876	0.705	4.75E-05
gpd-2	3.67E-08	0.35519242	0.889	0.714	0.00172309
F32D8.10	4.96E-10	0.36058985	0.111	0.035	2.32E-05
cpna-2	1.31E-07	0.36510365	0.547	0.393	0.00615602
enol-1	4.08E-07	0.37523818	0.863	0.762	0.01914576
ttn-1	6.81E-11	0.37779302	0.654	0.467	3.19E-06
cth-2	7.71E-07	0.38229604	0.739	0.576	0.03617513

Tissue enrichment | -log10 Q-values

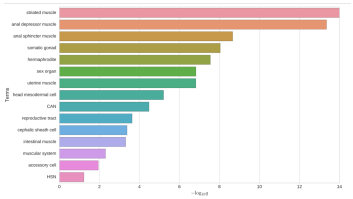

GO enrichment | -log10 Q-values

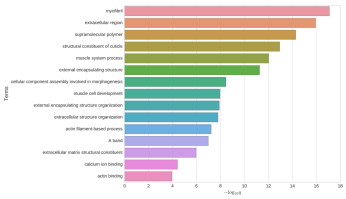

Phenotype enrichment | -log10 Q-values

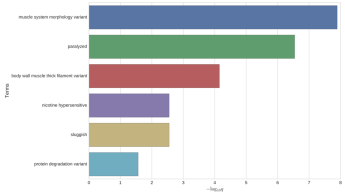

cht-3 (chitin binding activity in uterine epithelial and vulval cells)

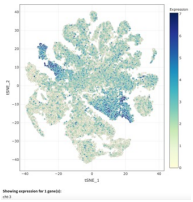

cluster	chromosome	cosmid	CDS	gene
CELK00113	4	C25A8	C25A8.4	x

acbp-6 (fatty acyl co-binding activity)*

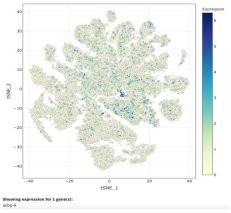

clone	cluster	chromosome	cosmid	CDS	gene	size
372e9	CELK06157	2	Y17G7B			1.55

t-SNE showing cell type 28

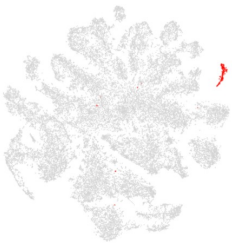

Top 20 enriched genes

	p_val	avg_log2FC	pct.1	pct.2	p_val_adj
dig-1	3.23E-202	8.57695228	0.959	0.23	1.51E-197
aman-1	0	7.8349216	0.933	0.031	0
ZC116.3	0	7.38400593	0.846	0.012	0
inos-1	8.18E-294	6.72525712	0.903	0.121	3.84E-289
T19C3.5	0	6.33563494	0.81	0.016	0
Y75B7AL.2	0	6.10029465	0.738	0.011	0
Y73F4A.1	0	5.89322697	0.918	0.025	0
mig-6	1.45E-149	5.81111125	0.974	0.361	6.78E-145
ttr-1	0	5.67612335	0.933	0.04	0
cup-4	0	5.49147265	0.867	0.021	0
clec-145	0	5.39558576	0.795	0.011	0
far-1	2.08E-126	5.11466402	0.995	0.628	9.77E-122
Y116A8C.3	0	4.90522801	0.882	0.022	0
lgc-26	0	4.87721062	0.795	0.008	0
clec-178	0	4.75455192	0.867	0.015	0
ZC513.7	7.55E-129	4.58470428	0.974	0.424	3.54E-124
F35C12.3	0	4.47929833	0.882	0.027	0
unc-122	0	4.32605415	0.723	0.008	0
wrk-1	5.55E-271	4.30351118	0.851	0.112	2.60E-266
lgc-25	0	4.15864043	0.687	0.004	0

Top 20 depleted genes

	p_val	avg_log2FC	pct.1	pct.2	p_val_adj
ule-4	2.25E-10	-2.6926624	0.297	0.509	1.06E-05
D1086.10	1.55E-08	-2.507027	0.205	0.394	0.00072772
ttn-1	9.59E-11	-2.1883218	0.251	0.471	4.50E-06
vit-4	1.01E-18	-1.5936053	0.379	0.684	4.75E-14
F57F5.1	2.85E-11	-1.5338714	0.297	0.501	1.34E-06
dod-6	3.10E-08	-1.5220349	0.108	0.287	0.00145238
perm-4	1.21E-10	-1.5159118	0.359	0.581	5.66E-06
vit-3	1.40E-22	-1.5103616	0.374	0.715	6.58E-18
ttr-51	2.49E-20	-1.5058136	0.385	0.683	1.17E-15
C23H5.8	1.15E-11	-1.5027429	0.226	0.454	5.41E-07
vit-1	1.11E-14	-1.4145753	0.431	0.677	5.23E-10
lys-1	5.25E-15	-1.4116604	0.308	0.573	2.46E-10
unc-54	2.97E-16	-1.3933393	0.395	0.686	1.39E-11
act-3	2.48E-21	-1.3773647	0.467	0.776	1.16E-16
mlc-3	8.12E-19	-1.3579575	0.385	0.685	3.81E-14
vit-5	1.04E-19	-1.3515589	0.482	0.766	4.86E-15
ketn-1	2.78E-11	-1.343711	0.19	0.411	1.30E-06
ftn-2	9.77E-18	-1.3416391	0.318	0.602	4.58E-13
C17F4.7	3.81E-17	-1.3296595	0.426	0.714	1.79E-12
mup-2	2.50E-11	-1.3293507	0.364	0.562	1.17E-06

Tissue enrichment | -log10 Q-values

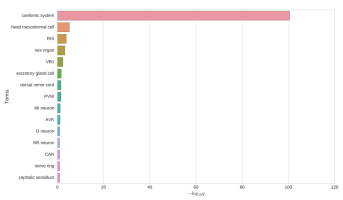

GO enrichment | -log10 Q-values

Nothing found on GO analysis

Phenotype enrichment | -log10 Q-values

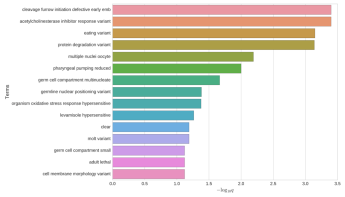

dig-1 (calcium ion binding, several structures including head mesodermal cell)

clone	cluster	chromosome	cosmid	CDS	gene	size
JAWN10	CEL.K09908	3		JK0781.2 JK0781.2.1		2.46

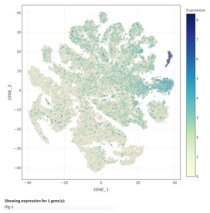

aman-1 (mannose metabolic processes predicted to be in lysosome)*

clone	cluster	chromosome	cosmid	CDS	gene	size
JAWN7	CEL.K01884	X		F55D10 F55D10.1		9.66

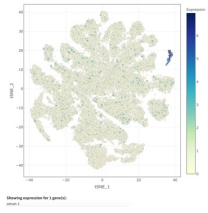

t-SNE showing cell type 29

Top 20 enriched genes

	p_val	avg_log2FC	pct.1	pct.2	p_val_adj
C35E7.5	0	4.46295818	0.811	0.037	0
sdz-29	0	4.46012328	0.396	0.007	0
odc-1	3.61E-68	4.32442019	0.523	0.084	1.69E-63
clec-266	1.13E-267	3.85284467	0.676	0.037	5.29E-263
pop-1	8.28E-75	3.53076343	0.55	0.083	3.88E-70
sdc-2	6.25E-167	3.40919513	0.739	0.074	2.93E-162
epg-2	7.35E-210	3.39618951	0.685	0.049	3.45E-205
cav-1	1.54E-121	3.38624962	0.649	0.075	7.21E-117
str-81	0	3.31258949	0.568	0.007	0
Y46H3C.7	8.18E-127	3.30984004	0.82	0.12	3.84E-122
C47D12.4	0	3.30398414	0.613	0.009	0
cht-1	6.75E-190	3.2026164	0.514	0.029	3.17E-185
Y82E9BR.17	0	3.18881549	0.649	0.01	0
T27A1.3	0	3.15315264	0.523	0.009	0
Y51H7C.15	4.24E-227	3.12242129	0.739	0.051	1.99E-222
his-24	5.65E-38	3.10260996	0.604	0.181	2.65E-33
Y45G5AM.5	0	3.09952927	0.441	0.006	0
chd-3	4.04E-80	3.09024482	0.703	0.138	1.89E-75
din-1	2.74E-61	3.07443022	0.784	0.224	1.28E-56
F53H1.4	1.14E-57	3.03436232	0.775	0.227	5.37E-53

Top 20 depleted genes

	p_val	avg_log2FC	pct.1	pct.2	p_val_adj
D1086.10	1.84E-08	-3.2291334	0.135	0.394	0.00086521
ule-4	9.19E-09	-3.1411727	0.243	0.508	0.00043083
lev-11	5.65E-29	-3.1115638	0.216	0.729	2.65E-24
far-2	2.01E-26	-2.9362263	0.36	0.768	9.45E-22
col-139	6.05E-12	-2.8962295	0.117	0.431	2.84E-07
col-124	4.31E-24	-2.8686186	0.27	0.708	2.02E-19
col-119	8.24E-25	-2.8547338	0.297	0.732	3.87E-20
unc-54	2.66E-24	-2.833011	0.18	0.685	1.25E-19
ttr-16	1.88E-19	-2.8327523	0.27	0.646	8.80E-15
col-93	1.21E-26	-2.8078882	0.351	0.768	5.67E-22
cpn-3	3.41E-23	-2.7989457	0.225	0.684	1.60E-18
K08D12.6	6.24E-21	-2.7922375	0.153	0.604	2.93E-16
col-20	2.77E-25	-2.7716992	0.252	0.725	1.30E-20
unc-27	2.47E-23	-2.7640237	0.207	0.668	1.16E-18
unc-15	5.13E-23	-2.7502167	0.162	0.649	2.40E-18
far-1	4.00E-21	-2.72896	0.171	0.634	1.87E-16
act-3	2.61E-25	-2.707055	0.387	0.775	1.22E-20
C39D10.7	7.01E-07	-2.7036447	0.072	0.284	0.03287574
mup-2	2.70E-21	-2.6529847	0.09	0.563	1.27E-16
col-122	1.98E-24	-2.6381536	0.324	0.74	9.28E-20

Tissue enrichment | -log10 Q-values

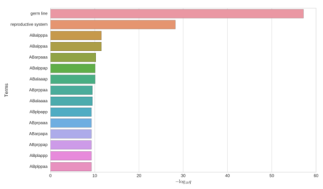

GO enrichment | -log10 Q-values

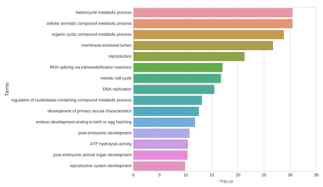

Phenotype enrichment | -log10 Q-values

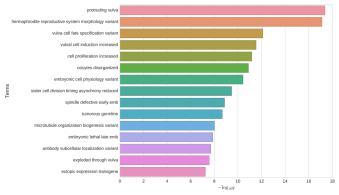

clec-266 (carbohydrate binding in plasma membrane, intestine

cluster	chromosome	cosmid	CDS	gene
CELK00113	4	C25A8	C25A8.6	x

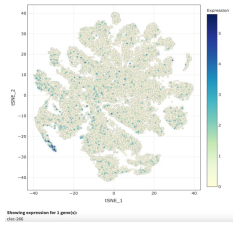

C35E7.5 (predicted to be involved in autophagy)*

cluster	chromosome	cosmid	CDS	gene
CELK00484	1	C35E7	C35E7.5	x

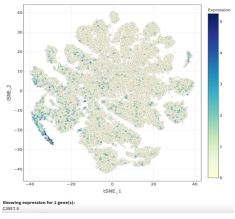

t-SNE showing cell type 30

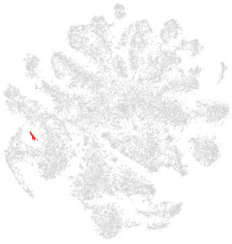

Top 20 enriched genes

	p_val	avg_log2FC	pct.1	pct.2	p_val_adj
MTCE.33	4.23E-20	6.41200122	0.763	0.266	1.98E-15
ctc-1	9.78E-21	5.15495749	0.895	0.437	4.59E-16
ctb-1	3.18E-18	3.8397139	0.816	0.383	1.49E-13
nduo-5	2.26E-22	3.60902475	0.868	0.372	1.06E-17
ctc-3	1.32E-26	3.35728548	1	0.575	6.19E-22
ctc-2	6.22E-24	3.32558884	0.947	0.439	2.92E-19
nduo-4	1.60E-24	3.14952748	0.921	0.344	7.49E-20
atp-6	3.31E-09	2.8378901	0.763	0.546	0.00015531
nduo-1	7.46E-16	2.79468754	0.816	0.362	3.50E-11
fln-1	3.01E-10	2.72370835	0.763	0.537	1.41E-05
nduo-6	5.71E-15	2.68922005	0.921	0.676	2.68E-10
rla-0	8.48E-08	2.46660321	0.789	0.572	0.00397621
rpl-11.1	1.60E-10	2.39478235	0.684	0.315	7.52E-06
nduo-2	6.93E-10	2.30895059	0.526	0.182	3.25E-05
MTCE.7	7.96E-07	2.29792725	0.632	0.345	0.03733506
ppw-2	3.85E-13	2.28241747	0.474	0.124	1.81E-08
rpoa-1	2.24E-15	2.15638609	0.605	0.176	1.05E-10
rla-1	3.65E-09	2.13590711	0.737	0.402	0.00017135
ndfl-4	1.72E-07	2.1061077	0.711	0.473	0.00805659
eea-1	4.01E-13	2.04993501	0.658	0.232	1.88E-08

Top 20 depleted genes

	p_val	avg_log2FC	pct.1	pct.2	p_val_adj
col-93	1.68E-15	-5.126399	0.079	0.767	7.87E-11
col-119	2.43E-13	-4.994781	0.132	0.731	1.14E-08
nlp-77	2.61E-14	-4.8577085	0	0.705	1.22E-09
col-140	2.25E-14	-4.8169383	0.053	0.738	1.05E-09
col-95	2.03E-10	-4.7165161	0.026	0.589	9.51E-06
F46H5.3	3.08E-16	-4.4789981	0.105	0.802	1.45E-11
col-20	1.80E-13	-4.4578894	0.079	0.723	8.43E-09
pat-10	3.77E-13	-4.4451127	0.053	0.708	1.77E-08
col-106	2.72E-13	-4.4186801	0.026	0.686	1.28E-08
col-181	1.83E-13	-4.3287726	0.079	0.726	8.57E-09
lev-11	1.40E-12	-4.1562704	0.158	0.728	6.55E-08
col-19	1.34E-11	-4.1228499	0.079	0.663	6.29E-07
act-4	5.58E-13	-4.0803911	0.079	0.719	2.62E-08
col-122	1.60E-13	-4.0798741	0.079	0.739	7.51E-09
unc-27	2.52E-11	-4.0473375	0.105	0.667	1.18E-06
mlc-3	4.32E-12	-3.9836271	0.079	0.683	2.03E-07
col-160	1.32E-14	-3.9245871	0.053	0.755	6.19E-10
F11E6.3	3.90E-12	-3.8870397	0.105	0.688	1.83E-07
col-8	9.44E-12	-3.8131409	0.053	0.646	4.43E-07
col-124	2.08E-11	-3.7723947	0.158	0.707	9.74E-07

Tissue enrichment | -log10 Q-values

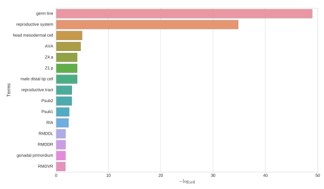

GO enrichment | -log10 Q-values

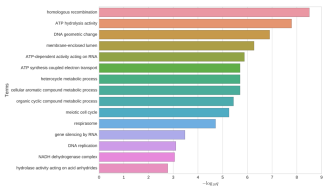

Phenotype enrichment | -log10 Q-values

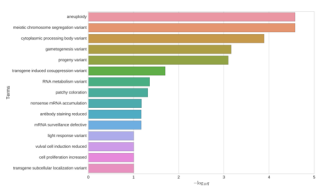

set-9 (histone methyltransferase activity, involved in determining adult

clone	cluster	chromosome	cosmid	CDS	gene	size
111d6	CELK03088	4	F15E6	F15E6.1		1.28

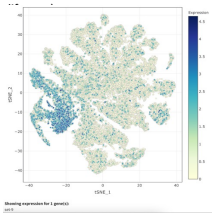

ppw-2 (predicted nucleic acid binding activity)*

cluster	chromosome	cosmid	CDS	gene
CELK00526	1	Y110A7A	Y110A7A.18	ppw-2

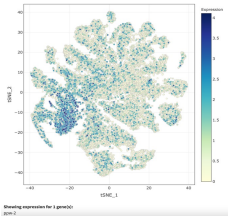

t-SNE showing cell type 0

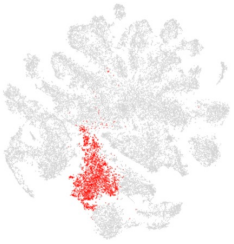

Top 20 enriched genes

	p_val	avg_log2FC	pct.1	pct.2	p_val_adj
vit-3	0	2.40753077	0.97	0.69	0
F57F5.1	0	2.36625453	0.945	0.461	0
vit-2	0	2.35693413	0.987	0.701	0
vit-5	0	2.33849234	0.981	0.745	0
H34I24.2	0	2.32123583	0.717	0.27	0
vit-1	0	2.23320352	0.954	0.651	0
lipl-5	0	2.20121706	0.939	0.567	0
vit-4	0	2.1749582	0.886	0.664	0
spp-17	0	2.12359357	0.843	0.41	0
fat-2	0	2.09367012	0.897	0.451	0
vit-6	0	2.08227724	0.984	0.735	0
lys-2	0	2.05854736	0.875	0.439	0
cpr-6	0	2.01385847	0.974	0.654	0
asp-3	0	2.01285413	0.961	0.56	0
asah-1	0	2.00459586	0.678	0.231	0
K12H4.7	0	1.96435666	0.879	0.442	0
dct-16	0	1.94856152	0.992	0.742	0
Y51F10.7	0	1.8522103	0.745	0.344	0
F28B4.3	0	1.83235041	0.691	0.29	0
cpr-1	0	1.83163546	0.866	0.417	0

Top 20 depleted genes

	p_val	avg_log2FC	pct.1	pct.2	p_val_adj
dig-1	5.96E-62	-3.3888185	0.071	0.251	2.80E-57
D1086.10	1.45E-61	-2.8996673	0.22	0.407	6.78E-57
ule-4	1.87E-50	-2.8347517	0.376	0.518	8.76E-46
ule-3	1.11E-20	-2.5996429	0.157	0.249	5.21E-16
ttr-1	5.59E-125	-2.5955658	0.203	0.492	2.62E-120
ZC513.7	1.05E-109	-2.439556	0.181	0.45	4.94E-105
D1054.10	9.83E-15	-2.3070872	0.251	0.327	4.61E-10
act-4	2.03E-254	-2.2836538	0.421	0.744	9.54E-250
ZK813.7	1.00E-18	-2.2766945	0.143	0.23	4.70E-14
unc-54	2.14E-220	-2.2620756	0.38	0.709	1.00E-215
far-2	1.19E-231	-2.2327528	0.555	0.784	5.60E-227
pat-10	1.21E-196	-2.1994722	0.481	0.726	5.66E-192
ule-2	2.64E-33	-2.1939963	0.175	0.304	1.24E-28
fasn-1	1.19E-45	-2.1630796	0.133	0.288	5.59E-41
ttr-16	3.83E-170	-2.1557018	0.403	0.665	1.80E-165
mlc-3	1.34E-200	-2.133881	0.425	0.704	6.29E-196
C10G8.4	1.38E-22	-2.128373	0.252	0.351	6.47E-18
Y62H9A.5	1.13E-14	-2.1111424	0.211	0.287	5.32E-10
lev-11	4.50E-229	-2.1049562	0.454	0.75	2.11E-224
cpn-3	5.60E-180	-2.0833823	0.449	0.701	2.63E-175

Tissue enrichment | -log10 Q-values

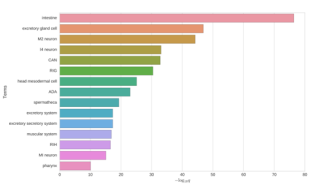

GO enrichment | -log10 Q-values

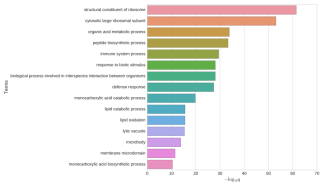

Phenotype enrichment | -log10 Q-values

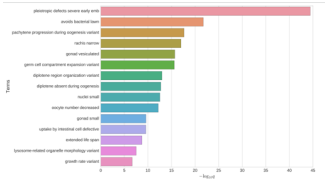

ges-1 (gut esterase in catabolic processes)

clone	cluster	chromosome	cosmid	CDS	gene	size
457a3	CEL.K06559	3	K12A1		ges-1	1.60

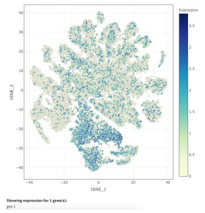

H34I24.2 (PVD, head mesodermal, intestine and pharyngeal muscle cells)*

clone	cluster	chromosome	cosmid	CDS	gene	size
145g4	CEL.F03662	3	H34I24	H34I24.2		1.04

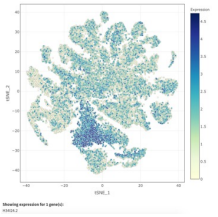

References

Alaimo, J. T., Davis, S. J., Song, S. S., Burnette, C. R., Grotewiel, M., Shelton, K. L., Pierce-Shimomura, J. T., Davies, A. G., & Bettinger, J. C. (2012). Ethanol metabolism and osmolarity modify behavioral responses to ethanol in C. elegans. *Alcoholism, Clinical and Experimental Research*, *36*(11), 1840–1850. https://doi.org/10.1111/J.1530-0277.2012.01799.X

Albarqi, M. M. Y., & Ryder, S. P. (2021). The endogenous mex-3 3´UTR is required for germline repression and contributes to optimal fecundity in C. elegans. *PLOS Genetics*, *17*(8), e1009775. https://doi.org/10.1371/JOURNAL.PGEN.1009775

Allard, P., Kleinstreuer, N. C., Knudsen, T. B., & Colaiácovo, M. P. (2013). A C. elegans screening platform for the rapid assessment of chemical disruption of germline function. *Environmental Health Perspectives*, *121*(6). https://doi.org/10.1289/ehp.1206301

Alvarez, M., Rahmani, E., Jew, B., Garske, K. M., Miao, Z., Benhammou, J. N., Ye, C. J., Pisegna, J. R., Pietiläinen, K. H., Halperin, E., & Pajukanta, P. (2020). Enhancing droplet-based single-nucleus RNA-seq resolution using the semi-supervised machine learning classifier DIEM. *Scientific Reports 2020 10:1*, *10*(1), 1–16. https://doi.org/10.1038/s41598-020-67513-5

Angeles-Albores, D., Raymond, R. Y., Chan, J., & Sternberg, P. W. (2016). Tissue enrichment analysis for C. elegans genomics. *BMC Bioinformatics*, *17*(1), 1–10. https://doi.org/10.1186/S12859-016-1229-9/FIGURES/6

Arneson, D., Zhang, G., Ying, Z., Zhuang, Y., Byun, H. R., Ahn, I. S., Gomez-Pinilla, F., & Yang, X. (2018). Single cell molecular alterations reveal target cells and pathways of concussive brain injury. *Nature Communications 2018 9:1*, *9*(1), 1–18. https://doi.org/10.1038/s41467-018-06222-0

Barton, M. K., & Kimble, J. (1990). fog-1, a regulatory gene required for specification of spermatogenesis in the germ line of Caenorhabditis elegans. *Genetics*, *125*(1), 29–39. https://doi.org/10.1093/GENETICS/125.1.29

Benjamini, Y., & Hochberg, Y. (1995). Controlling the False Discovery Rate: A Practical and Powerful Approach to Multiple Testing. *Journal of the Royal Statistical Society: Series B (Methodological)*, *57*(1), 289–300. https://doi.org/10.1111/J.2517-6161.1995.TB02031.X

Bozler, J., Kacsoh, B. Z., & Bosco, G. (2019). Transgeneratonal inheritance of ethanol preference is caused by maternal NPF repression. *ELife*, *8*. https://doi.org/10.7554/ELIFE.45391

Camacho, J., Truong, L., Kurt, Z., Chen, Y. W., Morselli, M., Gutierrez, G., Pellegrini, M., Yang, X., & Allard, P. (2018). The Memory of Environmental Chemical Exposure in C. elegans Is Dependent on the Jumonji Demethylases jmjd-2 and jmjd-3/utx-1. *Cell Reports*, *23*(8), 2392–2404. https://doi.org/10.1016/j.celrep.2018.04.078

Cao, J., Packer, J. S., Ramani, V., Cusanovich, D. A., Huynh, C., Daza, R., Qiu, X., Lee, C., Furlan, S. N., Steemers, F. J., Adey, A., Waterston, R. H., Trapnell, C., & Shendure, J. (2017). Comprehensive single-cell transcriptional profiling of a multicellular organism. *Science (New York, N.Y.)*, *357*(6352), 661–667. https://doi.org/10.1126/SCIENCE.AAM8940

Caputo, C., Wood, E., & Jabbour, L. (2016). Impact of fetal alcohol exposure on body systems: A systematic review. *Birth Defects Research. Part C, Embryo Today : Reviews*, *108*(2), 174–180. https://doi.org/10.1002/BDRC.21129

Dejong, K., Olyaei, A., & Lo, J. O. (2019). Alcohol Use in Pregnancy. *Clinical Obstetrics and Gynecology*, *62*(1), 142. https://doi.org/10.1097/GRF.0000000000000414

Dguzeh, U., Haddad, N. C., Smith, K. T. S., Johnson, J. O., Doye, A. A., Gwathmey, J. K., & Haddad, G. E. (2018). Alcoholism: A Multi-Systemic Cellular Insult to Organs. *International Journal of Environmental Research and Public Health*, *15*(6). https://doi.org/10.3390/IJERPH15061083

Gangisetty, O., Chaudhary, S., Palagani, A., & Sarkar, D. K. (2022). Transgenerational inheritance of fetal alcohol effects on proopiomelanocortin gene expression and methylation, cortisol response to stress, and anxiety-like behaviors in offspring for three generations in rats: Evidence for male germline transmission. *Plos One*, *17*(2), e0263340–e0263340. https://doi.org/10.1371/JOURNAL.PONE.0263340

Girault, V., Gilard, V., Marguet, F., Lesueur, C., Hauchecorne, M., Ramdani, Y., Laquerrière, A., Marret, S., Jégou, S., Gonzalez, B. J., Brasse-Lagnel, C., & Bekri, S. (2017). Prenatal alcohol exposure impairs autophagy in neonatal brain cortical microvessels. *Cell Death & Disease*, *8*(2), e2610. https://doi.org/10.1038/CDDIS.2017.29

Hollander, J., McNivens, M., Pautassi, R. M., & Nizhnikov, M. E. (2019). Offspring of male rats exposed to binge alcohol exhibit heightened ethanol intake at infancy and alterations in T-maze performance. *Alcohol (Fayetteville, N.Y.)*, *76*, 65–71. https://doi.org/10.1016/J.ALCOHOL.2018.07.013

Hunt, P. A. (1987). Ethanol-induced aneuploidy in male germ cells of the mouse. *Cytogenetic and Genome Research*, *44*(1), 7–10. https://doi.org/10.1159/000132333

Kaufman, M. H. (1983). Ethanol-induced chromosomal abnormalities at conception. *Nature 1983 302:5905*, *302*(5905), 258–260. https://doi.org/10.1038/302258a0

Kaufman, M. H., & Bain, I. M. (1984). Influence of ethanol on chromosome segregation during the first and second meiotic divisions in the mouse egg. *Journal of Experimental Zoology*, *230*(2), 315–320. https://doi.org/10.1002/JEZ.1402300217

Kelly, K. O., Dernburg, A. F., Stanfield, G. M., & Villeneuve, A. M. (2000). *Caenorhabditis elegans msh-5 Is Required for Both Normal and Radiation-Induced Meiotic Crossing Over but Not for Completion of Meiosis*.

Kelly, W. G. (2014). Transgenerational epigenetics in the germline cycle of Caenorhabditis elegans. *Epigenetics and Chromatin*, *7*(1), 1–17. https://doi.org/10.1186/1756-8935-7-6/FIGURES/6

Kishimoto, S., Uno, M., Okabe, E., Nono, M., & Nishida, E. (2017). Environmental stresses induce transgenerationally inheritable survival advantages via germline-to-soma communication in Caenorhabditis elegans. *Nature Communications*, *8*. https://doi.org/10.1038/NCOMMS14031

Klosin, A., Casas, E., Hidalgo-Carcedo, C., Vavouri, T., & Lehner, B. (2017). Transgenerational transmission of environmental information in C. elegans. *Science (New York, N.Y.)*, *356*(6335), 320–323. https://doi.org/10.1126/SCIENCE.AAH6412

La Vignera, S., Condorelli, R. A., Balercia, G., Vicari, E., & Calogero, A. E. (2013). Does alcohol have any effect on male reproductive function? A review of literature. *Asian Journal of Andrology*, *15*(2), 221. https://doi.org/10.1038/AJA.2012.118

Lacar, B., Linker, S. B., Jaeger, B. N., Krishnaswami, S., Barron, J., Kelder, M., Parylak, S., Paquola, A., Venepally, P., Novotny, M., O'Connor, C., Fitzpatrick, C., Erwin, J., Hsu, J. Y., Husband, D., McConnell, M. J., Lasken, R., & Gage, F. H. (2016). Nuclear RNA-seq of single neurons reveals molecular signatures of activation. *Nature Communications*, *7*. https://doi.org/10.1038/NCOMMS11022

Lam, M. K. P., Homewood, J., Taylor, A. J., & Mazurski, E. J. (2000). Second generation effects of maternal alcohol consumption during pregnancy in rats. *Progress in Neuro-Psychopharmacology & Biological Psychiatry*, *24*(4), 619–631. https://doi.org/10.1016/S0278-5846(00)00097-X

Lee, C., Seidel, H., Lynch, T., Sorensen, E., Crittenden, S., & Kimble, J. (2017). Single-molecule RNA Fluorescence in situ Hybridization (smFISH) in Caenorhabditis elegans. *Bio-Protocol*, *7*(12). https://doi.org/10.21769/BIOPROTOC.2357

Liu, W., Venugopal, S., Majid, S., Ahn, I. S., Diamante, G., Hong, J., Yang, X., & Chandler, S. H. (2020). Single-cell RNA-seq analysis of the brainstem of mutant SOD1 mice reveals perturbed cell types and pathways of amyotrophic lateral sclerosis. *Neurobiology of Disease*, *141*. https://doi.org/10.1016/J.NBD.2020.104877

Mueller, F., Senecal, A., Tantale, K., Marie-Nelly, H., Ly, N., Collin, O., Basyuk, E., Bertrand, E., Darzacq, X., & Zimmer, C. (2013). FISH-quant: automatic counting of transcripts in 3D FISH images. *Nature Methods 2013 10:4*, *10*(4), 277–278. https://doi.org/10.1038/nmeth.2406

Nizhnikov, M. E., Popoola, D. O., & Cameron, N. M. (2016). Transgenerational Transmission of the Effect of Gestational Ethanol Exposure on Ethanol Use-Related Behavior. *Alcoholism, Clinical and Experimental Research*, *40*(3), 497. https://doi.org/10.1111/ACER.12978

Obad, A., Peeran, A., Little, J. I., Haddad, G. E., & Tarzami, S. T. (2018). Alcohol-mediated organ damages: Heart and brain. *Frontiers in Pharmacology*, *9*(FEB), 81. https://doi.org/10.3389/FPHAR.2018.00081/BIBTEX

Packer, J. S., Zhu, Q., Huynh, C., Sivaramakrishnan, P., Preston, E., Dueck, H., Stefanik, D., Tan, K., Trapnell, C., Kim, J., Waterston, R. H., & Murray, J. I. (2019). A lineage-resolved molecular atlas of C. elegans embryogenesis at single-cell resolution. *Science (New York, N.Y.)*, *365*(6459). https://doi.org/10.1126/SCIENCE.AAX1971

R, E., & T, S. (2007). Sex determination in the germ line. *WormBook : The Online Review of C. Elegans Biology*. https://doi.org/10.1895/WORMBOOK.1.82.2

Selewa, A., Dohn, R., Eckart, H., Lozano, S., Xie, B., Gauchat, E., Elorbany, R., Rhodes, K., Burnett, J., Gilad, Y., Pott, S., & Basu, A. (2020). Systematic Comparison of High-throughput Single-Cell and Single-Nucleus Transcriptomes during Cardiomyocyte Differentiation. *Scientific Reports 2020 10:1*, *10*(1), 1–13. https://doi.org/10.1038/s41598-020-58327-6

Stuart, T., Butler, A., Hoffman, P., Hafemeister, C., Papalexi, E., Mauck, W. M., Hao, Y., Stoeckius, M., Smibert, P., & Satija, R. (2019). Comprehensive Integration of Single-Cell Data. *Cell*, *177*(7), 1888-1902.e21. https://doi.org/10.1016/J.CELL.2019.05.031

Ungerer, M., Knezovich, J., & Ramsay, M. (2013). In Utero Alcohol Exposure, Epigenetic Changes, and Their Consequences. *Alcohol Research : Current Reviews*, *35*(1), 37. /pmc/articles/PMC3860424/

Waltman, L., & Van Eck, N. J. (2013). A smart local moving algorithm for large-scale modularity-based community detection. *The European Physical Journal B 2013 86:11*, *86*(11), 1–14. https://doi.org/10.1140/EPJB/E2013-40829-0

Weinhouse, C., Truong, L., Meyer, J. N., & Allard, P. (2018). Caenorhabditis elegans as an emerging model system in environmental epigenetics. *Environmental and Molecular Mutagenesis*, *59*(7). https://doi.org/10.1002/em.22203

Yohn, N. L., Bartolomei, M. S., & Blendy, J. A. (2015). Multigenerational and Transgenerational Inheritance of Drug Exposure: The effects of alcohol, opiates, cocaine, marijuana, and nicotine. *Progress in Biophysics and Molecular Biology*, *118*(0), 21. https://doi.org/10.1016/J.PBIOMOLBIO.2015.03.002

Young, M. D., & Behjati, S. (2020). SoupX removes ambient RNA contamination from droplet-based single-cell RNA sequencing data. *GigaScience*, *9*(12), 1–10. https://doi.org/10.1093/GIGASCIENCE/GIAA151

CHAPTER 5

Summary and Discussion

Part of Chapter 5 was published as a review in Environmental and Molecular Mutagenesis titled

"*Caenorhabditis elegans* as an Emerging Model System in Environmental Epigenetics"

The elicitation of phenotypes due to environmental cues and the mechanism by which these changes are inherited across generations has been researched and debated for years (Heard *et al.,* 2014). In recent years, studies have begun to emerge that suggest epigenetics may be the key mediator in this process (Weinhouse *et al.,* 2018). To this end, *C. elegans* has proven to be a valuable model to study the effects of environmental exposures on the epigenome due to its ability to respond to a variety of environmental stressors: natural, including osmolarity (Kishimoto *et al.,* 2017), starvation (Rechavi *et al.,* 2014), and temperature (Klosin *et al.,* 2017); as well as made-made, such as heavy metals (Kishimoto *et al.,* 2017; Rudgalvyte *et al.,* 2017), nanoparticles (Schultz *et al.,* 2016) and others. The combination of the ease of manipulation of the organism and the availability of a multitude of molecular tools has allowed deep insight into the environmental influences on the epigenome. In addition, its fast generation time coupled with its high degree of conservation of epigenetic regulatory pathways (to the exception of 5mC) compared to humans has open the door to the examination of multi- and trans-generational effects.

Together, our work attempts to characterize the transgenerational effects of two environmental toxicants: Bisphenol A and ethanol. While the studies regarding each chemical differed extensively, both chemicals have been shown to transgenerationally elicit responses in the germline, leading to defects in reproduction. First, our work with BPA identified the mechanism of transgenerational inheritance of BPA exposure (Camacho *et al.,* 2018). Characterization of worms that were ancestrally exposed to BPA revealed both a direct F1 and transgenerational F3 deregulation of repressive histone modifications. In particular, using a strain carrying a highly repetitive GFP transgene that is normally epigenetically silenced in the germline similarly to the silencing of endogenous germline heterochromatin, we observed BPA exposure both directly and transgenerationally disrupting the silenced state and causing a de-silencing effect. Since this array is normally silenced through the addition of repressive histone marks, we next imaged pachytene-staged nuclei by immunofluorescence and showed that an

approximately 25% reduction in global H3K9me3 and H3K27me3 was observed transgenerationally between BPA and DMSO.

Since F3 germlines showed a strong alteration of their chromatin, we next investigated whether these changes were associated with reproductive defects. In particular, we analyzed two metrics for germline health: embryonic lethality and germline apoptosis. We observed a transgenerational increase in both metrics in worms ancestrally exposed to BPA when compared to DMSO control, suggesting that ancestral BPA exposure transgenerationally induces reproductive dysfunction. Further embryo analysis revealed both a higher incidence of F3 worms containing embryos with aneuploidies and an increase in the number of embryos containing aneuploidies per worm in the BPA treated groups. This aligns well with our observed increases in embryonic lethality which suggests possible chromosomal errors in embryos.

Additionally, since we had previously shown that ancestral BPA exposure caused an increase in apoptosis transgenerationally at the F3, we next explored whether this is due to an activation of the synapsis or DNA damage checkpoints. Here, we identify BPA's transgenerational apoptotic increase to be due to an activation of the synapsis checkpoint, not the DNA damage checkpoint. Furthermore, we analyzed a component of the synaptonemal complex and saw that ancestral BPA exposure causes an abnormal aggregation of SYP-3 and importantly, these SYP-3 aggregates correlated with increased embryonic lethality. Together, this suggests that transgenerational BPA exposure perturbs SC formation between homologous chromosomes, resulting in an activation of the synapsis checkpoint and increased germline apoptosis. However, not all of the nuclei with SC errors are caught by the synapsis checkpoint. Since it has been shown that synapsis is vital to ensure proper chromosome segregation in gametes, this results in nuclei that continue on to develop into embryos with aneuploidies. This in turn manifests as our observed increased embryonic lethality.

Next, we investigated the relationship between the observed reduction in H3K9me3 and H3K27me3 levels in the germline and BPA's transgenerational effects. Since it is known that in

addition to inheriting the genome from its parents, the progeny also inherits its associate epigenetic marks including histone modifications (Lind *et al.,* 2018), we hypothesized that the transgenerational effects of BPA exposure could be mediated through epigenetics. Since BPA exposure appears to reduce the repressive marks H3K9me3 and H3K27me3, we focused on targeting the histone demethylases for these marks in an attempt to rescue BPA's transgenerational effects. Using RNAi to knock-down the expression of *jmjd-2* (H3K9me3 KDM; Greer *et al.,* 2014; Whetstine *et al.,* 2006) and *jmjd-3/utx-1* (H3K27me3 KDM, Agger *et al.,* 2007), we were able to rescue BPA's transgenerational effects. The down-regulation of *jmjd-2* or *jmjd-3/utx-1* at the F2 returned BPA's transgenerational desilencing effects to basal levels. In addition, we also observed an increase in the levels of H3K9me3 and H3K27me3 in the germlines of F3 worms from the RNAi treatment. This was coupled with a rescue of BPA's reproductive effects including a decrease in embryonic lethality to basal levels. Next, we were interested in exploring whether BPA's transgenerational increase in apoptosis is also mediated through histone modifications. Here, we decided to use a different rescue paradigm. Since JMJD-1.2 controls multiple histone post-translation modifications including histone 3 lysine 9, lysine 23, and lysine 27 di-methylation (H3K9/K23/K27me2) in meiotic cells (Myers *et al.,* 2018), we used a *jmjd-1.2* mutant in order to rescue BPA's transgenerational apoptotic effects. We discovered that BPA's transgenerational increase in both apoptosis and embryonic lethality can be rescued by the *jmjd-1.2* mutant, further supporting the idea that BPA's transgenerational effects are mediated through histone modifications.

In comparison to BPA, for our work with ethanol, we decided to take a more high-throughput approach. While our exposure paradigm remained the same, rather than focusing on just the germline and exploring ethanol's transgenerational effects one gene at a time, we developed a single-nucleus extraction protocol that was robust enough to penetrate the *C. elegans'* rough cuticle while gentle enough not to damage the nuclei during the extraction process. These extracted single-nuclei were then sent for single nucleus RNA-seq library

preparation using the 10X Genomics Chromium system followed by 50 PE sequencing on the Illumina Novaseq 6000 platform.

In total, we generated transcriptomic data for 81,267 nuclei, each with more than 500 transcripts derived from 31 groups collected in 5 distinct batches. On average, 2,181 unique molecular identifiers (UMIs) and 992 genes were detected per nucleus with high sequencing depth (90.3% average sequencing depth). SnRNA-seq reads were demultiplexed and aligned to the ENSEMBL ce10 *C. elegans* transcriptome to generate gene expression matrices using CellRanger (10x Genomics) and filtered for empty droplets and corrected for ambient RNA contamination using DIEM (Alvarez *et al.,* 2020) and SoupX (Young *et al.,* 2020). Post-filtering, we retained the transcriptomic data from 41,750 droplets representing an average of 1627 UMIs and 1007 genes per nucleus. A total of 31 discrete clusters were identified following batch/group effect correction by canonical correlation analysis (CCA) in Seurat v3 followed by Louvain clustering algorithm [18,19]. Log-normalized expression levels in t-SNE (t-distributed stochastic neighbor embedding) plot projections were used to visualize cell clusters in two dimensions and dot heatmap were used to visualize marker expression across different cell types.

Analysis comparing the effects of two ethanol concentrations (0.05% and 0.50%) to water at two different generations (F1 and F3) revealed a significant number of Differentially Expressed Genes (DEGs) with an FDR<0.05 between both treatment conditions and water, both intergenerationally at the F1 and transgenerationally at the F3. Gene Ontology analysis of all DEGs revealed the enrichment of some functional categories that align with alcohol metabolism such as the GO category “carboxylic acid metabolic process” driven by the presence in our DEG list of alcohol dehydrogenase genes, which catalyze the first step of ethanol metabolism from ethanol to acetaldehyde, as well as aldehyde dehydrogenase genes, which catalyze the second step of ethanol metabolism from acetaldehyde into acetate, in both exposure groups at the F1 and F3. There were also GO categories that involve reproduction such as “embryo development ending in birth or egg hatching” and “cellular process involved in

reproduction in multicellular organism" that is shared between both exposure conditions at the F1 with many of them being shared across generations with the F3 as well.

Followed by analysis conducted on DEGs across all clusters, we conducted cluster-specific DEG analysis to investigate cell type specific effects at both the F1 and F3. Cluster-resolved DEG analysis clearly identified distinct transcriptional responses to parental ethanol exposure between different cell types. Euclidean distance analysis, which estimates the degree of global transcriptomic shifts between exposure and control groups, consistently ranked several clusters with a strong germline identity (1, 12, 15) to have the largest degree of transcriptomic shifts at both the F1 and F3. Analysis of cluster-specific changes to ethanol metabolism genes as a result of ancestral ethanol exposure revealed many cell type-specific changes with the cell types showing the highest increase in ethanol metabolism genes were also the ones that were the least sensitive to ethanol and vice versa, suggesting that upregulation of ethanol metabolism does protect a tissue from the inter- and trans-generational impact of ethanol exposure. Further DEG and pathway analysis reveals two important points: ethanol's effects are strongly dose-dependent and the pachytene region of the germline is most sensitive to both intergenerational and transgenerational ethanol exposure, carrying significant implication for ethanol's multigenerational reproductive effects.

Lastly, we validated our single-nucleus RNA-seq results both through single molecule fluorescence in situ hybridization (smFISH) (Lee *et al.,* 2016) and reproductive assays to reveal ethanol's multigenerational reproductive effects. We characterized the reproductive effects of ancestral ethanol exposure by looking at three metrics for germline health: apoptosis, aneuploidy, and embryonic lethality. Here, we observed a significant increase in the number of apoptotic nuclei per gonad in both the F1 and F3 who were ancestrally exposed to either ethanol concentrations. We monitored aneuploidy through the high incidence of male (XO) embryos caused by mis-segregation of the X-chromosome and identified a significant increase in the incidence of male embryos marked by expression of XOL-1::GFP for both ethanol

concentrations at both the F1 and F3 (Nicoll *et al.,* 1997; Miller *et al.,* 1998) . Lastly, we observed an increase in embryonic lethality between both ethanol conditions and water control at both F1 and F3. These results indicate a profound impact of intergenerational and transgenerational alcohol exposure on reproduction.

Together, these results demonstrate that both BPA and ethanol elucidate strong inter- and trans-generational reproductive effects. While studies involving BPA was much more mechanistic and focused specifically on germline effects, studies with ethanol were more holistic, allowing us to explore the transgenerational effects of ethanol on almost every tissue type. Mechanistic studies involving BPA demonstrated the key role of repressive histone modifications, H3K9me3 and H3K27me3, in the inheritance of reproductive dysfunction induced by an environmental exposure. These findings reveal how environmental exposures can affect reproductive phenotypes and how these effects can be transgenerationally inherited. Unfortunately, analysis of genes responsible for histone modifications in our single-nucleus RNA-seq data were not indicated to be strongly differentially expressed and pathways related to histone marks were not identified in our pathway analysis. This suggests that the effects of BPA exposure and ethanol exposure may be inherited across generations through different mechanisms.

Recent studies have highlighted the challenge of identifying a unifying mechanism of inheritance, if it indeed exists. Histone modifications are not the only epigenetic marks implicated in trans-generational inheritance. Rechavi *et al.,* (2014) observed that starvation-induced developmental arrest induced expression of small RNAs that were inherited for three generations. These small RNAs target genes important for nutrient reservoir activity and vitellogenins, yolk lipoglycoproteins that provision the egg (Rechavi *et al.*, 2014). Small RNA inheritance across generations required the argonaute factors *rde-4* and *hrde-1*, which are critical components of the small RNA generation pathway (Rechavi *et al.*, 2014). Interestingly, another study was able to functionally connect regulation of H3K9 methylation levels with that of

small RNAs. Worms mutant for the H3K9 methyltransferase *met-2* display a progressive mortal germline phenotype in which fertility declines over many generations (10–30 generations following homozygosity) (Lev *et al.*, 2017). Interestingly, the argonaute factor *hdre-1* is required for this progressive sterility phenotype (Lev *et al.*, 2017). Although RNA interference (RNAi) is heritable for a few generations in *C. elegans*, *met-2* mutants show greater persistence of RNAi effects, up to 15 generations (Lev *et al.*, 2017). This effect correlated with the presence and maintenance of small RNAs directed against the target locus across these generations (Lev *et al.*, 2017). Thus, a model emerges in which MET-2 controls the production of small RNAs *via* the regulation of H3K9me. These exciting findings directly link repressive histone marks and small RNAs, potentially implicating both types of epigenetic mechanisms in trans-generational inheritance. Since analysis of genes responsible for histone modifications in our single-nucleus RNA-seq data were not indicated to be strongly differentially expressed and pathways related to histone marks were not identified in our GO analysis, it is possible that ethanol's transgenerational effects may be mediated through small RNAs which our single-nucleus RNA-seq method would not encompass.

Future research should focus on mechanisms underlying trans-generational inheritance due to environmental exposure. Specifically, due to crosstalk among epigenetic pathways, there is a great need to systematically examine the interplay between the different modes of inheritance (histone or RNA-mediated). Furthermore, none of the aforementioned studies connected the initial environmental exposure mechanistically to reported epigenetic alterations. Further work should dissect the mechanisms linking the environmental cue with the alteration of the pathways important for epigenetic homeostasis. Lastly, future research should incorporate considerations of nonepigenetic parental contributions. For example, osmotic stress can alter the amount of glycogen packaged into embryos (Frazier and Roth 2009); this could be mediated by parental epigenetic changes, or accompany or induce epigenetic changes in offspring, but this could also occur with no epigenetic involvement. More broadly, stressors could simply alter

loading of many protein, lipid, and nucleic acid components without epigenetic involvement. In addition, chemical pollutants may be directly loaded into embryos in exposure experiments; for example, vitellogenin can be a vector for transport of contaminants to offspring in fish (Monteverdi and Di Giulio 2000). Thus, such loading should be ruled out or considered in interpretation of data from multi- or trans-generational epigenetics experiments.

Finally, our work as well as others have yet to answer another important question: For somatic phenotypes that are inherited across generations, how is this information transferred between germ cells and somatic cells, resulting in adult cell types with altered cellular programs and function. This would best be addressed in *C. elegans*, a model in which the location and timing of each cellular differentiation event are well explored and described. Thus, while there is still much work to be done, our current studies have identified one mode of inheritance of environmental cues across generations. In addition, our development of a new single-nucleus extraction protocol that is able to isolate single nuclei from the adult *C. elegans* will prove to be useful in understanding the underlying mechanisms of environmental exposures across generations.

References

Agger, K., Cloos, P. A. C., Christensen, J., Pasini, D., Rose, S., Rappsilber, J., Issaeva, I., Canaani, E., Salcini, A. E., & Helin, K. (2007). UTX and JMJD3 are histone H3K27 demethylases involved in HOX gene regulation and development. *Nature 2007 449:7163*, *449*(7163), 731–734. https://doi.org/10.1038/nature06145

Alvarez, M., Rahmani, E., Jew, B., Garske, K. M., Miao, Z., Benhammou, J. N., Ye, C. J., Pisegna, J. R., Pietiläinen, K. H., Halperin, E., & Pajukanta, P. (2020). Enhancing droplet-based single-nucleus RNA-seq resolution using the semi-supervised machine learning classifier DIEM. *Scientific Reports 2020 10:1*, *10*(1), 1–16. https://doi.org/10.1038/s41598-020-67513-5

Camacho, J., Truong, L., Kurt, Z., Chen, Y. W., Morselli, M., Gutierrez, G., Pellegrini, M., Yang, X., & Allard, P. (2018). The Memory of Environmental Chemical Exposure in C. elegans Is Dependent on the Jumonji Demethylases jmjd-2 and jmjd-3/utx-1. *Cell Reports*, *23*(8), 2392–2404. https://doi.org/10.1016/j.celrep.2018.04.078

Frazier, H. N., & Roth, M. B. (2009). Adaptive sugar provisioning controls survival of C. elegans embryos in adverse environments. *Current Biology : CB*, *19*(10), 859–863. https://doi.org/10.1016/J.CUB.2009.03.066

Greer, E. L., Beese-Sims, S. E., Brookes, E., Spadafora, R., Zhu, Y., Rothbart, S. B., Aristizábal-Corrales, D., Chen, S., Badeaux, A. I., Jin, Q., Wang, W., Strahl, B. D., Colaiácovo, M. P., & Shi, Y. (2014). A histone methylation network regulates transgenerational epigenetic memory in C. elegans. *Cell Reports*, *7*(1), 113–126. https://doi.org/10.1016/J.CELREP.2014.02.044

Heard, E., & Martienssen, R. A. (2014). Transgenerational Epigenetic Inheritance: myths and mechanisms. *Cell*, *157*(1), 95. https://doi.org/10.1016/J.CELL.2014.02.045

Kishimoto, S., Uno, M., Okabe, E., Nono, M., & Nishida, E. (2017). Environmental stresses induce transgenerationally inheritable survival advantages via germline-to-soma communication in Caenorhabditis elegans. *Nature Communications*, *8*. https://doi.org/10.1038/NCOMMS14031

Klosin, A., Casas, E., Hidalgo-Carcedo, C., Vavouri, T., & Lehner, B. (2017). Transgenerational transmission of environmental information in C. elegans. *Science (New York, N.Y.)*, *356*(6335), 320–323. https://doi.org/10.1126/SCIENCE.AAH6412

Lee, C. H., Sorensen, E. B., Lynch, T. R., & Kimble, J. (2016). C. elegans GLP-1/Notch activates transcription in a probability gradient across the germline stem cell pool. *ELife*, *5*(OCTOBER2016). https://doi.org/10.7554/ELIFE.18370

Lind, M. I., & Spagopoulou, F. (2018). Evolutionary consequences of epigenetic inheritance. *Heredity 2018 121:3*, *121*(3), 205–209. https://doi.org/10.1038/s41437-018-0113-y

Miller, L. M., Plenefisch, J. D., Casson, L. P., & Meyer, B. J. (1988). xol-1: a gene that controls the male modes of both sex determination and X chromosome dosage compensation in C. elegans. *Cell*, *55*(1), 167–183. https://doi.org/10.1016/0092-8674(88)90019-0

Monteverdi, G. H., & Di Giulio, R. T. (2000). Oocytic accumulation and tissue distribution of 2,3,7,8-tetrachlorodibenzo-p-dioxin and benzo[a]pyrene in gravid Fundulus heteroclitus. *Environmental Toxicology and Chemistry*, *19*(10), 2512–2518. https://doi.org/10.1002/ETC.5620191017

Myers, T. R., Amendola, P. G., Lussi, Y. C., & Salcini, A. E. (2018). JMJD-1.2 controls multiple histone post-translational modifications in germ cells and protects the genome from replication stress. *Scientific Reports 2018 8:1*, *8*(1), 1–11. https://doi.org/10.1038/s41598-018-21914-9

Nicoll, M., Akerib, C. C., & Meyer, B. J. (1997). X-chromosome-counting mechanisms that determine nematode sex. *Nature 1997 388:6638*, *388*(6638), 200–204. https://doi.org/10.1038/40669

Rechavi, O., Houri-Ze'Evi, L., Anava, S., Goh, W. S. S., Kerk, S. Y., Hannon, G. J., & Hobert, O. (2014). Starvation-induced transgenerational inheritance of small RNAs in C. elegans. *Cell*, *158*(2), 277–287. https://doi.org/10.1016/J.CELL.2014.06.020

Rudgalvyte, M., Peltonen, J., Lakso, M., & Wong, G. (2017). Chronic MeHg exposure modifies the histone H3K4me3 epigenetic landscape in Caenorhabditis elegans. *Comparative Biochemistry and Physiology. Toxicology & Pharmacology : CBP*, *191*, 109–116. https://doi.org/10.1016/J.CBPC.2016.10.001

Schultz, C. L., Wamucho, A., Tsyusko, O. V., Unrine, J. M., Crossley, A., Svendsen, C., & Spurgeon, D. J. (2016). Multigenerational exposure to silver ions and silver nanoparticles reveals heightened sensitivity and epigenetic memory in Caenorhabditis elegans. *Proceedings. Biological Sciences*, *283*(1832). https://doi.org/10.1098/RSPB.2015.2911

Weinhouse, C., Truong, L., Meyer, J. N., & Allard, P. (2018). Caenorhabditis elegans as an emerging model system in environmental epigenetics. *Environmental and Molecular Mutagenesis*, *59*(7), 560–575. https://doi.org/10.1002/EM.22203

Whetstine, J. R., Nottke, A., Lan, F., Huarte, M., Smolikov, S., Chen, Z., Spooner, E., Li, E., Zhang, G., Colaiacovo, M., & Shi, Y. (2006). Reversal of histone lysine trimethylation by the JMJD2 family of histone demethylases. *Cell*, *125*(3), 467–481. https://doi.org/10.1016/J.CELL.2006.03.028

Young, M. D., & Behjati, S. (2020). SoupX removes ambient RNA contamination from droplet-based single-cell RNA sequencing data. *GigaScience*, *9*(12). https://doi.org/10.1093/GIGASCIENCE/GIAA151